frontiers | Research Topics

Epigenetic and metabolic regulation of primary and metastatic brain cancers

Edited by
Ryan Gimple, Briana Prager and Qi Xie

Published in
Frontiers in Oncology

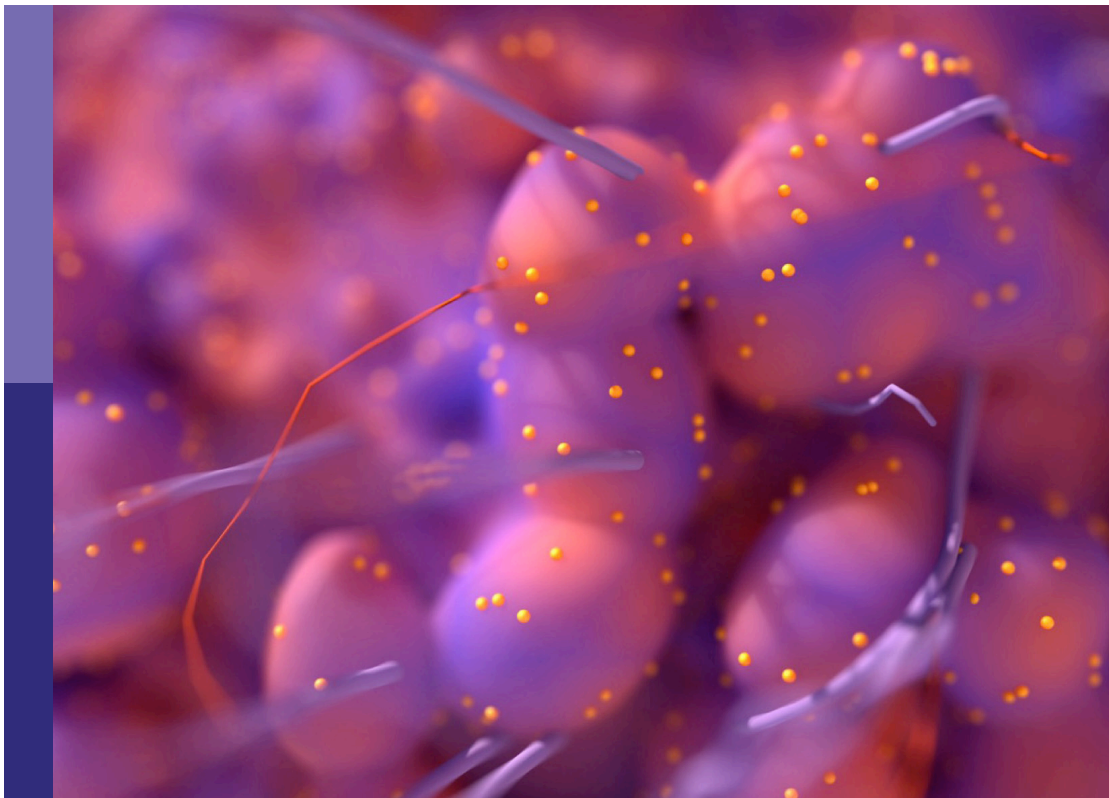

ISSN 1664-8714
ISBN 978-2-8325-3533-2
DOI 10.3389/978-2-8325-3533-2

About Frontiers

Frontiers is more than just an open access publisher of scholarly articles: it is a pioneering approach to the world of academia, radically improving the way scholarly research is managed. The grand vision of Frontiers is a world where all people have an equal opportunity to seek, share and generate knowledge. Frontiers provides immediate and permanent online open access to all its publications, but this alone is not enough to realize our grand goals.

Frontiers journal series

The Frontiers journal series is a multi-tier and interdisciplinary set of open-access, online journals, promising a paradigm shift from the current review, selection and dissemination processes in academic publishing. All Frontiers journals are driven by researchers for researchers; therefore, they constitute a service to the scholarly community. At the same time, the *Frontiers journal series* operates on a revolutionary invention, the tiered publishing system, initially addressing specific communities of scholars, and gradually climbing up to broader public understanding, thus serving the interests of the lay society, too.

Dedication to quality

Each Frontiers article is a landmark of the highest quality, thanks to genuinely collaborative interactions between authors and review editors, who include some of the world's best academicians. Research must be certified by peers before entering a stream of knowledge that may eventually reach the public - and shape society; therefore, Frontiers only applies the most rigorous and unbiased reviews. Frontiers revolutionizes research publishing by freely delivering the most outstanding research, evaluated with no bias from both the academic and social point of view. By applying the most advanced information technologies, Frontiers is catapulting scholarly publishing into a new generation.

What are Frontiers Research Topics?

Frontiers Research Topics are very popular trademarks of the *Frontiers journals series*: they are collections of at least ten articles, all centered on a particular subject. With their unique mix of varied contributions from Original Research to Review Articles, Frontiers Research Topics unify the most influential researchers, the latest key findings and historical advances in a hot research area.

Find out more on how to host your own Frontiers Research Topic or contribute to one as an author by contacting the Frontiers editorial office: frontiersin.org/about/contact

Epigenetic and metabolic regulation of primary and metastatic brain cancers

Topic editors

Ryan Gimple — Washington University in St. Louis, United States

Briana Prager — Massachusetts General Hospital, Harvard Medical School, United States

Qi Xie — Westlake University, China

Citation

Gimple, R., Prager, B., Xie, Q., eds. (2023). *Epigenetic and metabolic regulation of primary and metastatic brain cancers*. Lausanne: Frontiers Media SA.

doi: 10.3389/978-2-8325-3533-2

Table of contents

frontiers | Frontiers in Oncology

TYPE Editorial
PUBLISHED 07 September 2023
DOI 10.3389/fonc.2023.1271851

OPEN ACCESS

EDITED AND REVIEWED BY
Michael P. Lisanti,
University of Salford, United Kingdom

*CORRESPONDENCE
Ryan C. Gimple
ryangimple@gmail.com

RECEIVED 03 August 2023
ACCEPTED 23 August 2023
PUBLISHED 07 September 2023

CITATION
Gimple RC, Prager BC and Xie Q (2023) Editorial: Epigenetic and metabolic regulation of primary and metastatic brain cancers.
Front. Oncol. 13:1271851.
doi: 10.3389/fonc.2023.1271851

Editorial: Epigenetic and metabolic regulation of primary and metastatic brain cancers

Ryan C. Gimple[1]*, Briana C. Prager[2] and Qi Xie[3,4,5]

[1]Department of Medicine, Washington University School of Medicine, Washington University in St Louis, St. Louis, MO, United States, [2]Department of Neurosurgery, Massachusetts General Hospital, Boston, MA, United States, [3]Key Laboratory of Growth Regulation and Translational Research of Zhejiang Province, School of Life Sciences, Westlake University, Hangzhou, Zhejiang, China, [4]Westlake Laboratory of Life Sciences and Biomedicine, School of Life Sciences, Westlake University, Hangzhou, Zhejiang, China, [5]Institute of Basic Medical Sciences, Westlake Institute for Advanced Study, Hangzhou, Zhejiang, China

KEYWORDS

brain cancer, cancer, epigenetics, metabolism, metastasis, tumor microenvironment, primary brain cancer, brain cancer stem cells

Editorial on the Research Topic
Epigenetic and metabolic regulation of primary and metastatic brain cancers

Primary intrinsic brain tumors and brain metastases are among the most lethal of all human malignancies despite decades of scientific advances. The intersecting fields of cancer epigenetics and metabolism lie at the core of our current conceptual framework for the pathophysiology of these diseases (1, 2). While alterations in epigenetic pathways contribute to neoplastic metabolic dysregulation through transcriptional control mechanisms, metabolite abundance and availability reciprocally impinge upon epigenetic pathways. In this Research Topic, we highlight important advances focused on epigenetic and metabolic processes that enable brain tumors to thrive within the intracranial setting, along with key insights into the tumor microenvironment.

Epigenetic pathways integrate multiple sources of information regarding cell state and microenvironmental features to orchestrate an organized cellular response, mediating cellular adaptability, plasticity, and resilience. In this Research Topic, McCornack et al. discuss mechanisms by which histone methyltransferases and acetyltransferases mediate these diverse processes including reviewing downstream signaling elements and therapeutic targeting opportunities. Valproic acid is a commonly used anti-epileptic with anti-tumor effects through its histone deacetylase (HDAC) activity; however, in this Research Topic, Barciszewska et al. define a new epigenetic role for valproic acid in the induction of global hypermethylation. This study provides a rationale for the combination of valproic acid with temozolomide for enhancing DNA damage and oxidative stress in glioblastoma tissues. Although extrachromosomal circular DNA (eccDNA) had been originally observed nearly six decades ago (3), the relevance of this alternative mechanism of dynamic gene regulation to cancer survival and therapeutic resilience has only recently come into sharper focus (4, 5), particularly in brain tumors (6–9). Zhu et al. interrogate the landscape of eccDNAs in medulloblastoma, showing preferential inclusion

of genes involved in neuronal development and differentiation, RAS GTPase binding, and RAP1 signaling. They further identify the upregulation of genes via eccDNAs associated with poor prognosis in clinical datasets, highlighting eccDNAs as important mediators of medulloblastoma pathophysiology and implicating future therapeutic targets.

Tumor metabolism impinges on multiple key oncogenic processes through the coordination of signaling cascades, bioenergetics, and structural components both in a cell-intrinsic manner and in the coordination of cellular interactions within the brain tumor microenvironment. Bezawork-Geleta et al. review the importance of lipid metabolism in glioblastoma biology, focusing on lipid droplets as key substrates for cellular energy production and as intermediates that affect cellular signaling through affecting ferroptosis (a lipid peroxidation mediated and iron-dependent form of cell death), and lipophagy (a lipid specific form of autophagy). Autophagy is a finely tuned cellular process that enables cancer cell survival in nutrient- and energy-poor settings that define the tumor microenvironment, but can also be exploited for anti-cancer therapies (10). Induction of cytotoxic autophagy using the small molecule inhibitor ABTL0812 impairs glioblastoma stem cell proliferation and stem features *in vitro* and displays combinatorial efficacy in orthotopic xenograft models when combined with standard-of-care radiotherapy and temozolomide, primarily through inhibition of AKT/mTORC1 signaling and activation of ER stress responses (Mancini et al). These studies highlight the important metabolic adaptations utilized by primary brain tumors to survive in the intracranial setting and suggest a new approach to undermining these key dependencies.

Epigenetic and metabolic pathways further support tumor cell invasion. The blood-brain barrier preserves the integrity of the central nervous system and shields against toxins from the central circulation and from invading cancer cells. Breaching the blood-brain barrier is a critical step in the metastatic cascade responsible for the generation of brain metastases (11). Zhang et al. identify that the blood-brain barriers of patients with advanced lung cancers are more permeable than those of patients with early-stage lung cancers or healthy controls, suggesting that primary lung cancers may act at a distance to disrupt the blood-brain barrier and set the stage for future metastases. Further understanding of the processes underlying blood-brain barrier disruption may yield strategies to protect the brain from metastatic colonization. Meningiomas are among the most common primary brain tumors with widely variable prognoses based on molecular classification and morphologic features. Jiang et al. utilize imaging characteristics from MRI studies to improve the identification of the extent of tumor invasion to facilitate improved extent of resection. This study further identifies imaging features that serve as independent risk factors for predicting WHO tumor grades through deeper scrutiny of interactions within the brain-tumor interface.

This Research Topic further touches on therapeutics in the intracranial setting. Vasogenic edema is a major source of morbidity and mortality in intracranial malignancies with limited treatment options (12). While studies have shown the efficacy of bevacizumab in reducing edema and progression-free survival in primary brain tumor patients (13, 14), Bai and Zhou investigate the role of bevacizumab in patients with lung or colon brain metastases, showing differential effectiveness based on the tumor of origin. The prognosis for patients with brain metastases from non-small cell lung cancer remains dismal, particularly when patients are not candidates for surgical resection due to a variety of patient or tumor characteristics. Yang et al. study the use of an alternative radiation therapy delivery modality, 125-Iodide brachytherapy, compared to external beam radiotherapy (EBRT) and find improved 6-month survival and similar 12-month survival for the 125-iodide group compared to the EBRT group. This study provides further evidence for an additional modality for the treatment of brain metastases.

In a prescient and well-timed review, Johanssen et al. describe the current state of basic and translational research as it applies to glioblastoma with a discussion of the importance of understanding brain tumors through the lens of intratumoral heterogeneity and within the context of their tumor microenvironments. They suggest the use of both rationally designed and hypothesis-generating unbiased combinatorial screening approaches that incorporate heterogeneous tumor models as well as important microenvironmental features to identify compounds and combination therapies with the greatest clinical utility. Taken together, this Research Topic highlights some of the latest advances in the fields of brain tumor biology, specifically focused on the intersection between cancer epigenetics and metabolism and touching on key elements of the tumor microenvironment, with an eye towards improving outcomes for patients with primary and metastatic brain tumors.

Author contributions

RG: Writing – original draft, Writing – review & editing. BP: Writing – original draft, Writing – review & editing. QX: Writing – original draft, Writing – review & editing.

Conflict of interest

The authors declare that the research was conducted in the absence of any commercial or financial relationships that could be construed as a potential conflict of interest.

Publisher's note

References

1. Izzo LT, Affronti HC, Wellen KE. The bidirectional relationship between cancer epigenetics and metabolism. *Annu Rev Cancer Biol* (2021) 5:235–57. doi: 10.1146/annurev-cancerbio-070820-035832

2. Dai Z, Ramesh V, Locasale JW. The evolving metabolic landscape of chromatin biology and epigenetics. *Nat Rev Genet* (2020) 21:737–53. doi: 10.1038/s41576-020-0270-8

3. Cox D, Yuncken C, Spriggs AI. Minute chromatin bodies in Malignant tumours of childhood. *Lancet* (1965) 1:55–8. doi: 10.1016/s0140-6736(65)90131-5

4. Yi E, Chamorro Gonzalez R, Henssen AG, Verhaak RGW. Extrachromosomal DNA amplifications in cancer. *Nat Rev Genet* (2022) 23:760–71. doi: 10.1038/s41576-022-00521-5

5. Hung KL, Mischel PS, Chang HY. Gene regulation on extrachromosomal DNA. *Nat Struct Mol Biol* (2022) 29:736–44. doi: 10.1038/s41594-022-00806-7

6. Turner KM, Deshpande V, Beyter D, Koga T, Rusert J, Lee C, et al. Extrachromosomal oncogene amplification drives tumour evolution and genetic heterogeneity. *Nature* (2017) 543:122–5. doi: 10.1038/nature21356

7. deCarvalho AC, Kim H, Poisson LM, Winn ME, Mueller C, Cherba D, et al. Discordant inheritance of chromosomal and extrachromosomal DNA elements contributes to dynamic disease evolution in glioblastoma. *Nat Genet* (2018) 50:708–17. doi: 10.1038/s41588-018-0105-0

8. Morton AR, Dogan-Artun N, Faber ZJ, MacLeod G, Bartels CF, Piazza MS, et al. Functional enhancers shape extrachromosomal oncogene amplifications. *Cell* (2019) 179:1330–1341 e1313. doi: 10.1016/j.cell.2019.10.039

9. Nathanson DA, Gini B, Mogahedeh J, Visnyei K, Koga T, Gomez G, et al. Targeted therapy resistance mediated by dynamic regulation of extrachromosomal mutant EGFR DNA. *Science* (2014) 343:72–6. doi: 10.1126/science.1241328

10. Levy JMM, Towers CG, Thorburn A. Targeting autophagy in cancer. *Nat Rev Cancer* (2017) 17:528–42. doi: 10.1038/nrc.2017.53

11. Arvanitis CD, Ferraro GB, Jain RK. The blood-brain barrier and blood-tumour barrier in brain tumours and metastases. *Nat Rev Cancer* (2020) 20:26–41. doi: 10.1038/s41568-019-0205-x

12. Gerstner ER, Duda DG, di Tomaso E, Ryg PA, Loeffler JS, Sorensen AG, et al. VEGF inhibitors in the treatment of cerebral edema in patients with brain cancer. *Nat Rev Clin Oncol* (2009) 6:229–36. doi: 10.1038/nrclinonc.2009.14

13. Gilbert MR, Dignam JJ, Armstrong TS, Wefel JS, Blumenthal DT, Vogelbaum MA, et al. A randomized trial of bevacizumab for newly diagnosed glioblastoma. *N Engl J Med* (2014) 370:699–708. doi: 10.1056/NEJMoa1308573

14. Chinot OL, Wick W, Mason W, Henriksson R, Saran F, Nishikawa R, et al. Bevacizumab plus radiotherapy-temozolomide for newly diagnosed glioblastoma. *N Engl J Med* (2014) 370:709–22. doi: 10.1056/NEJMoa1308345

frontiers | Frontiers in Oncology

TYPE Original Research
PUBLISHED 29 September 2022
DOI 10.3389/fonc.2022.838670

OPEN ACCESS

EDITED BY
Lyndon Kim,
Mount Sinai Hospital, United States

REVIEWED BY
Muhammad Khan,
Guangzhou Medical University Cancer Hospital, China
Pinan Liu,
Beijing Tiantan Hospital, Capital Medical University, China

*CORRESPONDENCE
Meng Zhou
zmeng1119@163.com

SPECIALTY SECTION
This article was submitted to Cancer Imaging and Image-directed Interventions, a section of the journal Frontiers in Oncology

RECEIVED 07 January 2022
ACCEPTED 06 September 2022
PUBLISHED 29 September 2022

CITATION
Bai X and Zhou M (2022) The benefit of bevacizumab therapy in patients with refractory vasogenic edema caused by brain metastasis from lung and colon cancers.
Front. Oncol. 12:838670.
doi: 10.3389/fonc.2022.838670

The benefit of bevacizumab therapy in patients with refractory vasogenic edema caused by brain metastasis from lung and colon cancers

Xuexue Bai and Meng Zhou*

Neurosurgery of The First Affiliated Hospital, Jinan University, Guangzhou, China

Objective: This retrospective study investigated the efficacy of bevacizumab in refractory brain edema caused by brain metastasis from lung cancer and colon cancer.

Methods: A total of 72 patients with refractory brain edema were divided into the lung cancer and colon cancer groups according to their primary tumor. All patients received a single bevacizumab treatment for refractory brain edema. MRI was performed 1 week before the treatment and 4 weeks after the treatment. The edema and tumor volumes were calculated using imaging modalities.

Results: After a single bevacizumab treatment, the refractory brain edema of 61 patients was controlled, and the clinical symptoms of 65 patients were improved. The average edema volume before treatment was 201,708.97 $\pm$ 61,426.04 mm^3, which has decreased to 116,947.01 $\pm$ 43,879.16 mm^3 after treatment ($P < 0.05$). After treatment, the edema index decreased from 25.97 $\pm$ 7.15 to 17.32 $\pm$ 5.24 ($P < 0.05$).We found that brain edema was controlled in 40 patients (93.02%) in the lung cancer group and 21 patients (72.41%) in the colon cancer group ($P<0.05$). In addition, 22 patients (88.00%) in the radiotherapy group achieved edema control, compared to 39 (82.98%) in the non-radiotherapy group ($P>0.05$). Nine patients experienced hypertension after treatment, two patients exhibited decreased platelet counts, and no hemorrhage cases were observed.

Conclusion: Bevacizumab can significantly alleviate refractory brain edema, and there is a significant difference in the efficacy of bevacizumab on refractory brain edema caused by brain metastasis from lung and colon cancers.

KEYWORDS

bevacizumab, refractory brain edema, lung cancer, colon cancer, brain metastasis

Introduction

Brain metastases are 10 times more common than primary intracranial cancer and represent the most common intracranial malignancy in adults (1, 2). Brain edema often occurs around brain metastases due to the abnormal accumulation of fluid in the brain parenchyma (3), which increases brain volume and elevated intracranial pressure (ICP) within the skull (4). Elevated ICP may decrease cerebral blood flow, causing hypoxia in the brain tissue and even brain herniation. These factors can lead to irreversible damage to nerve function and even death. Mannitol, diuretics, and steroids are used to reduce brain edema, but their therapeutic effect on refractory brain edema is unsatisfactory. Previous studies have shown that the control rate of these drugs for refractory brain edema is 27%–39% (5–10). These drugs cannot eliminate potential pathogenic factors and have many adverse reactions (11). The long-term use of steroids can lead to significant systemic side effects, including immunosuppression and avascular necrosis (12, 13). Mannitol may cause systemic hypotension, decreased cerebral perfusion, and acute renal failure (14, 15). Vascular endothelial growth factor A (VEGF-A) promotes angiogenesis and vascular permeability (16). Therefore, it is considered to play a key role in brain tumor-related edema. Bevacizumab, a monoclonal antibody against VEGF-A, is an effective treatment for brain edema (17–20). The purpose of this study is to explore whether there is a difference in the efficacy of bevacizumab for refractory brain edema caused by brain metastasis from lung and colon cancers.

We divided 72 patients who met the inclusion criteria into a lung cancer group (n=43) and colon cancer group (n=29) according to their primary tumor site of origin. We demonstrated that bevacizumab is effective for the treatment of refractory cerebral edema. Furthermore, the efficacy of bevacizumab for the treatment of refractory cerebral edema caused by metastatic tumors with distinct anatomical origins is different.

Materials and methods

Patients

From January, 2014 to January, 2021, 287 patients were treated with bevacizumab in our hospital. The inclusion criteria were as follows: (1) peritumoral brain edema confirmed by magnetic resonance imaging (MRI) examination; (2) clinical symptoms were not improved after more than 5 days of mannitol or glucocorticoid treatment; and (3) patients underwent pathological testing. The exclusion criteria were as follows: (1) patients with a history of hypertension; (2) patients with a history of other tumors; (3) patients with incomplete clinical data; and (4) patients who refused to sign the informed consent. All patients signed a written informed consent form before receiving bevacizumab treatment. The academic and ethics committee of the First Affiliated Hospital of Jinan University approved this study.

Demographic characteristics

Table 1 summarizes the demographic characteristics of the enrolled patients. A total of 72 patients were divided into a lung cancer group (n=43) and colon cancer group (n=29) according to the source of the primary tumor. There were 39 male patients and 33 female patients in this study. The average age was 61.75 ± 12.60 (range, 29–87 years). Of the 72 patients, 64 were diagnosed with brain metastases for the first time and had not received any treatment. Eight patients experienced tumor recurrence after

TABLE 1 Demographic characteristics of two groups.

	Lung cancer	Colon cancer	P
Age (Y)	62.51 ± 12.31	60.62 ± 13.15	>0.05
Sex			>0.05
Male	23	16	
Female	20	13	
KPS	62.79 ± 9.84	60.00 ± 12.82	>0.05
Tumor size (mm)	8.95 ± 3.11	8.41 ± 3.26	>0.05
Edema volume	201,558.70 ± 59,327.27	201,931.79 ± 65,482.65	>0.05
Edema index	25.60 ± 7.47	26.52 ± 6.73	>0.05
Treatment time	1	1	>0.05
History of craniotomy	5	3	>0.05
Radiotherapy (mean ± SE)			>0.05
Stereotactic radiotherapy	8(13.56 ± 2.53 Gy)	5(14.72 ± 1.24 Gy)	
Whole-brain radiotherapy	5(16.31 ± 4.25 Gy)	4(17.76 ± 3.28 Gy)	
Intensity-modulated radiotherapy	1(20Gy)	2(20.50 ± 0.71 Gy)	

craniotomy. None of the patients had a history of radiation therapy prior to bevacizumab treatment. In total, 25 patients received radiotherapy during MRI examination.

Treatment

Previous studies have suggested that the therapeutic dose of bevacizumab was 5 or 10 mg/kg (21, 22). The relationship between the bevacizumab dose and adverse reactions is unclear (23, 24). The purpose of utilizing bevacizumab in this study was to control refractory brain edema, so the therapeutic dose we used was 5 mg/kg. All patients received a single dose of bevacizumab.

Imaging examination

MRI was performed 1 week before the treatment and 4 weeks after treatment (25, 26). The tumor volumes were measured using T1-weighted images, and edema volumes were calculated using FRFSE and T2-weighted images. The tumor and edema volumes were measured using a method previously described by Bitzer (27). It is assumed that the volume of the tumor and brain edema is an elliptical sphere. Therefore, $V = \pi/6 \times ABC$ calculates the volume. Figure 1 demonstrates the volume measurement technique. Volume is measured by drawing mutually perpendicular diameters (A and B) of the largest cross-section of cerebral edema in the axial plane and maximum height of sagittal cerebral edema (C). These measurements are substituted into the formula above to complete the volume calculation. The edema index (EI) was calculated as (volume of edema + tumor volume)/tumor volume (27). Edema volume reduction >10% was considered controlled, and volume increase or change ≤10% was considered uncontrolled (28). A total of 25 patients received radiotherapy during MRI examination. In total, 13 patients received stereotactic radiotherapy. Nine patients received whole-brain radiotherapy, and three patients received intensity-modulated radiotherapy.

Statistical analyses

Our data were analyzed using SPSS 26.0 statistical software. The Wilcoxon signed-rank test was used to compare the differences in the edema volume and EI before and after bevacizumab treatment. The edema control rate of each group was compared using the chi-square test. An arbitrary level of 5% was used to indicate statistical significance.

Results

Therapeutic effect

After treatment, the edema control rate was calculated by examining images. The results revealed that the refractory brain edema was controlled in 61 patients and the clinical symptoms were improved in 65 patients. Table 2 summarizes the changes in the edema volume and EI before and after treatment in each group. Figures 2, 3 describe the changes in edema volume and EI before and after treatment, respectively. The results showed that bevacizumab effectively treated refractory brain edema and reduced EI. Figure 4 shows the imaging changes in patients with lung cancer and colon cancer before and after treatment.

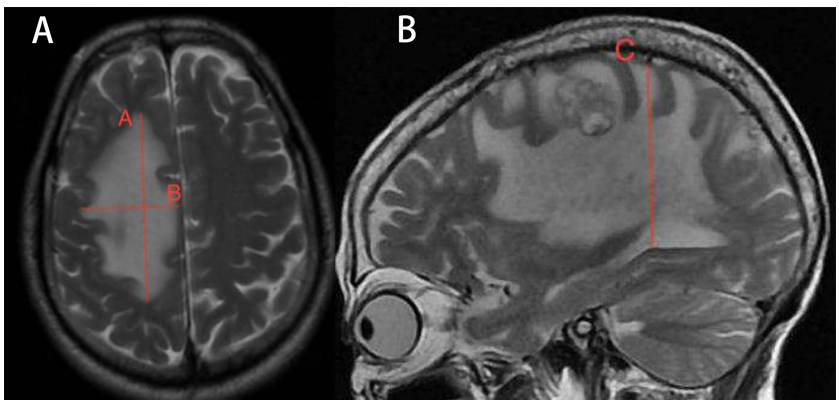

FIGURE 1
Demonstration of volume calculation technology. Volume calculation formula: $V = \pi/6 \times ABC$. Volume is measured by drawing the mutually perpendicular diameters **(A, B)** of the largest cross-section of cerebral edema in the axial plane and maximum height of sagittal cerebral edema **(C)**. These measurements are substituted into the formula above to complete the volume calculation.

TABLE 2 Changes in edema volume and edema index after treatment.

	Pretreatment (x ± s)	Posttreatment (x ± s)	P
All (n=72)			
Edema volume (mm^3)	201,708.97 ± 61,426.04	116,947.01 ± 43,879.16	<0.05
Edema index	25.97 ± 7.15	17.32 ± 5.24	<0.05
Lung cancer (n=43)			
Edema volume (mm^3)	201,558.70 ± 59,327.27	108,344.40 ± 35,299.96	<0.001
Edema index	25.60 ± 7.47	16.98 ± 5.21	<0.001
Colon cancer (n=29)			
Edema volume (mm^3)	201,931.79 ± 65,482.65	129,702.62 ± 52,258.17	<0.05
Edema index	26.52 ± 6.73	17.83 ± 5.34	<0.05
Radiotherapy (n=25)			
Edema volume (mm^3)	215,883.08 ± 56,569.51	123,312.40 ± 48,058.32	<0.001
Edema index	25.12 ± 6.73	16.88 ± 4.79	<0.05
Non-radiotherapy (n=47)			
Edema volume (mm^3)	194,169.55 ± 63,141.89	113,561.17 ± 41,629.79	<0.05
Edema index	26.43 ± 7.39	17.55 ± 5.50	<0.001

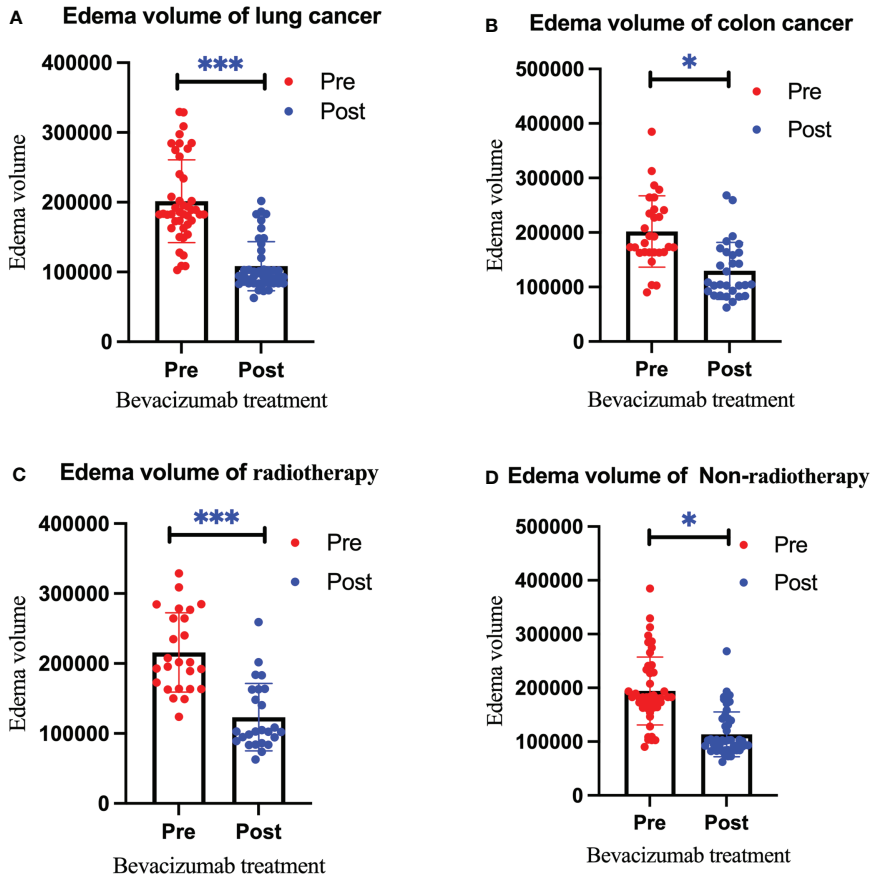

FIGURE 2
Changes in the edema volume before and after bevacizumab treatment in the lung cancer group **(A)**, colon cancer group **(B)**, radiotherapy group **(C)**, and non-radiotherapy group **(D)**. Red represents the edema volume before treatment, and blue represents the edema volume after treatment. We use * to indicate statistical difference. * for p<0.05, and *** for p<0.001.

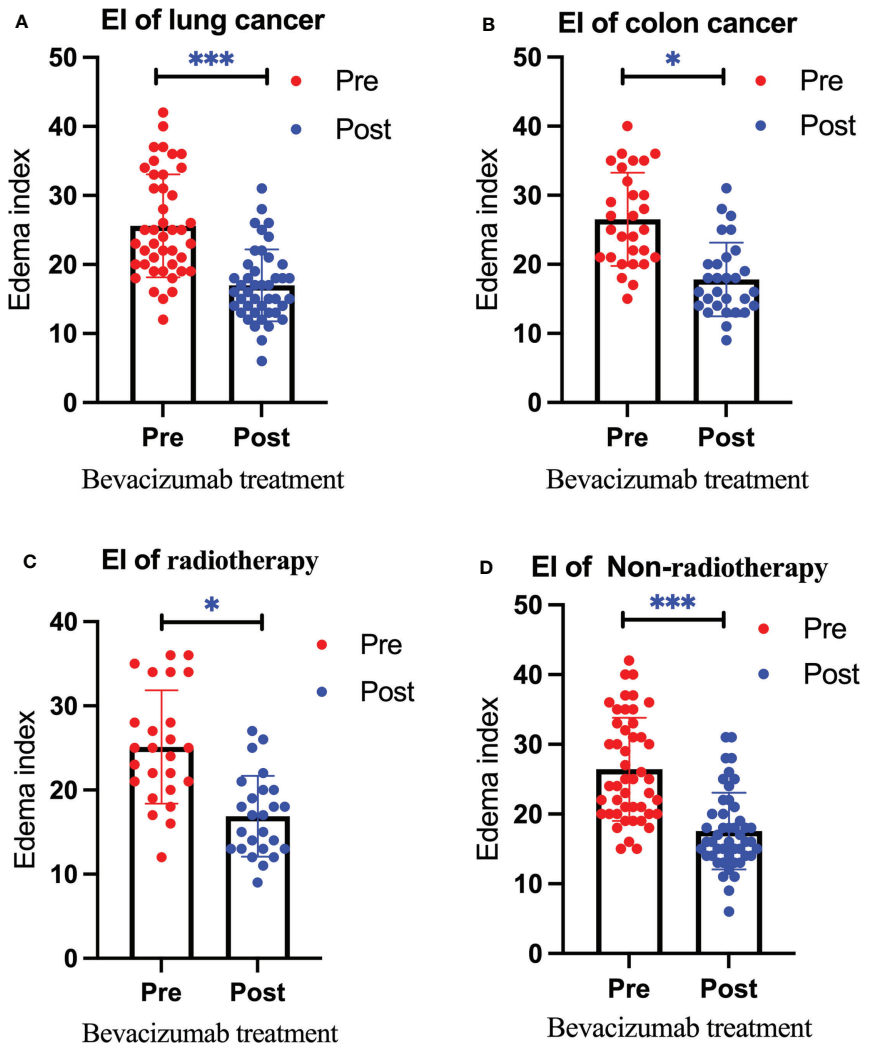

FIGURE 3
Changes in the edema index before and after bevacizumab treatment in the lung cancer group **(A)**, colon cancer group **(B)**, radiotherapy group **(C)**, and non-radiotherapy group **(D)**. Red represents the edema index before treatment, and blue represents the edema index after treatment. We use * to denote statistical differences. * for $p<0.05$, and *** for $p<0.001$.

Table 3 compares the edema control rate in each group after treatment.

Adverse reactions

Adverse reactions to bevacizumab included hypertension, several types of bleeding, venous thrombus exfoliation, and albuminuria (29, 30). The correlation between the drug dose and adverse reactions is unclear. Besse reported that the incidence of intracerebral hemorrhage in patients with brain metastases was 0.8%–3.3% after bevacizumab, while the incidence without bevacizumab was 1.0% (31). Khasraw reported that the incidence of intracerebral hemorrhage in patients with glioma or brain metastasis after bevacizumab treatment was 3.7%, while the incidence in those not administered bevacizumab was 3.6% (32). In addition, other complications after bevacizumab treatment have been reported, such as thrombocytopenia, intestinal perforation, and sepsis (33). In our study, nine patients experienced hypertension after treatment, two patients exhibited decreased platelet counts, and no cases of hemorrhage were observed.

Discussion

Surgery is often considered first-line treatment for patients with a large (usually defined as >3 cm in diameter) or

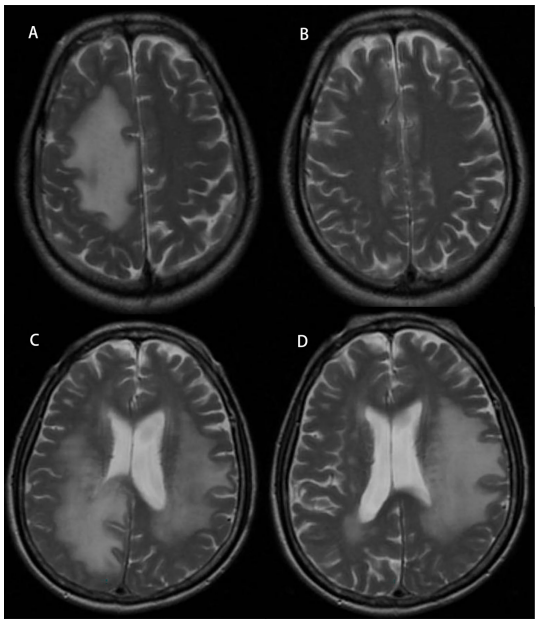

FIGURE 4
Radiographic images of brain edema before and after treatment with bevacizumab. Panel **(A)** represents edema in a lung cancer patient before treatment, and panel **(B)** represents after treatment. Panel **(C)** represents edema in a colon cancer patient before treatment, and panel **(D)** represents after treatment.

symptomatic brain metastasis; however, many patients are not optimal candidates for resection due to medical comorbidities, extensive extracranial burden of disease, or multiple intracranial metastases (34). None of the patients in this study were able to undergo craniotomy for various reasons. In these cases, radiation, either as whole-brain radiotherapy or stereotactic radiosurgery, is considered. There is a protracted response time following radiotherapy, with the earliest reaction observed within 2–3 months (35). Because the onset of radiation therapy was longer than our follow-up period, we believe that the effects of radiation therapy on cerebral edema in the patients during this study were small. Furthermore, although there is no definitive time limit, radiation-associated cerebral edema usually appears 3 or more months after radiation therapy (5).

Steroids are widely used to control clinical symptoms caused by perifocal edema (36). However, steroid treatment has side effects that impair the quality of life, including iatrogenic Cushing syndrome, which is frequently evident after only a few weeks of treatment (37). Steroid side effects such as mood changes, metabolic derailment, sleep disorders, and myopathy add to the symptoms of advanced cancer and can further impair the quality of life (9). Due to steroids' adverse complications, they often do not provide long-term efficacy. In addition, steroids combined with mannitol have poor efficacy in refractory cerebral edema, with a control rate of approximately 30% (38, 39). Bevacizumab has been reported to improve steroid-resistant cerebral edema. A previous study reported that bevacizumab treatment resolved edema in 82% of patients (5). In our study, the edema control rate was similar at 84.72%.

This study is the first to assess differences in the therapeutic efficacy of bevacizumab on refractory brain edema caused by brain metastasis from different tissues of origin: lung and colon. These findings may have important clinical significance for the treatment of these patients. Previous studies have shown that bevacizumab treats brain edema by blocking the binding of VEGF-A to its receptor (40–43). Zustovich reported on 18 patients with peritumoral cerebral edema treated with bevacizumab. The objective control rate was 100%, and the effective rate was 60% (44).

In this study, patients were reexamined by MRI 4 weeks after treatment. A total of 61 patients (84.72%) achieved edema control after a single bevacizumab treatment. We found that brain edema was controlled in 40 patients (93.02%) in the lung cancer group and 21 patients (72.41%) in the colon cancer group (P=0.023). This observation confirms that bevacizumab has differential efficacy in refractory cerebral edema caused by brain metastases from different organs. Refractory brain edema from colon cancer brain metastases may require higher doses of bevacizumab. In addition, 22 patients (88.00%) in the radiotherapy group achieved edema control compared to 39

TABLE 3 Edema control rate of each group after treatment.

	Controlled n/N (%)	Uncontrolled n/N (%)	P
All (n=72)	61/72 (84.72%)	11/72 (15.28%)	
Lung cancer (n=43)	40/43 (93.02%)	3/43 (6.98%)	
Colon cancer (n=29)	21/29 (72.41%)	8/29 (27.59%)	
			<0.05
Radiotherapy (n=25)	22/25 (88.00%)	3/25 (12.00%)	
Non-radiotherapy (n=47)	39/47 (82.98%)	8/47 (17.02%)	
			>0.05

(82.98%) in the non-radiotherapy group (P=0.573). We found no significant difference in the edema control rate between the radiotherapy and non-radiotherapy groups. This may suggest that bevacizumab can effectively alleviate radiation-induced brain edema.

Patients were followed up for 1 month. We only examined changes in refractory brain edema after a single bevacizumab treatment. In our study, the average edema volume before treatment was 201,708.97 ± 61,426.04 mm^3 which has decreased to 116,947.01 ± 43,879.16 mm^3 after treatment. These results showed that bevacizumab reduces the volume of refractory brain edema. Even if edema control is achieved after a single treatment, some patients retain a large volume of peritumoral edema. These patients continued bevacizumab treatment 4 weeks after the first treatment. Due to the short follow-up time, we could only observe the short-term effect of bevacizumab on refractory cerebral edema. Therefore, the long-term efficacy of bevacizumab after withdrawal is unclear. However, a previous study has reported that bevacizumab was effective in relapsed refractory cerebral edema (45). Furthermore, considering the short survival time of patients with brain metastases, we believe that the role of bevacizumab is worthy of recognition.

When bevacizumab was ≥0.3 mg/kg, free VEGF in the serum could not be detected (46). The currently recommended therapeutic dose of bevacizumab is 5–10 mg/kg (11–14). Although there is no evidence that adverse drug reactions are related to the dose, we still choose safer therapeutic doses. In our study, the treatment dose of bevacizumab was 5 mg/kg. Nine patients developed hypertension after a single bevacizumab treatment and returned to normal after nifedipine treatment. Platelet levels decreased in two patients and returned to normal without treatment. Some studies have shown that bevacizumab-induced hypertension significantly predicts progression-free survival and overall survival in patients with metastatic colorectal cancer, whereas its prediction for the objective response rate was non-significant (47, 48). Previous studies have reported that hypertension may be an indicator of positive antitumor effects, may predict the efficacy of antiangiogenic therapy, and could be associated with a favorable tumor prognosis (49). In our study, the edema volume was reduced by 98,237.81 ± 32,134.05 mm^3 in nine patients with new-onset hypertension, while the edema volume in the others was reduced by 83,351.25 ± 47,735.24 mm^3 ($P<0.05$). The edema control rate in the hypertension group was 88.89%, while the edema control rate in patients without new-onset hypertension was 84.13% ($P>0.05$). Compared to non-hypertensive patients, hypertensive patients exhibited a more significant reduction in the edema volume, but there were no significant differences in the edema control rate between the two groups. Hypertension may be used to predict the efficacy of bevacizumab in refractory cerebral edema, but more research is needed to demonstrate this.

Despite these findings, our study has some limitations. First, this was a single-center study. If we can conduct further multicenter research, the results will be more representative. Second, radiotherapy during follow-up may have an impact on the edema volume and edema index. Our study found for the first time that bevacizumab has a differential efficacy of refractory brain edema caused by brain metastases from primary lung and colon cancers. However, the reasons for the differences in efficacy need to be further studied. Finally, only 72 patients were included in this study. All patients received only a single dose of bevacizumab with a short follow-up period. Increasing the follow-up time and bevacizumab dose allows for a more precise assessment of bevacizumab efficacy.

Conclusion

This study suggests that bevacizumab may reduce refractory brain edema, and there is a significant difference in the efficacy of bevacizumab on refractory brain edema caused by the brain metastasis of lung cancer and colon cancer. A total of 11 patients experienced mild adverse reactions and quickly returned to normal. Therefore, bevacizumab is a safe and effective treatment option for refractory brain edema.

Data availability statement

The original contributions presented in the study are included in the article/supplementary material. Further inquiries can be directed to the corresponding author.

Ethics statement

The studies involving human participants were reviewed and approved by the Academic and Ethical Committee of the First Affiliated Hospital of Jinan University. The patients/participants provided their written informed consent to participate in this study.

Author contributions

XB and MZ participated in the design of this study and collected important background information. XB completed related literature retrieval, data acquisition and data analysis. XB drafted the manuscript, MZ completed the revision of the manuscript. All the authors read and approved the final manuscript. MZ are responsible for the final manuscript. The authors declare that there are no conflicts of interest. All authors contributed to the article and approved the submitted version.

Acknowledgments

The authors are grateful to all patients included in this study for their support.

Conflict of interest

The authors declare that the research was conducted in the absence of any commercial or financial relationships that could be construed as a potential conflict of interest.

Publisher's note

References

1. Villano JL, Durbin EB, Normandeau C, Thakkar JP, Moirangthem V, Davis FG. Incidence of brain metastasis at initial presentation of lung cancer. *Neuro Oncol* (2015) 17(1):122–8. doi: 10.1093/neuonc/nou099

2. Feng W, Zhang P, Zheng X, Chen M, Mao WM. Incidence and treatment of brain metastasis in patients with esophageal carcinoma. *World J Gastroenterol* (2015) 21(19):5805–12. doi: 10.3748/wjg.v21.i19.5805

3. Nag S, Manias JL, Stewart DJ. Pathology and new players in the pathogenesis of brain edema. *Acta Neuropathol* (2009) 118(2):197–217. doi: 10.1007/s00401-009-0541-0

4. Bosoi CR, Rose CF. Brain edema in acute liver failure and chronic liver disease: Similarities and differences. *Neurochem Int* (2013) 62(4):446–57. doi: 10.1016/j.neuint.2013.01.015

5. Tripathi M, Ahuja CK, Mukherjee KK, Kumar N, Dhandapani S, Dutta P, et al. The Safety and Efficacy of Bevacizumab for Radiosurgery - Induced Steroid - Resistant Brain Edema; Not the Last Part in the Ship of Theseus. *Neurol India* (2019) 67(5):1292–302. doi: 10.4103/0028-3886.271242

6. Ryken TC, McDermott M, Robinson PD, Ammirati M, Andrews DW, Asher AL, et al. The role of steroids in the management of brain metastases: A systematic review and evidence-based clinical practice guideline. *J Neurooncol* (2010) 96 (1):103–14. doi: 10.1007/s11060-009-0057-4

7. Marantidou A, Levy C, Duquesne A, Ursu R, Bailon O, Coman I, et al. Steroid requirements during radiotherapy for malignant gliomas. *J Neurooncol* (2010) 100 (1):89–94. doi: 10.1007/s11060-010-0142-8

8. Sturdza A, Millar BA, Bana N, Laperriere N, Pond G, Wong RK, et al. The use and toxicity of steroids in the management of patients with brain metastases. *Support Care Cancer* (2008) 16(9):1041–8. doi: 10.1007/s00520-007-0395-8

9. Roth P, Wick W, Weller M. Steroids in neurooncology: Actions, indications, side-effects. *Curr Opin Neurol* (2010) 23(6):597–602. doi: 10.1097/WCO.0b013e32833e5a5d

10. Taranova II, Kokhno VN. Brain edema treatment procedure using continuous controlled infusion of mannitol in neurosurgical patients. *Anesteziol Reanimatol* (2010) 4:29–34.

11. Walcott BP, Kahle KT, Simard JM. Novel treatment targets for cerebral edema. *Neurotherapeutics* (2012) 9(1):65–72. doi: 10.1007/s13311-011-0087-4

12. Vecht CJ, Hovestadt A, Verbiest HB, van Vliet JJ, van Putten WL. Dose-effect relationship of dexamethasone on karnofsky performance in metastatic brain tumors: A randomized study of doses of 4, 8, and 16 mg per day. *Neurology* (1994) 44(4):675–80. doi: 10.1212/WNL.44.4.675

13. Dietrich J, Rao K, Pastorino S, Kesari S. Corticosteroids in brain cancer patients: Benefits and pitfalls. *Expert Rev Clin Pharmacol* (2011) 4(2):233–42. doi: 10.1586/ecp.11.1

14. Palma L, Bruni G, Fiaschi AI, Mariottini A. Passage of mannitol into the brain around gliomas: A potential cause of rebound phenomenon. a study on 21 patients. *J Neurosurg Sci* (2006) 50(3):63–6.

15. Velho VL, Bhide AA, Ansari SAH. Effect of Mannitol Irrigation on Brain Edema in a Live Rat Model. *Asian J Neurosurg* (2018) 13(3):766–8. doi: 10.4103/ajns.AJNS_11_18

16. Tamura R, Tanaka T, Miyake K, Yoshida K, Sasaki H, et al. Bevacizumab for malignant gliomas: current indications, mechanisms of action and resistance, and markers of response. *Brain Tumor Pathol* (2017) 34(2):62–77. doi: 10.1007/s10014-017-0284-x

17. Kurkjian C, Kim ES. Risks and benefits with bevacizumab: Evidence and clinical implications. *Ther Adv Drug Saf* (2012) 3(2):59–69. doi: 10.1177/2042098611430109

18. Lu VM, Ravindran K, Graffeo CS, Perry A, Van Gompel JJ, Daniels DJ, et al. Efficacy and safety of bevacizumab for vestibular schwannoma in neurofibromatosis type 2: A systematic review and meta-analysis of treatment outcomes. *J Neurooncol* (2019) 144(2):239–48. doi: 10.1007/s11060-019-03234-8

19. Sadraei NH, Dahiya S, Chao ST, Murphy ES, Osei-Boateng K, Xie H, et al. Treatment of cerebral radiation necrosis with bevacizumab: the Cleveland clinic experience. *Am J Clin Oncol* (2015) 38(3):304–10. doi: 10.1097/COC.0b013e31829c3139

20. Pillay Smiley N, Alden T, Hartsell W, Fangusaro J. Severe radiation necrosis successfully treated with bevacizumab in an infant with low-grade glioma and tumor-associated intractable trigeminal neuralgia. *Pediatr Blood Cancer* (2016) 63 (9):1671–3. doi: 10.1002/pbc.26055

21. Alanin MC, Klausen C, Caye-Thomasen P, Thomsen C, Fugleholm K, Poulsgaard L, et al. Effect of bevacizumab on intracranial meningiomas in patients with neurofibromatosis type 2 - a retrospective case series. *Int J Neurosci* (2016) 126 (11):1002–6. doi: 10.3109/00207454.2015.1092443

22. Hawasli AH, Rubin JB, Tran DD, Adkins DR, Waheed S, Hullar TE, et al. Antiangiogenic agents for nonmalignant brain tumors. *J Neurol Surg B Skull Base* (2013) 74(3):136–41. doi: 10.1055/s-0033-1338262

23. Shih KC, Chowdhary S, Rosenblatt P, Weir AB3rd, Shepard GC, Williams JT, et al. A phase II trial of bevacizumab and everolimus as treatment for patients with refractory, progressive intracranial meningioma. *J Neurooncol* (2016) 129 (2):281–8. doi: 10.1007/s11060-016-2172-3

24. Nunes FP, Merker VL, Jennings D, Caruso PA, di Tomaso E, Muzikansky A, et al. Bevacizumab treatment for meningiomas in NF2: A retrospective analysis of 15 patients. *PloS One* (2013) 8(3):e59941. doi: 10.1371/journal.pone.0059941

25. Wang Y, Wang E, Pan L, Dai J, Zhang N, Wang X, et al. A new strategy of CyberKnife treatment system based radiosurgery followed by early use of adjuvant bevacizumab treatment for brain metastasis with extensive cerebral edema. *J Neurooncol* (2014) 119(2):369–76. doi: 10.1007/s11060-014-1488-0

26. Falk AT, Barrière J, François E, Follana P. Bevacizumab: A dose review. *Crit Rev Oncol Hematol* (2015) 94(3):311–22. doi: 10.1016/j.critrevonc.2015.01.012

27. Bitzer M, Opitz H, Popp J, Morgalla M, Gruber A, Heiss E, et al. Angiogenesis and brain oedema in intracranial meningiomas: influence of vascular endothelial growth factor. *Acta Neurochir (Wien)* (1998) 140(4):333–40. doi: 10.1007/s007010050106

28. Kreisl TN, Zhang W, Odia Y, Shih JH, Butman JA, Hammoud D, et al. A phase II trial of single-agent bevacizumab in patients with recurrent anaplastic glioma. *Neuro Oncol* (2011) 13(10):1143–50. doi: 10.1093/neuonc/nor091

29. Chen J, Lu Y, Zheng Y. Incidence and risk of hypertension with bevacizumab in non-small-cell lung cancer patients: A meta-analysis of randomized controlled trials. *Drug Des Devel Ther* (2015) 9:4751–60. doi: 10.2147/DDDT.S87258.

30. Matikas A, Kentepozidis N, Ardavanis A, Vaslamatzis M, Polyzos A, Emmanouilides Ch, et al. Efficacy and tolerance of frontline bevacizumab-based chemotherapy for advanced non-small cell lung cancer patients: A multicenter, phase IV study of the Hellenic oncology research group (HORG). *Cancer Chemother Pharmacol* (2016) 78(2):369–76. doi: 10.1007/s00280-016-3094-7

31. Besse B, Lasserre SF, Compton P, Huang J, Augustus S, Rohr UP, et al. Bevacizumab safety in patients with central nervous system metastases. *Clin Cancer Res* (2010) 16(1):269–78. doi: 10.1158/1078-0432.CCR-09-2439

32. Khasraw M, Holodny A, Goldlust SA, DeAngelis LM. Intracranial hemorrhage in patients with cancer treated with bevacizumab: The memorial Sloan-Kettering experience. *Ann Oncol* (2012) 23(2):458–63. doi: 10.1093/annonc/mdr148

33. Lou E, Sumrall AL, Turner S, Peters KB, Desjardins A, Vredenburgh JJ, et al. Bevacizumab therapy for adults with recurrent/progressive meningioma: A retrospective series. *J Neurooncol* (2012) 109(1):63–70. doi: 10.1007/s11060-012-0861-0

34. Gilbo P, Zhang I, Knisely J. Stereotactic radiosurgery of the brain: A review of common indications. *Chin Clin Oncol* (2017) 6:S14. doi: 10.21037/cco.2017.06.07

35. Ilyas A, Chen CJ, Ding D, Taylor DG, Moosa S, Lee CC, et al. Volume-staged versus dose-staged stereotactic radiosurgery outcomes for large brain arteriovenous malformations: A systematic review. *J Neurosurg* (2018) 128(1):154–64. doi: 10.3171/2016.9.JNS161571

36. Soffietti R, Abacioglu U, Baumert B, Combs SE, Kinhult S, Kros JM, et al. Diagnosis and treatment of brain metastases from solid tumors: Guidelines from the European association of neuro-oncology (EANO). *Neuro Oncol* (2017) 19 (2):162–74. doi: 10.1093/neuonc/now241

37. Roth P, Regli L, Tonder M, Weller M. Tumor-associated edema in brain cancer patients: Pathogenesis and management. *Expert Rev Anticancer Ther* (2013) 13(11):1319–25. doi: 10.1586/14737140.2013.852473

38. Barbero-Bordallo N, Gomez-Vicente L. Use of steroids in neuro-oncology. *Rev Neurol* (2019) 68(9):389–97. doi: 10.33588/rn.6809.2019083

39. Wang J, Ren Y, Zhou LJ, Kan LD, Fan H, Fang HM. Glycerol infusion versus mannitol for cerebral edema: A systematic review and meta-analysis. *Clin Ther* (2021) 43(3):637–49. doi: 10.1016/j.clinthera.2021.01.010

40. Furuse M, Kawabata S, Kuroiwa T, Miyatake S. Repeated treatments with bevacizumab for recurrent radiation necrosis in patients with malignant brain tumors: A report of 2 cases. *J Neurooncol* (2011) 102(3):471–5. doi: 10.1007/s11060-010-0333-3

41. Benoit A, Ducray F, Cartalat-Carel S, Psimaras D, Ricard D, Honnorat J. Favorable outcome with bevacizumab after poor outcome with steroids in a patient with temporal lobe and brainstem radiation necrosis. *J Neurol* (2011) 258(2):328–9. doi: 10.1007/s00415-010-5747-5

42. Williams BJ, Park DM, Sheehan JP. Bevacizumab used for the treatment of severe, refractory perilesional edema due to an arteriovenous malformation treated with stereotactic radiosurgery. *J Neurosurg* (2012) 116(5):972–7. doi: 10.3171/2012.1.JNS111627

43. Berghoff AS, Sax C, Klein M, Furtner J, Dieckmann K, Gatterbauer B, et al. Alleviation of brain edema and restoration of functional independence by bevacizumab in brain-metastatic breast cancer: A case report. *Breast Care (Basel)* (2014) 9(2):134–6. doi: 10.1159/000360930

44. Zustovich F, Ferro A, Lombardi G, Zagonel V, Fiduccia P, Farina P, et al. Bevacizumab as front-line treatment of brain metastases from solid tumors: A case series. *Anticancer Res* (2013) 33(9):4061–5.

45. Miyatake S, Furuse M, Kawabata S, Maruyama T, Kumabe T, Kuroiwa T, et al. Bevacizumab treatment of symptomatic pseudoprogression after boron neutron capture therapy for recurrent malignant gliomas. report of 2 cases. *Neuro Oncol* (2013) 15(6):650–5. doi: 10.1093/neuonc/not020

46. Gordon MS, Margolin K, Talpaz M, Sledge GW Jr, Holmgren E, Benjamin R, et al. Phase I safety and pharmacokinetic study of recombinant human anti-vascular endothelial growth factor in patients with advanced cancer. *J Clin Oncol* (2001) 19(3):843–50. doi: 10.1200/JCO.2001.19.3.843

47. Zhang CJ, Zhang SY, Zhang CD, Lin CR, Li XY, Li QY, et al. Usefulness of bevacizumab-induced hypertension in patients with metastatic colorectal cancer: An updated meta-analysis. *Aging (Albany NY)* (2018) 10(6):1424–41. doi: 10.18632/aging.101478

48. Lombardi P, Rossini D, Crespi V, Germani MM, Bergamo F, Pietrantonio F, et al. Bevacizumab-induced hypertension as a predictor of clinical outcome in metastatic colorectal cancer: An individual patient data-based pooled analysis of two randomized studies and a systematic review of the literature. *Cancer Treat Rev* (2022) 103:102326. doi: 10.1016/j.ctrv.2021.102326

49. Carvalho B, Lopes RG, Linhares P, Costa A, Caeiro C, Fernandes AC, et al. Hypertension and proteinuria as clinical biomarkers of response to bevacizumab in glioblastoma patients. *J Neurooncol* (2020) 147(1):109–16. doi: 10.1007/s11060-020-03404-z

frontiers | Frontiers in Oncology

TYPE Original Research
PUBLISHED 18 October 2022
DOI 10.3389/fonc.2022.1015011

OPEN ACCESS

EDITED BY
Chen Liu,
Army Medical University, China

REVIEWED BY
Wenxing Chen,
Nanjing University of Chinese Medicine, China
Gobinda Sarkar,
Mayo Clinic, United States

*CORRESPONDENCE
Xiu-Feng Xu
xfxu2004@sina.com
Ying-Ying Ding
dingyingying0428@163.com
Yu-Qi Cheng
yuqicheng@126.com

†These authors have contributed equally to this work

SPECIALTY SECTION
This article was submitted to Cancer Imaging and Image-directed Interventions, a section of the journal Frontiers in Oncology

RECEIVED 09 August 2022
ACCEPTED 27 September 2022
PUBLISHED 18 October 2022

CITATION
Zhang D-F, Ma H, Yang G-J, Zhang Z-P, He Y-F, Feng M-Y, Shan B-C, Xu X-F, Ding Y-Y and Cheng Y-Q (2022) Blood–brain barrier and brain structural changes in lung cancer patients with non-brain metastases. *Front. Oncol.* 12:1015011. doi: 10.3389/fonc.2022.1015011

Blood–brain barrier and brain structural changes in lung cancer patients with non-brain metastases

Da-Fu Zhang[1,2†], Huan Ma[2,3†], Guang-Jun Yang[2], Zhi-Ping Zhang[2], Yin-Fu He[2], Mao-Yang Feng[1], Bao-Ci Shan[4], Xiu-Feng Xu[1,5*], Ying-Ying Ding[2*] and Yu-Qi Cheng[1,5*]

[1]Department of Psychiatry, the First Affiliated Hospital of Kunming Medical University, Kunming, China, [2]Department of Radiology, the Third Affiliated Hospital of Kunming Medical University, Yunnan Cancer Hospital, Yunnan Cancer Center, Kunming, China, [3]Department of Psychiatry, the Second Affiliated Hospital of Kunming Medical University, Kunming, China, [4]Laboratory of Nuclear Analysis Techniques, Institute of High Energy Physics, Chinese Academy of Sciences, Beijing, China, [5]Yunnan Clinical Research Center for Mental Disorders, The First Affiliated Hospital of Kunming Medical University, Kunming, China

Purpose: To explore the relationship between blood-brain barrier (BBB) leakage and brain structure in non-brain metastasis lung cancer (LC) by magnetic resonance imaging (MRI) as well as to indicate the possibility of brain metastasis (BM) occurrence.

Patients and methods: MRI were performed in 75 LC patients and 29 counterpart healthy peoples (HCs). We used the Patlak pharmacokinetic model to calculate the average leakage in each brain region according to the automated anatomical labeling (AAL) atlas. The thickness of the cortex and the volumes of subcortical structures were calculated using the FreeSurfer base on Destrieux atlas. We compared the thickness of the cerebral cortex, the volumes of subcortical structures, and the leakage rates of BBB, and evaluated the relationships between these parameters.

Results: Compared with HCs, the leakage rates of seven brain regions were higher in patients with advanced LC (aLC). In contrast to patients with early LC (eLC), the cortical thickness of two regions was decreased in aLCs. The volumes of twelve regions were also reduced in aLCs. Brain regions with increased BBB penetration showed negative correlations with thinner cortices and reduced subcortical structure volumes ($P<0.05$, $R=-0.2$ to -0.50). BBB penetration was positively correlated with tumor size and with levels of the tumor marker CYFRA21-1 ($P<0.05$, $R=0.2–0.70$).

Conclusion: We found an increase in BBB permeability in non-BM aLCs that corresponded to a thinner cortical thickness and smaller subcortical structure volumes. With progression in LC staging, BBB shows higher permeability and may be more likely to develop into BM.

KEYWORDS

lung cancer, brain structure, blood-brain barrier, brain metastasis, dynamic contrast-enhanced MRI

1 Introduction

Brain metastasis (BM) are a serious public health problem on a global scale. It is estimated that approximately 20% of patients with cancer experience BM (1, 2), and that this is an important cause of cancer-associated mortality. Lung cancer (LC) is the most common cause of BM (3, 4). Approximately 25%-50% of LC patients have BM (5, 6). BMs may cause a range of focal neurological symptoms as well as cognitive impairment, thus greatly reducing patients' quality of life (7). The average survival time of untreated patients with BM is 2-3 months (8, 9). Even with existing treatments (e.g., surgery, radiotherapy, chemotherapy, targeted therapy, immunotherapy), the median survival time of patients with BM is only approximately 5 months (10).

The pathogenesis of BM are complicated, and BBB dysfunction is considered one of its mediating mechanisms. LC cells reach the vascular system of the brain through blood circulation, attach to microvascular endothelial cells, infiltrate the parenchyma, induce angiogenesis, proliferate in response to growth factors, and finally cross the BBB to form intracerebral metastases (11).

The BBB is composed of endothelial cells, a basement membrane, an astrocytic foot, and pericytes (12, 13). Its integrity is essential for blocking the entry of toxic substances into the peripheral circulation as well as blocking most tumor cells (14). However, metastatic cells can cross the multiple cell layers that comprise the BBB, including through the proteolysis of adhesion molecules (such as JAM-B, junctional adhesion molecule B) (15), leukocyte mimicry (15), and through the action of a variety of cytokines (e.g., cyclooxygenase2 (COX2, also known as PTGS2), heparin-binding EGF-like growth factor (HB-EGF), ST6GALNAC5, PLEKHA5, placental growth factor (PLGF)) (16, 17).

The process of transferring cells across the BBB leads to the destruction of the BBB as well as to an increase in permeability. Therefore, effective measurement of BBB permeability may potentially have application and clinical utility in terms of predicting BM. Although BBB leakage plays an important role in BM, it is difficult to measure human BBB permeability. The ratio of cerebrospinal fluid to serum albumin is a common and well- developed method for evaluating the permeability of the BBB. However, it is invasive and its reliability is controversial as it is easily affected by cerebrospinal fluid flow (18).

Progress in neuroimaging technology to date has suggested the utility of a direct, quantitative, and detailed method for evaluating BBB functionality (19). More specifically, DCE-MRI can quantify the spillover of contrast medium to the brain parenchyma and measure lower-level BBB leakage/permeability (20, 21). DCE-MRI has been successfully applied to study diseases related to BBB dysfunction, such as multiple sclerosis (22), stroke (23), traumatic brain injury (20), and dementia (24). Research on tumors is mainly focused on evaluating tumor grade and patient prognoses, distinguishing changes after treatment (e.g., progression, tumor recurrence), and evaluating treatment efficacy and curative effects (25, 26).

Although the results of research to date are encouraging, the aforementioned methodology has rarely been used in evaluating BMs. Instead, this methodology has mainly been deployed in evaluating therapeutic efficacy with respect to BMs. However, to the best of our knowledge, there have been few studies on BBB microleakage prior to BM or on micro-metastasis.

In the current study, we hypothesized that BBB permeability may increase prior to BM or micro-metastasis and that BBB permeability is related to the primary LC stage. Specifically, we hypothesized that a higher LC stage would be associated with more significant BBB damage and a greater likelihood that this damage would be to develop into BM. DCE-MRI volume transfer constant (K^{trans}) was used to detect changes in the BBB in order to predict the possibility of BM. Therefore, the purpose of this study was to quantify BBB permeability in LC patients without BM, and to explore the relationships between BBB permeability, brain structural changes, tumor staging, and tumor markers.

2 Materials and methods

2.1 Participants

This study was approved by the ethics committee of the third affiliated Hospital of Kunming Medical University (NO. SLKYLX202118). All participants provided their written informed consent prior to participating in this study. This work was conducted in accordance with the principles of the Declaration of Helsinki and its later amendments.

We conducted a cross-sectional study in LC patients. MRI was performed in untreated LC patients without a BM. We also enrolled age-and sex-matched HCs. Patients were enrolled into a group that had not received any treatment (e.g., surgery, radiotherapy, chemotherapy, immunotherapy) and had received a pathological diagnosis. Exclusion criteria were prophylactic craniocerebral irradiation, BM, stroke, craniocerebral trauma, epilepsy, Alzheimer's disease, Parkinson's disease, other acute mental or neurological diseases, a history of major medical diseases (e.g., anemia, severe heart disease, thyroid dysfunction, abnormal liver or kidney function), and severe vision or hearing loss. According to the TNM (tumor, node, metastasis) staging criteria (27), early-stage patients were categorized into stage I LC, and those in more advanced stages were categorized into stage II–IV LC(Supplementary material for detail). The study flowchart is shown in Figure 1.

2.2 Imaging

2.2.1 MRI acquisition

Images were acquired using a 3T MRI scanner (Discovery MR750, GE Healthcare, Waukesha, Wisconsin, USA) with a 21-channel MR Instruments head coil. Tight but comfortable foam pads was used to minimize head movement and earplugs and headphones were used to reduce scanner noise. Participants were instructed to lie down with their eyes closed, to stay awake, and not to think of anything special. For each participant, routine MRI sequences, including T2 and T1-weighted imaging and T2 fluid attenuated inversion recovery (FLAIR) imaging, was performed to ensure that there were no visible brain lesions or BMs.

The sequences for BBB assessment included the following steps: (1) a T1- weighted three-dimensional (3D) axial anatomical scan (BRAVO, TR=8.5ms, TE=3.2ms, field of view (FOV) 25.6×25.6, acquisition matrix 256×256, voxel size 1×1×1 mm, bandwidth 31.25kHz, FA 12°; (2) a T1- weighted 3D axial sequence with variable flip angles (3D-SPGR, TR 5.9ms, TE 2.0ms, flip angle 5° and 14°, FOV 24×20.4, acquisition matrix 256×180, slice thickness 4.0 mm, interval 0, bandwidth 62.5kHz); and (3) a T1- weighted 3D axial dynamic scan (LAVA, TR 5.9ms, TE 2.0ms, flip angle 14°, FOV 24×20.4, acquisition matrix 256×180, slice thickness 4.0 mm, interval 0, bandwidth 62.5 kHz) acquired within 650 s after intravenous injection of the magnetic contrast gadolinium (0.05 mmol/kg, flow rate 3.0 mL/s).

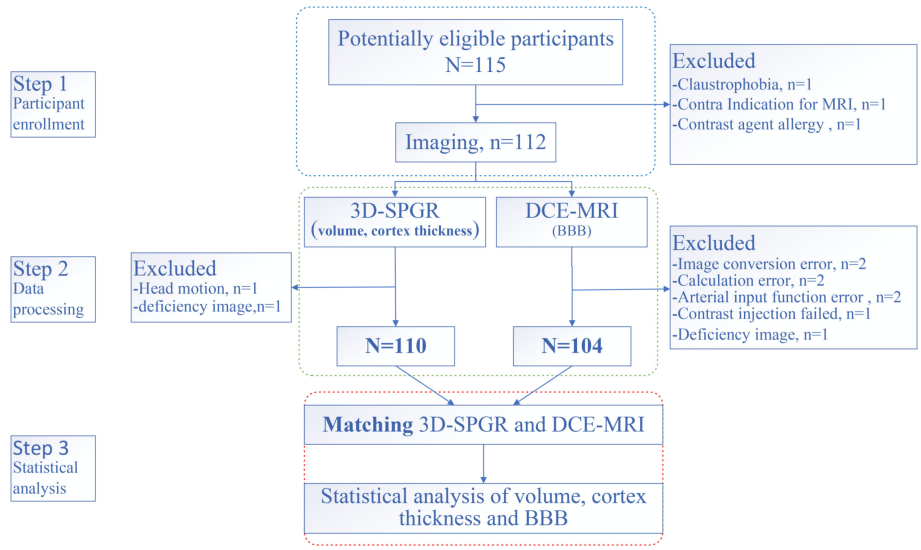

FIGURE 1
Study flowchart.

2.2.2 Analysis of the cerebral cortex and subcortical structures

High-resolution T1-weighted anatomical images were processed using the FreeSurfer 7.2 software package (https://surfer.nmr.mgh.harvard.edu/). Processing included: 1) motion correction and averaging of multiple volumetric T1-weighted images; 2) removal of non-brain tissue using a hybrid watershed/surface deformation procedure; 3) automated Talairach transformation; 4) segmentation of the subcortical white matter and deep gray matter volumetric structures (including the hippocampus, amygdala, caudate, putamen, ventricles); 5) intensity normalization; 6) tessellation of the gray matter white matter boundary with automated topology correction; and 7) surface deformation following intensity gradients to optimally place the gray/white and gray/cerebrospinal fluid borders at the location where the greatest shift in intensity defines the transition to the other tissue class. Cortical thickness and subcortical structure volume were calculated using the software template [i.e., the Destrieux atlas (28)]. We analyzed the cortical thicknesses of 74 structures as well as 16 subcortical volumes.

2.2.3 BBB data processing

The contrast medium leakage caused by BBB leakage leads to an increase in the T1-weighted signal in the affected tissue, thus enabling the contrast medium leakage to be calculated. To achieve this, we used SPM12 to register and normalize T1-weighted images acquired continuously after contrast injection to the MNI (Montreal Neurological Institute) coordinates (University College London, www.fil.ion.ucl.ac.uk/spm).

Previous studies have shown that the Patlak model is more accurate than other models in diseases presenting with slight BBB damage (29–31). Using DCE-MRI to measure the subtle leakage of the BBB has moderate to excellent repeatability (32). Therefore, in this study, the Patlak model was used to calculate K^{trans}. All dynamic images were registered to the same reference image, with an average flip angle of 14° to correct for head displacement. The Patlak method uses a two-compartment model, in which it is assumed that there is no reflux and infinite flow. Therefore, the leakage rate is similar to the product of vascular permeability (P) and the surface area (S) per unit tissue mass.

For the Patlak graphic method, the two main factors affecting the accurate measurement of BBB permeability are the estimation of the blood concentration curve based on T1 signal intensity and the determination of the VIF (variance inflation factor) (33) (Figure 2). A common method of T1 mapping is to change the flip angle (34). VIF measurements also play a key role in estimating kinetic parameters. VIF was calculated by selecting the region of interest (ROI) of the superior sagittal sinus (35). The sagittal sinus has a sufficiently large cross-section such that the VIF can be easily extracted from the superior sagittal sinus and is not affected by partial volume and inflow artifacts (35). Thereafter, K^{trans} (min^{-1}) was calculated using MATLAB software (MathWorks, Natick, MA, USA), implementing the Patlak model. The K^{trans} value was used to reflect BBB leakage.

K^{trans} is calculated as a voxel. The whole brain was divided into 116 brain regions based on the AAL atlas (36). Each brain region was considered as a ROI with respect to extracting the average K^{trans} value for statistical analysis.

3 Statistical analysis

SPSS (version 19.0; SPSS Inc., Chicago, IL, USA) and R statistical software (version 4.1.2, The R Project for Statistical Computing, Vienna, Austria; https://www.r-project.org/) were used for statistical analyses. Continuous variables with normal distributions are described as mean ± standard deviation. We evaluated classification variable usage (%) or the constituent ratio (%). If the data were normally distributed and the variance was uniform, an analysis of variance (ANOVA) test was implemented and LSD Test was used for *post hoc* multiple comparisons. Otherwise, the Kruskal-Wallis (KW) test was performed. Differences were considered statistically significant at a two-sided P-value of <0.05. The results were visualized using R statistical software or GraphPad Prism visualization software (San Diego, CA, USA). Multiple comparisons were performed with Bonferroni correction.

4 Results

4.1 Demographic and clinical characteristics

A total of 75 LC patients (39 eLCs and 36 aLCs) and 29 HCs (selected through online advertising) were enrolled from August 2021 to March 2022 at the Department of Thoracic Surgery of the Third Affiliated Hospital of Kunming Medical University (Kunming, China). Participants were age and sex matched. Eleven subjects were excluded due to excessive head movement, allergies to the contrast medium, or miscalculation during scanning. The number of participants assessed for eligibility and the reasons for exclusion is shown in Figure 1.

A summary of detailed demographic data, histological diagnoses, and tumor staging is shown in Table 1. There were no statistically significant differences in sex, age, smoking, or KPS (Karnofsky Performance Scale) scores between the LC patients and the control group (P>0.05). The tumor diameter in the eLC group was smaller than that in the aLC group (P<0.001). The levels of the tumor markers CEA (carcino embryonic antigen), NSE (neuron-specific enolase), CYFRA21-1 (cytokeratin 19 fragment), and SCC (squamous cell carcinoma

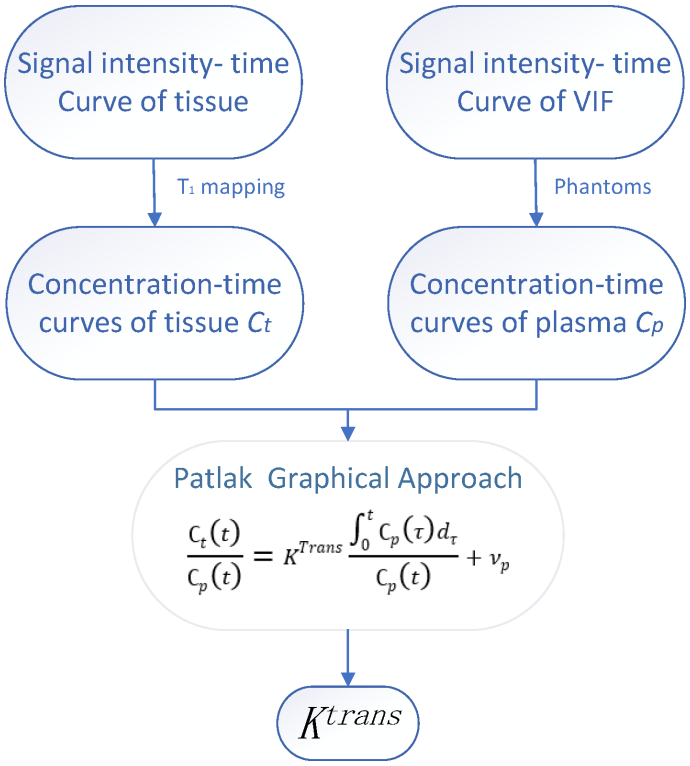

FIGURE 2
The time-signal intensity curve of tissue and vascular input function (VIF) was converted into time-concentration curve. The leakage rate (K^{trans}) and plasma volume (Vp) were calculated by Patlak graphic method.

antigen) were higher in the aLC group than those in the eLC group (P<0.05).

4.2 BBB leakage in patients with LC

Compared with the control group, the K^{trans} levels of seven brain regions and the whole cerebral gray matter in aLC group were higher than those in HC group (P<0.05) (i.e., the *left calcarine fissure and surrounding cortex (CAL.L), right superior occipital gyrus (SOG.R), right middle occipital gyrus (MOG.R), left inferior occipital gyrus (IOG.L), right inferior occipital gyrus (IOG.R), left Cerebelum Crus1, right Cerebelum 6*). The permeability of *left Temporal pole: superior temporal gyrus (TPOsup.L), right temporal pole: middle temporal gyrus (TPOmid.R), and TPOmid.L* was increased in eLC group (P<0.05). The permeability of *CAL.L, IOG.R, left Cerebellum Crus1, left Cerebellum Crus2 and right Cerebellum 6* was increased with the LC staging progression. There were no statistically significant differences in BBB permeability in the other brain regions (Figures 3A, S1–S16).

4.3 Changes in cerebral cortex thickness and volume

A comparison of 74 cortical thicknesses between eLCs, aLCs and HCs showed that cortical thickness in nine brain regions in aLC group was smaller than that of eLC group (i.e., *left Transverse frontopolar gyri and sulci, left Long insular gyrus and central sulcus of the insula, left Posterior ramus of the lateral sulcus, left. Anterior segment of the circular sulcus of the insula, left. Middle occipital sulcus and lunatus sulcus, left. Medial occipito-temporal sulcus and lingual sulcus, right Superior occipital gyrus, right Central sulcus and right Medial occipito-temporal sulcus and lingual sulcus*)(P<0.05). The cortical thickness of the *left aMCC* and *the left sulcus intermedius primus (Jensen)* in aLC group was statistically significantly lower than in HC group. The cortical thickness of *the left long insular gyrus and the central sulcus of the insula* increased in eLC group (P<0.05). The locations are shown in Figures 4A–H). There were no statistical differences with respect to the other cortical thicknesses. However, we found an increasing trend in cortical thickness, as well as a decreasing trend in the LC group (Figure 3B, Supplementary Material Tables S17–S19).

TABLE 1 Demographic and clinical features of patients with lung cancer.

	Controls (n = 29)	Early lung cancer (n = 39)	Advanced lung cancer (n = 36)	χ2/F/μ	pvalue
gender					
male/female	15/14	15/24	24/12	5.986	0.05[a]
Age(mean ± SD), year	51.07 ± 9.67	55.59 ± 8.23	56.06 ± 8.99	3.059	0.051[b]
Smoking(%)	10/29	9/30	16/20	3.84	0.147[a]
Tumor diameter (cm) (mean ± SD)		1.62 ± 0.94	4.93 ± 2.35	-8.103	0.000*c
KPS score(mean ± SD)	95.00 ± 7.77	96.15 ± 7.11	94.44 ± 6.95	0.568	0.568[b]
Clinical stage					NA[d]
I		39	0		
II		0	4		
III		0	20		
IV		0	12		
Pathological type				χ2	
Squamous cell carcinoma		7	13	7.396	0.092[a]
Adenocarcinoma		29	18		
Small Cell Lung Cancer		3	5		
Tumor markers (25%,50%,75%)				μ	
CEA		1.53, 2.25, 3.57	1.87,4.38, 10.33	446.50	0.007*e
NSE		9.60, 11.80, 13.40	11.75, 13.70,21.96	397.50	0.001*e
CYFRA21-1		1,40, 2.00,2.60	2.625,4.500,7.025	223.00	0.000*e
SCC		0.70,0.80,1.00	0.72,1.10,1.47	493.00	0.026*e

Data are expressed as Mean ± SD, n (%) or InterQuartile Range(P_{25},P_{50},P_{75}). [a]The P values are obtained by using χ2 test. [b]The P values are obtained by using one-way ANOVA. [c]The P values are obtained by using two sample t-test. [d]There is no statistical analysis. [e]The P values are obtained by Kruskal-Wallis test. *P<0.05 is considered significant. CEA, carcinoembryonic antigen; NSE, neuron-specific enolase; CYFRA21-1, cytokeratins21-1; SCC, squamous cell carcinoma antigen.

Compared with HCs, the volume of 12 brain regions in aLC group decreased (i.e., *bilateral thalamus, putamen, pallidum, ventral diencephalon, left hippocampus, amygdala and right cerebellum white matter, nucleus accumbens)*, whereas the volume of the *left temporal horn of lateral ventricle* increased (P<0.05). The specific locations are shown in Figures 4I–K. In eLC group, the volume decreased preferentially in the *bilateral Ventral Diencephalon* (P<0.05), but there were no statistically significant differences with respect to other volume changes. The volumes of *the bilateral thalamus, right pallidum, and right choroid plexus* in aLC group were smaller than those in eLC group (Figure 3C; Supplementary Material Tables S20–S22; Figures S1–S4).

4.4 The correlations between the tumor diameter, serum marker, cortical thickness, volume and BBB leakage

To examine whether the maximum diameter of the tumor, serum marker levels (CEA, NSE, CYFRA21-1, SCC), cortical thickness, and volume were related to BBB leakage, we analyzed the correlations between them. We found that the maximum diameter of the tumor was positively correlated with K^{trans} (*CAL.L, IOG.L, IOG.R, TPOmid.L, left Cerebellum Crus2*). CEA was positively correlated with K^{trans} of the cerebral gray matter, and CYFRA21-1 was positively correlated with *CAL.L, TPOmid.L, left cerebellum crus1, right cerebellum 6, and* K^{trans} *Gray* (P<0.05, R=0.25–0.51) (Figure 5A and Supplementary Material Table S23). Increased K^{trans} brain area was negatively correlated with the average cortical thickness of *the left aMCC, the left long insular gyrus, the central sulcus of the insula, the posterior ramus of the lateral sulcus, the left sulcus intermedius primus, the left medial occipitotemporal sulcus, the lingual sulcus, the right superior occipital gyrus, and the volumes of the left thalamus, the left pallidum, the left hippocampus, the left ventral diencephalon, the right cerebellum (white matter), the right thalamus, the right accumbens, and the right ventral diencephalon.* Increased K^{trans} brain area was also positively correlated with *the left temporal horn of lateral ventricle volume* (P<0.05, |R|=0.2-0.50) (Figure 5B and Supplementary Material Table S24).

5 Discussion

To the best of our knowledge, this is the first study to perform a quantitative analysis of BBB leakage in LCs without a BM. It was found that BBB leakage increased in patients with aLC and this was related to brain structure. Patients with aLC showed a higher level of BBB leakage in some brain regions. The BBB permeability was associated with a decrease in cerebral cortex thickness and volume. These findings present a key step in establishing the role of BBB dysfunction in the pathogenesis of BM in LC and highlight that the

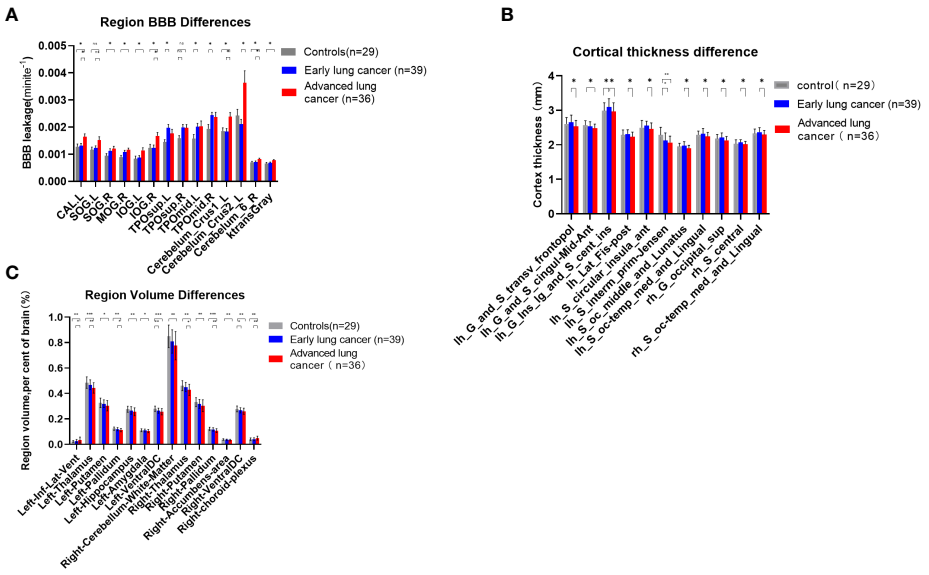

FIGURE 3
(A) Comparisons of BBB leakage between patients with LC at different stages and HCs. Quantify the leakage rate of BBB in different brain regions, and there were significant differences in 8 brain regions between patients with aLC and HCs ($p < 0.05$), which revealed the existence of BBB leakage in patients with aLC. There was no statistical difference between SOG.R and TPOsup.R after correction. **(B)** Comparisons of cerebral cortex thickness between patients with LC at different stages and HC. There was significant difference between patients with aLC and patients with eLC ($p < 0.05$). The thickness of 9 cerebral cortices decreased in patients with aLC. There was no statistical difference between the cerebral cortex of patients with LC and HC, but the cortex of patients with eLC showed an increasing trend and a decreasing trend in aLC. **(C)** Comparisons of subcortical structure volume between patients with LC at different stages and HC. There was significant difference between HC of patients with aLC ($p < 0.05$). In patients with aLC, the volume of 13 subcortical structures decreased, while the volume of 1 structure increased. The volume of bilateral VentralDC showed volume reduction in patients with eLC. The volume of 6 subcortical structures in patients with aLC was smaller than that in patients with eLC, while the volume of one structure increased in patients with aLC. *P<0.05, **P<0.01, ***P<0.001; ns, no statistical difference.

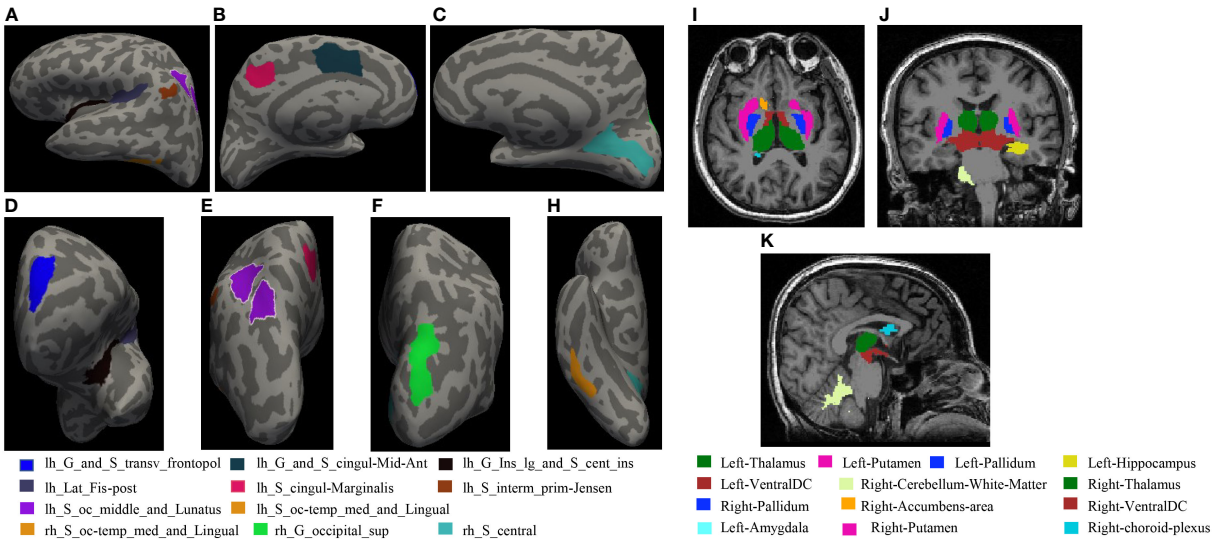

FIGURE 4
(A–H) shows statistical differences in the locations of cortical thickness: **(A)** Left hemisphere left side view; **(B)** Left hemisphere right side view; **(C)** Right hemisphere left side view; **(D)** Left hemisphere front view; **(E)** Left hemisphere rear view; **(F)** Right hemisphere rear view; H Right hemisphere bottom view. **(I–K)** The locations of subcortical structures with statistical differences: **(I)**: coronal, **(J)**: axial, **(K)**: sagittal.

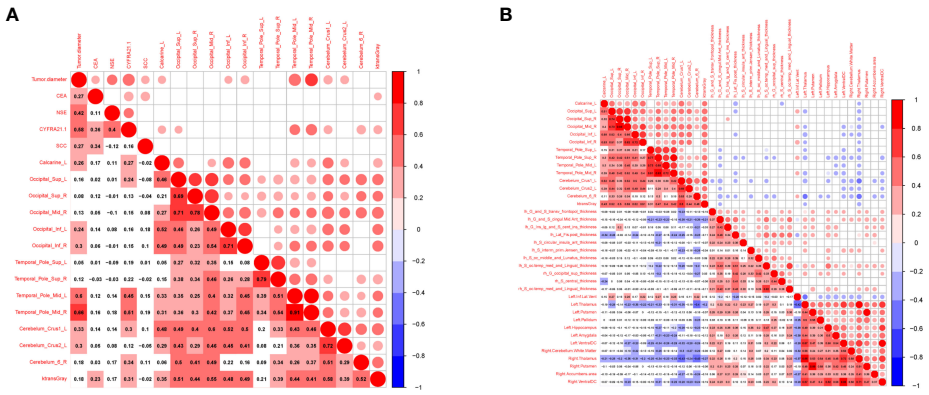

FIGURE 5
Correlation between tumor markers, differential cerebral cortical thickness, subcortical volume and BBB leakage in patients with LC. Red represents positive correlation, blue represents negative correlation, the darker the color, the higher the correlation. **(A)** Showed the correlation between tumor markers, tumor diameter and BBB leakage in LCs (n=75). **(B)** Showed the correlation between cerebral cortical thickness, subcortical volume and BBB leakage in LCs and HCs (n=104).

BBB may be a potential diagnostic and therapeutic target. BM can cause severe, uncontrollable symptoms and reduce quality of life, including by inducing paralysis, elevated intracranial pressure, and/or seizures. The incidence of BM has shown an upward trend in the past decade, but there has been little progress in treatment, and therapeutic effects have not been of sufficient quality (37). Therefore, it is particularly important to identify LC patients who are more prone to BM. Intensive treatment should be performed in these patients.

The occurrence of BM involves a series of interrelated steps, starting with the invasion of local cancer cells that progresses into the intravascular and/or circulatory and/or lymphatic system. Owing to the lack of a lymphatic system within the central nervous system, the only way for cancer cells to reach the brain is through blood circulation. The resulting circulating tumor cells (CTCs) may enter the microcirculation of the brain and adapt to the microenvironment of the brain tissue, thus resulting in the formation of micro-metastases that eventually form visible tumors through metastatic colonization (38, 39). However, metastatic cells that invade the parenchyma of the central nervous system must pass through the BBB. Cerebral vascular endothelial cells change in this process (40). These changes include damage to the tight junction structure and an increased perivascular space (41). In addition, windows corresponding to the surrounding vascular system can be found in these vessels, and the number and activity of pinocytic vacuoles have been shown to be increased (42). Therefore, these blood vessels may reflect the blood vessels of the tumor tissue rather than those of the endothelial cells of the central nervous system. Owing to these structural changes, the leakage of the BBB was found to increase in this study, and plasma was found to infiltrate into the extracellular space (43).

DCE-MRI can be used to evaluate the leakage of extracellular space in each voxel using pharmacokinetics parameters (K^{trans}) as well as to detect BBB leakage (i.e., reflecting BBB destruction). K^{trans} is defined as the volume transfer constant between the plasma and the extracellular space and is often used as a synonym for permeability. This parameter has been confirmed to be increased in patients with BMs (44), multiple sclerosis (22), stroke (23), traumatic brain injury (20), and dementia (24). Although DCE-MRI has been widely used in Neuro-oncology imaging, it is uncommon to measure relatively complete BBB leakage. Therefore, the level of leakage of BBB that we need to measure in order to establish prognoses may be small. Thus, the Patlak model was used to calculate K^{trans} in the current study, as this model is more accurate in measuring low level leakage (29, 31).

Our results confirm that BBB leakage is increased in patients with LC, especially in aLC. It is suggested that, with the progression of LC, the integrity of the BBB may be destroyed in a wider range of brain regions and that permeability may increase. These changes indicate changes in cerebral vascular endothelial cells in these brain regions (26), damage to tight junction structures, and an increase in the perivascular space (27). This in turn indicates that the potential occurrence of microtransfer or a transition from the BBB to the blood-tumor barrier (BTB), because the BTB is generally considered to be more prone to leaking than the BBB (45). Therefore, BM may develop if there is no further clinical intervention. Early detection of increased BBB permeability as well as strengthening clinical interventions is of great significance in preventing the occurrence of BM.

We observed an interesting phenomenon in the current study. Compared with HCs, the cortical thickness of patients with eLC showed an increasing trend, although this difference was not statistically significant. Compared with patients with eLC, the cortical thickness of patients with aLC showed a downward trend,

with statistically significant differences in the frontal transverse pole, the cingulate gyrus, the insular, the temporal pole, and the occipital pole cortices. At present, these findings have not been reported in the literature. Hence, our findings may represent a new discovery. However, these findings require more research support, including confirmed in studies with a larger sample size.

Our study further found that patients with aLC showed a larger tumor size, higher staging, and a higher incidence of BM compared with those with eLC (46, 47). With an increase in tumor diameter, BBB permeability was found to increase in the left peri-talar cortex, the bilateral suboccipital gyrus, the middle temporal pole, and the inferior cerebellum, probably because it is easier for tumor cells to invade the vascular or lymphatic system given a larger tumor volume (with CTCs entering the cerebral microcirculation). This may affect BBB integrity in the above-mentioned brain regions. CEA, CYFRA21-1, NSE, and SCC are biomarkers related to the LC and are suitable for LC screening and recurrence monitoring. In this study, the tumor markers CEA, NSE, CYFRA21-1, and SCC were high in advanced LC. BBB permeability of the cerebral gray matter increased with an increase in CEA and CYFRA21-1 levels. The BBB permeability of the left talar fissure, the left superior occipital gyrus, the bilateral middle temporal gyrus, and the superior cerebellum also increased with an increase in CYFRA21-1, indicating that the observed increase in serum tumor markers was correlated with BBB destruction. Therefore, the relationship between elevated tumor marker levels and BBB integrity may reflect tumor heterogeneity and may be a risk factor for BM (48, 49).

In contrast, in patients with aLC, cortical thickness and subcortical volume were smaller with increased BBB permeability. This may be because the development of LC is a long process, and that tumor tissue directly or indirectly affects the BBB by secreting cytokines or forming CTCs, which leads to changes in local microcirculation structure and hemodynamics, ultimately leading to a reduction in cortical structure and subcortical volume, an increase in space within this area, easier adhesion and retention of CTCs, and increased local invasion and micro-metastasis. The continuous expansion of tumor lesions causes local and distal changes, which directly damage the activity of neurons and vascular function (50), thus further aggravating leakage of the BBB and reducing the volume of the corresponding brain structure. However, the specific mechanisms underlying these changes are not clear. Therefore, BBB imaging may have the potential to identify biomarkers for BM risk in LC patients. Clinical adjuvant therapy should be strengthened for saboteurs of the BBB, including better chemotherapy for CTCs and prophylactic whole-brain radiotherapy for brain micro-metastasis, in order to achieve accurate individual treatment.

The advantages of this study include a lack of clear recruitment bias and a short time interval between clinical evaluation and neuroimaging regimens (usually after clinical evaluation). Moreover, MRI examination was completed within one week. However, the enrolled sample size of our cohort was small and our imaging scheme required a gadolinium-based contrast agent, which may potentially damage renal function and limit the wide applicability of this methodology.

6 Conclusion

In conclusion, this study provides convincing evidence of BBB leakage and its relationship with brain structure in patients with LC at different stages in patients without a BM. The accurate measurement of BBB leakage has the potential to be established as an effective biomarker for predicting BM.

Data availability statement

The original contributions presented in the study are included in the article/Supplementary Material. Further inquiries can be directed to the corresponding authors.

Ethics statement

The studies involving human participants were reviewed and approved by the ethics committee of the third affiliated Hospital of Kunming Medical University. The patients/participants provided their written informed consent to participate in this study.

Author contributions

D-FZ: Data curation, Methodology, Software, Writing- Original draft preparation. Y-QC: Conceptualization, Writing- Reviewing and Editing. G-JY: Visualization, Investigation. Y-YD: Supervision. HM, X-FX: Writing- Reviewing and Editing. B-CS, M-YF: Software. Z-PZ, Y-FH: Data curation. All authors contributed to the article and approved the submitted version.

Funding

This work was supported by National Natural Science Foundation of China (82060259, 81760296, 82001986); Yunnan Province High-Level Health Technical Talents (leading talents) (L-2019004, L-2019011); Yunnan Province Special Project for Famous Medical Talents of the "Ten Thousand Talents Program" (YNWRMY- 2018-040, YNWR-MY-2018-041); Yunnan digitalization, development and application of biotic resource (202002AA100007); The Outstanding Youth Science Foundation of Yunnan Basic Research Project (202101AW070001). Innovation Team of Kunming Medical University (CXTD202110). The Applied Basic Research Projects of Yunnan Province (2019FE001-083).

Acknowledgments

This study is a joint effort of many investigators and staff members, and their contribution is gratefully acknowledged. We especially thank all patients who participated in this study. We thank Elsevier Webshop - Author Services for editorial and language assistance.

Conflict of interest

The authors declare that the research was conducted in the absence of any commercial or financial relationships that could be construed as a potential conflict of interest.

Publisher's note

Supplementary material

The Supplementary Material for this article can be found online at: https://www.frontiersin.org/articles/10.3389/fonc.2022.1015011/full#supplementary-material

References

1. Achrol AS, Rennert RC, Anders C, Soffietti R, Ahluwalia MS, Nayak L, et al. Brain metastases. *Nat Rev Dis Primers* (2019) 5(1):5. doi: 10.1038/s41572-018-0055-y

2. Lauko A, Mu Z, Gutmann DH, Naik UP, Lathia JD. Junctional adhesion molecules in cancer: A paradigm for the diverse functions of cell-cell interactions in tumor progression. *Cancer Res* (2020) 80(22):4878–85. doi: 10.1158/0008-5472.Can-20-1829

3. Bertolini F, Spallanzani A, Fontana A, Depenni R, Luppi G. Brain metastases: an overview. *CNS Oncol* (2015) 4(1):37–46. doi: 10.2217/cns.14.51

4. Ostrom QT, Wright CH, Barnholtz-Sloan JS. Brain metastases: epidemiology. *Handb Clin Neurol* (2018) 149:27–42. doi: 10.1016/b978-0-12-811161-1.00002-5

5. Gavrilovic IT, Posner JB. Brain metastases: epidemiology and pathophysiology. *J Neurooncol* (2005) 75(1):5–14. doi: 10.1007/s11060-004-8093-6

6. Page S, Milner-Watts C, Perna M, Janzic U, Vidal N, Kaudeer N, et al. Systemic treatment of brain metastases in non-small cell lung cancer. *Eur J Cancer* (2020) 132:187–98. doi: 10.1016/j.ejca.2020.03.006

7. Noh T, Walbert T. Brain metastasis: clinical manifestations, symptom management, and palliative care. *Handb Clin Neurol* (2018) 149:75–88. doi: 10.1016/b978-0-12-811161-1.00006-2

8. Lah TT, Novak M, Breznik B. Brain malignancies: Glioblastoma and brain metastases. *Semin Cancer Biol* (2020) 60:262–73. doi: 10.1016/j.semcancer.2019.10.010

9. Schuler M, Wu YL, Hirsh V, O'Byrne K, Yamamoto N, Mok T, et al. First-line afatinib versus chemotherapy in patients with non-small cell lung cancer and common epidermal growth factor receptor gene mutations and brain metastases. *J Thorac Oncol* (2016) 11(3):380–90. doi: 10.1016/j.jtho.2015.11.014

10. Cagney DN, Martin AM, Catalano PJ, Redig AJ, Lin NU, Lee EQ, et al. Incidence and prognosis of patients with brain metastases at diagnosis of systemic malignancy: a population-based study. *Neuro Oncol* (2017) 19(11):1511–21. doi: 10.1093/neuonc/nox077

11. Denkins Y, Reiland J, Roy M, Sinnappah-Kang ND, Galjour J, Murry BP, et al. Brain metastases in melanoma: roles of neurotrophins. *Neuro Oncol* (2004) 6 (2):154–65. doi: 10.1215/s115285170300067x

12. Gupta S, Dhanda S, Sandhir R. Anatomy and physiology of blood-brain barrier. In: *Brain targeted drug delivery system*. Elsevier (2019). p. 7–31. doi: 10.1016/B978-0-12-814001-7.00002-0

13. Serlin Y, Shelef I, Knyazer B, Friedman A. Anatomy and physiology of the blood-brain barrier. *Semin Cell Dev Biol* (2015) 38:2–6. doi: 10.1016/j.semcdb.2015.01.002

14. Alexander JJ. Blood-brain barrier (BBB) and the complement landscape. *Mol Immunol* (2018) 102:26–31. doi: 10.1016/j.molimm.2018.06.267

15. Sevenich L, Bowman RL, Mason SD, Quail DF, Rapaport F, Elie BT, et al. Analysis of tumour- and stroma-supplied proteolytic networks reveals a brain-metastasis-promoting role for cathepsin s. *Nat Cell Biol* (2014) 16(9):876–88. doi: 10.1038/ncb3011

16. Li B, Wang C, Zhang Y, Zhao XY, Huang B, Wu PF, et al. Elevated PLGF contributes to small-cell lung cancer brain metastasis. *Oncogene* (2013) 32 (24):2952–62. doi: 10.1038/onc.2012.313

17. Jilaveanu LB, Parisi F, Barr ML, Zito CR, Cruz-Munoz W, Kerbel RS, et al. PLEKHA5 as a biomarker and potential mediator of melanoma brain metastasis. *Clin Cancer Res* (2015) 21(9):2138–47. doi: 10.1158/1078-0432.Ccr-14-0861

18. Reiber H. Flow rate of cerebrospinal fluid (CSF)–a concept common to normal blood-CSF barrier function and to dysfunction in neurological diseases. *J Neurol Sci* (1994) 122(2):189–203. doi: 10.1016/0022-510x(94)90298-4

19. Mackay M, Tang CC, Vo A. Advanced neuroimaging in neuropsychiatric systemic lupus erythematosus. *Curr Opin Neurol* (2020) 33(3):353–61. doi: 10.1097/wco.0000000000000822

20. Veksler R, Vazana U, Serlin Y, Prager O, Ofer J, Shemen N, et al. Slow blood-to-brain transport underlies enduring barrier dysfunction in American football players. *Brain* (2020) 143(6):1826–42. doi: 10.1093/brain/awaa140

21. Weissberg I, Veksler R, Kamintsky L, Saar-Ashkenazy R, Milikovsky DZ, Shelef I, et al. Imaging blood-brain barrier dysfunction in football players. *JAMA Neurol* (2014) 71(11):1453–5. doi: 10.1001/jamaneurol.2014.2682

22. Cramer SP, Simonsen H, Frederiksen JL, Rostrup E, Larsson HB. Abnormal blood-brain barrier permeability in normal appearing white matter in multiple sclerosis investigated by MRI. *NeuroImage Clin* (2014) 4:182–9. doi: 10.1016/j.nicl.2013.12.001

23. Merali Z, Huang K, Mikulis D, Silver F, Kassner A. Evolution of blood-brain-barrier permeability after acute ischemic stroke. *PloS One* (2017) 12(2): e0171558. doi: 10.1371/journal.pone.0171558

24. Sweeney MD, Sagare AP, Zlokovic BV. Blood-brain barrier breakdown in Alzheimer disease and other neurodegenerative disorders. *Nat Rev Neurol* (2018) 14(3):133–50. doi: 10.1038/nrneurol.2017.188

25. Li KL, Djoukhadar I, Zhu X, Zhao S, Lloyd S, McCabe M, et al. Vascular biomarkers derived from dynamic contrast-enhanced MRI predict response of vestibular schwannoma to antiangiogenic therapy in type 2 neurofibromatosis. *Neuro Oncol* (2016) 18(2):275–82. doi: 10.1093/neuonc/nov168

26. Ellingson BM, Bendszus M, Sorensen AG, Pope WB. Emerging techniques and technologies in brain tumor imaging. *Neuro Oncol* (2014) 16 Suppl 7(Suppl 7): vii12–23. doi: 10.1093/neuonc/nou221

27. Detterbeck FC, Boffa DJ, Kim AW, Tanoue LT. The eighth edition lung cancer stage classification. *Chest* (2017) 151(1):193–203. doi: 10.1016/j.chest.2016.10.010

28. Destrieux C, Fischl B, Dale A, Halgren E. Automatic parcellation of human cortical gyri and sulci using standard anatomical nomenclature. *Neuroimage* (2010) 53(1):1–15. doi: 10.1016/j.neuroimage.2010.06.010

29. Heye AK, Thrippleton MJ, Armitage PA, Valdés Hernández MDC, Makin SD, Glatz A, et al. Tracer kinetic modelling for DCE-MRI quantification of subtle blood-brain barrier permeability. *Neuroimage* (2016) 125:446–55. doi: 10.1016/j.neuroimage.2015.10.018

30. Patlak CS, Blasberg RG, Fenstermacher JD. Graphical evaluation of blood-to-brain transfer constants from multiple-time uptake data. *J Cereb Blood Flow Metab* (1983) 3(1):1–7. doi: 10.1038/jcbfm.1983.1

31. Barnes SR, Ng TS, Montagne A, Law M, Zlokovic BV, Jacobs RE. Optimal acquisition and modeling parameters for accurate assessment of low ktrans blood-brain barrier permeability using dynamic contrast-enhanced MRI. *Magn Reson Med* (2016) 75(5):1967–77. doi: 10.1002/mrm.25793

32. Wong SM, Jansen JFA, Zhang CE, Staals J, Hofman PAM, van Oostenbrugge RJ, et al. Measuring subtle leakage of the blood-brain barrier in cerebrovascular disease with DCE-MRI: Test-retest reproducibility and its influencing factors. *J Magn Reson Imaging* (2017) 46(1):159–1665. doi: 10.1002/jmri.25540

33. Larsson HB, Courivaud F, Rostrup E, Hansen AE. Measurement of brain perfusion, blood volume, and blood-brain barrier permeability, using dynamic contrast-enhanced T(1)-weighted MRI at 3 tesla. *Magn Reson Med* (2009) 62 (5):1270–81. doi: 10.1002/mrm.22136

34. Brookes JA, Redpath TW, Gilbert FJ, Murray AD, Staff RT. Accuracy of T1 measurement in dynamic contrast-enhanced breast MRI using two- and three-dimensional variable flip angle fast low-angle shot. *J Magn Reson Imaging* (1999) 9 (2):163–71. doi: 10.1002/(sici)1522-2586(199902)9:2<163::aid-jmri3>3.0.co;2-l

35. Lavini C, Verhoeff JJ. Reproducibility of the gadolinium concentration measurements and of the fitting parameters of the vascular input function in the superior sagittal sinus in a patient population. *Magn Reson Imaging* (2010) 28 (10):1420–30. doi: 10.1016/j.mri.2010.06.017

36. Tzourio-Mazoyer N, Landeau B, Papathanassiou D, Crivello F, Etard O, Delcroix N, et al. Automated anatomical labeling of activations in SPM using a macroscopic anatomical parcellation of the MNI MRI single-subject brain. *Neuroimage* (2002) 15(1):273–89. doi: 10.1006/nimg.2001.0978

37. Soffietti R, Abacioglu U, Baumert B, Combs SE, Kinhult S, Kros JM, et al. Diagnosis and treatment of brain metastases from solid tumors: guidelines from the European association of neuro-oncology (EANO). *Neuro Oncol* (2017) 19(2):162–74. doi: 10.1093/neuonc/now241

38. Paduch R. "The role of lymphangiogenesis and angiogenesis in tumor metastasis. *Cell Oncol (Dordr)* (2016) 39(5):397–410. doi: 10.1007/s13402-016-0281-9

39. Hanahan D, Weinberg RA. Hallmarks of cancer: the next generation. *Cell* (2011) 144(5):646–74. doi: 10.1016/j.cell.2011.02.013

40. Bart J, Groen HJ, Hendrikse NH, van der Graaf WT, Vaalburg W, de Vries EG. The blood-brain barrier and oncology: new insights into function and modulation. *Cancer Treat Rev* (2000) 26(6):449–62. doi: 10.1053/ctrv.2000.0194

41. Liebner S, Fischmann A, Rascher G, Duffner F, Grote EH, Kalbacher H, et al. Claudin-1 and claudin-5 expression and tight junction morphology are altered in blood vessels of human glioblastoma multiforme. *Acta Neuropathol* (2000) 100 (3):323–31. doi: 10.1007/s004010000180

42. Shibata S. Ultrastructure of capillary walls in human brain tumors. *Acta Neuropathol* (1989) 78(6):561–71. doi: 10.1007/bf00691283

43. Nduom EK, Yang C, Merrill MJ, Zhuang Z, Lonser RR. Characterization of the blood-brain barrier of metastatic and primary malignant neoplasms. *J Neurosurg* (2013) 119(2):427–33. doi: 10.3171/2013.3.Jns122226

44. Lüdemann L, Grieger W, Wurm R, Wust P, Zimmer C. Quantitative measurement of leakage volume and permeability in gliomas, meningiomas and brain metastases with dynamic contrast-enhanced MRI. *Magn Reson Imaging* (2005) 23(8):833–41. doi: 10.1016/j.mri.2005.06.007

45. Arvanitis CD, Ferraro GB, Jain RK. The blood-brain barrier and blood-tumour barrier in brain tumours and metastases. *Nat Rev Cancer* (2020) 20(1):26–41. doi: 10.1038/s41568-019-0205-x

46. Gong L, Wang QI, Zhao L, Yuan Z, Li R, Wang P. Factors affecting the risk of brain metastasis in small cell lung cancer with surgery: is prophylactic cranial irradiation necessary for stage I-III disease? *Int J Radiat Oncol Biol Phys* (2013) 85 (1):196–200. doi: 10.1016/j.ijrobp.2012.03.038

47. Chen Y, Li J, Zhang Y, Hu Y, Zhang G, Yan X, et al. Early versus late prophylactic cranial irradiation in patients with extensive small cell lung cancer. *Strahlenther Onkol* (2018) 194(10):876–85. doi: 10.1007/s00066-018-1307-1

48. Yang Q, Zhang P, Wu R, Lu K, Zhou H. Identifying the best marker combination in CEA, CA125, CY211, NSE, and SCC for lung cancer screening by combining ROC curve and logistic regression analyses: Is it feasible? *Dis Markers* (2018) 2018:2082840. doi: 10.1155/2018/2082840

49. Zhang L, Liu D, Li L, Pu D, Zhou P, Jing Y, et al. The important role of circulating CYFRA21-1 in metastasis diagnosis and prognostic value compared with carcinoembryonic antigen and neuron-specific enolase in lung cancer patients. *BMC Cancer* (2017) 17(1):96. doi: 10.1186/s12885-017-3070-6

50. Seano G, Nia HT, Emblem KE, Datta M, Ren J, Krishnan S, et al. Solid stress in brain tumours causes neuronal loss and neurological dysfunction and can be reversed by lithium. *Nat BioMed Eng* (2019) 3(3):230–45. doi: 10.1038/s41551-018-0334-7

frontiers | Frontiers in Oncology

TYPE Original Research
PUBLISHED 02 November 2022
DOI 10.3389/fonc.2022.943064

OPEN ACCESS

EDITED BY
Robert Clarke,
University of Minnesota Twin Cities, United States

REVIEWED BY
Jacqueline Noll,
University of Adelaide, Australia
Hao Zhang,
Xiangya Hospital Central South University, China

*CORRESPONDENCE
Claudio Festuccia
claudio.festuccia@univaq.it

†These authors have contributed equally to this work

SPECIALTY SECTION
This article was submitted to Pharmacology of Anti-Cancer Drugs, a section of the journal Frontiers in Oncology

RECEIVED 13 May 2022
ACCEPTED 13 October 2022
PUBLISHED 02 November 2022

CITATION
Mancini A, Colapietro A, Cristiano L, Rossetti A, Mattei V, Gravina GL, Perez-Montoyo H, Yeste-Velasco M, Alfon J, Domenech C and Festuccia C (2022) Anticancer effects of ABTL0812, a clinical stage drug inducer of autophagy-mediated cancer cell death, in glioblastoma models. *Front. Oncol.* 12:943064. doi: 10.3389/fonc.2022.943064

Anticancer effects of ABTL0812, a clinical stage drug inducer of autophagy-mediated cancer cell death, in glioblastoma models

Andrea Mancini[1†], Alessandro Colapietro[1†], Loredana Cristiano[2], Alessandra Rossetti[1], Vincenzo Mattei[3], Giovanni Luca Gravina[1,4], Héctor Perez-Montoyo[5], Marc Yeste-Velasco[5], Jose Alfon[5], Carles Domenech[5] and Claudio Festuccia[1*]

[1]Laboratory of Radiobiology, Department of Biotechnological and Applied Clinical Sciences, University of L'Aquila, L'Aquila, Italy, [2]Department of Clinical Medicine, Public Health, Life Sciences, University of L'Aquila, L'Aquila, Italy, [3]Biomedicine and Advanced Technologies Rieti Center, "Sabina Universitas", Rieti, Italy, [4]Division of Radiation Oncology, Department of Biotechnological and Applied Clinical Sciences, University of L'Aquila, L'Aquila, Italy, [5]R&D Department, Ability Pharmaceuticals, Parc Tecnològic del Vallès, Cerdanyola del Vallès, Barcelona, Spain

Background: Glioblastoma multiforme (GBM) is the most malignant adult brain tumor. Current standard of care treatments have very limited efficacy, being the patients´ overall survival 14 months and the 2-year survival rate less than 10%. Therefore, the treatment of GBM is an urgent unmet clinical need.

Methods: The aim of this study was to investigate *in vitro* and *in vivo* the potential of ABTL0812, an oral anticancer compound currently in phase II clinical stage, as a novel therapy for GBM.

Results: We showed that ABTL0812 inhibits cell proliferation in a wide panel of GBM cell lines and patient-derived glioblastoma stem cells (GSCs) with half maximal inhibitory concentrations (IC50s) ranging from 15.2 μM to 46.9 μM. Additionally, ABTL0812 decreased GSCs neurosphere formation. GBM cells aggressiveness is associated with a trans-differentiation process towards a less differentiated phenotype known as proneural to mesenchymal transition (PMT). ABTL0812 was shown to revert PMT and induce cell differentiation to a less malignant phenotype in GBM cell lines and GSCs, and consequently reduced cell invasion. As previously shown in other cancer types, we demonstrated that the molecular mechanism of action of ABTL0812 in glioblastoma involves the inhibition of Akt/mTORC1 axis by overexpression of TRIB3, and the activation of endoplasmic reticulum (ER) stress/unfolded protein response (UPR). Both actions converge to induce autophagy-mediated cell death. ABTL0812 anticancer efficacy was studied *in vivo* using subcutaneous and orthotopic intra-brain xenograft tumor models. We demonstrated that ABTL0812 impairs tumor growth and increases disease-free survival and overall survival of mice. Furthermore, the histological analysis of tumors indicated that ABTL0812 decreases angiogenesis. Finally, we investigated the combination of

ABTL0812 with the standard of care treatments for GBM radiotherapy and temozolomide in an orthotopic model, detecting that ABTL0812 potentiates the efficacy of both treatments and that the strongest effect is obtained with the triple combination of ABTL0812+radiotherapy+temozolomide.

Conclusions: Overall, the present study demonstrated the anticancer efficacy of ABTL0812 as single agent and in combination with the GBM standard of care treatments in models of glioblastoma and supports the clinical investigation of ABTL0812 as a potential novel therapy for this aggressive brain tumor type.

KEYWORDS

ABTL0812, glioblastoma, TRIB3, Akt, mTOR, ER stress, UPR, autophagy

Introduction

Glioblastoma multiforme (GBM) is a very aggressive cancer with a high frequency of resistance to chemotherapy and radiotherapy, which results in low patient survival (1, 2). Current standard of care treatments, radiotherapy, and chemotherapy (2, 3), have not improved the prognosis of GBM, which has a median overall survival of approximately 14 months and a 2-year survival rate of less than 10% (1–3). Recently, genotyping and expression profiling analyses have demonstrated that GBMs may be categorized into four subclasses dependent on their neural differentiation (4–6): proneural (PN), neural (N), classical (CL), and mesenchymal (MES). In particular, the MES subtype is associated with poorest prognosis among all subtypes (6). MES tumors show an inflammatory microenvironment, increased angiogenesis, and resistance to therapies. Moreover, it has been demonstrated that MES trans-differentiation from other subtypes occurs during GBM progression due to the microenvironment or therapeutic stimuli (7, 8). This phenomenon is similar to the epithelial-mesenchymal transition (EMT), a reversible biological process that occurs in epithelial cells. In glioblastoma, a specialized form of EMT is the "Proneural-Mesenchymal Transition" or PMT (6–8). The mesenchymal subtype of glioblastoma typically expresses neural stem cell markers and is associated with an aggressive phenotype (9, 10). Glioblastoma cells that express stem cell markers are highly invasive and resistant to chemotherapy and radiotherapy (11, 12).

ABTL0812 is a first-in-class orally administered small molecule with anti-cancer activity currently at phase 2 clinical stage. ABTL0812 kills cancer cells through the induction of cytotoxic autophagy by a dual mechanism of action: i) inhibition of Akt/mTORC1 axis by overexpressing TRIB3 (13), and ii) induction of endoplasmic reticular (ER) stress and, consequently, of the Unfolded Protein Response (UPR) (14). Both actions converge to induce a robust and persistent autophagy that results in cancer cell death, while non-tumoral cells are spared. ABTL0812 anticancer activity as a single agent by oral route has been demonstrated in preclinical animal models, including pancreatic cancer (13, 14), endometrial cancer (15), non-small cell lung carcinoma (NSCLC) (13, 14, 16), neuroblastoma (17) and breast cancer (18). Moreover, in these models ABTL0812 potentiates chemotherapy activity without increasing its toxicity (15, 16, 18). At clinical level, to date ABTL0812 has successfully completed a first-in-human phase 1 clinical trial showing a high safety profile and signs of efficacy in patients with advanced solid tumors (NCT02201823) (19). Subsequently, ABTL0812 was investigated in a phase I/IIa clinical trial where it was administered as a first-line therapy in combination with paclitaxel and carboplatin in patients with endometrial and squamous non-small cell lung cancers (NSCLC), showing improved efficacy without increasing toxicities compared to chemotherapy alone (NCT03366480) (20, 21). Currently, ABTL0812 is being studied in a phase 2b trial as a first-line therapy in combination with FOLFIRINOX in patients with metastatic pancreatic cancer (NCT04431258).

Autophagy is an evolutionarily conserved cellular process leading to the degradation of disposable or potentially harmful intracellular components in the autolysosome to preserve cell homeostasis and to adapt to stress (22, 23). Autophagy can be induced by multiple forms of cellular stress, such as nutrient deprivation, oxidative stress, hypoxia, or endoplasmic reticulum (ER) stress (22, 23) and is regulated by a multi-layered control system. A main regulator of the autophagic responses is the mechanistic target of rapamycin complex 1 (mTORC1), which maintains autophagy inhibited (24). In cancer, autophagy plays tumor-inhibiting and tumor-promoting functions depending on the tumorigenesis stage, tissue, and genetic context (25). Among the anti-tumor actions of autophagy is activation of cancer cell death; it

has been described that over-stimulation of autophagy in tumors leads to excessive cellular damage and triggers autophagic cell death. Therefore, the induction of cytotoxic autophagy is a novel and promising therapeutic strategy to treat cancers (25, 26).

Hyperactivation of the PI3K/Akt/mTOR (PAM) pathway is commonly observed in human cancers including colorectal cancers (27), head and neck cancer (28), non-small cell lung cancer (29), endometrial cancer (30) as well as glioblastoma (31), and results in induction of cell growth, survival, adhesion, and migration. PAM activation is also involved in chemoresistance in several cancers including GBM. Activation of PIK3 cascade has been shown to be associated with reduced patient survival (31) in GBM. Thus, the inhibition of this pathway is being used as an anticancer therapy and several inhibitors of this pathways are under clinical development.

Here, we have investigated the anticancer effects and underlying molecular effects of ABTL0812 as single therapy and in combination with standard of care treatments in glioblastoma *in vitro* and *in vivo* models. We have shown that ABTL0812 decreases cell proliferation, induces cell differentiation to a less malignant and less invasive phenotype, and activates autophagy-mediated cell death in glioblastoma cells and patient-derived stem cells. As previously found in other cancer types, the molecular mechanism of action of ABTL0812 in glioblastoma involves the inhibition of Akt/mTORC1 axis by overexpression of TRIB3, and the activation of ER stress and UPR. Overall, our findings support the clinical investigation of ABTL0812 for the treatment of glioblastoma, even for the most aggressive and less differentiated types that are more resistant to current standard of care therapies.

Materials and methods

Reagents, antibodies, and drugs preparation

Plasticware and materials for tissue culture were purchased from Euroclone (EuroClone S.p.A, Milan, Italy). Antibodies for β-actin [sc-130065], GFAP (2E1) [sc-33673], nestin [sc-23927], β-catenin [sc-7199], LC3 [sc-271625], beclin1 [sc-48341], p62 [sc-28359] caspase-9 [sc-56076] recognizing the proenzyme and caspase 9 [sc-56076] recognizing cleaved form were purchased from Santa Cruz (Santa Cruz, CA, USA). LAMP1, Caspase-8 (1C12) Mouse mAb #9746, and caspase 9 were purchased from Cell signaling (EuroClone, Milan, Italy). Antibodies against eIF2a, ATFF4 and CHOP were purchased from St John's Laboratory Ltd (London, UK). Ki67 was purchased from Dako (Carpenteria, CA). We used the ApopTag® peroxidase *in situ* apoptosis detection Kit purchased from Merck Millipore (Merck, Milan, Italy). Anti-Caspase-3 antibody [EPR18297] recognizing pro-form and cleaved form of caspase 3 was purchased from Abcam (Cambridge, MA). Vessel count was detected by using anti-mouse CD34 from eBioscience, Inc. (Prodotti Gianni SpA, Milan Italy). ABTL0812 was provided by Ability Pharmaceuticals (Barcelona, Spain). For *in vitro* cell viability assays, ABTL0812 was dissolved in Dimethyl sulfoxide (DMSO) and used at final concentrations of <0.2% DMSO. Everolimus was purchased from Sigma-Aldrich (St. Louis, MO) (for *in vitro* study). For *in vivo* study, pharmacological preparation of the drug was purchased from Novartis Oncology.

Cell lines

Ten human high-grade glioma cell lines (U251MG, U373, U118, U138, A172, U87MG, SW1783, LN229, T98G, and D54) were cultured at 37°C in 5% CO2 and were maintained in Dulbecco's modified eagle medium (DMEM) containing 10% (v/v) fetal bovine serum, 4 mM glutamine, 100 IU/ml penicillin and 100 µg/ml streptomycin (Thermo Fisher/Life Technologies, Inc., Carlsbad, CA, USA). Primary human brain microvascular endothelial cells (HBMVEs) were kindly provided from Dr. Emma Harper, Endothelium Biology Group (XB11), School of Biotechnology. Dublin City University. To minimize the risk of working with misidentified and/or contaminated cell lines, we stocked the cells used in this report at very low passages and used <20 subcultures. Periodically, a DNA profiling by GenePrint® 10 System (Promega Corporation, Madison, WI) was carried out to authenticate cell cultures. Luciferase transfected U87MG cells were kindly provided by Jari E. Heikkila, department of Biochemistry and Pharmacy, Abo Akademi University, Turku, Finland. Three GBM patient-derived stem cells (GSCs) BT12M, BT48EF and BT50EF were kindly provided by J. Gregory Cairncross, and Samuel Weiss (Hotchkiss Brain Institute, Faculty of Medicine, University of Calgary, Calgary, Alberta, Canada) (32), and GSCs-5 from Marta Izquierdo (Departamento de Biología Molecular, Universidad Autónoma de Madrid, Spain) (33). All GSCs were maintained as neurosphere cultures in Neurocult medium (Mixture DMEM: F12 1:1) supplemented with epidermal growth factor (20 ng/ml) and fibroblast growth factor (10 ng/ml). NHA (normal human astrocytes) cell line was obtained from LONZA (Rockville, MD)].

Cell viability assay

The cytotoxicity of ABTL0812 was measured by the Cell Counting Kit-8 (CCK-8; Dojindo Molecular Technologies Inc., Tokyo, Japan) following manufacturer indications. The optical density (OD) values were averaged and normalized against the controls to generate dose-response curves to calculate the IC50 values using Grafit software.

Sphere counts

As previously indicated (34, 35) and in order to evaluate effects on stem cell proliferation, we used two different modalities

of study: (i) a direct count and sizing of neurospheres at 1 week of culture from pre-formed spheres, and (ii) the evaluation of the clonal capacity of GSCs cultured as single cells after 14–30 days. For the analysis of sphere growth, pre-formed neurospheres were treated with different doses of ABTL0812 for 72 h. After treatment, spheres were photographed and counted at contrast phase microscopy. Spheres were recorded as either large colonies (>50 cells) or small colonies (<50 cells). Single cells were also manually counted per microscopic field at 100× magnification. For the clonogenic assay, GSCs were seeded in 96-well plates as a single cell suspension at a density of 2 cells/mL (equivalent of 1 cell every 3 wells). Cells were maintained for 14–30 days in their culturing media and then the wells were visually scanned using light microscopy to identify and count the clones (spheres) produced.

Immunofluorescence studies

GSCs-5, BT48EF, BT12M and BT50EF GSC cells were used for immunofluorescence analyses as previously described (36, 37). Spheres were seeded at a density of 10 000 cells/cm^2 on glass coverslips pretreated with Poly-L lysine 30μg/ml to allow the spheres to adhere. Then, slides were washed with PBS and fixed with 4% paraformaldehyde for 20 min at room temperature (RT). To stain cytoplasmatic markers, slides were permeabilized with 0.3% Triton-X-100, for 5 minutes, at RT. Next, spheres were incubated overnight at 4°C with the following primary antibodies accordingly to their data sheets: anti-OCT3/4, Ki67, nestin, βIII tubulin, NFH, GFAP, Sox2, Stro-1, CD90 and CD44. After washing with PBS, cells were incubated for 30 minutes at RT with AlexaFluor 488 anti-rabbit IgG, AlexaFluor 595 anti-goat IgG or AlexaFluor 633 anti-mouse IgG secondary antibodies (1:2000 Molecular Probes, Invitrogen, Carlsbad, CA, USA). Controls were performed by omitting the primary antibody. Cell nuclei were stained with DAPI (0.5 μg/ml). Coverslips were mounted with Vectashield Mounting Medium and examined at a confocal microscope (Leica TCS SP5, Mannheim, Germany).

FACS analyses

Expression of antigens on GSCs untreated or not with ABTL0812 (5 to 20 μM), were quantified by flow cytometry. Cells were fixed with 4% paraformaldehyde and permeabilized by 0.1% (v/v) Triton X-100. After washing, cells were incubated for 1 hr at 4°C with selected primary antibodies (see above) followed by CY5-conjugated anti-rabbit IgG H&L or PE-conjugated anti-mouse IgG purchased from Abcam for an additional 30 min. Negative controls were obtained by analyzing the autofluorescence of samples with only the secondary antibodies. All samples were analyzed by using the "BD Accuri™ C6 Plus" Flow cytometer (Becton Dickinson Italia Spa, Milan, Italy) equipped with a blue laser (488 nm) and a red laser (640 nm). At least 10,000 events were acquired.

Cell cycle and apoptosis analysis

The amount of subG1 cells and cell cycle profiles were analyzed by flow cytometry of propidium iodide-stained cells by using Tali™ instrument (Thermo Fisher Scientifics, Carlsbad, CA, USA). Cells were seeded into a 12-well plate at a density of 2.5 × 105 cells/mL per well. After treatment with 0.1, 1 or 2 μM ABTL0812, for 24, 48 and 72 h, cells were collected and separated from the culture medium by centrifugation. Subsequently, they were first washed with PBS and then fixed in 70% ethanol in PBS for 1 h at 4 °C. Then, cells were washed twice with PBS and resuspended in 125 μL of PBS, 12.5 μL of 5 μg/mL RNase (Sigma-Aldrich) and stained with 125 μL of 100 μg/mL PI (Sigma-Aldrich). Finally, cells were incubated for 30 min in the dark at room temperature before analyzing their DNA content. The fluorescence was measured using Tali™ instrument as above. In addition, apoptosis was analyzed by using different methods: (i) *In Situ* Application Abbkine TUNEL Apoptosis Detection Kit (Green Fluorescence), which relies on the presence of nicks in the DNA which can be identified by TdT, an enzyme that catalyzes the addition of dUTPs that are labeled with fluorescein; (ii) TiterTACS™ Colorimetric Apoptosis Detection Kit from Trevigen (BioTechne, Milan, Italy). (iii) All cells were then measured on a Tali® Image-Based Cytometer measuring the fluorescence emission at 530 nm (e.g., FL1) and >575 nm. The results were expressed as the percentage of cell death in controls and in treated cultures. (iv) Apoptosis was also evaluated measuring the enzyme activity of caspase 3 (CC3), caspase 8 (CC8) and caspase 9 (CC9) by using specific colorimetric substrates in particular N-Acetyl-Asp-Glu-Val-Asp p-nitroanilide (zDEVD-pNA) for caspase-3, Ac-Ile-Glu-Thr-Asp-pNA for caspase-8 and Ac-Leu-Glu-His-Asp-pNA for caspase 9. The ELISA plates were read at 450 nm using an Elisa reader (Tecan sunrise). Annexin V-propidium iodine staining was used to detect early and late apoptosis by FACS analyses. Tali™ Apoptosis Kit containing Annexin V Alexa Fluor™ 488 and propidium iodide was used for detecting the early and late apoptotic cells. The percentage of apoptotic cells acquired by BD FACS Caliber flow cytometer was analyzed following the procedures recommended by the manufacturer.

Preparation of cell lysates and immunoblotting analysis

Following treatments, cells, grown in 90 mm diameter Petri dishes, were washed with cold PBS, and immediately lysed with 1 ml lysis buffer containing a proteinase and phosphatase inhibitor cocktail. Cytosol and lysosome fractions were obtained by using the nuclear/cytosol fractionation and

Lysosome Purification Kit, respectively from Biovision (Vinci-biochem, Florence. Italy). Total lysates and sub-fractionated extracts were (i) electrophoresed in 10% SDS-PAGE, and separated proteins transferred to nitrocellulose and probed with the appropriate antibodies using the conditions recommended by the suppliers. Total extracts were normalized by using an anti β-actin antibody. (ii) Parallelly total lysates and sub-fractionated extracts were analyzed by ELISA as described above.

Animal experiments: subcutaneous xenograft model

For the *in vivo* experiments 6-week-old female CD1-nu/nu mice (Charles River, Milan, Italy), were used and followed under the guidelines established by our Institution (University of L'Aquila, Medical School and Science and Technology School Board Regulations, complying with the Italian government regulation n.116 January 27, 1992, for the use of laboratory animals (Protocol authorization number 555/2017-PR). Next, animals were randomly divided into different groups. All mice received subcutaneous flank injections (2 each) of 1 x 10^6 U87MG (20 animals) or T98G (20 animals) cells. In a first set of experiments 40 animals (5 mice per group with two tumors each) with tumor volumes of 0.8~1.3 cm^3 were randomized in 4 different groups as follow: group I: Vehicle (methylcellulose), n = 5; group II: ABTL0812 at 120 mg/Kg/day, n= 5; group III: ABTL0812 at 240 mg/Kg/day, n = 5; group IV: Everolimus 5 mg/Kg/2 days for week, n = 5). ABTL0812 and Everolimus were solubilized in DMSO and dissolved in 0.5% methylcellulose and 100 ml of suspension was administered. Tumor growth was assessed bi-weekly by measuring tumor diameters with a Vernier caliper. If we considered a xenograft as equivalent to an ovoid having three diameters: the formula used was 'TW (mg) = tumor volume (mm^3) = 4/3πR1xR2xR3 in which R1/R2/R3 are the 1/2 diameters (rays), shorter diameter is the thickness/height of tumor, larger diameters are the length and width of tumor (36–39). In a second set of experiences, 30 mice bearing T98G and U251 cells (5 mice per group with two tumors each) with tumor volumes of 0.8~1.3 cm^3 were retained and randomly divided into 3 groups (1) Control (vehicle, 0.5% methylcellulose); (2) ABTL0812 (120 mg mg/kg/5 Day/week, PO); (3) ABTL0812 (240 mg mg/kg/5 Day/week, PO). Animals were treated with 10μl vehicle or drugs. At the end of experiments (35 days after the start of treatments) animals were sacrificed by carbon dioxide inhalation and tumors were subsequently surgically removed. Half of the tumor were directly frozen in liquid nitrogen for protein analysis and the other half fixed and frozen in paraformaldehyde overnight for immunohistochemical and biochemical analyses, respectively.

For the evaluation of treatment response *in vivo*, the following parameters were used to quantify the antitumor effects upon different treatments as previously described (36, 37, 39): (1) Tumor volume measured during and at the end of experiments. (2) Tumor weight measured at the end of experiment; (3) Tumor progression (TP)) defined as an increase of greater than 100% of tumor volume with respect to baseline; (4) Time to Tumor progression (TTP) defined as the time (T) necessary to Tumor progression.

Orthotopic intra-brain model

Female CD1 nu/nu mice were inoculated intra-cerebrally as previously described (34) with luciferase transfected U87MG and patient-derived GBM stem cell line (GSCs-5). Just before treatment initiation (5 days after tumor injection), animals were randomized as described above in three groups of 10 mice each: (1) Control (vehicle); (2) ABTL0812 (120 mg mg/kg/5 Day/week, PO); (3) ABTL0812 (240 mg mg/kg/5 Day/week, PO). *In vivo* bioluminescence images were obtained using the UVITEC Cambridge Mini HD6 (UVItec Limited, Cambridge, United Kingdom). Animals were anesthetized and luciferin (150 mg/kg) was injected intra-peritoneally (IP) 15 min prior to imaging. Mice were photographed while placed on their front and the bioluminescence intensity (BLI) was measured in the region of interest. We deliberately inoculated a small number of cells (3 x10^3) to simulate a post-surgery clinical scenario. Treatments were started 5 days after cell injection when no luciferase activity was intracranially detectable. Mice were euthanized when they displayed neurological signs (e.g., altered gait, tremors/seizures, lethargy) or weight loss of 20% or greater of pre-surgical weight. Luciferase transfected cells for bioluminescence evaluations. We used luciferase transfected U87MG and CSCs-5 cells.

Immunohistochemical analyses

Indirect immuno-peroxidase staining was performed on 4 μm paraffin-embedded tissue sections. A consensus judgment as indicated in previous reports (40, 41) was adopted for immunohistochemical scoring of tumors based on the strength of positivity: negative (score 0), weak (score 1), moderate (score 2), or strong staining (score 3). In each category, the percentage of positive cells was assessed by scoring at least 1000 cells in the area with the highest density of antigen positive cells. Cytoplasmic/membrane staining intensity was graded as follow: 0 = negative; 1 = <10% positive cells; 2 = positive cells in a range of 10–50%; and 3 = >50% positive cells. Overall expression was defined by the staining index (SI) and ranged between 0 and 9, with an SI ≤ 4 indicating a low expression. Proliferation index (labeling index) was determined through the evaluation of the percentage of Ki67 positive cells by analyzing 500 cells at 100× magnification. A TACS Blue Label kit (R&D Systems, Inc., Minneapolis, MN, USA) was used for *in situ* apoptosis determination and the percentage of terminal deoxynucleotidyl transferase dUTP nick end labeling (TUNEL)

positive cells was determined in five random fields evaluated at 400× magnification. In order to count the number of CD31+ micro vessels, five arbitrarily selected fields were analysed for each group at 100× magnification (tumour micro vessels). Martius yellow-brilliant crystal scarlet, blue stain was used to stain erythrocytes, and consequently, the presence of micro-thrombi and bleeding zones.

Statistics

Continuous variables were summarized as mean and SD or as median with 95% CI. For continuous variables not normally distributed, statistical comparisons between control and treated groups were established by carrying out the Kruskal-Wallis Tests. When Kruskal-Wallis Tests test revealed a statistical difference, pair-wise comparisons were made by Dwass-Steel-Chritchlow-Fligner method and the probability of each presumed "non-difference" was indicated. For continuous variables normally distributed, statistical comparisons between control and treated groups were established by carrying out the ANOVA test or by Student t-test for unpaired data (for two comparisons). When the ANOVA revealed a statistical difference, pair-wise comparisons were made by Tukey's HSD (Honestly Significant Difference) test and the probability of each presumed "non-difference" was indicated. Dichotomous variables were summarized by absolute and/or relative frequencies. For Dichotomous variables, statistical comparisons between control and treated groups were established by carrying out Fisher's exact test. For multiple comparisons, the level of significance was corrected by multiplying the P value by the number of comparisons performed (n) according to Bonferroni correction. TTP was analyzed by Kaplan-Meier curves and Gehan's generalized Wilcoxon test. When more than two survival curves were compared, the Log rank test for trend was used to test the probability that there is a trend in survival scores across the groups. All tests were two-sided and were determined by Monte Carlo significance. P values <0.05 were considered statistically significant. SPSS® (statistical analysis software package) version 10.0 and StatDirect (version. 2.3.3., StatDirect Ltd) were used for statistical analyses and graphic presentations.

Results

ABTL0812 inhibits proliferation of glioblastoma cells and glioblastoma stem cells *in vitro*

ABTL0812 effects on cell proliferation was evaluated in a panel of ten glioblastoma cell lines and four patient-derived glioblastoma stem cells (GSCs). ABTL0812 reduced cell proliferation in a concentration-dependent manner in all glioblastoma cell lines (Figure 1A) with IC50s that ranged from 15.8 μM to 46.9 μM. Similarly, proliferation assays performed on glioma spheres from GSCs showed IC50s for ABTL0812 that ranged between 15.2 μM and 43.7 μM (Figure 1B). Statistical analysis showed no difference in IC50 calculated for glioblastoma compared to GSC cell lines (Supplementary Figures S1A, B). Importantly, in astrocytes and human brain derived endothelial cells (HBMVECs) the calculated IC50 values were 380 μM and 225 μM, respectively (Figure 1C), confirming previous published data showing that non-cancer cells are viable at the same ABTL0812 concentrations that are cytotoxic for cancer cells (13–18). Morphological changes were observed after administration of ABTL0812 with the acquisition of a more differentiated astrocyte phenotype, which was evident at ABTL0812 concentrations between 10 and 20 μM. At the highest dose tested of 40 μM, cell death and detachment was observed. Figure 1D shows these changes in U87MG cells as a representative model. Similar changes were observed in the other glioma cell lines studied. In GSCs it was observed that ABTL0812 affects neurosphere formation and growth, the number and size of spheres were reduced in a concentration-dependent manner and over time (Figure 1E, Supplementary Figures S1C, D, E). These results show that ABTL0812 decreases proliferation of glioblastoma cells and GSCs, and reduces neurospheres formation of GSCs.

ABTL0812 induces differentiation of glioblastoma cells to a less malignant phenotype

The morphologic changes induced by ABTL0812 in glioblastoma and GSCs suggested tumor cell differentiation and an associated reduction of malignancy. In glioblastoma, the induction of malignancy is associated to the acquisition of PMT (proneural to mesenchymal transition) phenotype, a process which is similar to EMT (epithelial to mesenchymal transition) found in epithelial cancers. We studied changes in the expression of PMT and stem cell markers in high grade glioblastoma cells (U87MG, U251 and A172) and GSCs (GSCs-5 and BT12M). U87MG cells show an undifferentiated phenotype with high expression of CD44, CD90 and Stro-1 mesenchymal markers. The administration of increasing concentrations of ABTL0812 (10-40 μM) decreased in a concentration-dependent manner the mesenchymal markers CD44, CD90 and Stro-1 and increased the expression of pro-neuronal markers βIII tubulin and NFH (Figure 2A) Additonally, the cell proliferation marker Ki67 was studied and, consistently with the decrease of cell proliferation observed in the previous section, a reduction of Ki67 by ABTL0812 was detected. Similar results were obtained in glioblastoma cell lines U251 and A172 (Supplementary Figure S2). Next, we analyzed

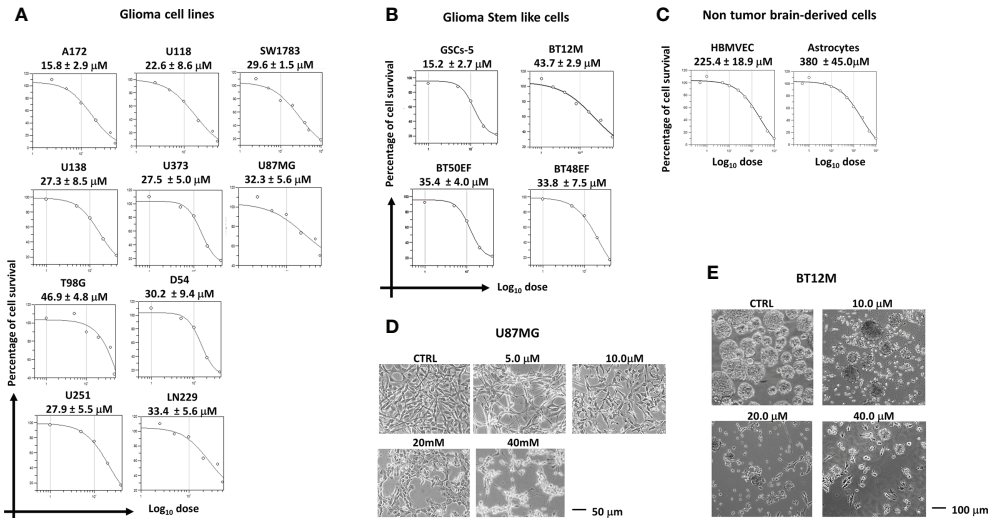

FIGURE 1
ABTL0812 inhibits proliferation of glioblastoma cells and glioblastoma stem cells. **(A)** ABTL0812 cell proliferation curves and IC_{50}s at 48 hours in glioblastoma cell lines, **(B)** at 96 hours in patient-derived glioblastoma stem cells (GSCs) and **(C)** at 48 hours in HBMVEC and astrocytes. **(D)** Images of U87MG cells treated for 48 hours with ABTL0812 showing that ABTL0812 induce cell extensions associated to type I astrocytic phenotype and cell death and detachment. Bar represents 50 μm **(E)** Neurosphere formation in BT12M cells treated for 96 hours with different concentrations of ABTL0812.

differentation and stem cell markers in the GSCs cell line GSCs-5, that has a mesenchymal phenotype, detecting that ABTL0812 decrease in a concentration-dependent manner the expression of mesenchymal markers Stro1, CD44 and CD90, and of stemness marker CXCR4 and an increase of proneuronal markers βIII tubulin and NFH (Figure 2B). In addition, Ki67 was reduced by ABTL0812 treatment. Furthermore, we analysed the expression and localization of the stemness marker Sox2 and proliferative marker Ki67 by confocal microscopy in BT12M neurospheres. The expression of Sox2 was decreased by ABTL0812 indicating a reduction of cell stemness (Figure 2C, Supplementary Figure S2). It is well known that glioblastoma mesenchymal phenotypes are more invasive. The treatment of U87MG, U251 and A172 cells with ABTL0812 for 24 hours reduced cell invasion (Figures 2D, E), which is consistent with an induction of a more differentiated pro-neural phenotype which is less invasive. Overall, these results indicate that ABTL0812 reverses the proneural to mesenchymal transition (PMT), a process associated to increased malignancy, and decreases cell invasion.

ABTL0812 induces autophagy-mediated apoptotic death of glioblastoma cells

ABTL0812 is known to impair tumor growth by inducing autophagy-mediated cancer cell death. During autophagy, the soluble form of LC3 conjugates with phosphatidylethanolamine and converts to the autophagosomal membrane-associated form LC3-II. Treatment of U87MG, A172 and U251 cells with ABTL0812 increased LC3-II in a concentration-dependent manner (Figure 3A). This was associated to an increase of acidic vesicular organelles (AVO), characteristic of autophagy, in U251 cells as detected by acridine orange staining (Figure 3B). Furthermore, ABTL0812 administration concentration-dependently induced the formation of vesicular structures with the morphologic features of autophagosomes in U87MG cells. Additionally, it was observed that mitochondria in cells treated with ABTL0812 were smaller and with damaged mitochondrial crests (Figure 3C). Moreover, the blockade of lysosomal content degradation with cathepsin inhibitors (E64d and pepstatin A) in U87MG cells resulted in increased levels of LC3-II, indicating that ABTL0812 induced dynamic autophagy (Figure 3D). Furthermore, the induction of dynamic autophagy was studied by the co-localization of the lysosomal marker LAMP1 and LC3. In U87MG cells ABTL0812 induced the co-localization of LC3 and LAMP1 in autolysosomes, and this co-localization was partially impaired by chloroquine, an autophagy inhibitor that blocks the binding of autophagosomes to lysosomes (Figure 3E).

Thereafter, we investigated if the autophagy-mediated cancer cell death induced by ABTL0812 affected mitochondria and involved apoptosis. Firstly, U251 cells were treated with increasing concentrations of ABTL0812 and, stained with JC-1, a dye used to monitor mitochondria status as an indicator of mitochondrial membrane potential. ABTL0812 treatment decreased the red/green fluorescence intensity ratio, which indicates mitochondrial depolarization, a process that precedes

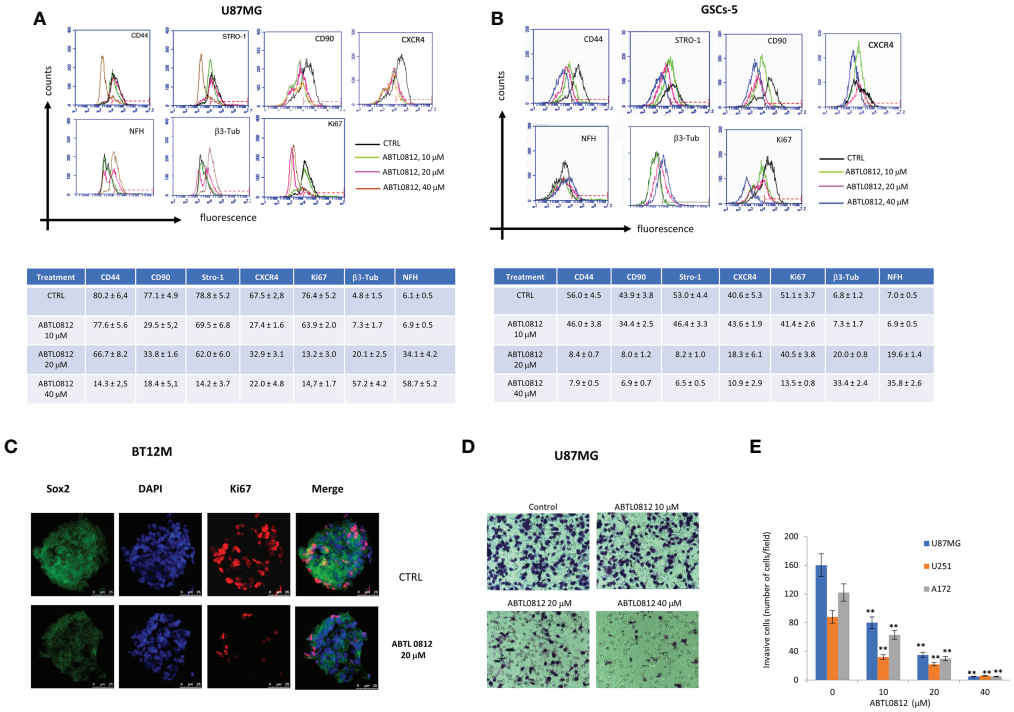

Treatment	CD44	CD90	Stro-1	CXCR4	Ki67	β3-Tub	NFH
CTRL	80.2 ± 6,4	77.1 ± 4.9	78.8 ± 5.2	67.5 ± 2,8	76.4 ± 5.2	4.8 ± 1.5	6.1 ± 0.5
ABTL0812 10 μM	77.6 ± 5.6	29.5 ± 5,2	69.5 ± 6.8	27.4 ± 1.6	63.9 ± 2.0	7.3 ± 1.7	6.9 ± 0.5
ABTL0812 20 μM	66.7 ± 8.2	33.8 ± 1.6	62.0 ± 6.0	32.9 ± 3.1	13.2 ± 3.0	20.1 ± 2.5	34.1 ± 4.2
ABTL0812 40 μM	14.3 ± 2,5	18.4 ± 5,1	14.2 ± 3.7	22.0 ± 4.8	14,7 ± 1.7	57.2 ± 4.2	58.7 ± 5.2

Treatment	CD44	CD90	Stro-1	CXCR4	Ki67	β3-Tub	NFH
CTRL	56.0 ± 4.5	43.9 ± 3.8	53.0 ± 4.4	40.6 ± 5.3	51.1 ± 3.7	6.8 ± 1.2	7.0 ± 0.5
ABTL0812 10 μM	46.0 ± 3.8	34.4 ± 2.5	46.4 ± 3.3	43.6 ± 1.9	41.4 ± 2.6	7.3 ± 1.7	6.9 ± 0.5
ABTL0812 20 μM	8.4 ± 0.7	8.0 ± 1.2	8.2 ± 1.0	18.3 ± 6.1	40.5 ± 3.8	20.0 ± 0.8	19.6 ± 1.4
ABTL0812 40 μM	7.9 ± 0.5	6.9 ± 0.7	6.5 ± 0.5	10.9 ± 2.9	13.5 ± 0.8	33.4 ± 2.4	35.8 ± 2.6

FIGURE 2
ABTL0812 induces glioblastoma and GSCs differentiation and reverts proneural to mesenchymal transition. **(A)** Representative FACS expression profiles of mesenchymal (CD44, Stro1 and CD90), stemness (CXCR4), neural (βIII tubulin, NFH and GAP43) and proliferation (Ki67) markers and table and histograms showing the percentage of cells expressing the markers analyzed by FACS in glioblastoma cells U87MG treated with ABTL0812 for 48 hours **(B)** and in glioblastoma stem cells GSCs-5 treated for 48 hours with ABTL0812 **(C)** Representative confocal images of BT12M cells stained with Sox2, βIII tubulin and Ki67. Cell nuclei were stained with DAPI. **(D)** Representative images from Boyden chamber assays showing invasive U87MG cells after a 6-hour assay that were pretreated with ABTL0812 for 48 hours **(E)** Quantification of invasive cells from a matrigel invasion assays performed in U87MG, U251 and A172 cells treated with ABTL0812. CTRL= control vehicle-treated cells. ** p<0.01 vs vehicle basal.

the release of apoptotic factors from the mitochondria cells (Figure 4A). Next, apoptosis was analysed by TUNEL assay, detecting that ABTL0812 induces apoptosis in a concentration-dependent manner in U87MG cells (Figure 4B). Additionally, apoptosis activation by ABTL0812 was confirmed by annexin V/propidium iodide staining in U87MG cells (Figure 4C) and by measuring subG1 apoptotic cell population in a wide panel of glioblastoma cells (Supplementary Figure S3). Moreover, we studied the cleavage of caspases by immunoblotting which showed that activator caspases 8 and 9 and effector caspase 3 were activated by ABTL0812 (Figure 4D). Caspase activation was further confirmed by measuring caspase 8, 9 and 3 enzimatic activity in U251, A172 and U87MG cells (Figure 4E). Finally, in order to study if autophagy precedes and is a necessary event for apoptosis activation, U87MG cells were treated with ABTL0812 and chloroquine. The analysis of caspase 3 activity showed that the increase induced by ABTL0812 was significantly reduced by co-treatment with chloroquine (Figure 4F), confirming that ABTL0812 induces autophagy-mediated apoptotic cell death. Overall, these data indicates that ABTL0812 induces a dynamic autophagy that results in the induction of apoptotic death of glioblastoma cells.

ABTL0812 inhibits Akt/mTORC1 axis and induces ER stress

Previously, it was demonstrated that ABTL0812 activates autophagy-mediated cancer cell death by inhibition of the Akt/mTORC1 axis and induction of ER stress, two well-known actions leading to autophagy (13, 14). Previous studies showed that ABTL0812 inhibits Akt by inducing TRIB3 a pseudokinase that binds to Akt and impedes its phosphorylation and activation by upstream kinases. We detected by immunoblotting that ABTL0812 induces TRIB3 in a concentration-dependent manner, which leads to a decrease of phosphorylation of Akt on residue Ser473 in U87MG and GSC-5 cells. The blockade of Akt resulted in inhibition of mTORC1 as detected by a decrease of phosphorylation of its target p70S6K (Figure 5A). The decrease of p-Akt Ser473, and also p-Akt Thr308, was confirmed by ELISA in

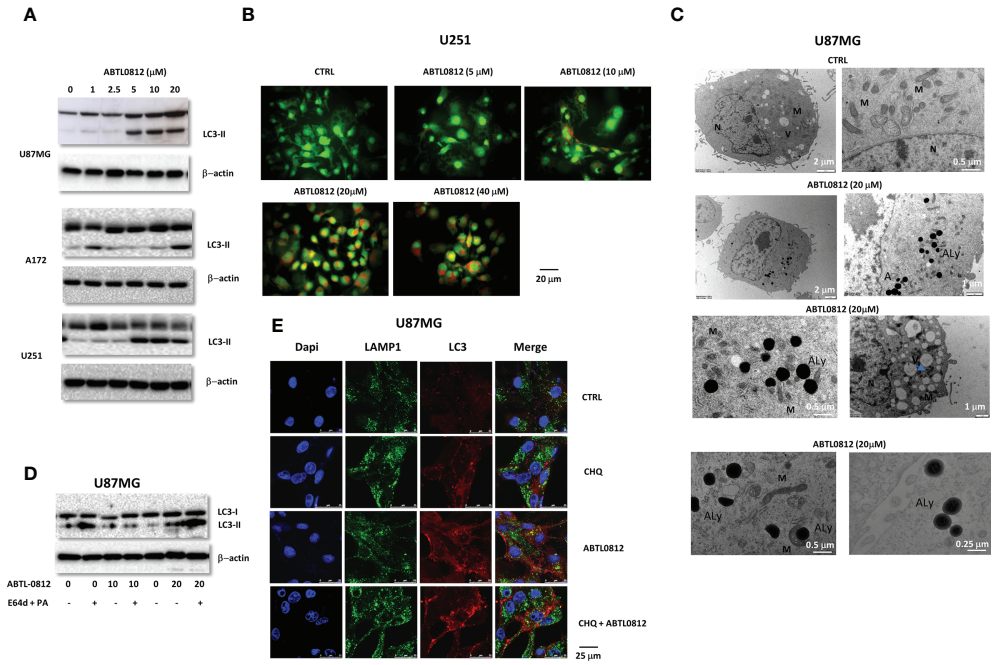

FIGURE 3
ABTL0812 induces autophagy in glioblastoma cells. **(A)** Representative immunoblotting images of LC3-II from U87MG, A172 and U251 cell lines treated with ABTL0812 for 12 hours. **(B)** Representative immunofluorescence images of staining with acridine orange, a green fluorophore that fluoresces red in acidic vesicular organelles (AVO) in U87MG cells treated for 12 hours with ABTL0812 (40X magnification). **(C)** Representative electron microscopy microphotographs of U87MG in cells treated with ABTL0812 at 20 and 40 μM for 12 hours. N= nucleus, Au=autophagosomes; M= mitochondria and V= vesicles. Blue arrows indicate small or unfunctional mitochondria. **(D)** Representative immunoblotting images of LC3-II from U87MG cells pretreated with lysosome protease inhibitors (E64 and pepstatin A at 10 mg/ml each) for 24 hours followed by 12 hours treatment with ABTL0812. **(E)** Representative immunofluorescence images of the staining of LAMP1 and LC3 in U87MG cells treated with ABTL0812 (20 μM) for 12 hours with or without a pretreatment of 1 hour with chloroquine (3 μM). LAMP1 in is a marker of endosomes/lysosomes (green signal), LC3 is a marker of autophagosomes (red signal) and DAPI stains nuclei (blue signal). The colocalization of red and green signal results in orange signal and corresponds to autolysosomes. CTRL, control vehicle-treated cells.

U251, U87MG, A172 and GSC-5 cells (Figure 5B). Moreover, it was previously shown that ABTL0812 induces sustained ER stress that results in activation of unfolded protein response (UPR) *via* PERK-eIF2α-ATF4-CHOP-TRIB3 (16–18). Immunoblotting analysis of this pathway showed that ABTL0812 induced pPERK, peIF2α, ATF4 and CHOP in a concentration-dependent manner in U87MG cells. ABTL0812 effects on this pathway were similar to the ones induced by Brefeldyn A, a compound widely used as an ER stress inducer. (Figure 5C). It is known that the accumulation of unfolded proteins in the ER triggers the unfolded protein response (UPR), a stress signaling pathway. This firstly leads to the promotion of a pro-adaptive signaling pathway by the inhibition of global protein synthesis and cell cycle, however, during conditions of prolonged ER stress, pro-adaptive responses fail, and apoptotic cell death is induced. It has been demonstrated that UPR induces growth arrest in G1 phase of the cell cycle. Thus, we analyzed whether ABTL0812 was able to modify cell cycle in glioblastoma cell models. Here, we demonstrated that ABTL0812 decreased in U87MG cells the levels of cyclin D1 and E as well as of CDK4 and CDK2 which are involved in G1/S cell cycle transition and induced the expression of the CDK inhibitors p27 and p16INK4A (Figure 5D). Accordingly, cell cycle analysis by flow cytometry using propidium iodide staining shows that ABTL0812 induces cell cycle arrest in G0/G1. It is worth mentioning that at lower concentrations of ABTL0812 (5 and 10 μM) the predominant effect is the arrest at G0/G1, whereas at higher concentrations (20 and 40 μM) the subG1 cell dead population is highly increased (Figure 5E). These data indicates that ABTL0812 inhibits Akt/mTORC1 axis and induces ER stress and both molecular events lead to autophagy and ultimately to glioblastoma cells death.

ABTL0812 treatment impairs tumor growth in glioblastoma subcutaneous xenograft tumor models

To study the therapeutic efficacy of ABTL0812 on tumor growth *in vivo*, U87MG and T98G cells were injected subcutaneously in athymic female cd1 nu/nu mice. Mice were

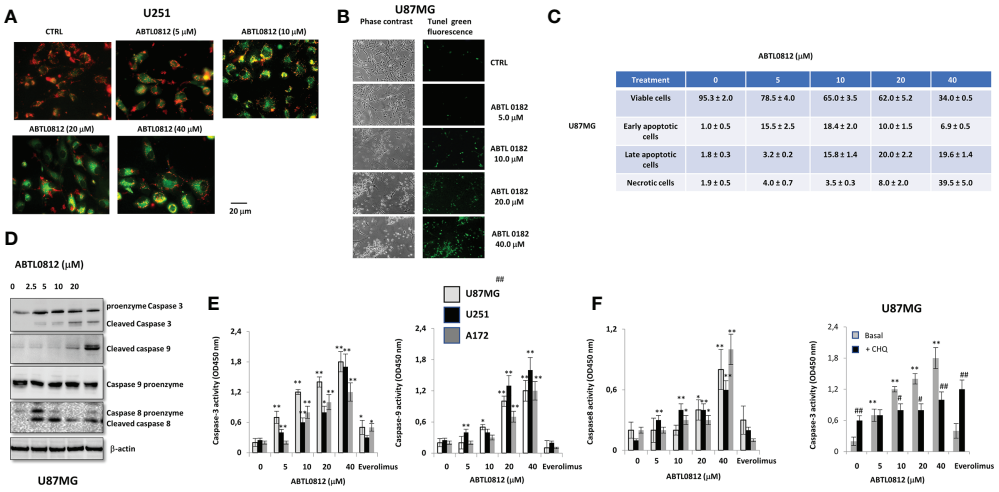

FIGURE 4
ABTL0812 induces mitochondrial depolarization and apoptosis in glioblastoma cells. **(A)** Representative immunofluorescence images of staining with JC-1, a dye indicator of mitochondrial membrane potential in U251MG cells treated for 16 hours with ABTL0812 (200X magnification). Red staining indicates polarized mitochondria and green indicates depolarized mitochondria. **(B)** Apoptosis TUNEL assay performed on U87MG cells treated with ABTL0812 for 16 hours. **(C)** Table showing the percentage of cell populations as determined by FACS analysis of annexin V/ propidium iodide staining of U87MG cells treated for 16 hours with ABTL0812. **(D)** Representative images of immunoblotting detection of caspase 3, 8 and 9 pro-enzymes and cleaved isoforms in U87MG cells treated with ABTL0812 for 16 hours. **(E)** Quantification of caspases 8, 9 and 3 activities by using caspase-specific chromogenic substrates in U87MG, A172 and U251 cells treated for 16 hours with ABTL0812. The mTORC1 inhibitor everolimus was used as a comparator to ABTL0812 *p<0.05 and ** p<0.01 vs vehicle treated cells. **(F)** Quantization of caspase 3 activity in U87MG cells treated for 16 hours with ABTL0812 and with or without a 1 hour chloroquine pretreatment. *p<0.05 and ** p<0.01 vs vehicle basal; $^{\#}$p<0.05 and $^{\#\#}$ p<0.01 vs vehicle+chloroquine.

orally treated with vehicle, ABTL0812 (120 mg/Kg or 240 mg/Kg) or everolimus, a mTOR inhibitor that was used as a comparator for antitumor activity. Both doses of ABTL0812 were well tolerated and animals did not show significant weight loss or signs of distress or toxicity (Table S1 and S2). In animals bearing U87MG tumors, ABTL0812 at 120 and 240 mg/Kg significantly reduced tumor weight; compared to vehicle, we detected a weight decrease of 38.1% and 58.6%, respectively. Everolimus at 5 mg/kg only achieved a decrease of 12% compared to vehicle (Figure 6A and Supplementary Table S1). In T98G cells-derived xenograft tumors, ABTL0812 treatment at 120 and 240 mg/Kg significantly decrease tumor weight by 36.4% and 62.5%, respectively, whereas with everolimus the decrease was 24.4% (Figure 6B and Supplementary Table S1). Additionally, ABTL0812 antitumor efficacy was evaluated by analyzing tumors time to progression (TTP), a parameter widely used in human clinical trials. In both U87MG and T98G xenograft tumors, ABTL0812 at 120 and 240mg/kg significantly increased TTP compared to vehicle (Supplementary Tables S1 and S2). Next, we investigated the molecular markers of ABTL0812 treatment in the surgically removed xenograft tumors. In both U87MG and T98G xenograft tumors, immuno-histochemical analyses revealed that TRIB3 expression was significantly increased in tumors treated with ABTL0812, whereas p-Akt Ser473, p-Akt Thr308 and the mTORC2 target p-p70S6K Ser411 were significantly decreased. Moreover, tumors treated with ABTL0812 showed a decrease of the cell proliferation marker Ki67, an induction of apoptosis as detected by an increase of caspase-3 and TUNEL staining, and a decrease of vascularization of the tumors as shown by CD34 staining and, consequently, an increase of hypoxia as shown by an increase of HIF-1α. The effect of ABTL0812 on all these parameters shows a clear trend towards a greater modification than with everolimus in both U87MG (Figure 6C) and T98G cells (Figure 6D). Supplementary Table S1 shows the numerical results of the IHC analyses. Overall, these *in vivo* studies have demonstrated the therapeutic efficacy of ABTL0812 against glioblastoma xenograft tumors. Additionally, the effect of ABTL0812 on the molecular markers of its mechanism of action have been shown, as well as that ABTL0812 decreases cell proliferation, activates apoptosis and reduces vascularization of tumors.

ABTL0812 treatment impairs tumor growth of glioblastoma orthotopic intra-brain xenograft tumor models and increases overall survival of mice

Next, we investigated the efficacy of ABTL0812 in orthotopic mice models that mimic the clinical setting of glioblastoma treatment. U87MG and GSC-5 luciferase-tagged cells were injected orthotopically into the brain of athymic female cd1

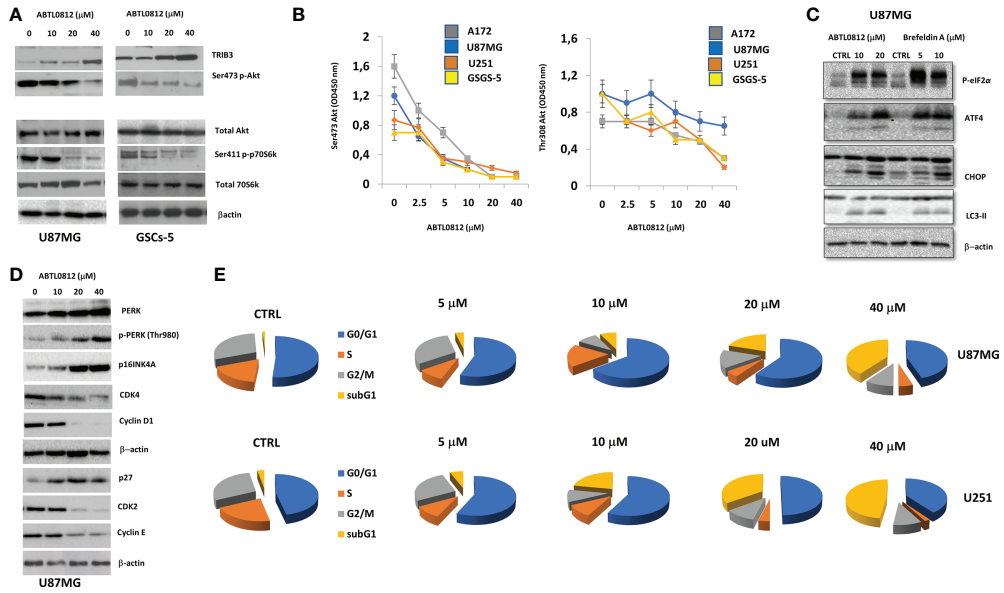

FIGURE 5
ABTL0812 inhibits Akt/mTORC1 axisA and induces ER stress **(A)** Representative immunoblotting images of Akt/mTORC1 axis markers TRIB3, Akt and p70S6K from U81MG cells treated with ABTL0812 for 16 hours. **(B)** ELISA quantification of p-Akt Ser473, and p-Akt Thr308 in U81MG, U251, A172 and GSCs-5 cells treated with ABTL0812 for 16 hours **(C)** Representative immunoblotting images of p-eIF2α, ATF4, CHOP and LC3-II from U81MG cells treated with ABTL0812 for 16 hours The ER stress inducer Brefeldin A was used as a positive control for ER stress response **(D)** Representative immunoblotting images of PERK and phase G1-S cell cycle regulators from U81MG cells treated with ABTL0812 for 16 hours. **(E)** Diagrams showing percentages of cell population in each cell cycle phase in U87MG and U251 cells treated with ABTL0812 for 16 hours determined by flow citometry analysis of propidium iodide-stained cells.

nu/nu mice. A low number of U87MG cells (3000) were injected into the brain to simulate an after surgery clinical setting where a few amounts of tumor cells cannot be removed. The oral treatment with vehicle, ABTL0812 or everolimus started 5 days after the injection when bioluminescence could not be detected intra-cranially yet. Animals were treated for 35 days and after this treatment period, mice were observed for 150 days (follow-up period) without being treated as indicated in the diagram of Figure 7A. Tumor growth was monitored over time by bioluminescence detection and two parameters were used to assess treatments efficacy: (i) disease free survival (DFS), which is defined as the time from tumor cells injection until luciferase activity was intracranially detectable; and, (ii) overall survival (OS) of mice over time. In the U87MG orthotopic model it was detected that ABTL0812 treatment at both 120 and 240mg/kg significantly increased the time of tumor onset in a concentration-dependent manner compared to vehicle-treated mice. When we compared ABTL0812 treatment with everolimus, we detected that DFS was significantly increased by ABTL0812 240mg/Kg (Figure 7B and Supplementary Tables S3 and S4). The overall survival was also significantly increased by ABTL0812 at both doses compared to vehicle and by ABTL0812 240mg/kg compared to everolimus (Figure 7C and Supplementary Tables S3 and S5). In order to investigate the anticancer efficacy of ABTL0812 treatment against glioblastoma stem cells, an orthotopic model using GSC-5 cells was generated in nude mice (Figure 7A). When comparing the DFS of each treatment again it was detected that compared to vehicle-treated animals, ABTL0812 240mg/kg was the most efficient in delaying the appearance of luminescence from tumor cells, followed by ABTL0812 120mg/Kg, whereas the less efficient was everolimus (Figure 7D and Supplementary Tables S3 and S4). Regarding overall survival, the efficiency of the treatments correlate with the DFS results: ABTL0812 increased overall survival in a concentration-dependent manner compared to vehicle, and both ABTL0812 doses increased overall survival compared to everolimus treatment although only the ABTL0812 240mg/kg dose was significantly different to everolimus. (Figure 7E and Supplementary Tables S3 and S5). All together these data demonstrates that ABTL0812 treatment has anticancer activity in orthotopic glioblastoma mouse models that reproduce the clinical setting after surgical removal of tumors. Moreover, the efficacy of ABTL0812 against glioblastoma stem cells *in vivo* was proven.

Currently, the standard of care treatment for GBM is surgery, followed by radiotherapy and temozolomide chemotherapy. To investigate the potential of combination of ABTL0812 with radiotherapy and temozolomide, we used the U87MG orthotopic model where ABTL0812 single therapy was studied. With the aim of mimicking the clinical practice, treatment doses and schedules were the following: 120 mg/Kg

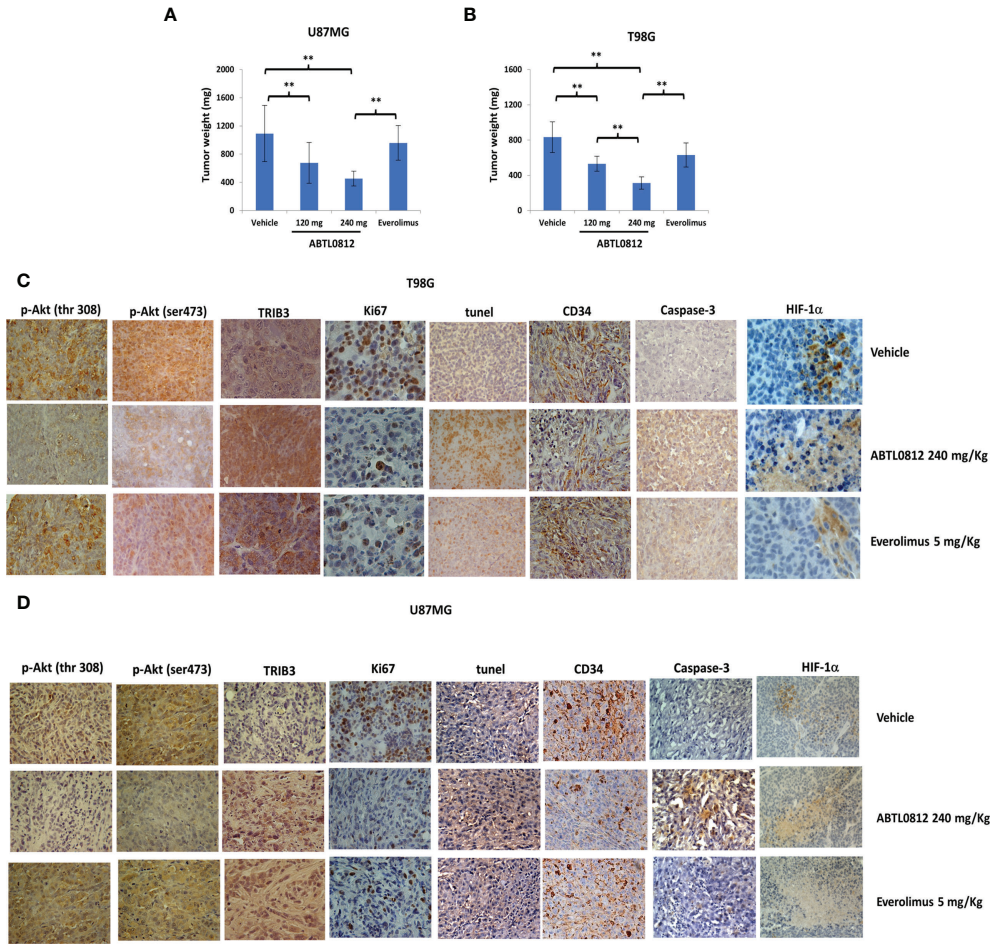

FIGURE 6
ABTL0812 impairs tumor growth in glioblastoma subcutaneous xenograft models. U87MG and T98G cells were injected subcutaneously in athymic female cd1 nu/nu mice (N=10 each group). Mice were treated daily with vehicle or ABTL0812 at 120 or 240 mg/Kg by oral administration. The mTORC inhibitor everolimus (ve) was used as a comparator for antitumor activity and was administered orally at dose of 5 mg/kg/2 days per week **(A, B)** Weight of U87MG and T98G cells-derived xenograft tumor removed from nude mice. **(C, D)** Representative immunohistochemistry images from U87MG **(C)** and T98G **(D)** xenograft tumors stained with Akt-mTORC axis markers (TRIB3, p-Akt Ser473 and p-Akt Thr308); the cell proliferation marker Ki67; the endothelial cell marker CD34; the apoptosis marker caspase3; the hypoxia marker HIF-1α; and TUNEL staining to measure apoptosis (Magnification 400X). Statistical significance levels: *p<0.05, **p<0.01 and n =10. CTRL= control vehicle-treated cells.

ABTL0812 administered orally 5 days a week from day 7; a single 4 Gy dose of radiotherapy at day 8; and 32mg/kg temozolomide from day 5 for 5 consecutive days, as shown in the diagram in Figure 8A. The investigated treatments were ABTL0812, radiotherapy and temozolomide as single agents; ABTL0812 in combination with radiotherapy or temozolomide; the combination of radiotherapy and temozolomide; and a triple combination of ABTL0812 with radiotherapy and temozolomide. The efficacy of the treatments was analyzed by performing Kaplan-Meier to calculate OS. We detected that ABTL0812 as a single agent had an efficacy similar to temozolomide and radiotherapy as single agents. When ABTL0812 was combined with radiotherapy or temozolomide the efficacy was significantly improved compared to any single treatment, however, when comparing ABTL0812 + radiotherapy or ABTL0812 + chemotherapy vs. the standard of care combination radiotherapy + temozolomide, despite detecting an increase of efficacy, it was not significant. Nevertheless, the triple combination of ABTL0812 + radiotherapy + temozolomide was the most efficacious treatment and the increase of OS was statistically significant when compared to the standard of care treatment of radiotherapy + temozolomide (Figure 8B and Supplementary Table S6). Therefore, these results have shown the efficacy of ABTL0812 in combination with radiotherapy and temozolomide to significantly increase the OS in a glioblastoma orthotopic mouse model.

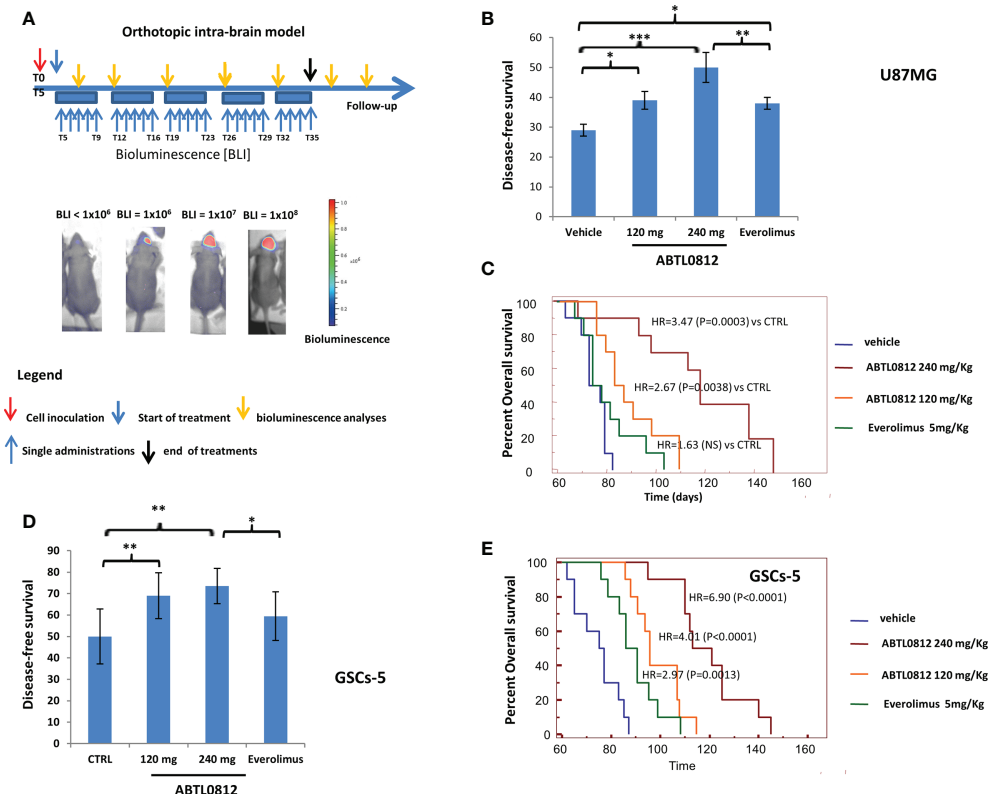

FIGURE 7
ABTL0182 inhibits tumor growth in an orthotopic model of glioblastoma in mice that reproduces the clinical setting after surgical removal of tumors. **(A)** Diagram showing the experimental design of the treatment of glioblastoma orthotopic models using U87MG and GSCs-5 luciferase-tagged cells ortotopically inoculated into the brain of athymic nude mice and treated with ABTL0812 (120 and 240 mg/Kg) and Everolimus (5 mg/Kg). Tumors were monitored by bioluminescence detection which was performed every 7 days in order to determine Disease Free Survival (DFS) and Overall Survival (OS). **(B)** DFS of mice bearing orthotopic tumor of U87MG-Luc cells. **(C)** Overall survival of mice bearing U87MG-Luc cells orthotopic tumors. **(D)** DFS of mice bearing orthotopic tumor of GSC-5 -Luc cells. **(E)** Overall survival of mice bearing GSC-5 -Luc cells orthotopic tumors. Statistical significance levels: *p<0.05, **p<0.01, ***p<0.01 n=10 in each group. CTRL= control vehicle-treated cells.

Discussion

Glioblastoma Multiforme (GBM) is the most malignant adult brain tumor. Unfortunately, glioblastoma tumors are often diagnosed once the patients become symptomatic when the lesion is already widely extended. GBMs are classified into four subtypes (classical, neural, proneural, and mesenchymal) based on their neural differentiation. It has been widely demonstrated that subtype changes have a strong impact on the prognosis, with mesenchymal subtype showing the worst outcome. Mesenchymal subtype glioblastomas usually express stem cell markers and are more invasive. Proneural to mesenchymal transition (PMT) has been shown to lead to resistance to standard of care therapies and to disease recurrence (6). PI3K/Akt/mTORC pathway is involved in the maintenance of PMT, therefore, the inhibition of this pathway may revert this phenotype (42).

The current available therapeutic options for GBMs require very aggressive treatments. The standard of treatment for GBM is surgery, followed by daily radiation and oral chemotherapy for six and a half weeks, then a six-month regimen of oral chemotherapy given five days a month (43). However, these therapies have very limited efficacy with a median overall survival of patients of 14 months. Therefore, the treatment of GBM remains an unmet clinical need. In the latest years, novel therapeutic agents have been actively investigated as additional therapeutic tools to be combined with standard of care treatments or as stand-alone therapies. Novel therapeutic agents currently under clinical investigation include targeted therapies, such as MET or FGFR inhibitors; immunotherapies, such as checkpoint inhibitors, cytokines, dendritic cell vaccines or CAR-Ts; and antiangiogenics among others (44).

ABTL0812 is a first-in-class anti-cancer drug that exerts its therapeutic action through the induction of autophagy-mediated

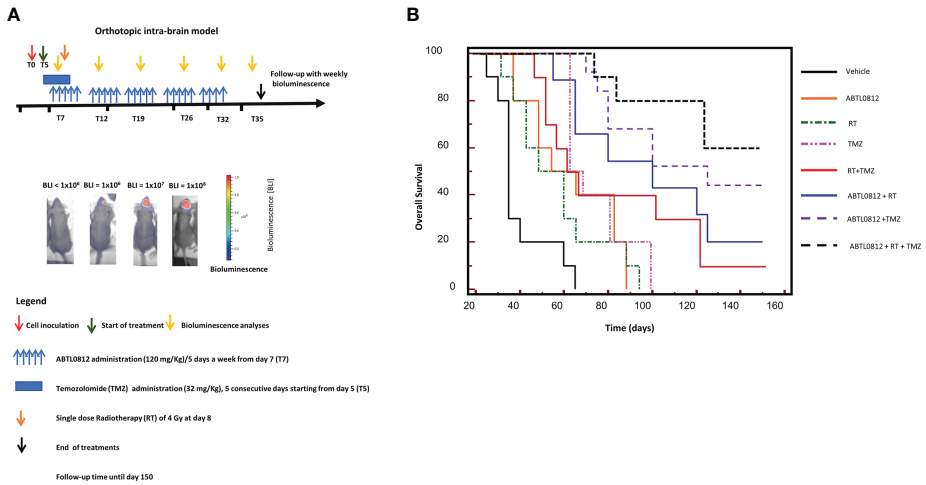

FIGURE 8
ABTL0182 potentiates the anticancer effect of the standard of care treatments radiotherapy and temozolomide in an orthotopic model of glioblastoma in mice **(A)** Diagram showing the experimental design of the treatment of glioblastoma orthotopic models using U87MG luciferase-tagged cells orthotopically inoculated into the brain of athymic nude mice and treated with ABTL0812 (120 mg/Kg), radiotherapy (4 Gy), temozolomide (32mg/kg) and combinatorial treatments. Tumors were monitored by bioluminescence detection which was performed every 7 days in order to determine Overall Survival (OS). **(B)** Overall survival of mice bearing U87MG-Luc cells orthotopic tumors. n=10 in each group.

cancer cell death (13, 14). To date, ABTL0812 has successfully completed a phase I clinical trial as a single therapy in advanced solid tumors (19) and a phase IIa clinical trial in combination with chemotherapy in Non-Small Cell Lung Carcinoma (NSCLC) and endometrial cancer showing superiority over standard of care chemotherapy (20, 21). In this study we investigated the therapeutic potential of ABTL0812 for the treatment of glioblastoma. We showed that ABTL0812 treatment inhibits cell proliferation and induces autophagy-mediated cell death in a wide panel of glioblastoma cell lines. Very importantly, ABTL0812 anticancer effects were also detected in glioblastoma stem cells, which are more resistant to chemotherapy and radiotherapy, at similar concentrations as for glioblastoma non-stem cells. Also noteworthy is the fact that ABTL0812 at supratherapeutic concentrations did not affect non-tumoral brain cells, as previously detected in other models (13–18).

Previously, it was shown that ABTL0812 inhibits the Akt/mTORC1 axis (13, 17) and induces ER stress and UPR response (14, 17) and both actions converge to induce a robust and persistent autophagy which eventually leads to cell death (15, 16). When interrogating the mechanism of action of ABTL0812 in glioblastoma models, we demonstrated that ABTL0812 induces TRIB3 and consequently inhibits Akt/mTORC1 axis, as indicated by a reduction of p-Akt and of the mTORC1 substrate p-p70S6K. Also, the involvement of the activation of ER stress and UPR was shown as indicated by the activation of the PERK-eIF2α-ATF4-CHOP-TRIB3 signaling pathway. As expected, both actions resulted in the induction of autophagy as shown by an increase of autophagy markers and by the presence of autophagosomes detected by electronic microscopy. Ultimately, in all the glioblastoma models studied here, the activation of autophagy led to cancer cell death by apoptosis as detected by TUNEL and annexin V staining. Additionally, we detected that ABTL0812 treatment induces caspases activation in a dose-dependent manner, including the initiator caspases 8 (death receptor/extrinsic apoptotic pathway) and 9 (mitochondrial/intrinsic apoptotic pathway) and the effector caspase 3.

As mentioned before, glioblastoma cells through PMT can progress to a more invasive and aggressive phenotype that correlates with treatment resistance and disease recurrence. Considering the therapeutics implications of PMT we studied the phenotype of glioblastoma cells after treatment with ABTL0812. We detected that ABTL0812 reverted the mesenchymal phenotype of glioblastoma cells to a more differentiated phenotype. Consequently, when cell invasion was assessed, ABTL0812 was shown to decrease cell invasiveness. This is the first report showing that ABTL0812 can revert mesenchymal phenotype and invasion in cancer cells, an effect that support the therapeutic potential of ABTL0812 against metastasis, development of anticancer therapy resistance, and disease recurrence. Additionally, in this study, we found for the first time that ABTL0812 decreases vascularization and induces hypoxia. Angiogenesis is a key step in tumor progression and, therefore, its inhibition might also contribute to ABTL0812 anticancer action.

The anticancer efficacy of ABTL0812 was studied in animal models using xenograft subcutaneous and intra-brain orthotopic models. ABTL0812 was tested in two subcutaneous models using glioblastoma cell lines U87MG and T98G. In both models

ABTL0812 significantly reduced tumor weight compared to vehicle. Moreover, ABTL0812 efficacy was dose dependent as shown by a significantly higher effect of ABTL0812 at 240mg/kg compared to 120mg/kg. For the intra-brain models the U87MG cell line and the GSCs-5 patient stem cells were used. In both models, ABTL0812 increased disease-free survival (time to tumor onset) and overall survival in a dose dependent manner.

The PAM pathway has a key role in the development and progression of glioblastoma, as well as in the development of resistance to current treatments. PAM inhibitors are being investigated for the treatment of human glioma, however, the clinical results obtained to date have not met the expectations. The clinical use of PAM inhibitors is restricted by its poorly tolerance, and by its limited efficacy, that might come by complex regulation of the pathway (45). ABTL0812 has been demonstrated to be safe and well tolerated. In addition, ABTL0812 uses a novel mechanism of action to inhibit the Akt/mTORC axis by inducing TRIB3, a pseudokinase that binds to Akt and impedes its phosphorylation and activation. This novel mechanism to inhibit the PAM pathway avoids some feedback loops that might be limiting the efficacy of other PAM inhibitors. Moreover, ABTL0812 has a second action by inducing ER stress and UPR. In order to compare ABTL0812 anticancer efficacy with mTORC inhibitors, the most clinically advanced mTORC1 inhibitor everolimus was tested in *in vivo* models. Previous preclinical studies have shown the efficacy of the rapamycin derivative everolimus in glioblastoma mice models (46, 47). In the two subcutaneous xenograft models studied, both doses of ABTL0812 were significantly more efficacious than everolimus. The superiority of ABTL0812 compared to everolimus was also demonstrated in the two intra-brain xenograft models used. Therefore, these results support the clinical investigation of ABTL0812 for the treatment of glioblastoma.

Cancer cells due to its fast proliferation need to synthesize a vast amount of protein which can result in misfolded proteins that can induce ER stress and UPR. These characteristic of tumor cells can be exploited as a therapeutic strategy by overstimulating ER stress and UPR to induce cancer cell death (48, 49). Preclinical studies in glioblastoma models have shown the anticancer efficacy of ER stress inducers that include small molecules and natural compounds (50). This therapeutic strategy is already being tested in clinical trials, currently, an ongoing study is investigating TN-TC11G (9-tetrahydrocannabinol + CBD) in combination with temozolomide and radiotherapy in patients with newly diagnosed GBM (NCT03529448). As mentioned above, in this study we have shown that ABTL0812 induces the ER stress UPR, more specifically the PERK-eIF2α-ATF4-CHOP-TRIB3 pathway. This action in conjunction with the Akt/mTORC1 inhibition leads to the activation of cytotoxic autophagy. Therefore, ABTL0812 treatment combines two therapeutic strategies that are under clinical investigation for the treatment of glioblastoma: the inhibition of PAM pathway and the activation of ER stress/UPR, highlighting its potential as novel therapy for these aggressive tumors.

Previous preclinical and clinical data has shown that the most promising therapeutic strategy for the clinical use of ABTL0812 to treat cancer is in combination with standard of care chemotherapies (15, 16, 18, 20, 21). Hence, we decided to study the potential of combining ABTL0812 with the standard of care therapies for glioblastoma: radiotherapy and temozolomide. In a glioblastoma orthotopic mouse model we evaluated OS, and we detected that ABTL0812 efficacy in monotherapy is similar to temozolomide and radiotherapy as single agents. The combination of ABTL0812 with either radiotherapy or temozolomide significantly increase its anticancer efficacy, however, the highest efficacy was detected with the combination of ABTL0812 with both radiotherapy and temozolomide. Therefore, these data shows that the most promising therapeutic option for the treatment of glioblastoma with ABTL0812 is in combination with the standard of care regimen of radiotherapy and chemotherapy and supports the clinical investigation of a triple combination of ABTL0812 + radiotherapy + temozolomide, even more considering that ABTL0812 is well tolerated in humans.

In summary, this study demonstrated the anticancer efficacy of ABTL0812 as single agent and in combination with glioblastoma standard of care treatments in preclinical glioblastoma models including patient-derived stem cells. We showed that the therapeutics actions of ABTL0812 in glioblastoma models included decrease of cell proliferation, induction of differentiation to a less malignant phenotype, induction of autophagy-mediated cell death and decrease of angiogenesis. In conclusion, our findings support ABTL0812 as a potential novel therapeutic agent for the treatment of glioblastoma.

Data availability statement

The raw data supporting the conclusions of this article will be made available by the authors, without undue reservation.

Ethics statement

The animal study was reviewed and approved by Medical School and Science and Technology and Ministero della Salute Animale Rome Italy.

Author contributions

CF, HP-M, MY-V, JA, CD designed and supervised research. AM, AC, LC, AR and VM performed the experiments. VM, GG, HP-M, MY-V, JA, and CF wrote or reviewed the manuscript. All authors contributed to the article and approved the submitted version.

Funding

This research was funded by Ability Pharmaceuticals and the ALCLI "Giorgio e Silvia" a Not-for-Profit cancer association in Rieti.

Conflict of interest

HP-M, MY-V, JA, and CD are employees of Ability Pharmaceuticals.

The remaining authors declare that the research was conducted in the absence of any commercial or financial relationships that could be constructed as a potential conflict of interest.

Publisher's note

Supplementary material

The Supplementary Material for this article can be found online at: https://www.frontiersin.org/articles/10.3389/fonc.2022.943064/full#supplementary-material

References

1. Huang Q, Li F, Chen Y, Hong F, Wang H, Chen J. Prognostic factors and clinical outcomes in adult primary gliosarcoma patients: a surveillance, epidemiology, and end results (SEER) analysis from 2004 to 2015. *Br J Neurosurg* (2019) 12:1–7. doi: 10.1080/02688697.2019.1699903

2. Alifieris C, Trafalis DT. Glioblastoma multiforme: Pathogenesis and treatment. *Pharmacol Ther* (2015) 152:63–82. doi: 10.1016/j.pharmthera.2015.05.005

3. Katsigiannis S, Krischek B, Barleanu S, Grau S, Galldiks N, Timmer M, et al. Impact of time to initiation of radiotherapy on survival after resection of newly diagnosed glioblastoma. *Radiat Oncol* (2019) 14:73. doi: 10.1186/s13014-019-1272-6

4. Sonoda Y. Clinical impact of revisions to the WHO classification of diffuse gliomas and associated future problems. *Int J Clin Oncol* (2020) 25:1004–09. doi: 10.1007/s10147-020-01628-7

5. Saito N, Hirai N, Aoki K, Sato S, Suzuki R, Hiramoto Y, et al. Genetic and lineage classification of glioma-initiating cells identifies a clinically relevant glioblastoma model. *Cancers (Basel)* (2019) 11:1564–79. doi: 10.3390/cancers11101564

6. Fedele M, Cerchia L, Pegoraro S, Sgarra R, Manfioletti G. Proneural-mesenchymal transition: Phenotypic plasticity to acquire multitherapy resistance in glioblastoma. *Int J Mol Sci* (2019) 20(11):2746. doi: 10.3390/ijms20112746

7. Iser IC, Pereira MB, Lenz G, Wink MR. The epithelial-to-Mesenchymal transition-like process in glioblastoma: An updated systematic review and in silico investigation. *Med Res Rev* (2017) 37:271–313. doi: 10.1002/med.21408

8. Tejero R, Huang Y, Katsyv I, Kluge M, Lin JY, Tome-Garcia J, et al. Gene signatures of quiescent glioblastoma cells reveal mesenchymal shift and interactions with niche microenvironment. *EBioMedicine* (2019) 42:252–69. doi: 10.1016/j.ebiom.2019.03.064

9. Zhao K, Cui X, Wang Q, Fang C, Tan Y, Wang Y, et al. RUNX1 contributes to the mesenchymal subtype of glioblastoma in a TGFβ pathway-dependent manner. *Cell Death Dis* (2019) 10:877. doi: 10.1038/s41419-019-2108-x

10. Stanzani E, Martínez-Soler F, Mateos TM, Vidal N, Villanueva A, Pujana MA, et al. Radioresistance of mesenchymal glioblastoma initiating cells correlates with patient outcome and is associated with activation of inflammatory program. *Oncotarget* (2017) 8:73640–53. doi: 10.18632/oncotarget.18363

11. Kaffes I, Szulzewsky F, Chen Z, Herting CJ, Gabanic B, Velázquez Vega JE, et al. Human mesenchymal glioblastomas are characterized by an increased immune cell presence compared to proneural and classical tumors. *Oncoimmunology* (2019) 8:e1655360. doi: 10.1080/2162402X.2019.1655360

12. Guardia GDA, Correa BR, Araujo PR, Qiao M, Burns S, Penalva LOF, et al. Proneural and mesenchymal glioma stem cells display major differences in splicing and lncRNA profiles. *NPJ Genom Med* (2020) 5:2. doi: 10.1038/s41525-019-0108-5

13. Erazo T, Lorente M, López-Plana A, Munoz-Guardiola P, Ferńandez-Nogueira P, Garcia-Martínez JA, et al. The new antitumor drug ABTL0812 inhibits the Akt/mTORC1 axis by upregulating tribbles-3 pseudokinase. *Clin Cancer Res* (2016) 22:2508–19. doi: 10.1158/1078-0432.CCR-15-1808

14. Muñoz-Guardiola P, Casas J, Megías-Roda E, Solé S, Perez-Montoyo H, Yeste-Velasco M, et al. The anti-cancer drug ABTL0812 induces ER stress-mediated cytotoxic autophagy by increasing dihydroceramide levels in cancer cells. *Autophagy* (2020) 17:1349–66. doi: 10.1080/15548627.2020.1761651

15. Felip I, Moiola CP, Megino-Luque C, Lopez-Gil C, Cabrera S, Solé-Sánchez S, et al. Therapeutic potential of the new TRIB3-mediated cell autophagy anticancer drug ABTL0812 in endometrial cancer. *Gynecol Oncol* (2019) 153(2):425–35. doi: 10.1016/j.ygyno.2019.03.002

16. López-Plana A, Fernández-Nogueira P, Muñoz-Guardiola P, Solé-Sánchez S, Megías-Roda E, Pérez-Montoyo H, et al. The novel proautophagy anticancer drug ABTL0812 potentiates chemotherapy in adenocarcinoma and squamous nonsmall cell lung cancer. *Int J Cancer* (2020) 147(4):1163–79. doi: 10.1002/ijc.32865

17. París-Coderch L, Soriano A, Jiménez C, Erazo T, Muñoz-Guardiola P, Masanas M, et al. The antitumour drug ABTL0812 impairs neuroblastoma growth through endoplasmic reticulum stress-mediated autophagy and apoptosis. *Cell Death Dis* (2020) 11(9):773. doi: 10.1038/s41419-020-02986-w

18. Polonio-Alcalá E, Solé-Sánchez S, Muñoz-Guardiola P, Megías-Roda E, Perez-Montoyo H, Yeste-Velasco M, et al. ABTL0812 enhances antitumor effect of paclitaxel and reverts chemoresistance in triple-negative breast cancer models. *Cancer Commun (Lond)* (2022) 42(6):567–71. doi: 10.1002/cac2.12282

19. Vidal L, Victoria I, Gaba L, Martín MG, Brunet M, Colom H, et al. A first-in-human phase I/Ib dose-escalation clinical trial of the autophagy inducer ABTL0812 in patients with advanced solid tumours. *Eur J Cancer* (2021) 146:87–94. doi: 10.1016/j.ejca.2020.12.019

20. Leary A, Estévez-García P, Sabatier R, Estévez-García P, Sabatier R, Fariñas-Madrid L, Pérez-Fidalgo JA, Romeo M, et al. Phase II of ABTL0812, a pro-autophagic drug, in combination with paclitaxel and carboplatin (P/C) as first-line treatment in advanced/recurrent endometrial cancer. *Ann Oncol* (2020) 31(Suppl 4):S639–40. doi: 10.1016/j.annonc.2020.08.1003

21. Bosch-Barrera J, Moran T, Estévez-García P, Martin-Martorell P, Sabatier R, Nadal E, et al. Phase 2 of pro-autophagic drug ABTL0812 in combination with first-line paclitaxel and carboplatin in IIIb/IV squamous NSCLC. *J Thor Oncol* (2021) 16(3):S130–1. doi: 10.1016/j.jtho.2021.01.202

22. Galluzzi L, Baehrecke EH, Ballabio A, Boya P, Bravo-San Pedro JM, Cecconi F, et al. Molecular definitions of autophagy and related processes. *EMBO J* (2017) 40:280–93. doi: 10.15252/embj.201796697

23. Kroemer G, Mariño G, Levine B. Autophagy and the integrated stress response. *Mol Cell* (2010) 20:243-51. doi: 10.1016/j.molcel.2010.09.023

24. Rybstein MD, Bravo-San Pedro JM, Kroemer G, Galluzzi L. The autophagic network and cancer. *Nat Cell Biol* (2018) 4:e892. doi: 10.1038/s41556-018-0042-2

25. Liu B, Wen X, Cheng Y. Survival or death: Disequilibrating the oncogenic and tumor suppressive autophagy in cancer. *Cell Death Dis* (2013) 18:1959–81. doi: 10.1038/cddis.2013.422

26. Byun S, Lee E, Lee KW. Therapeutic implications of autophagy inducers in immunological disorders, infection, and cancer. *Int J Mol Sci* (2017) 119:2460-9. doi: 10.3390/ijms18091959

27. Bahrami A, Khazaei M, Hasanzadeh M, ShahidSales S, Joudi Mashhad M, Farazestanian M, et al. Therapeutic potential of targeting PI3K/AKT pathway in

treatment of colorectal cancer: Rational and progress. *J Cell Biochem* (2018) 119:2460–9. doi: 10.1002/jcb.25950

28. Marquard FE. Jücker m PI3K/AKT/mTOR signaling as a molecular target in head and neck cancer. *Biochem Pharmacol* (2020) 172:113729. doi: 10.1016/j.bcp.2019.113729

29. Tan AC. Targeting the PI3K/Akt/mTOR pathway in non-small cell lung cancer (NSCLC). *Thorac Cancer* (2020) 11(3):511–8. doi: 10.1111/1759-7714.13328

30. Roncolato F, Lindemann K, Willson ML, Martyn J. Mileshkin L.PI3K/AKT/mTOR inhibitors for advanced or recurrent endometrial cancer. *Cochrane Database Syst Rev* (2019) 10:CD012160. doi: 10.1002/14651858.CD012160.pub2

31. Li X, Wu C, Chen N, Gu H, Yen A, Cao L, et al. PI3K/Akt/mTOR signaling pathway and targeted therapy for glioblastoma. *Oncotarget* (2016) 7(22):33440–50. doi: 10.18632/oncotarget.7961

32. Luchman HA, Stechishin OD, Dang NH, Blough MD, Chesnelong C, Kelly JJ, et al. An *in vivo* patient-derived model of endogenous IDH1-mutant glioma. *Neuro-Oncology* (2012) 14:184–91. doi: 10.1093/neuonc/nor207

33. Mendiburu-Elicabe M, Gil-Ranedo J, Izquierdo M. Efficacy of rapamycin against glioblastoma cancer stem cells. *Clin Transl Oncol* (2014) 16:495–502. doi: 10.1007/s12094-013-1109-y

34. Gravina GL, Mancini A, Colapietro A, Delle Monache S, Sferra R, Pompili S, et al. The brain penetrating and dual TORC1/TORC2 inhibitor, RES529, elicits anti-glioma activity and enhances the therapeutic effects of anti-angiogenetic compounds in preclinical murine models. *Cancers (Basel)* (2019) 11:1604–20. doi: 10.3390/cancers11101604

35. Laks DR, Crisman TJ, Shih MY, Mottahedeh J, Gao F, Sperry J, et al. Large-Scale assessment of the gliomasphere model system. *Neuro Oncol* (2016) 18:1367–78. doi: 10.1093/neuonc/now045

36. Gravina GL, Mancini A, Colapietro A, Delle Monache S, Sferra R, Vitale F, et al. The small molecule ephrin receptor inhibitor, GLPG1790, reduces renewal capabilities of cancer stem cells, showing anti-tumour efficacy on preclinical glioblastoma models. *Cancers* (2019) 11:359. doi: 10.3390/cancers11030359

37. Colapietro A, Mancini A, Vitale F, Martellucci S, Angelucci A, Llorens S, et al. Crocetin extracted from saffron shows antitumor effects in models of human glioblastoma. *Int J Mol Sci* (2020) 21(2):423. doi: 10.3390/ijms21020423

38. Gravina GL, Marampon F, Sherris D, Vittorini F, Di Cesare E, Tombolini V, et al. Torc1/Torc2 inhibitor, palomid 529, enhances radiation response modulating CRM1-mediated survivin function and delaying DNA repair in prostate cancer models. *Prostate* (2014) 74:852–68. doi: 10.1002/pros.22804

39. Festuccia C, Gravina GL, Giorgio C, Mancini A, Pellegrini C, Colapietro A, et al. UniPR1331, a small molecule targeting eph/ephrin interaction, prolongs survival in glioblastoma and potentiates the effect of antiangiogenic therapy in mice. *Oncotarget* (2018) 9:24347–63. doi: 10.18632/oncotarget.25272

40. Festuccia C, Gravina GL, Muzi P, Pomante R, Ventura L, Vessella RL, et al. Bologna Bicalutamide increases phospho-akt levels through Her2 in patients with prostate cancer. *M. Endocr Relat Cancer* (2007) 14(3):601–11. doi: 10.1677/ERC-07-0118

41. Takiyama A, Teramoto T, Suzuki H, Yamashiro K, Tanaka S. Persistent homology index as a robust quantitative measure of immunohistochemical scoring. *Sci Rep* (2017) 7(1):14002. doi: 10.1038/s41598-017-14392-y

42. Guo M, Goudarzi KM, Abedi S, Pieber M, Sjöberg E, Behnan J, et al. SFRP2 induces a mesenchymal subtype transition by suppression of SOX2 in glioblastoma. *Oncogene* (2021) 40(32):5066–80. doi: 10.1038/s41388-021-01825-2

43. Ma R, Taphoorn MJB, Plaha P. Advances in the management of glioblastoma. *J Neurol Neurosurg Psychiatry* (2021) 92(10):1103–11. doi: 10.1136/jnnp-2020-325334

44. Yang K, Wu Z, Zhang H, Zhang N, Wu W, Wang Z, et al. Glioma targeted therapy: insight into future of molecular approaches. *Mol Cancer* (2022) 21(1):39. doi: 10.1186/s12943-022-01513-z

45. Papavassiliou KA, Papavassiliou AG. The bumpy road towards mTOR inhibition in glioblastoma: Quo vadis? *Biomedicines* (2021) 9(12):1809. doi: 10.3390/biomedicines9121809

46. Poore B, Yuan M, Arnold A, Price A, Alt J, Rubens JA, et al. Inhibition of mTORC1 in pediatric low-grade glioma depletes glutathione and therapeutically synergizes with carboplatin. *Neuro Oncol* (2019) 21(2):252–63. doi: 10.1093/neuonc/noy150

47. Yang L, Clarke MJ, Carlson BL, Mladek AC, Schroeder MA, Decker P, et al. PTEN loss does not predict for response to RAD001 (Everolimus) in a glioblastoma orthotopic xenograft test panel. *Clin Cancer Res* (2008) 14(12):3993–4001. doi: 10.1158/1078-0432.CCR-07-4152

48. Shi P, Xu J, Xia F, Wang Y, Ren J, Liang P, et al. MOXD1 knockdown suppresses the proliferation and tumor growth of glioblastoma cells *via* ER stress-inducing apoptosis. *Cell Death Discovery* (2022) 8(1):174. doi: 10.1038/s41420-022-00976-9

49. Peñaranda-Fajardo NM, Meijer C, Liang Y, Dijkstra BM, Aguirre-Gamboa R, den Dunnen WFA, et al. ER stress and UPR activation in glioblastoma: identification of a noncanonical PERK mechanism regulating GBM stem cells through SOX2 modulation. *Cell Death Dis* (2019) 10(10):690. doi: 10.1038/s41419-019-1934-1

50. Shi P, Zhang Z, Xu J, Zhang L. Cui h endoplasmic reticulum stress–induced cell death as a potential mechanism for targeted therapy in glioblastoma (Review). *Int J Oncol* (2021) 59(2):60. doi: 10.3892/ijo.2021.5240

frontiers | Frontiers in Oncology

TYPE Original Research
PUBLISHED 08 November 2022
DOI 10.3389/fonc.2022.934159

OPEN ACCESS

EDITED BY
Shengwen Calvin Li,
Children's Hospital of Orange County, United States

REVIEWED BY
Marie Mirouze,
Institut de Recherche Pour le Développement (IRD), France
Roberta Poceviciute,
Bionaut Labs, United States

*CORRESPONDENCE
Lixin Ma
mlx_182019@163.com

†These authors have contributed equally to this work and share first authorship

SPECIALTY SECTION
This article was submitted to Neuro-Oncology and Neurosurgical Oncology, a section of the journal Frontiers in Oncology

RECEIVED 02 May 2022
ACCEPTED 12 October 2022
PUBLISHED 08 November 2022

CITATION
Zhu Y, Liu Z, Guo Y, Li S, Qu Y, Dai L, Chen Y, Ning W, Zhang H and Ma L (2022) Whole-genome sequencing of extrachromosomal circular DNA of cerebrospinal fluid of medulloblastoma.
Front. Oncol. 12:934159.
doi: 10.3389/fonc.2022.934159

Whole-genome sequencing of extrachromosomal circular DNA of cerebrospinal fluid of medulloblastoma

Yi Zhu[1†], Zhihui Liu[2†], Yuduo Guo[3], Shenglun Li[4], Yanming Qu[4], Lin Dai[1], Yujia Chen[4], Weihai Ning[4], Hongwei Zhang[4] and Lixin Ma[4,5*]

[1]Department of Neurosurgery, Binzhou Medical University Hospital, Binzhou, China, [2]Department of Obstetrics and Gynecology, Beijing Chaoyang Hospital, Capital Medical University, Beijing, China, [3]Chinese Academy of Sciences (CAS) Key Laboratory of Infection and Immunity, Institute of biophysics, Chinese Academy of Sciences, Beijing, China, [4]Department of Neurosurgery, Sanbo Brain Hospital, Capital Medical University, Beijing, China, [5]Department of Neurosurgery, Beijing Chaoyang Hospital, Capital Medical University, Beijing, China

Background: Medulloblastoma (MB) is a malignant tumor associated with a poor prognosis in part due to a lack of effective detection methods. Extrachromosomal circular DNA (eccDNA) has been associated with multiple tumors. Nonetheless, little is currently known on eccDNA in MB.

Methods: Genomic features of eccDNAs were identified in MB tissues and matched cerebrospinal fluid (CSF) and compared with corresponding normal samples using Circle map. The nucleotides on both sides of the eccDNAs' breakpoint were analyzed to understand the mechanisms of eccDNA formation. Bioinformatics analysis combined with the Gene Expression Omnibus (GEO) database identified features of eccDNA-related genes in MB. Lasso Cox regression model, univariate and multivariate Cox regression analysis, time-dependent ROC, and Kaplan–Meier curve were used to assess the potential diagnostic and prognostic value of the hub genes.

Results: EccDNA was profiled in matched tumor and CSF samples from MB patients, and control, eccDNA-related genes enriched in MB were identified. The distribution of eccDNAs in the genome was closely related to gene density and the mechanism of eccDNA formation was evaluated. EccDNAs in CSF exhibited similar distribution with matched MB tissues but were differentially expressed between tumor and normal. Ten hub genes prominent in both the eccDNA dataset and the GEO database were selected to classify MB patients to either high- or low-risk groups, and a prognostic nomogram was thus established.

Conclusions: This study provides preliminary evidence of the characteristics and formation mechanism of eccDNAs in MB and CSF. Importantly, eccDNA-associated hub genes in CSF could be used as diagnostic and prognostic biomarkers for MB.

KEYWORDS

extrachromosomal circular DNAs (eccDNAs), medulloblastoma (MB), liquid biopsy, differentially expressed genes, GEO

Introduction

Medulloblastoma (MB) is one of the most common malignant tumors of the central nervous system (CNS) in children, with an annual incidence of about five cases per 1 million people (1), and an overall 5-year survival rate of 70%–85% in the standard-risk group (2, 3) and less than 30% in the high-risk group (4, 5). The diagnosis of MB is mainly based on clinical symptoms, imaging findings, cerebrospinal fluid (CSF) examination, and histopathological examination. With the addition of molecular pathology, the 2016 edition of the World Health Organization (WHO) CNS tumor classification classifies MB into four subgroups (6): wingless pathway (WNT), sonic hedgehog (SHH), Group 3, and Group 4, making the diagnosis and treatment of MB more individualized. However, this raises the demand for accurate detection tools to select the optimal treatment regimen and assess treatment response and monitor relapse. Currently, clinical monitoring of MB is commonly done by magnetic resonance imaging (MRI) and CSF cytology, but the sensitivity of these two methods can be limited by the extent of tumor growth and affect the assessment of the disease (7, 8). Accordingly, there is an urgent clinical need for a more sensitive way to reliably monitor tumor status that may not have changed on imaging.

Extrachromosomal circular DNA (eccDNA) is a type of circular DNA located outside of chromosomes, independent of the traditional genome structure previously thought. Wu et al. published electron microscopy photographs of eccDNA and supported the widespread presence of eccDNA in human tumor cells and normal tissues in 2019 (9). Several studies published subsequently revealed the unique topological structure and genetic properties of eccDNA, which can rapidly remodel the genome through diversity (including structural, functional, and quantitative diversity) and thus are directly and effectively involved in cancer development (9–13). An increasing body of evidence suggests that eccDNAs can be derived from multiple genes and contain one or more gene fragments, intact genes, or regulatory regions; in tumors, eccDNA contains oncogenes or genes associated with drug resistance in cancer therapy (10, 14), tumor heterogeneity, and adaptability. In addition, eccDNA leads to an increase in the copy number of oncogenes (15), resulting in high levels of oncogene products; indeed, oncogene amplification on eccDNA is significantly more efficient than on chromosomes (10, 16). Current evidence suggests that eccDNA abundance is significantly associated with cancer progression and poor prognosis in various tumors (16). Taken together, the above findings indicate the great potential of eccDNA in cancer therapy.

Ana C. de Carvalho et al. found that the regulation of epidermal growth factor receptor (EGFR) VIII expression by eccDNA in glioblastoma (GBM) is significantly associated with resistance to EGFR inhibitors (11). Another report found that eccDNA is involved in and promotes most genomic rearrangements in neuroblastoma that induce mutant phenotypes, leading to tumor development and affecting patient survival (10). It is highly conceivable that eccDNA in MB may have some hitherto unexplored but important functions and molecular mechanisms. That eccDNA has potential in clinical diagnosis is demonstrated by the fact that fetal- and maternal-derived eccDNAs exist simultaneously in the plasma of pregnant women, with significant differences in fragment size and chromosome distribution (17), Similarly, eccDNA also holds promise in cancer diagnostics because eccDNA could be released from tumors (18). Importantly, eccDNAs are more stable than linear DNAs in blood circulation, suggesting that eccDNAs have the potential for clinical application as a novel cancer biomarker in liquid biopsies (19).

Considering the importance of eccDNA in cancer, here we investigated the mechanism of eccDNA formation in MB and the diagnostic potential of profiling eccDNA in CSF samples. We reasoned that, for diagnostic purposes, CSF samples are superior to both MB tissue and plasma samples, are relatively easy to obtain, and are in direct contact with MB tissue. For this purpose, eccDNA was profiled in matched tumor and CSF samples from $n = 3$ MB samples and $n = 1$ control; one separate MB tissue was also included in the MB group. To classify MB patients into high- or low-risk groups, 10 hub genes prominent in both our eccDNA data and gene expression profiles in high- and low-risk MB patients as well as controls from databases were selected. Finally, the selected genes were

used to establish a prognostic nomogram and evaluate the diagnostic potential of eccDNA in MB.

Materials and methods

Sample collection and DNA preparation

MB tissue samples and matched CSF samples were obtained from four patients who underwent surgery at the Department of Neurosurgery, Sanbo Brain Hospital, Capital Medical University (Beijing, China) between January 2020 and November 2021, with a pathological diagnosis of MB. After harvesting, the tumor tissues were rapidly frozen in liquid nitrogen and stored in a −80°C refrigerator. CSF was processed using a standardized protocol and immediately stored in a −80°C refrigerator. All patients provided informed consent, and the protocols used in this study were approved by the local institutional review board.

Sequencing and analysis of eccDNA

The eccDNA extraction, enrichment, and amplification procedures were conducted as previously described in the literature with slight modifications (19, 20). DNA quantification and detection of DNA integrity were performed by a Qubit 3.0 fluorometer (Table S1) and agarose gel electrophoresis (Figure S1A), respectively. Agilent 2100 Bioanalyzer (Agilent Technologies, Inc., USA) was used to determine the library quality (Figure S1B) (Table S2). Circle-Seq and Circulome-seq eccDNA sequencing Service was provided by CloudSeq Biotech Inc. (Shanghai, China).

(1) Tissue DNA Library Preparation and Sequencing (19): Tissue samples (6 mg) were placed in a 600-μl L1 buffer (Plasmid Mini AX; A&A Biotechnology: #010-50), and 15 μl of Proteinase K (ThermoFisher: #4333793) was added for incubation overnight at 50°C. The lysed samples were alkaline treated and purified through an ion exchange membrane column, according to the instructions (Plasmid Mini AX; A&A Biotechnology). Column-purified DNAs were digested for 16 h by FastDigest MssI (Thermo Scientific: #FD1344) at 37°C to remove mitochondrial circular DNA, as recommended by the manufacturer's protocol. DNAs were then incubated at 37°C with exonuclease (Plasmid-Safe ATP-dependent DNase, Epicentre: #E3101K); additional ATP (2 μl) and DNase (2.5 μl) were added every 24 h continuously for 1 week to remove the remaining linear DNA, as recommended by the manufacturer's protocol (Plasmid-Safe ATP-dependent DNase, Epicentre). The processed DNAs were used as a template for eccDNA amplification *via* phi29 polymerase reactions (REPLI-g Midi Kit, Qiagen: #150043) at 30°C for 2 days (46–48 h), as recommended by the manufacturer's protocol. Amplified DNAs were sheared with sonication (Bioruptor), and the sequencing libraries were prepared using the NEBNext® Ultra II DNA Library Prep Kit for Illumina (New England Biolabs; #E7645) following the manufacturer's manual. Sequencing was performed on Illumina NovaSeq 6000 with 150-bp paired-end mode according to the manufacturer's instructions.

(2) DNA of CSF library preparation and sequencing (20): The QIAamp Circulating Nucleic Acid Kit (Qiagen: #55114) was used to extract DNA in CSF of four samples (1 ml/sample), as recommended by the manufacturer's protocol. To remove linear DNA, the DNA was digested for 5 min with exonuclease V (New England Biolabs: #M0345S) at 37°C, as recommended by the manufacturer's protocol. The circular structure of eccDNA was opened by transposable enzymes, and the ends of the DNA fragments were attached to the joints. Next, the Klenow enzyme (New England Biolabs: #M0210L) was used to fill these gaps and ends, as recommended by the manufacturer's protocol. Then, these products were amplified and purified by PCR. The sequencing libraries were prepared with the NEBNext® Ultra™ DNA Library Prep Kit (New England Biolabs: #E7645S) following the manufacturer's manual. Agilent 2100 Bioanalyzer (Agilent Technologies, Inc., USA) was used to determine the library quality. DNA libraries were sequenced on Illumina NovaSeq 6000 with 150-bp paired-end mode according to the manufacturer's instructions.

Quantitative PCR was performed with SYBR Premix Ex Taq (Takara: #RR420A) under conditions of 40 cycles of PCR, as recommended by the manufacturer's protocol. COX5B was amplified with the forward primer GGGCACCATTTTCCTTG ATCAT and reverse primer AGTCGCCTGCTCTTCATCAG. Paired-end reads were obtained from the Illumina NovaSeq 6000 sequencer and were quality controlled by Q30 (Table S3). After 3' adaptor-trimming and low-quality read removal by cutadapt software (v1.9.1) (21), the high-quality clean reads were aligned to the reference genome with Burrows–Wheeler Alignment (BWA) software (v0.7.12) (22). Then, Circle-Map (v1.1.4) (23) was used to detect eccDNA within all samples, and Samtools (v0.2) (24) was used to obtain raw soft-clipped read counts of the breakpoint. Then, edgeR (25) (v0.6.9) was used to perform normalization and differentially expressed eccDNA filter by *p*-value and fold change. Bedtools (v2.27.1) (26) was used to annotate the eccDNAs. IGV (27) software (v2.4.10) was used for eccDNA visualization.

Gene enrichment analysis

To better understand the functions of the known or predicted genes, Gene Ontology (GO) analysis was conducted in terms of biological process (BP), cellular component (CC), and molecular function (MF) by the "clusterProfiler" R package (4.0.5). The "clusterProfiler" was used to understand the

relationship between genes and pathways provided by the Kyoto Encyclopedia of Genes and Genomes (KEGG) pathway database (28).

Acquisition of gene expression and clinical data

The patient's data for MB tissues and normal brain tissues gene expression and platform profiles of GSE85217 (29) and GSE124814 (30) were downloaded from the National Center for Biotechnology Information Gene Expression Omnibus (NCBI-GEO) (http://www.ncbi.nlm.nih.gov/geo). According to the annotation information on the platform, the probes were converted into corresponding gene symbols. A total of 337 patients with clinical survival and follow-up information from dataset GSE85217 were included in the survival analysis as the training cohort.

Construction of the gene signature model and validation

The univariate analysis was performed by the "survival" and "survminer" R packages (https://github.com/therneau/survival) (https://github.com/kassambara/survminer) to identify OS-related hub genes. Lasso-penalized Cox regression analysis (31) was performed to construct the prognostic gene signature. The prognostic gene signature was presented as a risk score obtained by the "survival" R package. Taking the median risk score as the cutoff value, 337 patients were divided into high- and low-risk groups. Kaplan–Meier (KM) survival curves and time-dependent receiver operational feature (ROC) curve analyses were generated to assess the predictive capacity of the model (32). Univariate and multivariate Cox regression analyses were performed to evaluate the survival status. The hazard ratio (HR) and 95% confidence interval (CI) were calculated to identify genes related to overall survival (OS). The area under the curve (AUC) of the ROC was used to compare the diagnostic and prognostic abilities of different indexes. All independent prognostic parameters and corresponding clinical data were included in a prognostic nomogram constructed by a stepwise Cox regression model to predict the 3-, 5-, and 10-year OS of MB patients in the training set.

Statistical analysis

All statistical analyses were performed by R software version 4.1.2 and visualized by GraphPad Prism 8.0 (GraphPad Software, La Jolla, CA, USA) and the "ggplot" R package (https://ggplot2.tidyverse.org/). Average and standard deviations were calculated for all data; as the underlying data distribution was unknown, Wilcoxon rank-sum test and Friedman test were applied to compare data from two or more groups using GraphPad Prism 8.0. In the enrichment analysis, the Benjamini and Hochberg (1995) test (33) has been applied to evaluate GO ID; a false discovery rate (FDR) < 0.25 and adj.p <0.05 were considered statistically significant. Lasso-penalized Cox regression analysis was performed to construct the prognostic gene signature. The KM method was used to compare OS between the two groups, and the logarithmic rank test was used to assess the difference in survival curves. Univariate and multivariate Cox regression analyses were performed to evaluate the survival status, and the hazard ratio (HR) and 95% confidence interval (CI) estimated the hazard risk of the individual indicators. p-value < 0.05 was statistically significant unless otherwise specified. * represents $p < 0.05$, ** represents $p < 0.01$, and *** represents $p < 0.001$.

Results

Identification and verification of eccDNAs from tissue and CSF

We adopted two different processes based on the Circle-Seq (19, 34, 35) method for better extraction and enrichment of eccDNAs in tissue and CSF, respectively. The samples were divided into two groups, one with tissue and matched CSF from MB ($n = 3$) and the other with normal ($n = 1$); one separate MB tissue sample was also included in the MB group. For tissue samples, column separation of eccDNA was used and incubated with exonuclease for better removal of linear genomic DNA. Then, the products were rolling-circle amplified before being sheared by sonication, and the fragmented DNAs were later used for library preparation for next-generation sequencing. For CSF samples, linear DNAs were removed directly using exonuclease V (Exo V), the circular structure of eccDNAs was opened by transposable enzyme, and the Klenow enzyme was used for gap/end repair. Finally, a polymerase chain reaction (PCR) was performed to amplify and purify the products for sequencing. Referring to Circle-Seq (19), COX5B, a gene absent from eccDNA, was measured using quantitative PCR (qPCR) to verify that linear DNA was removed after exonuclease treatment (Table S3). The overall process is shown in Figure 1A. Original reads were quality controlled by Q30 (Table S4), low-quality reads were removed, and the high-quality clean reads were aligned to the reference genome with BWA (22) (Table S5). Then, Circle-Map (23) software was used to detect eccDNA within all samples and obtain raw soft-clipped read counts of the breakpoint. Finally, more than 30,000 different eccDNAs (average: 6,718; median: 5,472) were identified from nine samples.

10.3389/fonc.2022.934159

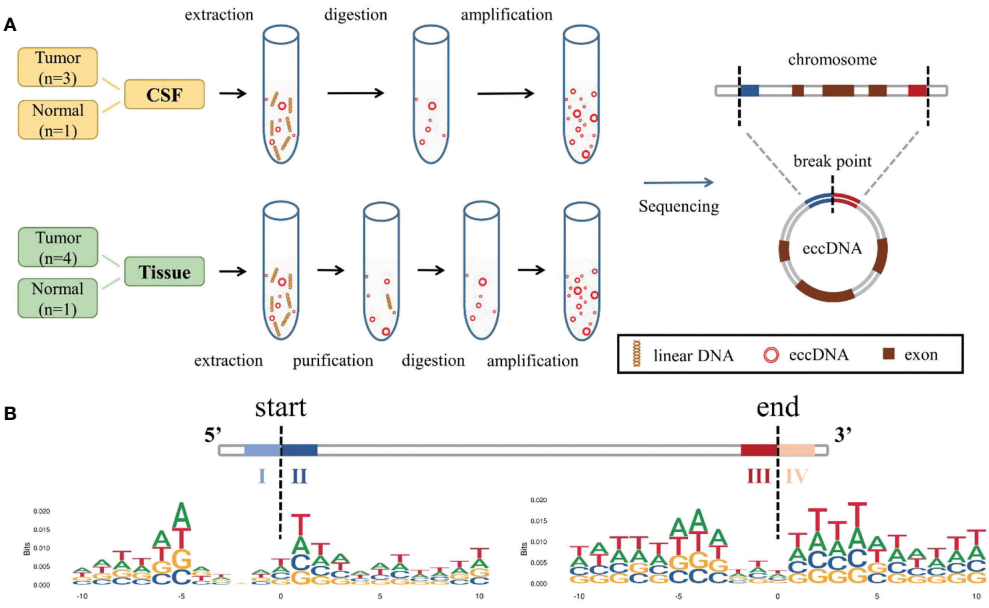

FIGURE 1
Identification and mapping process of eccDNAs in samples. **(A)** Two different methods were used to extract, enrich, and amplify eccDNAs from MB tissue samples and CSF samples, respectively, then compared to the reference genome. **(B)** Trinucleotide motif sequences flanking the start and end positions of eccDNA in normal CSF were labeled as I, II, III, and IV. eccDNAs, extrachromosomal circular DNAs; MB, medulloblastoma; CSF, cerebrospinal fluid.

We explored the possible mechanism of eccDNA formation by analyzing DNA sequences from 10 bp upstream to 10 bp downstream of the start and end positions of each eccDNA; the eccDNA sequences were acquired from our data, while sequences besides the eccDNA sequences were inferred from the reference genome. Trinucleotide motif sequences flanking the start and end positions of eccDNA in each group were labeled as I, II, III, and IV, respectively (Figure 1B, Figures S2A–C).

Detection and analysis of eccDNAs in different samples

A total of 35,179 eccDNAs was detected in nine samples, containing 34,308 eccDNAs in tissue samples and 12,058 eccDNAs in CSF samples. These eccDNAs originated from all chromosomes; however, chromosome 17 exhibited the highest density of eccDNAs and was associated with more DNA damage-repair-related genes (Figures 2A, B) (36, 37). Interestingly, we found the least number of eccDNA on chromosome Y in normal tissue and CSF samples, consistent with the eccDNA profile reported in the previous literature (19). Localization of eccDNA to different component regions of the genome was conducted as previously described in the literature, defined as the percentage of eccDNA localized to that class of genomic regions divided by the percentage of the genome covered by that class of genomic regions (17). We found that eccDNAs were enriched in 5'-untranslated regions (5'UTRs) and Alu repeat regions, with the lowest distributions in the intronic regions (Figure 2C). The size of eccDNAs of all samples ranged from 32 to 7,239,203 bp, with 16 eccDNAs larger than 1 MB (0.4548‰), and most (35,098/35,179, 99.77%) eccDNAs were less than 2 kb with the median size of 272 and 279 bp in tissue and CSF, respectively (Figure S3A). Both tissue and CSF eccDNAs showed no variability in length distribution and exhibited two distinctive peaks at 201 bp and 360 bp (Figure 2D).

Meanwhile, after mapping all eccDNAs detected onto the whole genomic chromosomal region, 47.57% (16,733/35,179) of eccDNA overlapped with gene regions, of which 47.50% (16,297/34,308) and 50.07% (6,038/12,058) of eccDNAs covered gene fragments in tissue and CSF samples, respectively; 97.87% (34,428/35,179) of the detected eccDNAs were mapped to only one gene region. Unexpectedly, some could carry multiple gene fragments (Figures 2E, F); eight of all eccDNAs contained more than 15 gene fragments, which are not shown here considering that they may be due to chromosomal rearrangements. In addition, we found that 77.35% (13,943/18,026) of genes were

10.3389/fonc.2022.934159

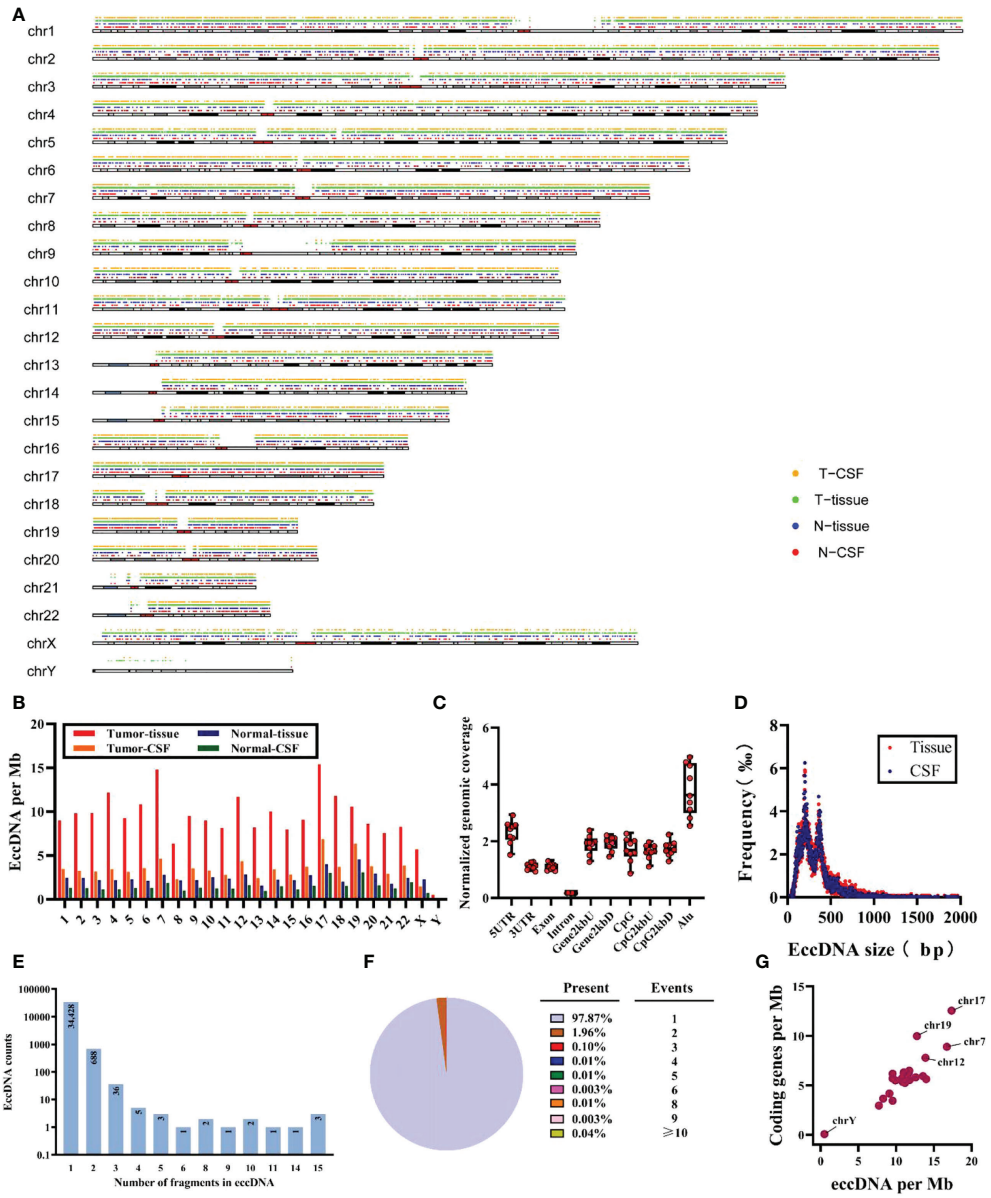

FIGURE 2
Characteristics of total eccDNAs. **(A)** Distribution for eccDNAs of four sample groups in chromosomes. **(B)** Frequency (per Mb) of distribution of eccDNAs in 23 pairs of chromosomes for each group. **(C)** The distribution of all samples of eccDNAs in different genomic regions. **(D)** Size distribution and relative abundance of eccDNAs in tissue (red) and CSF (blue), data from all samples. **(E, F)** The counts and proportion of eccDNAs in all samples cover different numbers of gene fragments. **(G)** The ratio of coding genes/Mb and eccDNAs/Mb in 23 pairs of chromosomes from analysis of all samples. Mb, megabase.

present on more than two eccDNAs (Figure S3B), and the CNTNAP2 gene formed 43 unique eccDNAs, which may be related to the fact that CNTNAP2 encompasses almost 1.5% of chromosome 7 and is one of the largest genes in the human genome (38). Finally, as shown in Figure 2G, a positive correlation was found between eccDNAs/Mb and encoding genes/Mb, with a significantly higher average rate of eccDNA/Mb for chromosome 17 compared to other chromosomes.

Differentially expressed eccDNAs between MB and normal tissues

Next, we compared whether there were differences in eccDNAs between tumor and normal samples. As shown in Figure 3A, 24,873 out of 35,179 eccDNAs were present only in all tumor samples, 3,553 were present in the normal samples, and 6,753 were detected in both samples. However, tumor and

10.3389/fonc.2022.934159

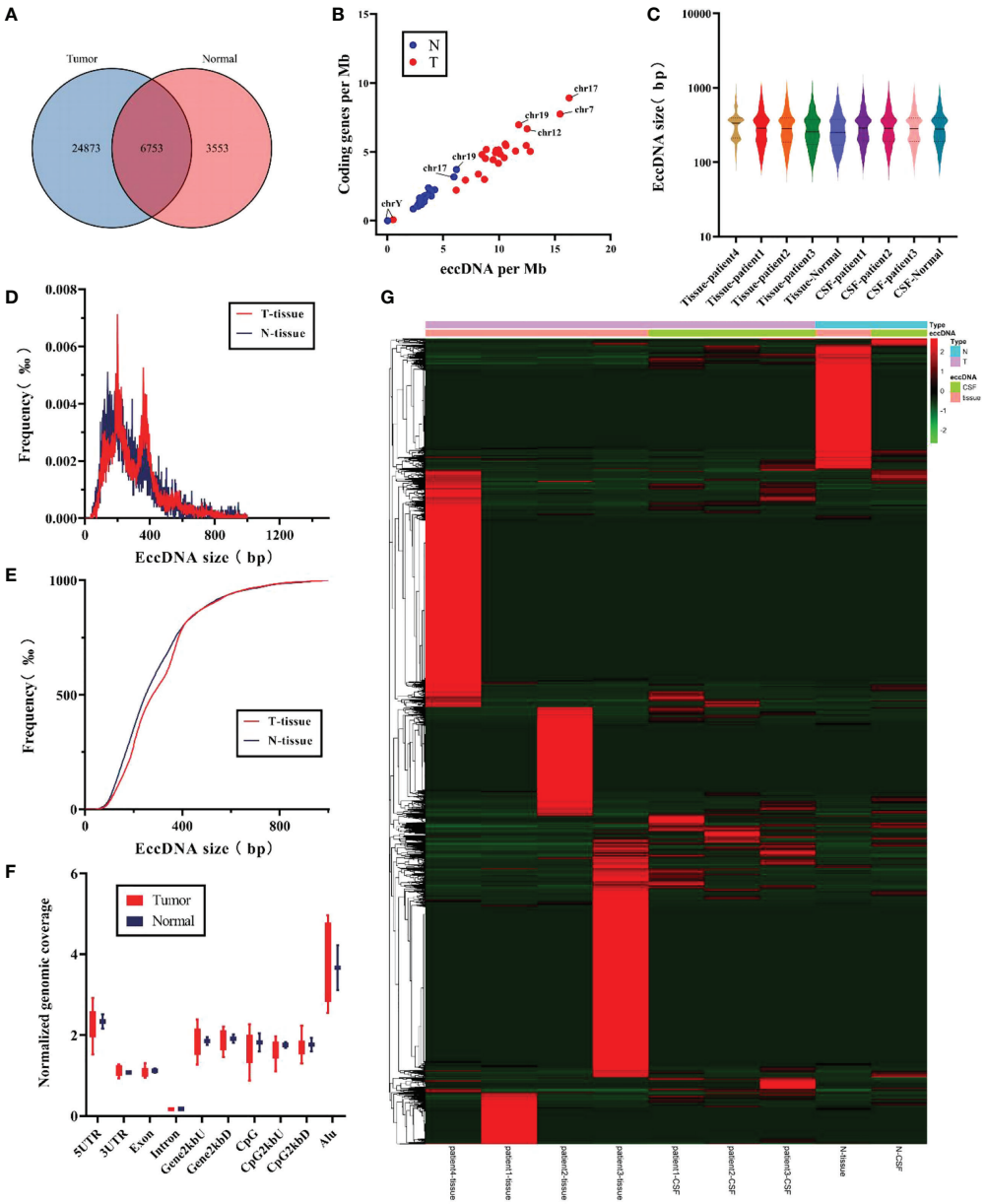

FIGURE 3
Comparison of the characteristics for eccDNAs in tumor samples and normal samples. **(A)** Differences in the counts for eccDNAs were detected in tumor and normal samples. **(B)** The ratio for coding genes/Mb and eccDNAs/Mb of chromosomes in tumor and normal samples. **(C)** Distribution of eccDNA length in each independent sample. **(D, E)** Size distribution of eccDNAs in tissue for tumor (red) and normal (blue). **(F)** Genomic distributions of eccDNAs between tumor (red) and normal (blue). **(G)** Heat map of abundance of eccDNAs in each sample.

normal samples did not show differences between eccDNAs/Mb and encoding genes/Mb (Figure 3B). No significant variation in the length distribution of eccDNAs was found in each sample (Figure 3C). Interestingly, by comparing the length characteristics of eccDNAs of normal and tumor tissue samples, we found peaks of eccDNA at ~201 and ~306 bp in tumor tissues and 140 and 206 bp in normal tissues (Figure 3D). Subsequently, we analyzed the cumulative frequency to further explore the differences in their length characteristics (Figure 3E) and found that the length of normal tissue eccDNAs was smaller than tumor tissues. We compared the distribution of eccDNA length between tumor and normal CSF samples, and no

significant differences were found (Figures S4A, B). Notably, we did not find significant differences in genomic elements of annotated eccDNAs between tumor and normal samples (Figure 3F).

Finally, the abundance of eccDNA in all samples was evaluated, and no significant difference was found (Figure 3G), probably due to the limited number of samples. However, analysis of the abundance of eccDNA in CSF samples showed that some eccDNAs were overexpressed in all three tumor CSF samples compared with normal samples (Figure S4E), suggesting that these eccDNAs have huge prospects for clinical application to distinguish tumors from the normal brain and may be involved in tumorigenesis and progression.

EccDNAs between tissue and matched CSF in MB

To verify whether the states of eccDNAs in tumor tissue and matched CSF were consistent, we investigated the characteristics and abundance levels of eccDNA in three groups of patients,

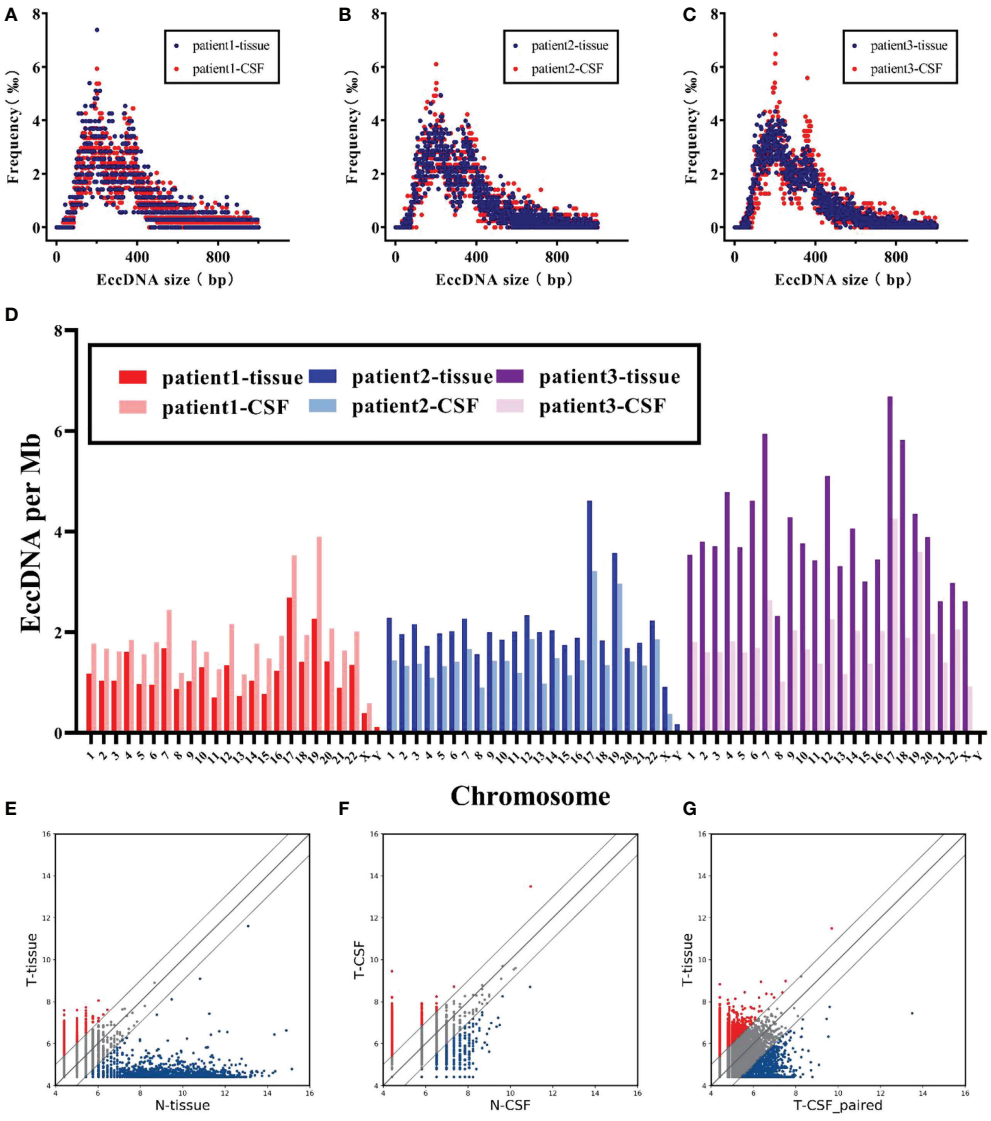

FIGURE 4
Characteristics of eccDNAs were comparable in MB and matched CSF. **(A–C)** Size distribution of eccDNAs in tissue (red) and CSF (blue) for each patient. **(D)** Comparison of chromosomal density trend of eccDNAs in tissue and CSF for three patients. **(E, F)** Scatter plots showing the differential abundance of eccDNAs between MB and normal in tissue and CSF, respectively. **(G)** Correlation of eccDNAs abundance between MB tumors and matched CSF.

respectively. The eccDNA counts of tissue samples and matched CSF samples in the three groups of patients were as follows: group 1 (tissue: 3,508, CSF: 5,340), group 2 (tissue: 6,199, CSF: 4,221), and group 3 (tissue: 12,071, CSF: 5,471), with minimal interindividual differences in each group. As shown in Figures 4A–C, eccDNAs in both the tissue and matched CSF samples of the three groups did not exhibit significant differences in length distribution. On the other hand, tissue samples exhibited similar chromosome distribution with their matched CSF samples to a certain extent (Figure 4D). Finally, we compared the levels of eccDNA abundance between tumor and normal tissue samples, between tumor and normal CSF samples, and between tumor tissue samples and match CSF samples (Figures 4E–G). No significant difference in eccDNA abundance was found between tumor samples and matched CSF samples, suggesting that CSF has huge prospects to replace tumor samples as a means of detection and provides a new direction for monitoring eccDNA abundance levels in MB.

Functional and pathways enrichment of the CSF differentially expressed eccDNAs

GO and KEGG pathway enrichment analyses were used to analyze the biological processes and functions of genes associated with the differentially expressed eccDNAs in CSF samples. As shown in Figure 5A, the top three enriched terms of the biological process associated with upregulated eccDNAs were “dendrite development”, “axonogenesis”, and “regulation of cell morphogenesis involved in differentiation”; the top three enriched terms of the cellular component were “glutamatergic synapse”, “cation channel complex”, and “ion channel complex”; the top three enriched terms of the molecular function were “Ras GTPase binding”, “small GTPase binding”, and “calmodulin binding”. Similarly, the top three enriched biological process terms associated with downregulated eccDNAs were “regulation of ion transmembrane transport”, “axonogenesis”, and “dendrite development”; the top three enriched cellular component terms

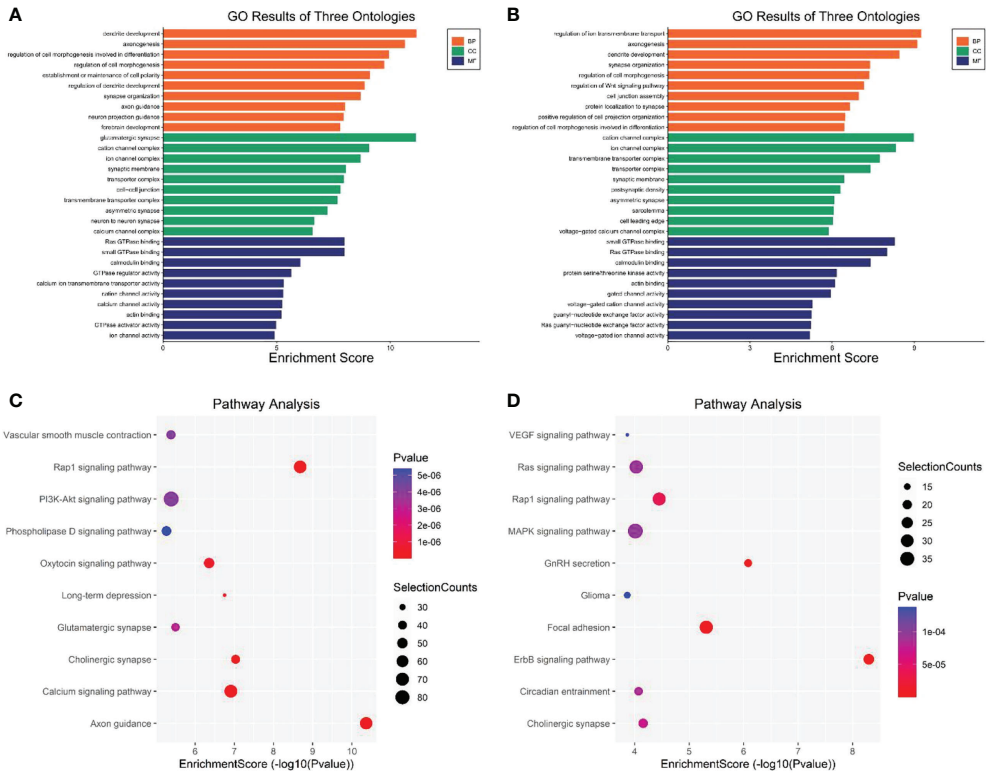

FIGURE 5
GO and KEGG pathway analysis of genes associated with the differentially expressed eccDNAs in CSF between MB and normal tissues. **(A)** Top 10 enriched BP, CC, and MF terms associated with the upregulated eccDNA genes. **(B)** Top 10 enriched BP, CC, and MF terms associated with the downregulated eccDNA genes. **(C, D)** KEGG pathway analysis of the upregulated and downregulated eccDNA genes, respectively. GO, Gene Ontology; KEGG, Kyoto Encyclopedia of Genes and Genomes; BP, biological processes; CC, cellular components, MF molecular functions (http://www.bioinformatics.com.cn/).

were "cation channel complex", "ion channel complex", and "transmembrane transporter complex"; the top three enriched molecular function terms were "small GTPase binding", "Ras GTPase binding", and "calmodulin binding" (Figure 5B). In addition, KEGG pathway analysis showed that genes associated with differentially expressed eccDNA were significantly enriched in "Axon guidance pathway" (upregulated), "Rap1 signaling pathway" (upregulated), and "Cholinergic synapse pathway" (upregulated), and "ErbB signaling pathway" (downregulated), "GnRH secretion pathway" (downregulated), and "Focal adhesion pathway" (downregulated) (Figures 5C, D).

Identification of survival-related hub genes associated with the differentially expressed eccDNAs in the CSF derived from normal and MB subjects

A total of 380 eccDNAs were expressed in three CSFs but not in normal samples. As previously mentioned, these eccDNAs contained 220 gene fragments, considered differential genes between the tumor and normal groups (Figure 6A). These genes were then intersected with genes in datasets GSE85217 and GSE124814, yielding 161 genes for subsequent analysis (Figure 6B). A total of 337 patients with clinical survival and follow-up information from the GEO dataset GSE85217 were included in the following survival analysis as the training cohort. Based on the univariate Cox regression model, 21 hub genes significantly correlated with the OS. Lasso-penalized Cox analysis identified 18 genes to be incorporated in multivariate Cox analysis (Figure 6C), and 10 genes were finally used to establish a prognostic model comprising MSH6, NUP85, TBCK, HERPUD2, ZNF750, BAIAP2L1, IFNGR2, FAM172A, FBXO45, and CFLAR. Interestingly, when we compared the expression of these hub genes with samples in the GSE214814 dataset (n = 1,641: 1,350 MB and 291 normal brain samples), 9 of these genes were differentially expressed ($p < 0.05$) (Figure 6D). Univariate Cox regression analysis demonstrated that these genes were independent prognostic factors of OS ($p < 0.05$), although the multivariate Cox regression analysis showed no significant association between FBXO45 and CFLAR and OS (Table S6). Finally, we included all 10 genes to establish the risk score model (Figure 6E).

Establishment of the prognostic signature of hub genes

The risk score was calculated based on the expression value of hub genes using the R package "survival". Taking the median risk score as a cutoff value, 337 patients were assigned to high- or low-risk groups. The KM survival curve was plotted to compare OS between the two groups, and a significant difference was found ($p < 0.001$) (Figure 7A). The survival curves in Figure S5A demonstrate that the expressions of MSH6 ($p = 0.028$), NUP85 ($p = 0.001$), IFNGR2 ($p = 0.017$), and FBXO45 ($p = 0.05$) were negatively correlated with OS, and TBCK ($p = 0.037$), HERPUD2 ($p = 0.001$), and BAIAP2L1 ($p = 0.008$) were positively correlated. In addition, to assess the predictive power of the hub genes, time-dependent receiver operational characteristic (ROC) curves were used, yielding area under the curve (AUC) values of 0.759, 0.799, and 0.781 for 1-year, 3-year, and 10-year survival, respectively (Figure 7B). This finding suggests that these genes have a high sensitivity and specificity in predicting OS. Meanwhile, we found that the 3- and 10-year AUCs were higher than the 1-year AUC, indicating the stronger predictive power of hub genes for long-term outcomes. Moreover, ROC curve analysis showed that the AUCs of the intersected hub genes were >80% (Figure 7C), suggesting that they have a significant diagnostic value for MB. The individual ROCs for each gene are shown in Figure S5B, revealing the positive value of MSH6 and IFNGR2 as independent diagnostic factors. A comparison of the OS and the expression of 10 genes between the high-risk and low-risk groups showed that the high-risk group was associated with a poorer prognosis (Figure 7D). The expression of the upregulated genes correlated with worse patient prognosis (Figure 7E). As shown in Figure S5C, we established a clinically applicable nomogram for predicting the prognosis of MB patients based on the expression of these hub genes. All independent prognostic and associated gene expression parameters were included in the prognostic nomograms constructed by stepwise Cox regression models to predict 1-, 5-, and 10-year OS of MB patients in the training cohort.

Construction and validation of the predictive nomogram

After verifying that the risk score could be used as an independent factor to predict OS of MB patients ($p < 0.001$), age, gender, tumor metastasis, and molecular subtype were included in our prognostic model (Table S7). Univariate and multivariate Cox regression analysis suggested that risk score ($p < 0.001$), age ($p < 0.05$), and tumor metastasis ($p < 0.01$) were all independent prognostic factors of OS in MB patients, unlike gender and molecular subtype (Figure 8A), consistent with the literature. Next, we established a nomogram to predict the OS of this patient population. The prognostic nomogram was constructed by a stepwise Cox regression model that included risk score, age, tumor metastasis, prognostic parameters, and relevant clinical data, to predict 3-, 5-, and 10-year OS of MB patients in the training cohort (Figure 8B). Finally, we compared the nomogram-predicted 3-

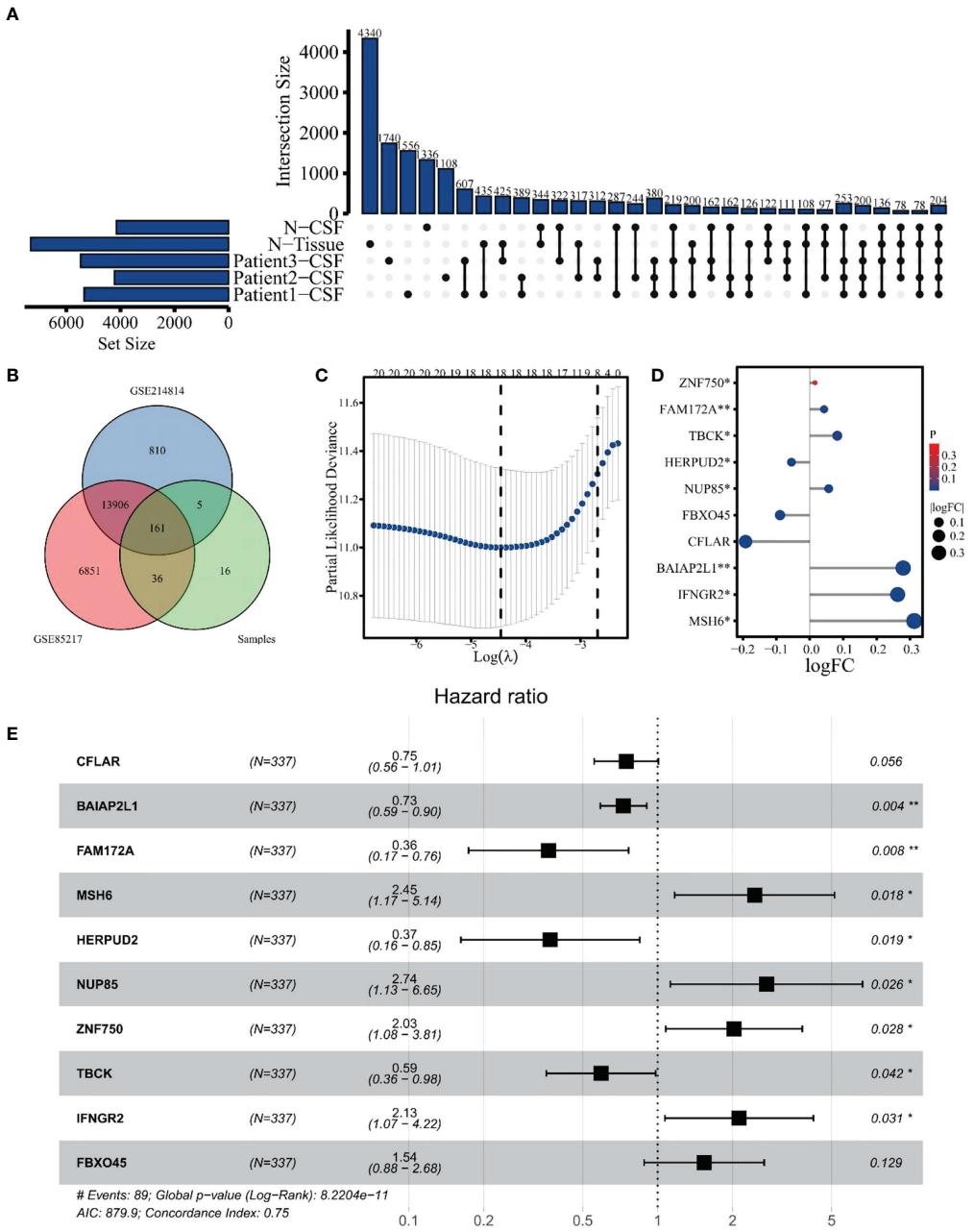

FIGURE 6
Identification of hub genes for differentially expressed eccDNAs in CSF. **(A)** A total of 380 differentially expressed eccDNAs between normal and MB in CSF. **(B)** Venn plot of genes among GSE124814, GSE85217, and data from our cohort. **(C)** Eighteen genes were selected by Lasso-penalized Cox analysis. **(D)** Differential expression of 10 hub genes between normal and tumor samples in dataset GSE124814. **(E)** Ten hub genes associated with OS in the training cohort. The symbol * means FDR adjusted p value for the labeled correlation was less than 0.05, ** means FDR adjusted p value for the labeled correlation was less than 0.01.

, 5-, and 10-year OS with the observed 3-, 5-, and 10-year OS to validate the accuracy of the prognostic model, and both were generally consistent (Figure 8C), highlighting the reliability of our nomogram to predict the survival probability of MB patients.

Discussion

Several studies suggest the presence of eccDNA in human plasma and tissues (17, 19, 39). Here, we extracted eccDNA from MB tumor tissue and matched CSF using two different methods

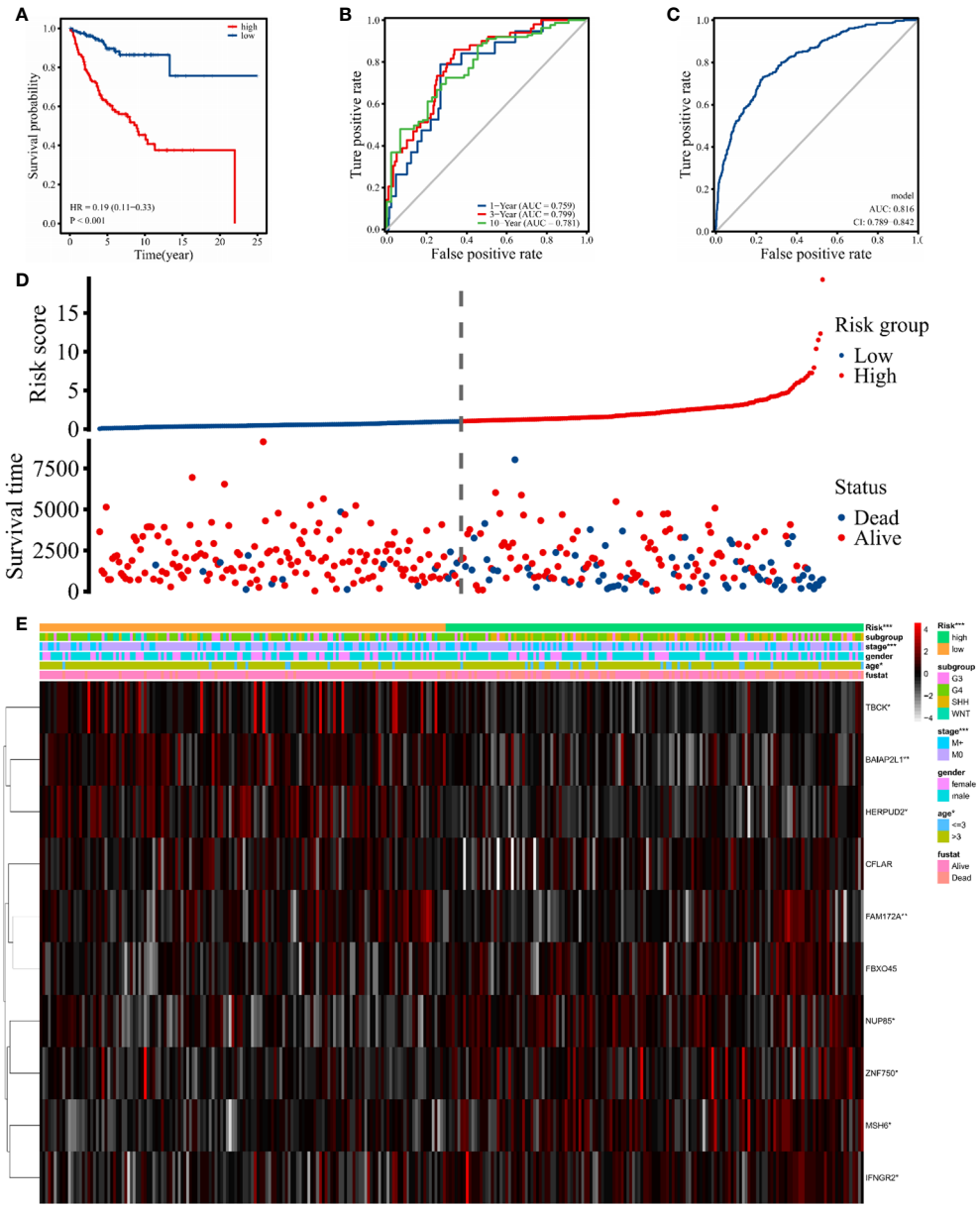

FIGURE 7
Signature-based risk score in the training cohort. **(A)** The Kaplan–Meier survival curves of the high (red) and low (blue) risk groups are based on the 10 hub gene signature. **(B)** The time-dependent ROC curves (1 year, 3 years, and 10 years) of the 10 hub gene signature. **(C)** ROC curve of the sensitivity for MB diagnostic through the 10 hub gene signatures. **(D, E)** Distribution of risk score, survival overview, and heatmap of hub genes in the training cohort. The symbol "*" means FDR adjusted p value for the labeled correlation was less than 0.05, "**" means FDR adjusted p value for the labeled correlation was less than 0.01, and "***" means FDR adjusted p value for the labeled correlation was less than 0.001.

based on Circle-Seq (17, 19, 35), substantiating the existence of eccDNA in CSF. It has been shown that eccDNA is closely related to the development of CNS tumors and affects the prognosis (10, 11, 16). An increasing body of evidence suggests that the genetic characteristics of cell-free tumor DNA (ctDNA) in CSF are consistent with matched CNS tumors and could be a reliable approach for monitoring the status of tumors (40–43). In the present study, we hypothesized that eccDNA might exhibit the genetic characteristics of MB tumors, and detecting the genetic characteristics of eccDNAs in CSF may provide a new direction for clinical diagnosis, treatment, and prognosis.

Importantly, the eccDNAs revealed in this study can be derived from all genomes and are roughly proportional to the

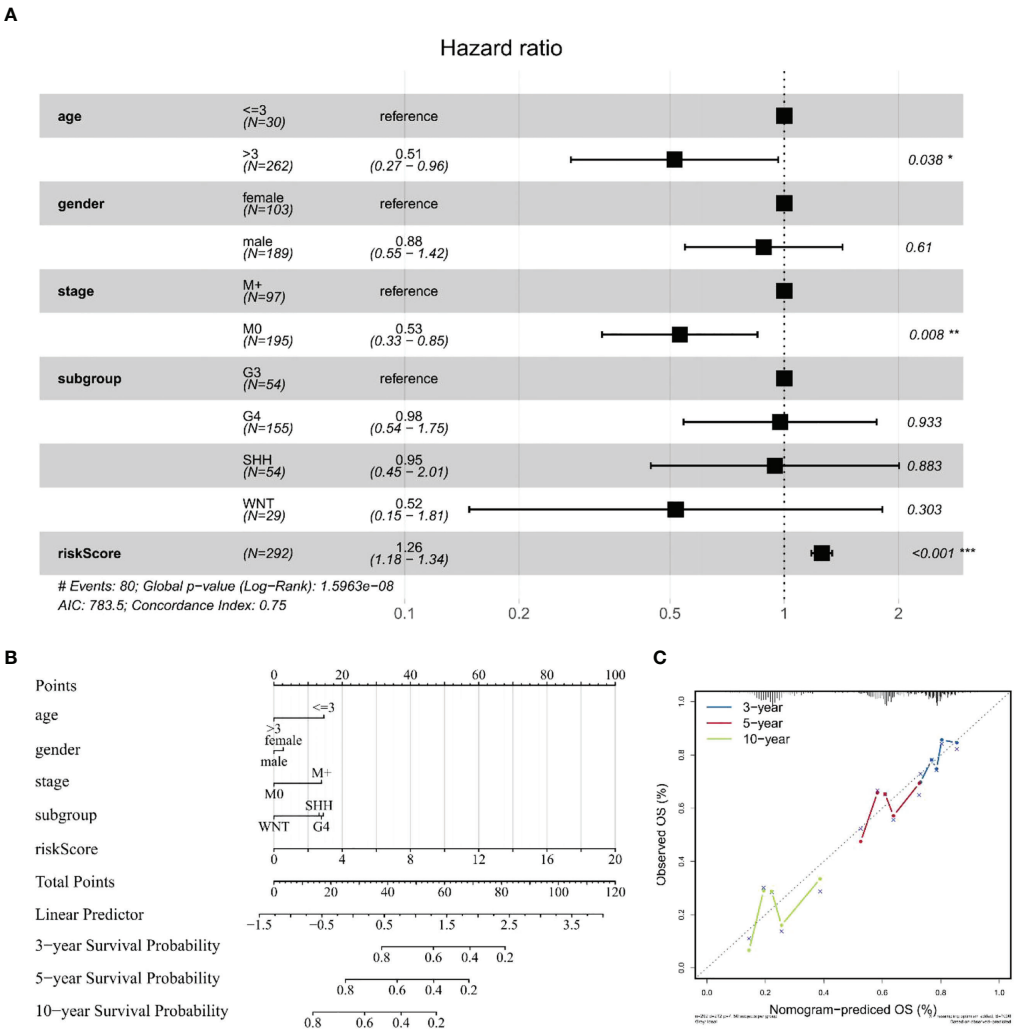

FIGURE 8
Construction and validation of a nomogram for survival prediction. **(A)** Multivariate Cox regression analysis of the association among clinical factors, risk score, and OS. **(B)** Nomogram combining the 10 hub gene signature and clinical factors. **(C)** Validation of the accuracy of the prognostic model with dataset GSE85217. The symbol "*" means FDR adjusted p value for the labeled correlation was less than 0.05, "**" means FDR adjusted p value for the labeled correlation was less than 0.01, and "***" means FDR adjusted p value for the labeled correlation was less than 0.001.

overall abundance of non-repetitive and repetitive sequences in the genome, consistent with the literature (44, 45). Interestingly, the highest density of eccDNA distribution was found on chromosome 17, which may be because human autosomes have the highest gene density on chromosome 17 (46). The least amount of eccDNA was observed on chromosome Y, which has a low gene density. Consistently, when we mapped eccDNA to different classes of genomic elements to investigate their formation preferences, eccDNA was most enriched in the 5'UTR and the Alu repeat regions, which have the highest gene densities (47, 48). The pattern identified here was slightly different from that previously reported in the literature for eccDNAs in mice (49), human plasma (17), and esophageal squamous cell carcinoma (ESCC) (50), possibly due to the unique intracranial environment, although the exact reason remains to be further investigated. This distribution characteristic of eccDNA suggests that its formation may be inextricably linked to high gene density. To further search for the potential mechanism of eccDNA formation, we performed motif analysis of the nucleotide patterns around the breakpoints on both sides of eccDNAs. It has been suggested that double-repeat trinucleotide sequences on both sides of the breakpoints may be associated with eccDNA formation (17, 51), with increasing reports highlighting the presence of microhomologous base

patterns at the junctions of eccDNAs, which can be formed by homologous recombination, microhomology end joining, or nonhomologous end joining-mediated cyclization of DNA (17, 18, 50, 52). A large number of repetitive bases were also identified in our data; unfortunately, after comparison with the repetitive sequences reported in the literature, we did not find any prominent features to prove an association with eccDNA formation. The current method of eccDNA purification is mainly through exonuclease digestion after alkaline lysis to obtain the product (19); this presents a problem that a trace amount of endonuclease activity in the exonuclease can cause eccDNA loss and thereby affect the yield. Mann et al. demonstrated that current research methods on eccDNA may produce false positives in rolling circle amplification (RCA) (53), because of its dependence on many cycles of amplification, and susceptibility to template-switching artifacts. These factors contribute to the general limitations of eccDNA research. A recently published study describes a new three-step eccDNA purification (3SEP) procedure by adding a new step that allows eccDNA purification with high purity and reproducibility (39); however, further details of the comparison between the different methods deserve to be discovered in more studies.

Of 35,179 eccDNAs, 16,733 (47.57%) overlapped with regions encoding genes. Surprisingly, some genes corresponded to multiple eccDNAs. Identification of genes that could form more than 20 eccDNAs showed that they were larger than 1 Mb (Table S8), which may reveal a genetic preference for eccDNA formation.

Consistent with previous studies, most eccDNAs (99.77%) were smaller than 2 kb and exhibited two distinct peaks at 201 bp and 360 bp (19, 54). Comparison of the eccDNA characteristics between the normal and tumor groups showed that the length of normal tissue eccDNAs was smaller than that of tumor tissues, similar to the difference between fetal and maternal eccDNA in the plasma (17). Although we did not observe differences in chromosome distribution, genomic elements of annotated eccDNAs, and repetitive sequences between the tumor and normal groups, the two groups exhibited greater variability in eccDNA abundance level, a phenomenon previously reported in a study on ESCC (50). Surprisingly, the abundance levels of eccDNAs in tumor tissue samples and matched CSF samples were related, while tumor and normal brain tissue samples were significantly different. Furthermore, the morphological characteristics and genomic distribution of eccDNAs in tumor tissue samples and matched CSF samples were consistent, highlighting that eccDNA levels in the CSF of MB patients can reflect the status of eccDNA levels in MB, warranting further investigation. Interestingly, we found that some eccDNAs were expressed in all three tumor CSF samples, which were lowly expressed in normal samples, suggesting that these eccDNAs may be potential biomarkers in distinguishing tumor from normal brain tissue and may be involved in tumorigenesis, progression, and evolution. Although our findings are clinically positive, unfortunately, there were not enough matched normal samples to further validate the differences between the tumor and normal groups, and the samples did not cover all MB subtypes, leaving us unable to investigate the characteristics of eccDNA in each MB subtype, which requires more patient data to increase its robustness.

To understand the underlying mechanisms, GO and KEGG pathway analyses of differentially expressed eccDNA-related genes in tumor CSF samples and normal CSF samples were conducted and revealed enrichment in “dendrite development”, “axonogenesis”, “Axon guidance pathway”, and “Rap1 signaling pathway”, which have been associated with CNS tumors (55, 56).

MB is one of the most common malignant tumors of the CNS in children with a poor prognosis (1, 4, 5). After the new addition of molecular biological markers in the 2016 edition of the World Health Organization (WHO) CNS tumor classification (6), genetic testing plays an important role in the staging and treatment of MB, including CTNNB for the WNT group (57), TP53 for the SHH group (58), MYC or MYCN for group 3 (59), and methylation for group 4 (60); these mutations are strongly associated with poor prognosis in MB patients. The sensitivity of magnetic resonance imaging (MRI) and CSF cytology, currently used in the clinical setting for patients with MB, is limited by the extent of tumor growth (7, 8), and monitoring tumor status that may not be found by imaging techniques can help physicians diagnose and treat earlier, contributing to the OS of patients (61). Importantly, previous literature has shown that the abundance of eccDNA is closely correlated with gene expression profiles (10, 62); thus, we hypothesized that a set of eccDNA-related genes might exhibit better performance in predicting the prognosis of MB patients. Subsequently, we analyzed two mRNA microarray datasets (GSE85217 and GSE124814), combined with the expression data of eccDNA overlapping genes measured in our cohort samples. Univariate Cox analysis, Lasso Cox regression analysis, and multivariate Cox analysis were performed, and 10 hub genes were incorporated to construct the risk model comprising MSH6, NUP85, TBCK, HERPUD2, ZNF750, BAIAP2L1, IFNGR2, FAM172A, FBXO45, and CFLAR. Although these eccDNA-related genes expressed some correlation after comparing our data with GSE124814, which is consistent with previous studies (10, 62), the overall association between the two datasets was not significant due to the different sources. More work will be carried out to reveal the correlation between eccDNA and gene expression profiles in MB by including a larger sample in the future. A total of 337 patients with clinical survival and follow-up information from the GEO dataset GSE85217 were included in the following survival

analysis. We evaluated the model's performance using ROC curves of the risk score obtained from the combined analysis of hub gene expression. ROC curve analysis yielded AUCs of 0.759, 0.799, and 0.781 for survival at 1, 3, and 10 years, respectively, implying that the risk score had high sensitivity and specificity. We also assessed the diagnostic performance of the hub gene in MB patients. Finally, we constructed a nomogram to predict the OS of MB patients, which exhibited better performance than traditional clinical factors (gender, grading, age, etc.), and validated its accuracy and sensitivity using prognostic data from real patients. Compared to previous literature that identified a 12-gene signature (AUC of 1 year = 0.889, AUC of 3 years = 0.681, and AUC of 5 years = 0.703) to predict OS in MB by considering only the GEO database (63), our data (AUC of 1 year = 0.759, AUC of 3 years = 0.799, and AUC of 10 years = 0.781) show stronger long-term predictive power in prognosis, and one strength of eccDNA is the ability to profile it in the CSF. However, this model has not been further validated in experiments and was based on a relatively small sample size of data.

In addition, 7 of these 10 hub genes reportedly participate in the biological processes of the tumor. MSH6 is a protein-coding gene component of the post-replicative DNA mismatch repair system (MMR) and forms a heterodimer with MSH2 to form MutS α, which is involved in DNA repair. Growing evidence suggests that MSH6 expression is significantly associated with tumor drug resistance and poor clinical outcomes, especially in MB, glioblastoma, bladder cancer, and breast cancer (64–66). MSH6 also showed high accuracy and sensitivity in diagnosis and prognosis in our data analysis, highlighting that it is an area worthy of our focus. NUP85 is related to the composition of the Nup107–160 subunit of the nuclear pore complex, mostly associated with nephrotic syndrome (67). Recent studies have identified its possible involvement in tumor development through the immune system and its potential as a new therapeutic target (68). ZNF750 is mainly expressed in squamous epithelial cells, with a nuclear localization signal and a conserved C2H2 zinc finger domain, and has been reported to correlate with the prognosis of ESCC, colonic cancer, and nasopharyngeal carcinoma patients (69–71). BAIAP2L1 is a protein-coding gene belonging to the IRSp53 family, which acts as an insulin receptor (IR) adapter that activates the IR-irs1/2 (insulin receptor substrate 1/2)–AKT signaling pathway by stimulating tyrosine phosphorylation of IR (72). BAIAP2L1 has been reported as a potential biomarker in various tumors (73–75). FAM172A is a newly discovered protein-coding gene whose specific function has not been studied, although it is widely thought to regulate alternative splicing by interacting with AGO2 and CHD7 (76), especially in pancreatic cancer and papillary thyroid carcinoma (76, 77). FBOX45 belongs to the FBXO protein subfamily and has been closely associated with the development of the nervous system. Recent studies have shown that FBOX45 is also involved in cancer development (78, 79), but the exact mechanism has not yet been studied. Moreover, CFLAR (CASP8 And FADD Like Apoptosis Regulator) plays an important role in several cellular processes such as apoptosis, necrosis, autophagy, and inflammation and is structurally similar to caspase-8 (80). An increasing body of evidence from recently published studies suggests that CFLAR overexpression contributes to tumor progression and correlates with a poor clinical outcome in cancers such as prostate, colorectal, gastric cancers, head and neck squamous cell carcinoma (HNSCC), and non-small cell lung cancer, which may be related to the cell death inhibitory function of FLIP (81, 82). Moreover, the protein encoded by HERPUD2 may be involved in the endoplasmic reticulum (ER)-associated degradation and mediates ER stress-induced inflammation (83). Furthermore, TBCK (TBC1 domain containing kinase) may be involved in the transcriptional regulation of components of the mammalian target of the rapamycin (mTOR) complex and has also been associated with neuronal developmental disorders (84, 85). Finally, IFNGR2 (interferon-gamma receptor 2) encodes a protein that is the non-ligand binding β-chain of the gamma interferon receptor, and its possible involvement in interleukin (IL)-1β-dependent inflammation was noted in recent studies (86, 87).

Notwithstanding that several articles have studied the potential functional mechanisms of eccDNAs in various tumors by combining next-generation sequencing, few have explored the association between eccDNAs and MB. Herein, we demonstrated the presence of eccDNAs in CSF, described the characteristics and genomic landscape of eccDNAs, and researched the possible mechanisms of its production. EccDNAs exhibit similarities between MB and matched CSF, suggesting their potential as a biomarker in the diagnosis and prognosis of MB. Based on the differentially expressed eccDNA-related genes between tumor and normal CSF samples, combined with the GEO database analysis, we screened 10 hub genes associated with MB diagnosis and prognosis and established a model to benefit patients and physicians in clinical practice. Our findings also reveal the potential of eccDNA in targeted interventions. However, limited by the relatively small clinical sample size, individual variations in eccDNAs among the samples from this study may affect the robustness of our findings to a certain extent, emphasizing the need for more studies with larger sample sizes.

Data availability statement

The data presented in the study are deposited in the Gene Expression Omnibus (https://www.ncbi.nlm.nih.gov/geo/) repository, accession number GSE205178.

Ethics statement

The studies involving human participants were reviewed and approved by Department of Neurosurgery, Sanbo Brain Hospital, Capital Medical University. Written informed consent to participate in this study was provided by the participants' legal guardian/next of kin. Written informed consent was obtained from the individual(s), and minor(s)' legal guardian/next of kin, for the publication of any potentially identifiable images or data included in this article.

Author contributions

All authors contributed to the study conception, design, and writing. All authors have given approval for the final version of the manuscript.

Funding

This work was supported by the National Key R&D Program (No. 2019YFC1316104), the National Science Foundation of China (No. 22077120), the China Postdoctoral Science Foundation (No. 2019M660715), and the independent project of Sanbo Brain Hospital (No. 2022ZZLX01).

Conflict of interest

The authors declare that the research was conducted in the absence of any commercial or financial relationships that could be construed as a potential conflict of interest.

Publisher's note

All claims expressed in this article are solely those of the authors and do not necessarily represent those of their affiliated organizations, or those of the publisher, the editors and the reviewers. Any product that may be evaluated in this article, or claim that may be made by its manufacturer, is not guaranteed or endorsed by the publisher.

Supplementary material

The Supplementary Material for this article can be found online at: https://www.frontiersin.org/articles/10.3389/fonc.2022.934159/full#supplementary-material

References

1. Ostrom QT, Gittleman H, Truitt G, Boscia A, Kruchko C, Barnholtz-Sloan JS. CBTRUS statistical report: Primary brain and other central nervous system tumors diagnosed in the united states in 2011-2015. *Neuro Oncol* (2018) 20(suppl_4):iv1–iv86. doi: 10.1093/neuonc/noy131

2. Gajjar A, Chintagumpala M, Ashley D, Kellie S, Kun LE, Merchant TE, et al. Risk-adapted craniospinal radiotherapy followed by high-dose chemotherapy and stem-cell rescue in children with newly diagnosed medulloblastoma (St Jude medulloblastoma-96): long-term results from a prospective, multicentre trial. *Lancet Oncol* (2006) 7(10):813–20. doi: 10.1016/S1470-2045(06)70867-1

3. Packer RJ, Gajjar A, Vezina G, Rorke-Adams L, Burger PC, Robertson PL, et al. Phase III study of craniospinal radiation therapy followed by adjuvant chemotherapy for newly diagnosed average-risk medulloblastoma. *J Clin Oncol* (2006) 24(25):4202–8. doi: 10.1200/JCO.2006.06.4980

4. Gandola L, Massimino M, Cefalo G, Solero C, Spreafico F, Pecori E, et al. Hyperfractionated accelerated radiotherapy in the Milan strategy for metastatic medulloblastoma. *J Clin Oncol* (2009) 27(4):566–71. doi: 10.1200/JCO.2008.18.4176

5. Jakacki RI, Burger PC, Zhou T, Holmes EJ, Kocak M, Onar A, et al. Outcome of children with metastatic medulloblastoma treated with carboplatin during craniospinal radiotherapy: a children's oncology group phase I/II study. *J Clin Oncol* (2012) 30(21):2648–53. doi: 10.1200/JCO.2011.40.2792

6. Louis DN, Perry A, Reifenberger G, von Deimling A, Figarella-Branger D, Cavenee WK, et al. The 2016 world health organization classification of tumors of the central nervous system: a summary. *Acta Neuropathol* (2016) 131(6):803–20. doi: 10.1007/s00401-016-1545-1

7. Weintraub L, Miller T, Friedman I, Abbott R, Levy AS. Misdiagnosing recurrent medulloblastoma: the danger of examination and imaging without histological confirmation. *J Neurosurg Pediatr* (2014) 13(1):33–7. doi: 10.3171/2013.10.PEDS13231

8. Northcott PA, Robinson GW, Kratz CP, Mabbott DJ, Pomeroy SL, Clifford SC, et al. Medulloblastoma. *Nat Rev Dis Primers* (2019) 5(1):11. doi: 10.1038/s41572-019-0063-6

9. Wu S, Turner KM, Nguyen N, Raviram R, Erb M, Santini J, et al. Circular ecDNA promotes accessible chromatin and high oncogene expression. *Nature* (2019) 575(7784):699–703. doi: 10.1038/s41586-019-1763-5

10. Koche RP, Rodriguez-Fos E, Helmsauer K, Burkert M, MacArthur IC, Maag J, et al. Extrachromosomal circular DNA drives oncogenic genome remodeling in neuroblastoma. *Nat Genet* (2020) 52(1):29–34. doi: 10.1038/s41588-019-0547-z

11. deCarvalho AC, Kim H, Poisson LM, Winn ME, Mueller C, Cherba D, et al. Discordant inheritance of chromosomal and extrachromosomal DNA elements contributes to dynamic disease evolution in glioblastoma. *Nat Genet* (2018) 50(5):708–17. doi: 10.1038/s41588-018-0105-0

12. Morton AR, Dogan-Artun N, Faber ZJ, MacLeod G, Bartels CF, Piazza MS, et al. Functional enhancers shape extrachromosomal oncogene amplifications. *Cell* (2019) 179(6):1330–41.e13. doi: 10.1016/j.cell.2019.10.039

13. Tandon I, Pal R, Pal JK, Sharma NK. Extrachromosomal circular DNAs: an extra piece of evidence to depict tumor heterogeneity. *Future Sci OA* (2019) 5(6):FSO390. doi: 10.2144/fsoa-2019-0024

14. Dennin RH. Overlooked: Extrachromosomal DNA and their possible impact on whole genome sequencing. *Malays J Med Sci* (2018) 25(2):20–6. doi: 10.21315/mjms2018.25.2.3

15. Zhang CZ, Spektor A, Cornils H, Francis JM, Jackson EK, Liu S, et al. Chromothripsis from DNA damage in micronuclei. *Nature* (2015) 522(7555):179–84. doi: 10.1038/nature14493

16. Kim H, Nguyen NP, Turner K, Wu S, Gujar AD, Luebeck J, et al. Extrachromosomal DNA is associated with oncogene amplification and poor outcome across multiple cancers. *Nat Genet* (2020) 52(9):891–7. doi: 10.1038/s41588-020-0678-2

17. Sin STK, Jiang P, Deng J, Ji L, Cheng SH, Dutta A, et al. Identification and characterization of extrachromosomal circular DNA in maternal plasma. *Proc Natl Acad Sci U S A* (2020) 117(3):1658–65. doi: 10.1073/pnas.1914949117

18. Kumar P, Dillon LW, Shibata Y, Jazaeri AA, Jones DR, Dutta A. Normal and cancerous tissues release extrachromosomal circular DNA (eccDNA) into the

circulation. *Mol Cancer Res* (2017) 15(9):1197–205. doi: 10.1158/1541-7786.MCR-17-0095

19. Moller HD, Mohiyuddin M, Prada-Luengo I, Sailani MR, Halling JF, Plomgaard P, et al. Circular DNA elements of chromosomal origin are common in healthy human somatic tissue. *Nat Commun* (2018) 9(1):1069. doi: 10.1038/s41467-018-03369-8

20. Shoura MJ, Gabdank I, Hansen L, Merker J, Gotlib J, Levene SD, et al. Intricate and cell type-specific populations of endogenous circular DNA (eccDNA) in caenorhabditis elegans and homo sapiens. *G3 (Bethesda)* (2017) 7(10):3295–303. doi: 10.1534/g3.117.300141

21. Kechin A, Boyarskikh U, Kel A, Filipenko M. cutPrimers: A new tool for accurate cutting of primers from reads of targeted next generation sequencing. *J Comput Biol* (2017) 24(11):1138–43. doi: 10.1089/cmb.2017.0096

22. Li H, Durbin R. Fast and accurate short read alignment with burrows-wheeler transform. *Bioinformatics* (2009) 25(14):1754–60. doi: 10.1093/bioinformatics/btp324

23. Prada-Luengo I, Krogh A, Maretty L, Regenberg B. Sensitive detection of circular DNAs at single-nucleotide resolution using guided realignment of partially aligned reads. *BMC Bioinf* (2019) 20(1):663. doi: 10.1186/s12859-019-3160-3

24. Li H, Handsaker B, Wysoker A, Fennell T, Ruan J, Homer N, et al. The sequence Alignment/Map format and SAMtools. *Bioinformatics* (2009) 25 (16):2078–9. doi: 10.1093/bioinformatics/btp352

25. Robinson MD, McCarthy DJ, Smyth GK. edgeR: a bioconductor package for differential expression analysis of digital gene expression data. *Bioinformatics* (2010) 26(1):139–40. doi: 10.1093/bioinformatics/btp616

26. Quinlan AR, Hall IM. BEDTools: a flexible suite of utilities for comparing genomic features. *Bioinformatics* (2010) 26(6):841–2. doi: 10.1093/bioinformatics/btq033

27. Thorvaldsdottir H, Robinson JT, Mesirov JP. Integrative genomics viewer (IGV): high-performance genomics data visualization and exploration. *Brief Bioinform* (2013) 14(2):178–92. doi: 10.1093/bib/bbs017

28. Yu G, Wang LG, Han Y, He QY. clusterProfiler: an r package for comparing biological themes among gene clusters. *OMICS* (2012) 16(5):284–7. doi: 10.1089/omi.2011.0118

29. Cavalli FMG, Remke M, Rampasek L, Peacock J, Shih DJH, Luu B, et al. Intertumoral heterogeneity within medulloblastoma subgroups. *Cancer Cell* (2017) 31(6):737–54.e6. doi: 10.1016/j.ccell.2017.05.005

30. Weishaupt H, Johansson P, Sundstrom A, Lubovac-Pilav Z, Olsson B, Nelander S, et al. Batch-normalization of cerebellar and medulloblastoma gene expression datasets utilizing empirically defined negative control genes. *Bioinformatics* (2019) 35(18):3357–64. doi: 10.1093/bioinformatics/btz066

31. Tibshirani R. The lasso method for variable selection in the cox model. *Stat Med* (1997) 16(4):385–95. doi: 10.1002/(SICI)1097-0258(19970228)16:4<385::AID-SIM380>3.0.CO;2-3

32. Heagerty PJ, Lumley T, Pepe MS. Time-dependent ROC curves for censored survival data and a diagnostic marker. *Biometrics* (2000) 56(2):337–44. doi: 10.1111/j.0006-341X.2000.00337.x

33. Klipper-Aurbach Y, Wasserman M, Braunspiegel-Weintrob N, Borstein D, Peleg S, Assa S, et al. Mathematical formulae for the prediction of the residual beta cell function during the first two years of disease in children and adolescents with insulin-dependent diabetes mellitus. *Med Hypotheses* (1995) 45(5):486–90. doi: 10.1016/0306-9877(95)90228-7

34. Moller HD, Bojsen RK, Tachibana C, Parsons L, Botstein D, Regenberg B. Genome-wide purification of extrachromosomal circular DNA from eukaryotic cells. *J Vis Exp* (2016) 110):e54239. doi: 10.3791/54239

35. Moller HD, Parsons L, Jorgensen TS, Botstein D, Regenberg B. Extrachromosomal circular DNA is common in yeast. *Proc Natl Acad Sci U S A* (2015) 112(24):E3114–22. doi: 10.1073/pnas.1508825112

36. McCabe MG, Backlund LM, Leong HS, Ichimura K, Collins VP. Chromosome 17 alterations identify good-risk and poor-risk tumors independently of clinical factors in medulloblastoma. *Neuro Oncol* (2011) 13 (4):376–83. doi: 10.1093/neuonc/noq192

37. Rausch T, Jones DT, Zapatka M, Stutz AM, Zichner T, Weischenfeldt J, et al. Genome sequencing of pediatric medulloblastoma links catastrophic DNA rearrangements with TP53 mutations. *Cell* (2012) 148(1-2):59–71. doi: 10.1016/j.cell.2011.12.013

38. de Jong JO, Llapashtica C, Genestine M, Strauss K, Provenzano F, Sun Y, et al. Cortical overgrowth in a preclinical forebrain organoid model of CNTNAP2-associated autism spectrum disorder. *Nat Commun* (2021) 12(1):4087. doi: 10.1038/s41467-021-24358-4

39. Wang Y, Wang M, Djekidel MN, Chen H, Liu D, Alt FW, et al. eccDNAs are apoptotic products with high innate immunostimulatory activity. *Nature* (2021) 599(7884):308–14. doi: 10.1038/s41586-021-04009-w

40. De Mattos-Arruda L, Mayor R, Ng CKY, Weigelt B, Martinez-Ricarte F, Torrejon D, et al. Cerebrospinal fluid-derived circulating tumour DNA better represents the genomic alterations of brain tumours than plasma. *Nat Commun* (2015) 6:8839. doi: 10.1038/ncomms9839

41. Pentsova EI, Shah RH, Tang J, Boire A, You D, Briggs S, et al. Evaluating cancer of the central nervous system through next-generation sequencing of cerebrospinal fluid. *J Clin Oncol* (2016) 34(20):2404–15. doi: 10.1200/JCO.2016.66.6487

42. Miller AM, Shah RH, Pentsova EI, Pourmaleki M, Briggs S, Distefano N, et al. Tracking tumour evolution in glioma through liquid biopsies of cerebrospinal fluid. *Nature* (2019) 565(7741):654–8. doi: 10.1038/s41586-019-0882-3

43. Li J, Zhao S, Lee M, Yin Y, Li J, Zhou Y, et al. Reliable tumor detection by whole-genome methylation sequencing of cell-free DNA in cerebrospinal fluid of pediatric medulloblastoma. *Sci Adv* (2020) 6(42):eabb5427. doi: 10.1126/sciadv.abb5427

44. Hull RM, King M, Pizza G, Krueger F, Vergara X, Houseley J. Transcription-induced formation of extrachromosomal DNA during yeast ageing. *PloS Biol* (2019) 17(12):e3000471. doi: 10.1371/journal.pbio.3000471

45. Moller HD, Ramos-Madrigal J, Prada-Luengo I, Gilbert MTP, Regenberg B. Near-random distribution of chromosome-derived circular DNA in the condensed genome of pigeons and the larger, more repeat-rich human genome. *Genome Biol Evol* (2020) 12(1):3762–77. doi: 10.1093/gbe/evz281

46. Zody MC, Garber M, Adams DJ, Sharpe T, Harrow J, Lupski JR, et al. DNA Sequence of human chromosome 17 and analysis of rearrangement in the human lineage. *Nature* (2006) 440(7087):1045–9. doi: 10.1038/nature04689

47. Leppek K, Das R, Barna M. Functional 5' UTR mRNA structures in eukaryotic translation regulation and how to find them. *Nat Rev Mol Cell Biol* (2018) 19(3):158–74. doi: 10.1038/nrm.2017.103

48. Lubelsky Y, Ulitsky I. Sequences enriched in alu repeats drive nuclear localization of long RNAs in human cells. *Nature* (2018) 555(7694):107–11. doi: 10.1038/nature25757

49. Shibata Y, Kumar P, Layer R, Willcox S, Gagan JR, Griffith JD, et al. Extrachromosomal microDNAs and chromosomal microdeletions in normal tissues. *Science* (2012) 336(6077):82–6. doi: 10.1126/science.1213307

50. Sun Z, Ji N, Zhao R, Liang J, Jiang J, Tian H. Extrachromosomal circular DNAs are common and functional in esophageal squamous cell carcinoma. *Ann Transl Med* (2021) 9(18):1464. doi: 10.21037/atm-21-4372

51. Dillon LW, Kumar P, Shibata Y, Wang YH, Willcox S, Griffith JD, et al. Production of extrachromosomal MicroDNAs is linked to mismatch repair pathways and transcriptional activity. *Cell Rep* (2015) 11(11):1749–59. doi: 10.1016/j.celrep.2015.05.020

52. Yang H, He J, Huang S, Yang H, Yi Q, Tao Y, et al. Identification and characterization of extrachromosomal circular DNA in human placentas with fetal growth restriction. *Front Immunol* (2021) 12:780779. doi: 10.3389/fimmu.2021.780779

53. Mann L, Seibt KM, Weber B, Heitkam T. ECCsplorer: a pipeline to detect extrachromosomal circular DNA (eccDNA) from next-generation sequencing data. *BMC Bioinf* (2022) 23(1):40. doi: 10.1186/s12859-021-04545-2

54. Ling X, Han Y, Meng J, Zhong B, Chen J, Zhang H, et al. Small extrachromosomal circular DNA (eccDNA): major functions in evolution and cancer. *Mol Cancer* (2021) 20(1):113. doi: 10.1186/s12943-021-01413-8

55. Barrett A, Evans IM, Frolov A, Britton G, Pellet-Many C, Yamaji M, et al. A crucial role for DOK1 in PDGF-BB-stimulated glioma cell invasion through p130Cas and Rap1 signalling. *J Cell Sci* (2014) 127(Pt 12):2647–58. doi: 10.1242/jcs.158576

56. Akino T, Han X, Nakayama H, McNeish B, Zurakowski D, Mammoto A, et al. Netrin-1 promotes medulloblastoma cell invasiveness and angiogenesis, and demonstrates elevated expression in tumor tissue and urine of patients with pediatric medulloblastoma. *Cancer Res* (2014) 74(14):3716–26. doi: 10.1158/0008-5472.CAN-13-3116

57. Waszak SM, Northcott PA, Buchhalter I, Robinson GW, Sutter C, Groebner S, et al. Spectrum and prevalence of genetic predisposition in medulloblastoma: a retrospective genetic study and prospective validation in a clinical trial cohort. *Lancet Oncol* (2018) 19(6):785–98. doi: 10.1016/S1470-2045(18)30242-0

58. Kool M, Jones DT, Jager N, Northcott PA, Pugh TJ, Hovestadt V, et al. Genome sequencing of SHH medulloblastoma predicts genotype-related response to smoothened inhibition. *Cancer Cell* (2014) 25(3):393–405. doi: 10.1016/j.ccr.2014.02.004

59. Shih DJ, Northcott PA, Remke M, Korshunov A, Ramaswamy V, Kool M, et al. Cytogenetic prognostication within medulloblastoma subgroups. *J Clin Oncol* (2014) 32(9):886–96. doi: 10.1200/JCO.2013.50.9539

60. Northcott PA, Buchhalter I, Morrissy AS, Hovestadt V, Weischenfeldt J, Ehrenberger T, et al. The whole-genome landscape of medulloblastoma subtypes. *Nature* (2017) 547(7663):311–7. doi: 10.1038/nature22973

61. Cristiano S, Leal A, Phallen J, Fiksel J, Adleff V, Bruhm DC, et al. Genome-wide cell-free DNA fragmentation in patients with cancer. *Nature* (2019) 570 (7761):385–9. doi: 10.1038/s41586-019-1272-6

62. Lin C, Chen Y, Zhang F, Liu B, Xie C, Song Y. Encoding gene RAB3B exists in linear chromosomal and circular extrachromosomal DNA and contributes to cisplatin resistance of hypopharyngeal squamous cell carcinoma *via* inducing autophagy. *Cell Death Dis* (2022) 13(2):171. doi: 10.1038/s41419-022-04627-w

63. Zhu S, Lin F, Chen Z, Jiang X, Zhang J, Yang Q, et al. Identification of a twelve-gene signature and establishment of a prognostic nomogram predicting overall survival for medulloblastoma. *Front Genet* (2020) 11:563882. doi: 10.3389/fgene.2020.563882

64. Zhang H, Xiao X, Wei W, Huang C, Wang M, Wang L, et al. CircLIFR synergizes with MSH2 to attenuate chemoresistance *via* MutSalpha/ATM-p73 axis in bladder cancer. *Mol Cancer* (2021) 20(1):70. doi: 10.1186/s12943-021-01360-4

65. Aasland D, Gotzinger L, Hauck L, Berte N, Meyer J, Effenberger M, et al. Temozolomide induces senescence and repression of DNA repair pathways in glioblastoma cells *via* activation of ATR-CHK1, p21, and NF-kappaB. *Cancer Res* (2019) 79(1):99–113. doi: 10.1158/0008-5472.CAN-18-1733

66. Couch FJ, Shimelis H, Hu C, Hart SN, Polley EC, Na J, et al. Associations between cancer predisposition testing panel genes and breast cancer. *JAMA Oncol* (2017) 3(9):1190–6. doi: 10.1001/jamaoncol.2017.0424

67. Braun DA, Lovric S, Schapiro D, Schneider R, Marquez J, Asif M, et al. Mutations in multiple components of the nuclear pore complex cause nephrotic syndrome. *J Clin Invest* (2018) 128(10):4313–28. doi: 10.1172/JCI98688

68. Terashima Y, Toda E, Itakura M, Otsuji M, Yoshinaga S, Okumura K, et al. Targeting FROUNT with disulfiram suppresses macrophage accumulation and its tumor-promoting properties. *Nat Commun* (2020) 11(1):609. doi: 10.1038/s41467-020-14338-5

69. Qu J, Zhang X, Lv X. Zinc finger protein 750(ZNF750), negatively regulated by miR-17-5p, inhibits proliferation, motility and invasion of colonic cancer cells. *J Gene Med* (2020) 22(8):e3195. doi: 10.1002/jgm.3195

70. Kong P, Xu E, Bi Y, Xu X, Liu X, Song B, et al. Novel ESCC-related gene ZNF750 as potential prognostic biomarker and inhibits epithelial-mesenchymal transition through directly depressing SNAI1 promoter in ESCC. *Theranostics* (2020) 10(4):1798–813. doi: 10.7150/thno.38210

71. Zhang P, He Q, Lei Y, Li Y, Wen X, Hong M, et al. m(6)A-mediated ZNF750 repression facilitates nasopharyngeal carcinoma progression. *Cell Death Dis* (2018) 9(12):1169. doi: 10.1038/s41419-018-1224-3

72. Huang LY, Wang YP, Wei BF, Yang J, Wang JQ, Wu BH, et al. Deficiency of IRTKS as an adaptor of insulin receptor leads to insulin resistance. *Cell Res* (2013) 23(11):1310–21. doi: 10.1038/cr.2013.99

73. Chao A, Tsai CL, Jung SM, Chuang WC, Kao C, Hsu A, et al. BAI1-associated protein 2-like 1 (BAIAP2L1) is a potential biomarker in ovarian cancer. *PloS One* (2015) 10(7):e0133081. doi: 10.1371/journal.pone.0133081

74. Pipatpanyanugoon N, Wareesawetsuwan N, Prasopporn S, Poolex W, Pisitkun T, Kaewkong W, et al. BAIAP2L1 enables cancer cell migration and facilitates phospho-cofilin asymmetry localization in the border cells. *Cancer Commun (Lond)* (2022) 42(1):75–9. doi: 10.1002/cac2.12239

75. Park JS, Pierorazio PM, Lee JH, Lee HJ, Lim YS, Jang WS, et al. Gene expression analysis of aggressive clinical T1 stage clear cell renal cell carcinoma for identifying potential diagnostic and prognostic biomarkers. *Cancers (Basel)* (2020) 12(1):222. doi: 10.3390/cancers12010222

76. Xu PP, Zeng S, Xia XT, Ye ZH, Li MF, Chen MY, et al. FAM172A promotes follicular thyroid carcinogenesis and may be a marker of FTC. *Endocr Relat Cancer* (2020) 27(11):657–69. doi: 10.1530/ERC-20-0181

77. Chen Y, Liu P, Shen D, Liu H, Xu L, Wang J, et al. FAM172A inhibits EMT in pancreatic cancer *via* ERK-MAPK signaling. *Biol Open* (2020) 9(2):bio048462. doi: 10.1242/bio.048462

78. Lin M, Wang ZW, Zhu X. FBXO45 is a potential therapeutic target for cancer therapy. *Cell Death Discovery* (2020) 6:55. doi: 10.1038/s41420-020-0291-2

79. Diaz VM, de Herreros AG. F-box proteins: Keeping the epithelial-to-mesenchymal transition (EMT) in check. *Semin Cancer Biol* (2016) 36:71–9. doi: 10.1016/j.semcancer.2015.10.003

80. Brenner C, Galluzzi L, Kepp O, Kroemer G. Decoding cell death signals in liver inflammation. *J Hepatol* (2013) 59(3):583–94. doi: 10.1016/j.jhep.2013.03.033

81. Humphreys L, Espona-Fiedler M, Longley DB. FLIP as a therapeutic target in cancer. *FEBS J* (2018) 285(22):4104–23. doi: 10.1111/febs.14523

82. Budd RC, Yeh WC, Tschopp J. cFLIP regulation of lymphocyte activation and development. *Nat Rev Immunol* (2006) 6(3):196–204. doi: 10.1038/nri1787

83. Dong YF, Chen ZZ, Zhao Z, Yang DD, Yan H, Ji J, et al. Potential role of microRNA-7 in the anti-neuroinflammation effects of nicorandil in astrocytes induced by oxygen-glucose deprivation. *J Neuroinflamm* (2016) 13(1):60. doi: 10.1186/s12974-016-0527-5

84. Ortiz-Gonzalez XR, Tintos-Hernandez JA, Keller K, Li X, Foley AR, Bharucha-Goebel DX, et al. Homozygous boricua TBCK mutation causes neurodegeneration and aberrant autophagy. *Ann Neurol* (2018) 83(1):153–65. doi: 10.1002/ana.25130

85. Wu J, Lu G. Multiple functions of TBCK protein in neurodevelopment disorders and tumors. *Oncol Lett* (2021) 21(1):17. doi: 10.3892/ol.2020.12278

86. Xia Y, Zhang Q, Ye Y, Wu X, He F, Peng Y, et al. Melatonergic signalling instructs transcriptional inhibition of IFNGR2 to lessen interleukin-1beta-dependent inflammation. *Clin Transl Med* (2022) 12(2):e716. doi: 10.1002/ctm2.716

87. Bustamante J, Boisson-Dupuis S, Abel L, Casanova JL. Mendelian susceptibility to mycobacterial disease: genetic, immunological, and clinical features of inborn errors of IFN-gamma immunity. *Semin Immunol* (2014) 26 (6):454–70. doi: 10.1016/j.smim.2014.09.008

frontiers | Frontiers in Oncology

TYPE Original Research
PUBLISHED 16 November 2022
DOI 10.3389/fonc.2022.1033035

OPEN ACCESS

EDITED BY
Navnath S Gavande,
Wayne State University, United States

REVIEWED BY
Diana Ainembabazi,
Purdue University Indianapolis, United States
Naresh Murty Venneti,
Wayne State University, United States

*CORRESPONDENCE
Mirosława Z. Naskręt-Barciszewska
mbarcisz@ibch.poznan.pl

†These authors have contributed equally to this work

SPECIALTY SECTION
This article was submitted to Cancer Molecular Targets and Therapeutics, a section of the journal Frontiers in Oncology

RECEIVED 31 August 2022
ACCEPTED 24 October 2022
PUBLISHED 16 November 2022

CITATION
Barciszewska A-M, Belter A, Gawrońska I, Giel-Pietraszuk M and Naskręt-Barciszewska MZ (2022) Cross-reactivity between histone demethylase inhibitor valproic acid and DNA methylation in glioblastoma cell lines. *Front. Oncol.* 12:1033035. doi: 10.3389/fonc.2022.1033035

Cross-reactivity between histone demethylase inhibitor valproic acid and DNA methylation in glioblastoma cell lines

Anna-Maria Barciszewska[1,2†], Agnieszka Belter[3†], Iwona Gawrońska[3], Małgorzata Giel-Pietraszuk[3] and Mirosława Z. Naskręt-Barciszewska[3*]

[1]Intraoperative Imaging Unit, Chair and Department of Neurosurgery and Neurotraumatology, Karol Marcinkowski University of Medical Sciences, Poznan, Poland, [2]Department of Neurosurgery and Neurotraumatology, Heliodor Swiecicki Clinical Hospital, Poznan, Poland, [3]Institute of Bioorganic Chemistry, Polish Academy of Sciences, Poznan, Poland

Currently, valproic acid (VPA) is known as an inhibitor of histone deacetylase (epigenetic drug) and is used for the clinical treatment of epileptic events in the course of glioblastoma multiforme (GBM). Which improves the clinical outcome of those patients. We analyzed the level of 5-methylcytosine, a DNA epigenetic modulator, and 8-oxodeoxyguanosine, an cellular oxidative damage marker, affected with VPA administration, alone and in combination with temozolomide (TMZ), of glioma (T98G, U118, U138), other cancer (HeLa), and normal (HaCaT) cell lines. We observed the VPA dose-dependent changes in the total DNA methylation in neoplastic cell lines and the lack of such an effect in a normal cell line. VPA at high concentrations (250-500 μM) induced hypermethylation of DNA in a short time frame. However, the exposition of GBM cells to the combination of VPA and TMZ resulted in DNA hypomethylation. At the same time, we observed an increase of genomic 8-oxo-dG, which as a hydroxyl radical reaction product with guanosine residue in DNA suggests a red-ox imbalance in the cancer cells and radical damage of DNA. Our data show that VPA as an HDAC inhibitor does not induce changes only in histone acetylation, but also changes in the state of DNA modification. It shows cross-reactivity between chromatin remodeling due to histone acetylation and DNA methylation. Finally, total DNA cytosine methylation and guanosine oxidation changes in glioma cell lines under VPA treatment suggest a new epigenetic mechanism of that drug action.

KEYWORDS

valproic acid, temozolomide, glioblastoma, DNA methylation, 8-oxo-deoxyguanosine

Introduction

Valproic acid (2-propylvaleric acid, 2-propylpentanoic acid, VPA) is used primarily in the treatment of epilepsy, bipolar disorders neuropathic pain, and migraine prophylaxis. It is also a first-line antiepileptic drug (AED) for glioblastoma (GBM) patients (1). Although the mechanism of the VPA action is not fully understood, its action includes increased GABAergic activity, a reduction in excitatory neurotransmission, and modification of monoamines (2). VPA is mostly known due to its histone deacetylase (HDAC)-inhibitory activity (3), which is believed to be responsible for the antitumor action defined as epigenetic effects of this drug (4). Through the HDAC inhibition, VPA promotes transcription activity of chromatin, and a better access to transcription factors as well as the transcriptional machinery to DNA (5). Furthermore, it has been shown that VPA affects tumor cells by inhibiting proliferation, angiogenesis and promoting apoptosis. However, these activities on glioma cells are somewhat contradictory (4, 6, 7), and may allow more durable benefits from its anti-glioma properties.

VPA (Figure 1A) is a branched short-chain fatty acid with a half-life of 9-16 h. Maximum plasma concentrations range from 25 to 100 mg/l following administration of 250 to 1000 mg dose. The protein binding capacity of VPA in plasma is approximately 90% in healthy persons. It is almost completely absorbed after oral administration, and dose-dependent peak plasma concentrations are attained within 1 to 10 hours. The bioavailability of VPA is nearly 100%, and its therapeutic concentration is 50–100 μg/ml (340–700 μM/l) (8). However, VPA penetration through the blood–brain barrier (BBB) changes because of an asymmetric transport of valproate, such that the brain-to-blood flux exceeds the blood-to-brain flux. Only a free, non-protein-bound, portion of VPA crosses the BBB and shows its antiepileptic effect (9). Valproate concentration in the cerebral cortex is remarkably low, compared with either total or unbound VPA concentration in plasma. The respective brain-to-serum partition ratios based on the total and free drug in serum are 0.11 ± 0.05 and 0.54 ± 0.18, respectively (10). Other studies showed brain levels of VPA at 6.8-27.9% and CSF levels at 7.6-25.0% of the plasma level (11). Altogether, understanding the mechanism of action of VPA is necessary.

The best known chemotherapeutic agent for GBM is temozolomide (TMZ). Temozolomide, (4-methyl-5-oxo-2,3,4,6,8-pentazabicyclo[4.3.0]nona-2,7,9-triene-9- carboxamide) (Figure 1B) is an oral alkylating agent that significantly prolongs survival in GBM patients when administered during and after radiotherapy (12). It is used as first-line chemotherapy, but also shows significant activity against recurrent glioblastoma (13). TMZ is available to the central nervous system (CNS) because its lipophilic properties allow efficient crossing of the BBB. TMZ interferes with the mechanism of development of cancer, slowing down its growth and spread in the body. O^6-methylguanine (O^6-mG) is regarded as the primary cytotoxic lesion of TMZ in DNA, although, it constitutes only ca. 5% of the TMZ-mediated methylation reaction products. Therefore, it is not clear why methylation of the O^6 position of guanine can be the major player in cytotoxic drug action.

Glioblastoma is the most frequent, highly recurrent, and rapidly progressing type of astrocytic brain tumor in adults. It is characterized by uncontrolled proliferation, dynamic angiogenesis, invasiveness, and the ability to evade apoptosis and infiltrate the neighboring brain. There are much data showing that GBM is mainly driven by genetic and epigenetic aberrations (14). The standard therapy for glioblastoma patients consists of surgical resection followed by radiation therapy and concomitant chemotherapy with temozolomide (12). However, even with that therapeutic scheme, the median survival time of GBM patients is still below 12 months from diagnosis, and the 5-year survival rate is less than 5%. Therapy failure, observed in the vast majority of glioblastoma patients, and bad prognosis are probably due to high intrinsic resistance to chemo- and radiotherapy on the one hand, as well as the rapid spread of glioblastoma cells in the brain on the other. Therefore, a new strategy to treat GBM is still urgently needed. Up to 50% of

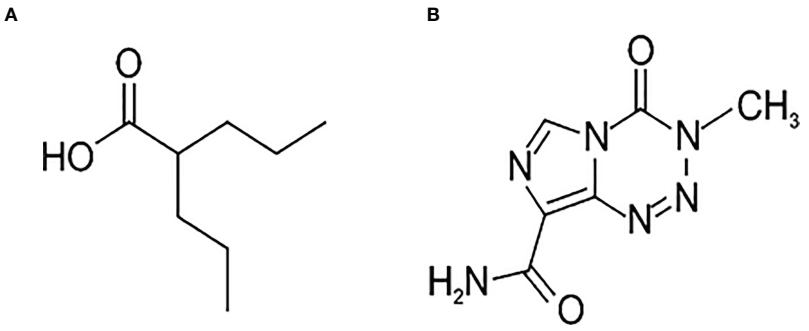

FIGURE 1
Chemical formulae of Valproic acid – **(A)** and temozolamide – **(B)**.

glioblastoma patients develop tumor-associated epileptic seizures that are treated with AEDs. Glioma patients with a history of seizures have a better prognosis than patients without seizures, and it has been reported that this phenomenon could be related to the VPA used for seizure prophylaxis or treatment (15). It has been shown that VPA might have a synergistic antitumor effect with radiation therapy because of the radiosensitizing properties of VPA (16). On the other hand, there are clinical trials suggesting that the addition of VPA to the standard radiotherapy with temozolomide in newly diagnosed glioblastoma patients may prolong survival (17), but others show no significant difference in overall survival (18). In addition to that, a meta-analysis confirmed some survival benefits unequally (19). Even mechanism of VPA action is vague and the impact on GBM patients' survival is doubtful, still VPA is the most commonly used AED during glioblastoma treatment. Therefore, we decided to look more precisely at the mode of action, of this epigenetic drug.

Epigenetics provides a new explanatory area for many pathological processes. It offers a connection between genetic and environmental factors that influence the development of the disease. Epigenetic regulation of gene expression is a dynamic, responsive, and reversible process. It plays a critical role in the pathophysiology of diseases, from neurological to metabolic disorders, to cancer and rare diseases thus leading to the tailoring of conventional therapies and ultimately better outcomes. DNA methylation is an essential mechanism for gene expression regulation, genomic imprinting, development, and genomic stability. DNA methylation status can significantly alter transcription factor binding and is thought to be inversely proportional to the level of expression of gene products. The bestcharacterized epigenetic marker is 5-methylcytosine (m^5C) in DNA (20). Therefore, the implications of DNA methylation changes are numerous (21, 22). Recently, we have shown that m^5C is a diagnostic marker for brain tumors' malignancy and the severity of other diseases (23, 24). In other studies we have found that temozolomide which modifies DNA through methylation (damage) of oxygen 6 of guanosine in DNA, affects methylated cytosine (m^5C) level, causing oxidative demethylation (25, 26).

Another DNA damage product is 8-hydroxydeoxy guanosine (8-oxo-dG), formed by the reaction of guanosine residue with hydroxyl radical (•OH). It induced base paring not only with cytosine (Watson-Crick base pair) but also with adenosine causing G-T transversion. A high level of 8-oxo-dG as a result of oxidative stress contributes to genome instability, elevated proliferation rate, and metastasis. A mutual monitoring of m^5C and 8-oxo-dG level in DNA will provide data for discussion of VPA effects on the cell.

The aim of the present work was to look for a new mechanism of VPA action in glioblastoma cells. We showed that it works not only as HDAC inhibitors but also as an effector of DNA methylation. It is known that epigenetic modifications respond to environmental changes more rapidly than genetic ones. Therefore, the level of their changes seems to be most promising in the treatment of such diseases as cancer.

In the paper, we showed that VPA stimulates DNA cytosine methylation, and did not change significantly red-ox potential of the GBM cells. The effect of combined treatment of VPA and TMZ is toxic to the cell.

Materials and methods

Chemicals and reagents

Sodium valproate (Sanofi-Aventis, France) stock solution of 100 mg/ml in water was used to prepare the required concentration with a complete medium. Temozolomide (Merck, Germany) was dissolved in dimethyl sulfoxide (DMSO, Sigma) at a concentration of 0.103 M. [γ-P^{32}] ATP (6000 Ci/mmol) was purchased from Hartmann Analytic GmbH (Germany), T4 polynucleotide kinase was purchased from USB (UK), micrococcal nuclease, spleen phosphodiesterase II, apyrase, RNase P1, thiazolyl blue tetrazolium bromide, and inorganic salts were purchased from Sigma Aldrich/Merck (Germany), cellulose plates and methanol were purchased from Merck (Germany), and the Genomic Mini kit for DNA isolation was supplied by A&A Biotechnology (Poland).

Cell line and culture conditions

The human glioblastoma cell lines (T98G, U138, U118), the cervical cancer cell line (HeLa), and the human keratinocyte cell line (HaCaT) were purchased from ATCC (USA). T98G and U138 cell lines were cultured in EMEM medium (ATCC), U118 in DMEM (ATCC), HeLa, and HaCaT in EMEM (Sigma-Aldrich). Each medium was supplemented with 10% (v/v) fetal bovine serum (FBS, Sigma-Aldrich) and 10 mg/ml antibiotics (penicillin 100 U/ml and streptomycin 100 µg/ml). Cells were cultured at 37°C with 5% CO_2 in humidified air. After 24 *h*, cells were washed with phosphate-buffered saline (PBS, Sigma-Aldrich/Merck), placed in a fresh medium, and treated with VPA alone or a mixture of VPA and TMZ.

Cell viability/proliferation assay

Cell viability was evaluated with a dye-staining method, using 3-(4,5-dimethyl-2-thiazolyl)-2,5-diphenyl-2H-tetrazolium bromide (MTT) (27). Cell lines (HaCaT, HeLa, T98G, U118, U138) were seeded in 96-well culture plates at a density of 1×10^4 cells/well and grown in the supplemented medium at 37°C under 5% CO_2 atmosphere. Next the cell lines were treated with VPA at concentrations (20, 39, 78, 156, 313, 625, 1250, 2500, 5000, 10000, 20000 µM). The combinations

of TMZ concentrations of 0, 1, 30, and 100 μM with the above mentioned VPA concentrations were performed to show the concomitant effect of dual treatment. After 24 *h*, the supernatant was washed out, and 100 μl of MTT solution in medium (0.5 mg/ml final concentration of MTT) was added to each well for 2 *h*. After the incubation, the unreacted dye was removed through aspiration. The formazan crystals were dissolved in 100 μl/well DMSO and measured spectrophotometrically in a multi-well Synergy2 plate reader (BioTek Instruments, USA) at a test wavelength of 492 nm and a reference wavelength of 690 nm. The half-maximal inhibitory concentrations (IC_{50}) were calculated by fitting experimental values to the sigmoidal bell-shaped equation using GraphPad Prism v5.01 (GraphPad Software, Inc., USA). Values represent the means from three independent experiments.

Treatment of the cell lines with valproic acid

VPA stock solution was added directly to the culture medium (with 90–95% confluence) to get the required concentrations (30, 50, 100, 250, 500 μM) and incubated for 3, 12, 24, and 48 *h*. For the control reaction the cells were treated with H_2O only. After 3–48 h of VPA treatment, cells were washed with PBS, trypsinized, and collected by centrifugation at 4000 rpm for 10 *min*. The cellular pellets were quickly frozen and stored at 20°C for DNA isolation.

Treatment of the cell lines with the combination of valproic acid and temozolamide

VPA and TMZ stock solutions were added directly to the culture medium to get the designed concentration. In experiments with TMZ, the final DMSO concentration in each cell culture was 0.8%. Cell cultures (with 90–95% confluence) were washed with PBS and placed in fresh medium, and treated with: 50 μM VPA and 0, 1, 30, or 100 μM TMZ for 3, 24 and 48 *h*; 200 μM VPA and 0, 1, 30, or 100 μM TMZ for 3, 24 and 48 *h*; 350 μM VPA and 0, 1, 30, or 100 μM TMZ for 3, 24 and 48 *h*. The control cells were treated with H_2O (for VPA) and DMSO (for TMZ). After incubation, the cells were washed with PBS, trypsinized, and collected by centrifugation at 4000 rpm for 5 *min*. The cellular pellets were quickly frozen and stored at 20°C for DNA isolation.

DNA isolation from cell cultures

DNA from tissue samples was extracted with the Genomic Mini kit according to the manufacturer's instructions. Shortly, tissue samples were incubated with RNase A first and then with proteinase K. After centrifugation (15000 rpm for 3 *min*), the supernatant was applied to a mini-column, and DNA bound to the column was eluted with Tris-buffer pH 8.5 and stored at 20° C for further analysis. The purity of DNA preparations was assessed by measuring UV absorbance at 260 and 280 nm. The A_{260}/A_{280} ratio was 2.0–2.1.

Analysis of m^5C contents in DNA

DNA (dried, 1μg) was dissolved in a succinate buffer (pH 6.0) containing 10 mM $CaCl_2$ and digested with 0.001 units of spleen phosphodiesterase II and 0.02 units of micrococcal nuclease in 4 μl total volume for 5 h at 37°C. DNA digest was labeled with 1μCi [γ-P^{32}]ATP (6000 Ci/mmol) and 1.5 units of T4 polynucleotide kinase in 10 mM bicine-NaOH pH 9.7 buffer containing 10 mM $MgCl_2$, 10 mM DTT, and 1 mM spermidine. After 0.5 *h* at 37°C, apyrase (10 units/ml) in the same buffer was added and incubated for another 0.5 h. The 3'nucleotide phosphate was cleaved off with 0.2 μg RNase P1 in 500 mM ammonium acetate buffer, pH 4.5. Identification of [γ-P^{32}]m^5C was performed with two-dimensional thin-layer chromatography (TLC) on cellulose plates using the solvent system isobutyric acid:NH_4OH:H_2O (66:1:17 v/v) in the first dimension and 0.2 M sodium phosphate (pH 6.8)-ammonium sulfate-n-propyl alcohol (100 ml/60 g/2 ml) in the second dimension. Radioactivity was subsequently measured using a Fluoro Image Analyzer FLA-5100 with Multi Gauge 3.0 software (FujiFilm). Each analysis was repeated three times. For precise calculations, we evaluated spots corresponding not only to m^5C, but also to products of its degradation, such as cytosine (C) and thymine (T). The amount of m^5C was calculated as R = [(m^5C/m^5C+C+T)]*100 (23).

Analysis of 8-oxo-dG contents in DNA

DNA was dissolved in 200 μl of a buffer (pH 5.3) containing 40 mM sodium acetate and 0.1 mM $ZnCl_2$, then mixed with nuclease P1 (Sigma-Aldrich, St. Louis, MO, USA) solution (30 μg), and incubated for 3 h at 37°C. Then, 30 μl of 1M Tris–HCl pH 8.0 and 5 μl of alkaline phosphatase (1.5 units) solution was added, followed by 1 h incubation at 37°C. DNA hydrolysate was purified using a cut-off 10,000 Da filter. 8-oxo-dG amount in DNA was determined using HPLC (Agilent Technologies 1260 Infinity, CA, USA) with two detectors working in series: 1260 Diode Array Detector and Coulochem III Electrochemical Detector (ESA Inc., Chelmsford, MA, USA). Isocratic chromatography of DNA hydrolysate was performed using a solution of 50 mM CH_3COONH_4 at pH 5.3 and methanol (93:7). Analysis of dG for reference was performed at 260 nm. 8-oxo-dG was determined with the following electrochemical detection

settings: guard cell +400 mV, detector 1: +130 mV (screening electrode), detector 2: + 350 mV (measuring electrode set on the 100 nA sensitivity) (28).

Calculation of the genomic amount of m^5C and 8-oxo-dG in human DNA

The amount of modified bases in DNA was calculated on the basis of global genome composition - 3.05×10^9 bases (100%), where C - 624×10^6 (20,5%), T - 905×10^6 (29,6%), G - 623×10^6 (20,4%), A - 901×10^6 (29,5%), and m^5C - 31×10^6 (1%). The amount of m^5C (%) in pyrimidines in DNA was determined from TLC analysis with the formula $R[\%] = m^5C \times 100/(C + T)$. The total number of m^5C in the genome was calculated from the formula $m^5C = (1\ 498\ 333\ 975) \times R/100$. The input amount of guanosine was necessary to determine 8-oxo-dG contents. It was calculated from Diode Array Detector (PAD) measurements using Avogadro number $N_G = 6.02 \times 10^{20} \times b(mAU)/a(mAU)$ standard. 8-oxo-dG nucleoside amount was estimated with electrochemical detector $N_{8\text{-oxo-dG}} = 6.02 \times 10^{20} \times d(nA)/c(nA)$ standard. The total number of 8-oxo-dG = $623 \times 10^6 \times N_{8\text{-oxo-dG}}/N_G$ (29).

Statistical analysis

STATISTICA software, (StatSoft Polska), was used for analyses of all data, as previously (30). The data are the result of three independent experiments. The descriptive statistics function was used to generate the mean and SD. The one-tailed t-test was used to calculate significant differences in R values for tested samples as compared with the control. Standard deviations were indicated as error bars on graphs.

Results

Cytotoxic effect of VPA in neoplastic and normal cell lines

Cell viability was determined by MTT assay at concentrations in the range of 20 μM–20 mM (1.29 - 4.3 on the logarithmic scale) and 1 μM–2 mM (0 - 3.301 on the logarithmic scale) for VPA and TMZ, respectively. VPA below 1000 μM (3 on logarithmic scale) showed no effect either on U118 or T98G glioma cells (Figures 2A, D, E), in a range 1 000 – 10 000 μM (3 – 4 on logarithmic scale) slight, and above 10 000 μM (4 on logarithmic scale) significant decrease of these cells viability

Interestingly, no toxicity of VPA at concentrations below 5 000 μM (3.7 on logarithmic scale) toward U138 and HaCaT cells was observed. What is more, a slight increase in cells viability in a range of 40 - 1 250 μM (1.6 – 3.1 on logarithmic scale) and 625 – 10 000 μM (2.8 – 4 on logarithmic scale) VPA was reported for U138 and HaCaT cells, respectively (Figures 2A, C). TMZ is much more toxic for all tested cell lines than VPA (Figures 2C–F). TMZ at concentrations above 50 μM shows a significant decrease in the viability of human glioblastoma cell lines (T98G, U118), a keratinocyte cell line (HaCaT), and a cervical cancer cell line (HeLa) (Figures 2B–F). Calculated IC50 for T98G and HaCaT cell lines were 2.3 and 1.2 mM, respectively (31, 32).

Combination index (CI) of VPA and TMZ was calculated with CompuSyn software (31, 32), for T98G cells, treated simultaneously with different concentrations VPA (up to 20 mM) and 100uM TMZ or VPA only. Clearly combination index, $CI_{VPA\text{-}TMZ}$ value is above >1 (IC = 2.55, for fa = 0.5), which suggests antagonistic effect of these drugs on cell viability.

The effect of VPA on genomic DNA methylation level in cell lines

The total DNA methylation level (expressed as R) in the cell lines was analyzed in after treatment with 30-500 μM of VPA for 3-48 *h* (Figure 3). We noticed concentration and time dependent m^5C contents changes. Small fluctuations of DNA methylation were observed for a normal cell line (HaCaT), where are m^5C level increased slightly for other cell lines after 12 and 24 *h* of incubation. For the HeLa cell line we observed the highest increase in total DNA methylation. For glioblastoma cell lines at the concentrations of 250-500 μM (for U138 and U118 also in 100 μM), we noticed that m^5C content increased in a dose-dependent manner. For T98G, a significant increase in DNA methylation at all concentrations was visible after 24 *h*. However, a longer incubation time (48 *h*) showed a lower level of m^5C, which suggests demethylation (Figure 3). The differences in R values between different VPA concentrations in all cell lines were statistically significant (Supplementary Table S1).

The effect of VPA and TMZ on genomic DNA methylation level in cell lines

We analyzed the combined effect of VPA (0, 50, 200, and 350 μM) and of TMZ (0, 1, 30, and 100 μM) for 3, 24, and 48 *h* on human glioblastoma (T98G, U138, U118) and keratinocyte (HaCaT) cell lines (Figure 4). In control experiments, cell lines were treated with H_2O and DMSO for VPA and TMZ, respectively. The effect of VPA/TMZ action on glioblastoma cell lines is variable. One can see VPA alone produces a clear dose-dependent increase in genomic DNA methylation in glioblastoma cell lines and scarcely in a non-neoplastic cell line. For HaCaT cell line, longer incubation (24 *h*) was crucial

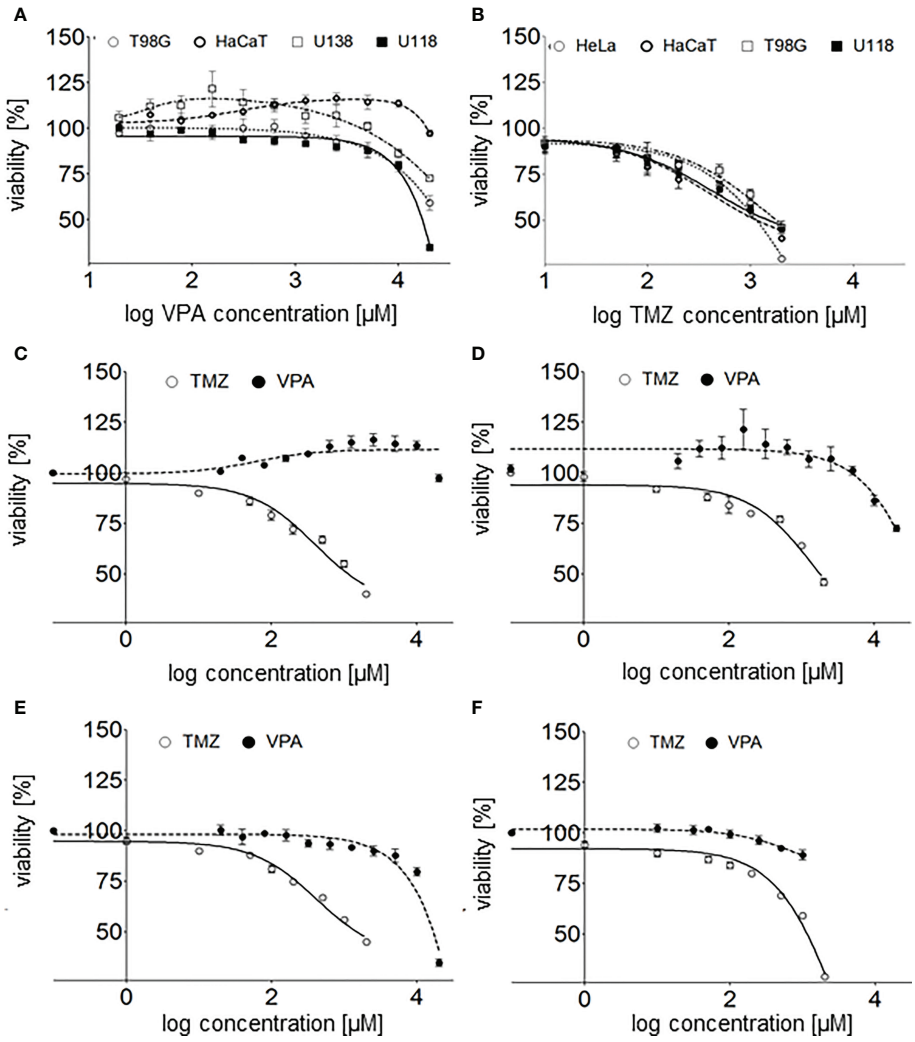

FIGURE 2
(A) - valproic acid's effect on human glioblastoma cell lines (T98G, U118, and U138) and a keratinocyte cell line (HaCaT) viability 24 h after cell culture supplementation with VPA (20-20000 μM; log concentration, 1.3 - 4.3 μM). **(B)** - TMZ's effect on human glioblastoma cell lines (T98G, U118), a keratinocyte cell line (HaCaT) and an adenocarcinoma cell line (HeLa) viability 24 h after cell culture supplementation with TMZ (1 μM - 2 mM, log concentration 0–3.3 μM). The comparison of TMZ and VPA effect on the viability of **(C)** - U118, **(D)** - T98G, **(E)** - HaCaT, and **(F)** - HeLa cells. Values are the means ± SE of at least four experiments.

to obtain a statistically significant increase in total DNA methylation with VPA and TMZ (Supplementary Table S2). On the other hand for T98G, U138, and U118 cell lines, TMZ catalyzes the removal of m^5C, which clearly proves DNA demethylation. The decrease in m^5C contents in the DNA of T98G cell line is negatively correlated with treatment with TMZ (100 μM) and VPA (350 μM), for 3 *h* (Figure 4). Similar observations can see for U118 for 24h (Figure 4). A slightly higher increase in m^5C contents induced with the increasing amount of TMZ was observed only for the U138 cell line at 50 μM of VPA after 48 *h* of incubation. The differences in R values are statistically significant (Supplementary Table S2).

Cytotoxic effect of a combination of VPA and TMZ in neoplastic and normal cell lines

Cell viability of glioblastoma (T98G) and keratinocyte (HaCaT) cell lines undergoing combined therapy was determined with MTT assay in the range of 20 μM - 20 mM (1.3 – 4.3 on logarithmic scale) VPA and 1, 30 and 100 μM (0, 1.5 and 2 on logarithmic scale TMZ (Figure 5).

T98G cells seem to be more sensitive than HaCaT to TMZ (Figures 2B, 5D–F), VPA (Figure 2A) and a combination of TMZ and VPA (Figures 5A–F). VPA, in a concentration range of

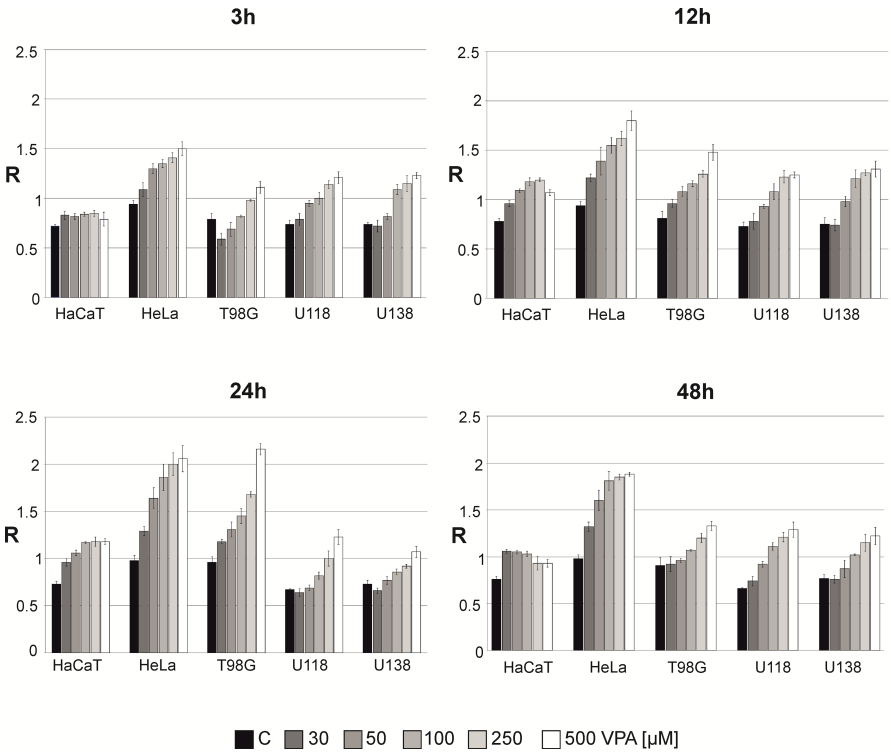

FIGURE 3
The effect of valproic acid (VPA) on DNA (m^5C) methylation level (R) in different cell lines. The analysis was performed after 3, 12, 24, and 48 h of incubation in a given VPA concentrations (0, 50, 100, 250, 500 μM). For control experiment cells were treated with H_2O. The R values are means from three experiments.

625 – 10 000 μM (2.8 – 4 on logarithmic scale), increases the viability of HaCaT cells (Figures 2A, 5A, C). Such an effect was observed (but is much lower) in the case of HaCaT cells treated already with TMZ (Figures 5A, D–F). It means that VPA in such concentrations protects healthy cells (HaCaT) from cell death being a result of TMZ (30 or 100 μM). In the case of T98G, in the range of 20 μM - 10 mM VPA no additional toxicity of T98G cells treated already with TMZ was observed (Figures 5B, D–F). However, VPA above 625 μM (2.8 on logarithmic scale), excelerates the cytotoxic effect of TMZ on T98G cells (Figures 5B, D–F).

Analysis of m^5C and 8-oxo-dG contents in DNA of T98G cell lines treated with VPA and TMZ

The total level of m^5C and 8-oxo-dG in genomic DNA from the T98G cell line after treatment with TMZ, VPA, and their mixture was analyzed. One can see that treatments with TMZ and VPA separately, show an increase of m^5C contents and a decrease of the 8-oxo-dG amount in DNA (Figure 6). On the contrary combined TMZ and VPA action induced cellular stress and DNA cytosine hypomethylation, and small changes in 8-oxo-dG. A decrease in the amount of 8-oxo-dG suggests the induction of DNA repair mechanisms.

Discussion

In a search for an understanding of the mechanism of VPA action, we analyzed changes in the total genomic contents of 5-methylcytosine, the main epigenetic modification of DNA in cell lines. The reason for focusing on that marker is that the DNA methylation (m^5C) profile changes dynamically under the influence of environmental, nutritional, and pathogenic conditions, viruses, and many other factors, as well as development and aging (33). The presence or absence of DNA (m^5C) methylation functions as a "switch", repressing or activating gene transcription, respectively, and therefore providing an essential mechanism for tissue-specific, developmentally regulated, and environmentally influenced genetic processes (14). In parallel to the analysis of m^5C, we also looked at 8-oxo-dG level in DNA, which is well known DNA oxidative damage marker.

In the present study, we analyzed the influence of VPA on genome wide methylation. It turned out that VPA alone

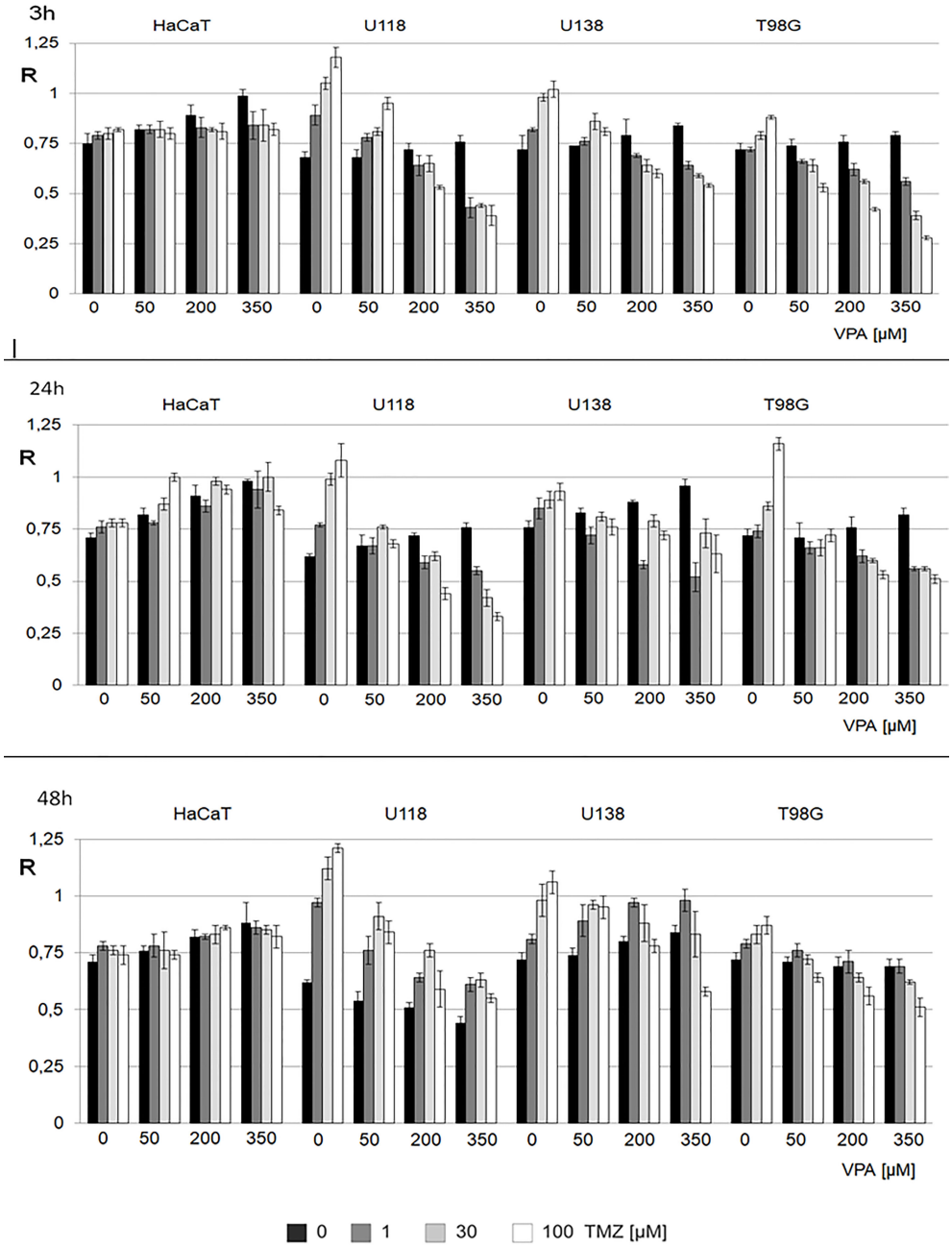

FIGURE 4
The effect of action of VPA/TMZ on total DNA (m^5C) methylation level in different cell lines. The analysis was performed after 3, 24 and 48 h of incubation in a given VPA (0, 50, 200, 350 μM) and TMZ concentration (0, 1, 30, 100 μM). For control experiments cells were treated with DMSO only. The R values are means from three experiments. The reference (100%) is the viability of cells not treated with TMZ and VPA. Values are means from three experiments.

increases total DNA methylation in a dose-dependent manner. We adjusted VPA doses to those virtually achieved in the central nervous system during treatment (11). While therapeutic serum concentrations of VPA are 340–700 μM, its brain concentration is approximately 7-30% of that in plasma. Therefore, to analyze the real VPA impact on the central nervous system, one should focus on the VPA concentration in the range between 23 and 490 μM. Therefore, in our experiments, we used a concentration of

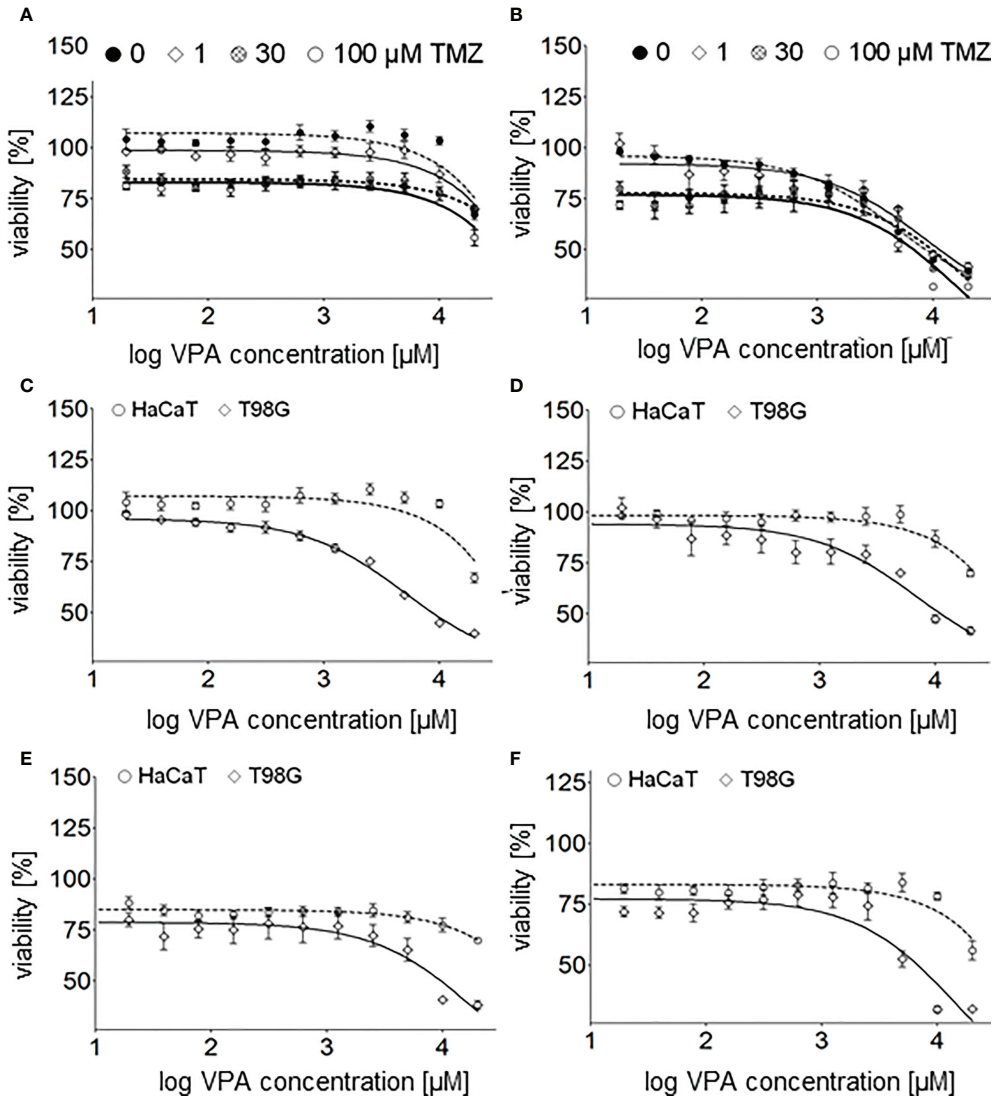

FIGURE 5
Cell viability assay of the glioblastoma cell line T98G – **(A)**, and the keratinocyte cell line HaCaT – **(B)** 24 h after cell culture supplementation with both TMZ (0, 1, 30, 100 μM) and different concentrations (20, 39, 78, 156, 313, 625, 1250, 2500, 5000, 10000, 20000 μM) of VPA. Cell viability assay of the glioblastoma cell line T98G and the keratinocyte cell line HaCaT 24 h after cell culture supplementation with different concentrations (20–20000 μM, log concentration 1.3 - 4.3 μM) of VPA – **(C)** and both VPA and 1 μM – **(D)**, 30 μM – **(E)** and 100 μM - **(F)** of TMZ. Values are means ± SE of at least four experiments.

30-500 μM. VPA concentration of 1 mM is already double our maximum. Based on our previous observations with high doses of TMZ, one can presume that in such high concentrations, DNA demethylation can be an effect of oxidative stress and DNA modification as well as induction of the DNA repair mechanism (25). However, DNA demethylation in VPA-treated HeLa cell lines has been observed (34) although that analysis has been done with FT-IR microspectroscopy, at high VPA concentration (1 and 20 mM) for 24 h. In another study, the glioma stem cell colonies were treated with 2 mM VPA for 24 h and up to 30 days, and TMZ of 50-400 μM for 48 or 72 h. VPA in that conditions, does not increase TMZ efficacy (35). This is understandable in the scope of our observations, showing that the joining of VPA and TMZ action causes global DNA demethylation (Figure 4). Interestingly it has been previously shown that VPA downregulates MGMT expression in glioma cells (36). In the case of 0.5–10 μM TMZ, DNA hypomethylation in glioblastoma cell lines depends on the cell line. This effect is particularly interesting because that range of concentration is observed in the brain during TMZ treatment (26). At the concentration of 10 μM of TMZ (3 μM in the case of U118), dose-dependent DNA hypermethylation was observed. The

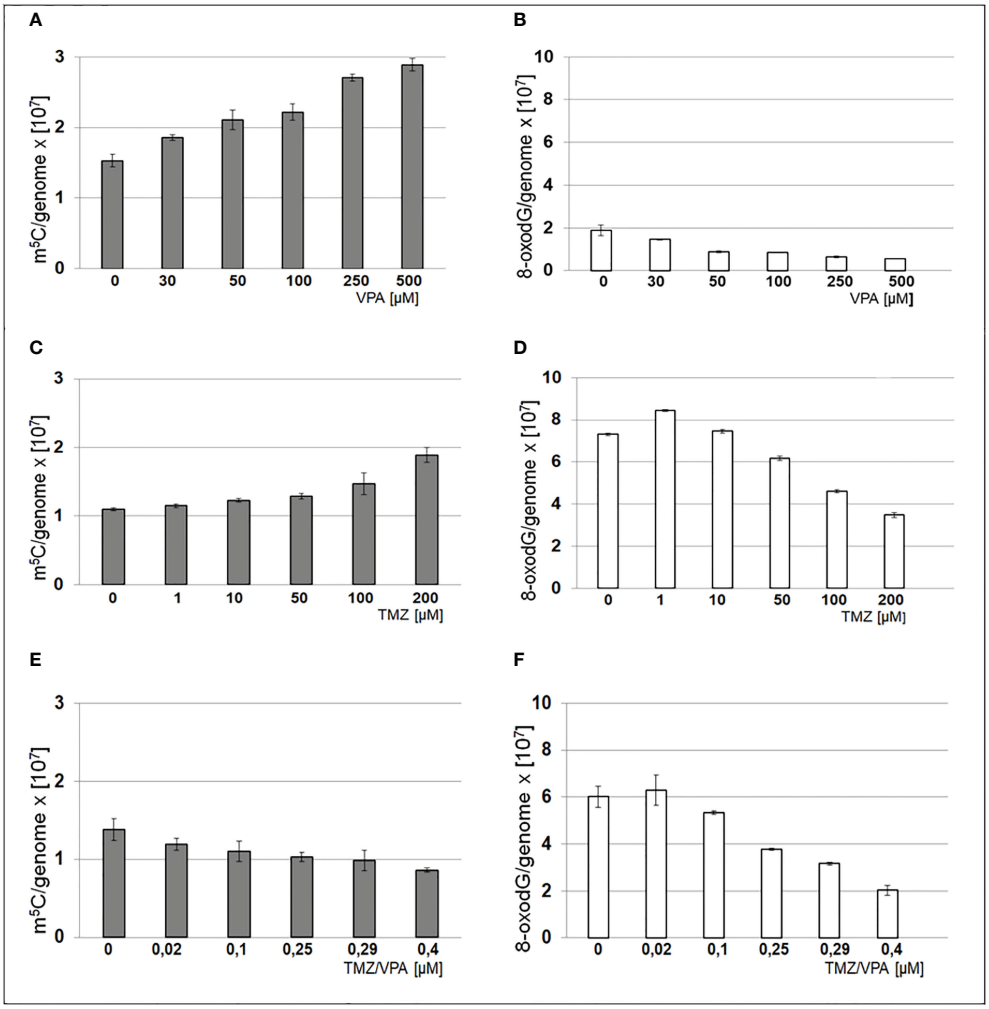

FIGURE 6
Contents of m^5C – **(A, C, E)** and 8-oxo-dG – **(B, D, F)** in DNA from T98G cell line after treatment with TMZ, VPA or their mixture. The analysis was performed after 24 h of incubation in given TMZ (0, 1, 10, 50, 100 and 200 μM), and VPA (0, 30, 50, 100, 250, 500 μM) concentration and mixtures of both of TMZ/VPA at ratio (0, 0.02, 0.1, 0.25, 0.29, 0.4). In control experiment cells were treated with DMSO only. The R values are means from three experiments.

hypomethylating effect of VPA/TMZ treatment is most striking after 3 h and is more balanced after a long time of incubation (24 and 48 h) (Figure 4). It has been frequently observed for different environmental pollutants (37). Comparing the results for drug combination (Figures 6C–F) with the single drug effects (Figures 2D, E), one can say that VPA shows a positive effect on longer cells' viability under TMZ treatment. Several mechanisms underlying the anti-tumor effect of VPA have already been considered (38). One of them regards VPA as histone deacetylase (HDAC) inhibitor, which increases lysine acetylation on histones, as well as other nonhistone proteins, by downregulating the HDAC activity. Removal of positive charge from lysine residue induces loosening of the chromatin structure and provides better accessibility to transcription factors to their target DNA sequence (39). Therefore, HDAC inhibitors induce numerous downstream effects such as cell cycle arrest, induction of apoptosis, affection of angiogenesis, inhibition of cellular stress response pathways, and changing ncRNA expression (39). However, VPA is a relatively weak HDAC inhibitor at millimolar concentrations, and is only an active inhibitor at relatively high concentrations (40). It actually excludes that mechanism from place in the brain because of the very small penetration of the drug through BBB. One should remember that HDAC inhibitors can reverse CpG methylation by the down-regulation of DNMT1 expression or by the repression of ERK1, and gene silencing (41). Those observations provide support for our concept of the novel epigenetic mechanism of VPA action which stimulates genome-wide DNA methylation. A

possible reason for that can be drug-induced DNA hypermethylation (42). 5-methylcytosine is a product of an enzymatic reaction catalyzed by DNA methyltransferases (DNMTs), where S-adenosyl methionine (SAM) is the only methyl donor. VPA is not a substrate for DNMTs, therefore, the only possible mechanism where a drug can increase m^5C contents is the allosteric activation of DNMTs (43). The induction of DNA hypermethylation with drugs, hormones, and other biological compounds has already been observed (42). The other indirect evidence for such a mechanism is the blockage of cancer-specific processes by SAM supplementation, which results in DNA hypermethylation and gene downregulation (44, 45). Taking this into account, it seems reasonable that VPA, either *in vitro* studies or phase I/II clinical trials, induced cell growth inhibition on both benign cells, such as vascular pericytes, cancers, as well as acute myeloid leukemia and solid malignancies (46).

The mechanism of action of VPA, which we propose, is based on allosteric enzyme activation from one side, but also on the oxidative demethylation (hypomethylation) through ROS. That negative association between DNA methylation and oxidative stress was recently confirmed (28). In this paper, we showed that the level of 8-oxo-dG is a good marker of the oxidative stress. As a product of ROS reaction with DNA, we can assume the red-ox state of the cell. The formation of 8-oxo-dG provides information on how deep is the DNA methylation process due to the reaction of the methyl group of m^5C with ROS.

The most important aspect of our studies is clinical relevance. The meta-analysis of 210 patients with GBM treated with different AEDs (VPA, carbamazepine, phenytoin) showed significantly longer survival than those who were not, and patients treated with VPA had significantly longer survival than those who had received other AEDs (17). However, that work did not specify the kind of chemotherapy that was used in the analyzed patients (whether it was temozolomide or not).

The observation that GBM patients may benefit from VPA therapy, supports our results. We have recently shown that the DNA methylation level in the cell depends on oxidative damage and is reversely correlated with ROS reaction products (28). It is also known that elevated ROS levels in the cell promote tumor development and progression (47). However, the relationship between DNA methylation level with cancer is less obvious. DNA hypermethylation leads to gene down expression including tumor suppressor gene promoters. The methylation of DNA diminishes the affinity of transcriptional factors to the target sequence. On the other hand, global DNA hypomethylation, resulting in total gene expression deregulation, is observed in many tumors (27). For many years, the research focus was directed toward DNA hypomethylating events, and the antineoplastic effect of various drugs was regarded as a consequence of oxidative stress induction and ROS-mediated cell damage (48). However, the efficacy of DNA demethylation agents is limited, and indications are selected (49). The reason for this is the occurrence of global oxidative damage of the cell under such oncological treatment. Surviving cells are highly resistant to any treatment and produce aggressive recurrences. The factors affecting global DNA hypomethylation are recently within the scope of many studies (50, 51), especially because it was proven that the hypermethylated phenotype signifies better survival in glioma (52).

The results of our study clearly identify the DNA hypermethylating effect of VPA (Figure 7), which can be regarded as the antineoplastic one. The hypomethylation with TMZ in our experiments identifies possible obstacles to the combined therapy of temozolomide, a standard for chemotherapy of primary and recurrent GBM (53), with valproic acid, which is recommended in symptomatic tumor-related epilepsy as a first-line treatment, especially during temozolomide therapy (1). Despite some cell lines studies showing a promising additive effect of VPA on TMZ (54–56), no significant positive impact on overall survival was observed in clinical trials while incorporating the VPA together with TMZ

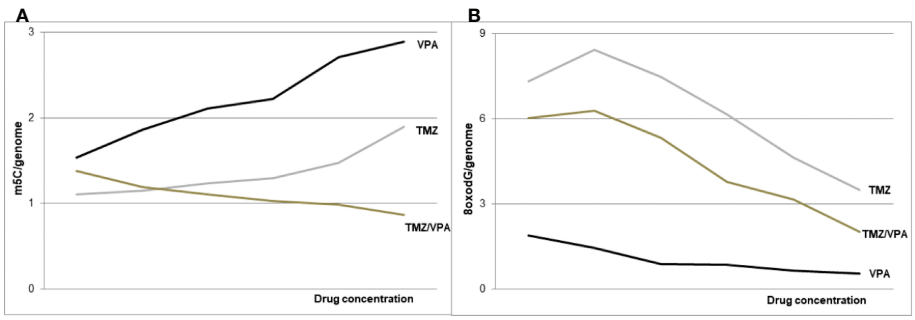

FIGURE 7
The schematic of VPA and TMZ impact on DNA (m^5C) methylation – **(A)** and DNA (8-oxo-dG) oxidation – **(B)**, alone and in combination. The concomitant application of the both drugs induces DNA hypomethylation.

(18). VPA shows the ability to affect TMZ sensitivity in GBM cell lines suggesting that it is the chemosensitizing drug (54). Our experiments show that combined therapy with both drugs leads to total DNA hypomethylation, which suggests the lack of a clearly positive clinical effect of VPA in GBM.

Generally, it turned out that valproic acid acts on two levels of epigenetic cell's machinery. In addition to histone acetylation, VPA induces reprogramming and increases the total DNA methylation level in glioblastoma cell lines in a dose-dependent manner. The DNA hypermethylation effect of VPA alone can be beneficial for GBM treatment, but not in a combination with TMZ, which induces DNA demethylation (Figure 7). Therefore, further clinical trials, are needed to evaluate the combining VPA/TMZ treatment effects.

Data availability statement

The original contributions presented in the study are included in the article/Supplementary Material. Further inquiries can be directed to the corresponding author.

Author contributions

MZN-B data curation, created the concept of the research, methodology formal analysis, funding acquisition, writing–original draft, writing–review and editing. AMB created the concept of the research, methodology, writing–original draft. AMB planned and carried out experiments, methodology, writing–original draft. IG performed the experiments, project administration. MG-P performed the experiments. All authors contributed to the article and approved the submitted version.

Funding

This work was supported with funding from the National Science Center Poland (grant nr.: 2020/37/B/NZ5/03249) to MZN-B.

Conflict of interest

The authors declare that the research was conducted in the absence of any commercial or financial relationships that could be construed as a potential conflict of interest.

Publisher's note

All claims expressed in this article are solely those of the authors and do not necessarily represent those of their affiliated organizations, or those of the publisher, the editors and the reviewers. Any product that may be evaluated in this article, or claim that may be made by its manufacturer, is not guaranteed or endorsed by the publisher.

Supplementary material

The Supplementary Material for this article can be found online at: https://www.frontiersin.org/articles/10.3389/fonc.2022.1033035/full#supplementary-material

References

1. Englot DJ, Chang EF, Vecht CJ. Epilepsy and brain tumors. *Handb Clin Neurol* (2016) 134:267–85. doi: 10.1016/B978-0-12-802997-8.00016-5

2. Johannessen CU, Johannessen SI. Valproate: past present and future. *CNS Drug Rev* (2003) 9(2):199–216. doi: 10.1111/j.1527-3458.2003.tb00249.x

3. Göttlicher M, Minucci S, Zhu P, Krämer OH, Schimpf A, Giavara S, et al. Valproic acid defines a novel class of HDAC inhibitors inducing differentiation of transformed cells. *EMBO J* (2001) 20(24):6969–78. doi: 10.1093/emboj/20.24.6969

4. Duenas-Gonzalez A, Candelaria M, Perez-Plascencia C, Perez-Cardenas E, de la Cruz-Hernandez E, Herrera LA. Valproic acid as epigenetic cancer drug: preclinical clinical and transcriptional effects on solid tumors. *Cancer Treat Rev* (2008) 34(3):206–22. doi: 10.1016/j.ctrv.2007.11.003

5. Silva MR, Correia AO, Dos Santos GCA, Parente LLT, de Siqueira KP, Lima DGS, et al. Neuroprotective effects of valproic acid on brain ischemia are related to its HDAC and GSK3 inhibitions. *Pharmacol Biochem Behav* (2018) 167:17–28. doi: 10.1016/j.pbb.2018.02.001

6. Chen Y, Tsai YH, Tseng SH. Valproic acid affected the survival and invasiveness of human glioma cells through diverse mechanisms. *J Neurooncol* (2012) 109(1):23–33. doi: 10.1007/s11060-012-0871-y

7. Berendsen S, Broekman M, Seute T, Snijders T, van Es C, de Vos F, et al. Valproic acid for the treatment of malignant gliomas: review of the preclinical rationale and published clinical results. *Expert Opin Investig Drugs* (2012) 21 (9):1391–415. doi: 10.1517/13543784.2012.694425

8. Löscher W. Valproate: a reappraisal of its pharmacodynamic properties and mechanisms of action. *Prog Neurobiol* (1999) 58(1):31–59. doi: 10.1016/s0301-0082 (98)00075-6

9. Patsalos PN, Zugman M, Lake C, James A, Ratnaraj N, Sander JW. Serum protein binding of 25 antiepileptic drugs in a routine clinical setting: A comparison of free non-protein-bound concentrations. *Epilepsia* (2017) 58(7):1234–43. doi: 10.1111/epi.13802

10. Shen DD, Ojemann GA, Rapport RL, Dills RL, Friel PN, Levy RH. Low and variable presence of valproic acid in human brain. . *Neurol* (1992) 42(3 Pt 1):582–5. doi: 10.1212/wnl.42.3.582

11. Wieser HG. Comparison of valproate concentrations in human plasma CSF and brain tissue after administration of different formulations of valproate or valpromide. *Epilepsy Res* (1991) 9(2):154–9. doi: 10.1016/0920-1211(91)90028-e

12. Stupp R, Hegi ME, Mason WP, van den Bent MJ, Taphoorn MJ, Janzer RC, et al. European Organisation for research and treatment of cancer brain tumour and radiation oncology groups; national cancer institute of Canada clinical trials group. effects of radiotherapy with concomitant and adjuvant temozolomide versus radiotherapy alone on survival in glioblastoma in a randomised phase III study: 5-

year analysis of the EORTC-NCIC trial. *Lancet Oncol* (2009) 10(5):459–66. doi: 10.1016/S1470-2045(09)70025-7

13. Kong DS, Lee JI, Kim JH, Kim ST, Kim WS, Suh YL, et al. Phase II trial of low-dose continuous (metronomic) treatment of temozolomide for recurrent glioblastoma. *Neuro Oncol* (2010) 12(3):289–96. doi: 10.1093/neuonc/nop030

14. Baylin SB, Jones PA. A decade of exploring the cancer epigenome - biological and translational implications. *Nat Rev Cancer* (2011) 11(10):726–34. doi: 10.1038/nrc3130

15. Vecht CJ, Kerkhof M, Duran-Pena A. Seizure prognosis in brain tumors: new insights and evidence-based management. *Oncologist* (2014) 19(7):751–9. doi: 10.1634/theoncologist.2014-0060

16. Barker CA, Bishop AJ, Chang M, Beal K, Chan TA. Valproic acid use during radiation therapy for glioblastoma associated with improved survival. *Int J Radiat Oncol Biol Phys* (2013) 86(3):504–9. doi: 10.1016/j.ijrobp.2013.02.012

17. Guthrie GD, Eljamel S. Impact of particular antiepileptic drugs on the survival of patients with glioblastoma multiforme. *J Neurosurg* (2013) 118(4):859–65. doi: 10.3171/2012.10.JNS12169

18. Tsai HC, Wei KC, Tsai CN, Huang YC, Chen PY, Chen SM, et al. Effect of valproic acid on the outcome of glioblastoma multiforme. *Br J Neurosurg* (2012) 26 (3):347–54. doi: 10.3109/02688697.2011.638996

19. Yuan Y, Xiang W, Qing M, Yanhui L, Jiewen L, Yunhe M. Survival analysis for valproic acid use in adult glioblastoma multiforme: a meta-analysis of individual patient data and a systematic review. *Seizure* (2014) 23(10):830–5. doi: 10.1016/j.seizure.2014.06.015

20. Kumar S, Chinnusamy V, Mohapatra T. Epigenetics of modified DNA bases: 5-methylcytosine and beyond. *Front Genet* (2018) 9:640. doi: 10.3389/fgene.2018.00640

21. Moore LD, Le T, Fan G. DNA Methylation and its basic function. *Neuropsychopharmacology* (2013) 38(1):23–38. doi: 10.1038/npp.2012.112

22. Ehrlich M, Lacey M. DNA Methylation and differentiation: silencing upregulation and modulation of gene expression. *Epigenomics* (2013) 5(5):553–68. doi: 10.2217/epi.13.43

23. Barciszewska AM, Nowak S, Naskręt-Barciszewska MZ. The degree of global DNA hypomethylation in peripheral blood correlates with that in matched tumor tissues in several neoplasia. *PloS One* (2014) 9(3):e92599. doi: 10.1371/journal.pone.0092599

24. Barciszewska AM. Global DNA demethylation as an epigenetic marker of human brain metastases. *Biosci Rep* (2018) 38(5):BSR20180731. doi: 10.1042/BSR20180731

25. Barciszewska AM, Gurda D, Głodowicz P, Nowak S, Naskręt-Barciszewska MZ. A new epigenetic mechanism of temozolomide action in glioma cells. *PloS One* (2015) 10(8):e0136669. doi: 10.1371/journal.pone.0136669

26. Belter A, Barciszewski J, Barciszewska AM. Revealing the epigenetic effect of temozolomide on glioblastoma cell lines in therapeutic conditions. *PloS One* (2020) 15(2):e0229534. doi: 10.1371/journal.pone.0229534

27. Ehrlich M, Lacey M. DNA Hypomethylation and hemimethylation in cancer. *Adv Exp Med Biol* (2013) 754:31–56. doi: 10.1007/978-1-4419-9967-2_2

28. Barciszewska AM, Giel-Pietraszuk M, Perrigue PM, Naskręt-Barciszewska M. Total DNA methylation changes reflect random oxidative DNA damage in gliomas. *Cells* (2019) 8(9):1065. doi: 10.3390/cells8091065

29. Nurk S, Koren S, Rhie A, Rautiainen M, Bzikadze AV, Mikheenko A, et al. The complete sequence of a human genome. *Science* (2022) 376(6588):44–53. doi: 10.1126/science.abj6987

30. Michalak M, Barciszewska MZ, Barciszewski J, Plitta BP, Chmielarz P. Global changes in DNA methylation in seeds and seedlings of pyrus communis after seed desiccation and storage. *PloS One* (2013) 8(8):e70693. doi: 10.1371/journal.pone.0070693

31. Chou TC, Martin N. *CompuSyn for drug combinations: PC software and user's guide: A computer program for quantitation of synergism and antagonism in drug combinations, and the determination of IC50 and ED50 and LD50 values*. Paramus, (NJ: ComboSyn Inc (2005). Available at: www.combosyn.com.

32. Chou TC, Talalay P. Quantitative analysis of dose-effect relationships: the combined effects of multiple drugs or enzyme inhibitors. *Adv Enzyme Regul* (1984) 22:27–55. doi: 10.1016/0065-2571(84)90007-4

33. Feil R, Fraga MF. Epigenetics and the environment: emerging patterns and implications. *Nat Rev Genet* (2012) 13(2):97–109. doi: 10.1038/nrg3142

34. Veronezi GM, Felisbino MB, Gatti MS, Mello ML, Vidal BC. DNA Methylation changes in valproic acid-treated HeLa cells as assessed by image analysis immunofluorescence and vibrational microspectroscopy. *PloS One* (2017) 12(1):e0170740. doi: 10.1371/journal.pone.0170740

35. Riva G, Butta V, Cilibrasi C, Baronchelli S, Redaelli S, Dalprà L, et al. Epigenetic targeting of glioma stem cells: Short-term and long-term treatments with valproic acid modulate DNA methylation and differentiation behavior but not temozolomide sensitivity. *Oncol Rep* (2016) 35(5):2811–24. doi: 10.3892/or.2016.4665

36. Eckert M, Klumpp L, Huber SM. Cellular effects of the antiepileptic drug valproic acid in glioblastoma. *Cell Physiol Biochem* (2017) 44(4):1591–605. doi: 10.1159/000485753

37. Martin EM, Fry RC. Environmental influences on the epigenome: Exposure-associated DNA methylation in human populations. *Annu Rev Public Health* (2018) 39:309–33. doi: 10.1146/annurev-publhealth-040617-014629

38. Nakada M, Furuta T, Hayashi Y, Minamoto T, Hamada J. The strategy for enhancing temozolomide against malignant glioma. *Front Oncol* (2012) 2:98. doi: 10.3389/fonc.2012.00098

39. Eckschlager T, Plch J, Stiborova M, Hrabeta J. Histone deacetylase inhibitors as anticancer drugs. *Int J Mol Sci* (2017) 18:1414. doi: 10.3390/ijms18071414

40. Hontecillas-Prieto L, Flores-Campos R, Silver A, de Alava E, Hajji N, Garcia-Dominguez D. Synergistic enhancement of cancer therapy using HDAC inhibitors: Opportunity for clinical trials. *Front Genet* (2020) 11:578011. doi: 10.3389/fgene.2020.578011

41. Sarkar S, Abujamra AL, Loew JE, Forman LW, Perrine SP, Faller DV. Histone deacetylase inhibitors reverse CpG methylation by regulating DNMT1 through ERK signaling. *Anticancer Res* (2011) 31(9):2723–32.

42. Nyce J. Drug-induced DNA hypermethylation and drug resistance in human tumors. *Cancer Res* (1989) 49(21):5829–36.

43. Jeltsch A, Jurkowska RZ. Allosteric control of mammalian DNA methyltransferases - a new regulatory paradigm. *Nucleic Acids Res* (2016) 44 (18):8556–75. doi: 10.1093/nar/gkw723

44. Wang Y, Sun Z, Szyf M. S-adenosyl-methionine (SAM) alters the transcriptome and methylome and specifically blocks growth and invasiveness of liver cancer cells. . *Oncotarget* (2017) 8(67):111866–81. doi: 10.18632/oncotarget.22942

45. Mahmood N, Cheishvili D, Arakelian A, Tanvir I, Khan HA, Pépin AS, et al. Methyl donor s-adenosylmethionine (SAM) supplementation attenuates breast cancer growth invasion and metastasis *in vivo*; therapeutic and chemopreventive applications. *Oncotarget* (2017) 9(4):5169–83. doi: 10.18632/oncotarget.23704

46. Ververis K, Hiong A, Karagiannis TC, Licciardi PV. Histone deacetylase inhibitors (HDACIs): multitargeted anticancer agents. *Biologics* (2013) 7:47–60. doi: 10.2147/BTT.S29965

47. Aggarwal V, Tuli HS, Varol A, Thakral F, Yerer MB, Sak K, et al. Role of reactive oxygen species in cancer progression: Molecular mechanisms and recent advancements. *Biomolecules* (2019) 9(11):735. doi: 10.3390/biom9110735

48. Yang H, Villani RM, Wang H, Simpson MJ, Roberts MS, Tang M, et al. The role of cellular reactive oxygen species in cancer chemotherapy. *J Exp Clin Cancer Res* (2018) 37(1):266. doi: 10.1186/s13046-018-0909-x

49. Mehdipour P, Murphy T, De Carvalho DD. The role of DNA-demethylating agents in cancer therapy. *Pharmacol Ther* (2020) 205:107416. doi: 10.1016/j.pharmthera.2019.107416

50. Mahmood N, Rabbani SA. Targeting DNA hypomethylation in malignancy by epigenetic therapies. *Adv Exp Med Biol* (2019) 1164:179–96. doi: 10.1007/978-3-030-22254-3_14

51. Milutinovic S, D'Alessio AC, Detich N, Szyf M. Valproate induces widespread epigenetic reprogramming which involves demethylation of specific genes. *Carcinogenesis* (2007) 28(3):560–71. doi: 10.1093/carcin/bgl167

52. van den Bent MJ, Gravendeel LA, Gorlia T, Kros JM, Lapre L, Wesseling P, et al. A hypermethylated phenotype is a better predictor of survival than MGMT methylation in anaplastic oligodendroglial brain tumors: a report from EORTC study 26951. *Clin Cancer Res* (2011) 17(22):7148–55. doi: 10.1158/1078-0432.CCR-11-1274

53. Schritz A, Aouali N, Fischer A, Dessenne C, Adams R, Berchem G, et al. Systematic review and network meta-analysis of the efficacy of existing treatments for patients with recurrent glioblastoma. *Neurooncol Adv* (2021) 3(1):1–12. doi: 10.1093/noajnl/vdab052

54. Tsai H, Wei K, Chen PY, Huang C, Chen KT, Lin YJ, et al. Valproic acid enhanced temozolomide-induced anticancer activity in human glioma through the p53-PUMA apoptosis pathway. *Front Oncol* (2021) 11:722754. doi: 10.3389/fonc.2021.722754

55. Han W, Guan W. Valproic acid: A promising therapeutic agent in glioma treatment. *Front Oncol* (2021) 11:687362. doi: 10.3389/fonc.2021.687362

56. Chen J, Lee I, Huang Ch, Wu Y, Chung Ch, Lee M, et al. Valproic acid-induced amphiregulin secretion confers resistance to temozolomide treatment in human glioma cells. *BMC Cancer* (2019) 19(1):756. doi: 10.1186/s12885-019-5843-6

frontiers | Frontiers in Oncology

TYPE Original Research
PUBLISHED 15 December 2022
DOI 10.3389/fonc.2022.1005876

OPEN ACCESS

EDITED BY
Avraham Eisbruch,
Michigan Medicine, University of Michigan, United States

REVIEWED BY
Yvonne Dzierma,
Saarland University Hospital, Germany
Hongtao Zhang,
Hebei General Hospital, China

*CORRESPONDENCE
Xiaokun Hu
huxiaokun770@163.com
Man Hu
hu5770@sina.com
Huanting Li
lihuanting26@163.com

†These authors have contributed equally to this work

SPECIALTY SECTION
This article was submitted to Head and Neck Cancer, a section of the journal Frontiers in Oncology

RECEIVED 28 July 2022
ACCEPTED 25 November 2022
PUBLISHED 15 December 2022

CITATION
Yang L, Wang C, Zhang W, Liu S, Xuan T, Jiang H, Hu X, Hu M and Li H (2022) Iodine-125 brachytherapy treatment for newly diagnosed brain metastasis in non-small cell lung cancer: A biocentric analysis. *Front. Oncol.* 12:1005876. doi: 10.3389/fonc.2022.1005876

Iodine-125 brachytherapy treatment for newly diagnosed brain metastasis in non-small cell lung cancer: A biocentric analysis

Lili Yang[1†], Congxiao Wang[1†], Wei Zhang[1], Shifeng Liu[1], Tiantian Xuan[2], Han Jiang[1], Xiaokun Hu[1*], Man Hu[3*] and Huanting Li[4*]

[1]Department of the Interventional Medical Center, The Affiliated Hospital of Qingdao University, Qingdao, Shandong, China, [2]Department of Oncology, Qilu Hospital, Qingdao, Shandong, China, [3]Department of Radiation Oncology, Shandong Cancer Hospital and Institute, Shandong First Medical University and Shandong Academy of Medical Sciences, Jinan, Shandong, China, [4]Department of Neurosurgery, The Affiliated Hospital of Qingdao University, Qingdao, Shandong, China

Purpose: The aim of the present study is to evaluate the safety and efficacy of iodine-125 brachytherapy for newly diagnosed brain metastasis in patients with non-small cell lung cancer (NSCLC).

Materials and methods: The study included 158 NSCLC patients diagnosed with brain metastasis from December 2003 to August 2017. Ninety-nine patients underwent external beam radiotherapy (EBRT group), and 59 patients received iodine-125 brachytherapy (^{125}I group). In addition, the 6- and 12-month progression-free survival (PFS) rates and the 12- and 24-month overall survival (OS) rates were compared between the EBRT group and the ^{125}I group. Median OS and PFS were analyzed using the Kaplan–Meier method with a log-rank test.

Results: The 6-month PFS rate was significantly higher in the ^{125}I group (p = 0.002) than in the EBRT group, while no differences were found in the 12-month PFS rate (p = 0.184). Additionally, the 12- (p = 0.839) and 24-month (p = 0.284) OS rates were not significantly different between the two groups. No significant differences in median OS (p = 0.525) or PFS (p = 0.425) were found between the two groups.

Conclusions: Iodine-125 brachytherapy is an alternative therapy for patients unable to undergo surgical resection.

KEYWORDS

iodine-125, brachytherapy, brain metastasis, non-small cell lung cancer, external beam radiotherapy

Introduction

Lung cancer is one of the leading causes of cancer-related mortality. Approximately 57% of patients with non-small cell lung cancer (NSCLC) present with metastasis. At the time of diagnosis, 20% of patients have brain metastases (BMs) (1, 2). Approximately 25% to 50% of patients will present with BMs during the course of the disease (3).

For BMs, surgical resection is often the option to alleviate symptoms. Various studies have confirmed the efficacy of surgical resection combined with postoperative radiation therapy (4). However, some of the patients presenting with BMs could not undergo surgical resection because of location, tumor volume, or poor medical conditions. Additionally, some patients reject the surgery and fear the side effects. The efficacy of radiotherapy without surgical resection has been approved. However, the prescribed dose of external beam radiotherapy (EBRT) should not be further increased in consideration of the safety of the surrounding normal tissues.

In contrast to primary brain tumors, infiltration of metastases seldom occurs in the brain. Based on these characteristics, local treatment was superior in controlling metastases (3). Numerous data confirmed the efficacy of ^{125}I brachytherapy for local control. The minimally invasive, precise therapy allows a higher prescribed dose within the tumor and continuously releases low-dose rate γ-rays, which is different from EBRT. Various studies have confirmed the safety and efficacy of ^{125}I brachytherapy for a variety of tumors (5). In the present study, we aimed to evaluate the safety and efficacy of ^{125}I brachytherapy for newly diagnosed BMs in patients with NSCLC.

Materials and methods

Patient selection

The present study was approved by the institutional review boards of the two centers. The requirement for informed consent of the patients was waived. Patients' data between December 2003 and 25 August 2017 were analyzed. The inclusion criteria were as follows: a) NSCLC patients diagnosed with BMs, b) patients who previously received systemic treatment, and c) patients who received ^{125}I brachytherapy or EBRT as their initial treatment for BMs. The exclusion criteria were as follows: a) the BMs involved the bilateral cerebral hemisphere, b) the number of BMs was more than three, and c) patients with intratumoral hemorrhage. All patients could continue systemic treatment after EBRT or ^{125}I implantation.

Implantation of ^{125}I seeds

^{125}I seeds were implanted as we previously reported (6, 7). As shown in Figure 1, the implantation of ^{125}I seeds was performed with the guidance of a treatment planning system (TPS, Beijing Astro Technology Ltd. Co., Beijing, China). Patients were fixed on the CT bed with a vacuum pad. The puncture point was confirmed with a homemade locator. Holes were drilled after general anesthesia according to the preoperative plan. Flat needles were used to implant the ^{125}I seeds (0.7 mCi, Model 7711, Beijing Atom and High Technique Industries, Inc., Beijing, China). After the operation, vital signs were monitored, and dehydration medications were given.

EBRT

As shown in Figure 2, EBRT plans were carried out with a VMAT (RapidArc, Eclipse Treatment Planning System version 13, Varian, Palo Alto, USA) treatment planning system. EBRT planning was carried out with the CT images with a 2-mm slice thickness. According to the standard institutional protocols, the clinical target volumes (CTVs) were delineated. The head was immobilized with a thermoplastic mask. Photon beams which were generated through a linear accelerator and synchrotron were emitted and shaped with ridge filters, double-scattering sheets, multicollimators, and custom-made boluses.

Study outcomes

Basic characteristics were compared between the two groups. In addition, the 6- and 12-month PFS and the 12- and 24-month OS rates were compared between the two groups. OS was measured from the time of ^{125}I implantation or EBRT to the time of death or last follow-up. PFS was calculated from the time of ^{125}I implantation or EBRT to the time of tumor recurrence, progression, or death.

Statistical analysis

The date of the last follow-up was 13 December 2018. SPSS (Version 18.0, IBM, NY, USA) was used to analyze the data. χ^2 or Fisher's exact tests were used for categorical variable comparisons, and two-tailed Student's *t*-tests were used for continuous variable comparisons. Survival curves were evaluated using the Kaplan–Meier method with a log-rank test. For all analyses, a *p*-value <0.05 was considered of significant difference.

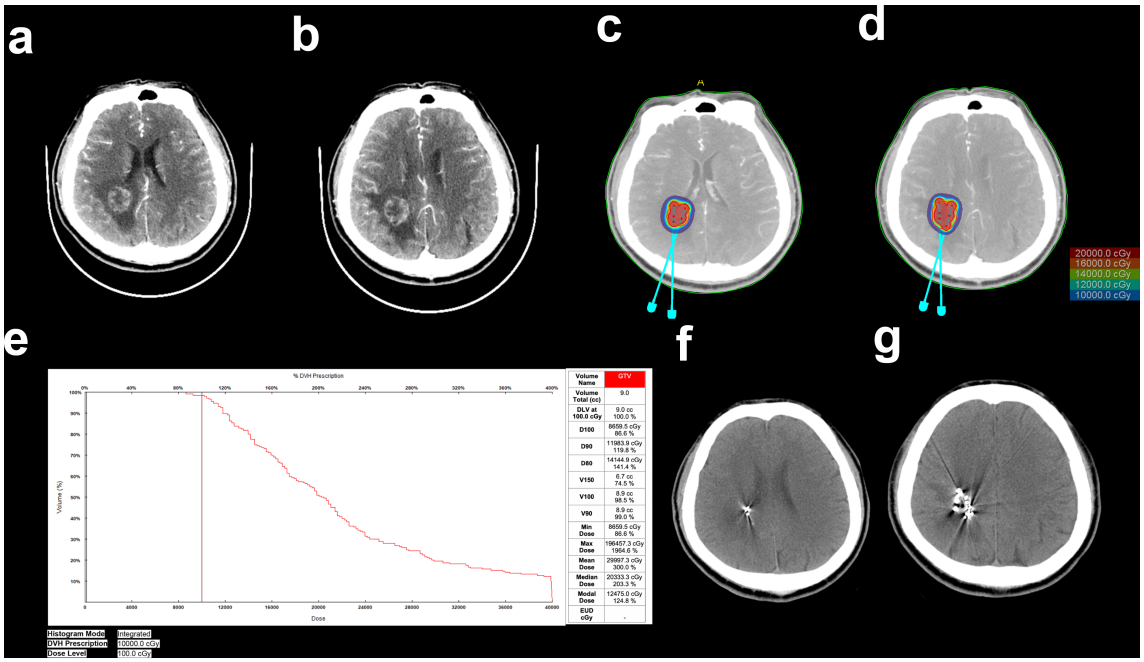

FIGURE 1
Implantation of ^{125}I seeds with the guidance of TPS. **(A, B)** Enhanced CT images of BMs resulting from NSCLC. **(C, D)** Needle paths were designed with TPS. **(E)** Preimplantation dose volume histogram (DVH) of GTV. **(F, G)** CT images of the brain after ^{125}I seed implantation.

Results

Patient characteristics

Basic data were compared between the two groups preoperatively. No differences were found in terms of sex, age, Karnofsky performance score (KPS), neurological symptoms, or chemotherapy. In the EBRT group, 5, 42, and 52 BMs were located in the right, left, and both hemispheres, respectively. In the ^{125}I group, 32, 21, and 6 BMs were located in the right, left, and both hemispheres ($p < 0.001$), respectively. The ratio of patients with BM diameters greater than 3 cm in the ^{125}I group was greater than that in the EBRT group ($p < 0.001$). The median diameter of the tumor was 2 cm (range, 0.6–4.8 cm) in the EBRT group and 3 cm in the ^{125}I group (range, 1.5–5 cm). The median prescribed dose (PD) was 41.3 Gy in the EBRT group and 93.5 Gy in the ^{125}I

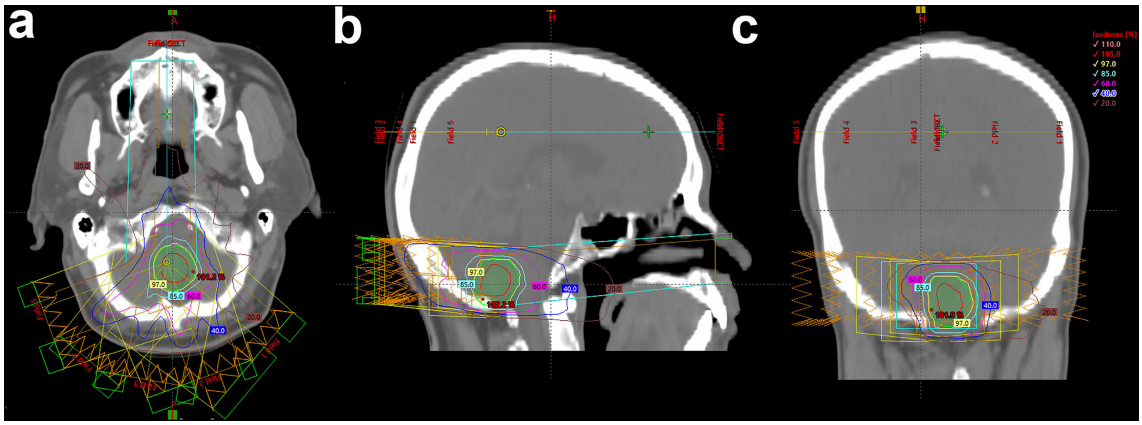

FIGURE 2
Example of the treatment planning of EBRT. **(A)** Traverse, **(B)** sagittal, and **(C)** coronal views of the treatment planning.

10.3389/fonc.2022.1005876

group. The differences were significant ($p < 0.001$) (Table 1). Brain stem was recognized as the organ at risk. The maximum tolerated dose is 79.6 Gy. Thus, the BED and EQD2 were calculated according to the following formulae (8): BED = $D[1 + R0/(\mu + \lambda)\ (\alpha/\beta)] = 83.3$ Gy; EQD2 = BED/$[1 + 2/(\alpha/\beta)] = 50.0$ Gy.

Postoperative complications

No fatal complications occurred after treatment. No radiation-related necrosis was found in either of the groups. Three patients in the ^{125}I group suffered a minor cerebral hemorrhage during the operation. Edema was exacerbated in 15 and 2 patients in the EBRT and ^{125}I groups, respectively. No severe neurological symptoms or infections occurred during the therapies.

Analysis of survival

As shown in Table 2, the 6-month PFS rates were 51.5% and 76.3% in the EBRT and ^{125}I groups, respectively. The differences were significant ($p = 0.002$). The 12-month PFS rates were 30.3% and 40.0% in the EBRT and ^{125}I groups, respectively. No significant differences were found ($p = 0.184$). The 12-month OS rates were 66.1% and 67.7% in the EBRT and ^{125}I groups, respectively ($p = 0.839$). The 24-month OS rates were 35.4% and 27.1% in the EBRT and ^{125}I groups, respectively ($p = 0.284$). The median PFS was 6 and 10 months in the EBRT and ^{125}I groups, respectively ($p = 0.425$) (Figure 3). The median OS was 18 and 16 months in the EBRT and ^{125}I groups, respectively. The log-rank test indicated that no differences were found between OS in the two groups ($p = 0.525$) (Figure 3).

TABLE 1 Characteristics of NSCLC patients with BMs in the two groups.

Characteristic	EBRT	^{125}I	*p*-value
Gender			0.284
Male	59	30	
Female	40	29	
Age			0.366
≥60	43	30	
<60	56	29	
KPS			0.117
≥90	39	16	
<90	60	43	
Neurological symptoms			0.034
Yes	69	50	
No	30	9	
Tumor location			<0.001
Right	5	32	
Left	42	21	
Both	52	6	
Diameter (cm)			
≥3	24	35	<0.001
<3	75	24	
Median (range)	2 (0.6–4.8)	3 (1.5–5)	
Time between diagnosis and treatment (months)			
Median (range)	2 (0.5–5.5)	2 (0.5–6.5)	
Chemotherapy			0.126
Yes	95	53	
No	4	6	
Dose (Gy)			<0.001
Mean (range)	41.3 (22.8–60)	93.5 (80–120)	

EBRT, external beam radiotherapy; KPS, Karnofsky performance score.

TABLE 2 PFS and OS control rate at different time points.

Rate	^{125}I (%)	EBRT (%)	*p*-value[a]
6-month PFS	76.3	51.5	0.002
12-month PFS	40.7	30.3	0.184
12-month OS	67.7	66.1	0.839
24-month OS	27.1	35.4	0.284

[a]Data were compared with the χ^2 tests.

Discussion

The present study indicated that both external beam radiotherapy and ^{125}I brachytherapy resulted in excellent local control of the disease. The retrospective study suggested that both ^{125}I brachytherapy and EBRT are effective therapeutic choices for NSCLC patients with BMs. The ^{125}I group had a higher 6-month PFS control rate than the EBRT group.

The prognosis of lung cancer patients with BMs is poor (9). As shown in a Swedish cohort study, the median survival time of lung cancer patients with BMs was only 2.5 months, and the 24-month OS rate was only 10.4% (10). Surgical resection is the best option for patients with single-brain metastasis. Surgery provides a debulking of the mass effect, an effective local control, and tissue for diagnosis. Numerous studies have reported the efficacy of surgical resection for brain metastasis. Nakagawa et al. (11) reported that the overall mean survival was 11.6 months, and the 1-year survival rate was 24% in 89 NSCLC patients with brain metastasis (12). However, surgery was not an option for patients with a large tumor volume in a limited location or in a poor medical condition. For those patients, EBRT is the best option. A series of studies confirmed the therapeutic safety and efficacy of EBRT (9). In recent years, ^{125}I brachytherapy has been widely used for various tumors, including prostate cancer, lung cancer, pancreatic cancer, esophageal cancer, colorectal cancer, cervical cancer, head and neck cancer, and liver cancer (13–19).

In the present study, we compared ^{125}I brachytherapy with EBRT for NSCLC patients with BMs in whom surgery was not an option. According to the K-M analysis with a log-rank test, there were no statistically significant differences between the two groups in terms of the median OS and PFS. The results indicated that ^{125}I brachytherapy could be chosen as an alternative treatment to EBRT for NSCLC patients with BMs. Interestingly, when we compared the 6-month PFS rate between the two groups, ^{125}I brachytherapy showed better results than EBRT. The 6-month PFS rates were 51.5% and 76.3% in the EBRT and ^{125}I groups, respectively. These results may support that ^{125}I brachytherapy was better than EBRT at achieving 6-month local control for NSCLC patients with BMs. Because patients were mostly afraid of radiation damage to normal tissue, the increase in PD was limited during EBRT. ^{125}I seeds were implanted within the tumors, and the half-value layers of the seeds in the soft tissue were 1.7 cm. Thus, for BM treatment, the mean PD of the ^{125}I seeds was elevated to an average of 93.5 Gy in this study. No severe radiation damage was found. The underlying reason could be that the ^{125}I seeds were implanted within the tumor, continuously releasing low-dose γ-rays, which is different from EBRT. The half-life period of ^{125}I is 60.2 days (11), and the duration of the therapy is generally

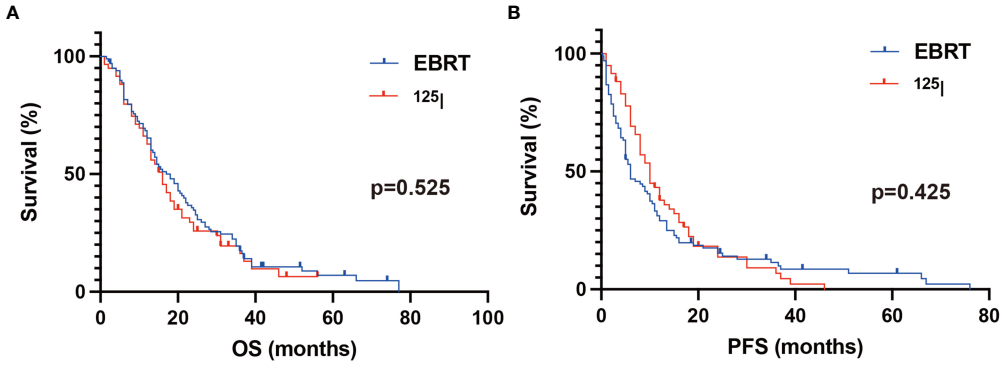

FIGURE 3
Kaplan–Meier analysis of OS and PFS. **(A)** The median OS was 18 and 16 months in the EBRT and ^{125}I groups, respectively. The log-rank test showed no statistical differences between the two groups (p = 0.525). **(B)** The median PFS in the ^{125}I and EBRT groups was 10 and 6 months, respectively. No significant difference was found between the groups with a log-rank test (p = 0.425).

considered to be 6 to 8 months, which may partly explain why the 6-month PFS rate was higher in the ^{125}I group than in the EBRT group. No significant differences were found when comparing the 12-month PFS rate with the 12- and 24-month OS rates. These results indicated that repeated ^{125}I implantation might be needed to obtain a higher 6-month PFS rate.

However, ^{125}I seed implantation is a minimally invasive treatment compared with surgical resection. Edema, bleeding, and infection sometimes occur. The complications are typically not severe and can be controlled after conservative treatment. Safety has been proven in several studies (5, 15, 16). No fetal complications were found in either of the groups. Although previous studies reported radiation-induced normal brain tissue necrosis around the lesion during radiation therapy, the risk of radionecrosis is approximately 10%, 15%, or 20% for patients with brain metastases who received single-fraction stereotactic radiosurgery. The volume of the tissues receiving 12 Gy was 5, 10, or >15 cm^3, respectively (20, 21), while no radiation-related necrosis was found in the present study even with a higher PD in the ^{125}I group. As we previously reported, flat needles were used during ^{125}I implantation (6, 7). However, bleeding still occurred in 3 patients in the ^{125}I group during the operation. Edema was worsened in 2 patients and 15 patients in the EBRT group and the ^{125}I group, respectively, which was relieved after routine dehydration medication.

Patients received EBRT Monday–Friday each week for approximately 4–6 weeks. For patients who received ^{125}I implantation, the therapy was mostly completed at one time, and patients were discharged from the hospital approximately 3–5 days after the operation. The patients made a one-time payment of approximately $3,000 to $5,000 for EBRT or ^{125}I therapy. Although ^{125}I is an invasive therapy, it is more convenient for patients than EBRT.

In the present study, we compared ^{125}I brachytherapy with EBRT for the treatment of BMs in patients with NSCLC. No significant differences were found between the two groups, except for the 6-month PFS rate. The safety of ^{125}I brachytherapy was confirmed. The results indicated that for NSCLC patients with BMs unsuitable for surgery, ^{125}I brachytherapy was a safe and effective therapy choice.

Data availability statement

The data analyzed in this study are subject to the following licenses/restrictions: The dataset is not publicly available, but it can be obtained under reasonable request from the authors. Requests to access these datasets should be directed to Xiaokun Hu, huxiaokun770@163.com.

Ethics statement

The studies involving human participants were reviewed and approved by The Affilated Hospital of Qingdao University. Written informed consent for participation was not required for this study in accordance with the national legislation and the institutional requirements.

Author contributions

CW and LY conducted all the experiments, integrated the data, edited the figures, and wrote the manuscript. WZ, SL, TX, and HJ provided essential assistance. XH, MH, and HL directed this study, designed the research, and gave key advice. All authors contributed to the article and approved the submitted version.

Funding

This work was supported by the Ministry of Science and Technology of the People's Republic of China (No. 2019YFE0120100); National Science Foundation for Youths of China (No. 81901800); Foundation of Taishan Scholars Project; China Postdoctoral Science Foundation (No. 2021M701812); Chinese Medical Education Association (No. 2020KTZ003); Science and Technology Plan of Shinan District, Qingdao (2022-2-001-YY); and Qingdao Postdoctoral Applied Research Project.

Conflict of interest

The authors declare that the research was conducted in the absence of any commercial or financial relationships that could be construed as a potential conflict of interest.

Publisher's note

All claims expressed in this article are solely those of the authors and do not necessarily represent those of their affiliated organizations, or those of the publisher, the editors and the reviewers. Any product that may be evaluated in this article, or claim that may be made by its manufacturer, is not guaranteed or endorsed by the publisher.

References

1. Siegel RL, Miller KD, Jemal A. Cancer statistics, 2019. *CA Cancer J Clin* (2019) 69:7–34. doi: 10.3322/caac.21551

2. Barnholtz-Sloan JS, Sloan AE, Davis FG, Vigneau FD, Lai P, Sawaya RE. Incidence proportions of brain metastases in patients diagnosed (1973 to 2001) in the metropolitan Detroit cancer surveillance system. *J Clin Oncol* (2004) 22:2865–72. doi: 10.1200/JCO.2004.12.149

3. Stinchcombe TE, Ernani V. Management of brain metastases in non–Small-Cell lung cancer. *J Oncol Pract* (2019) 15:9. doi: 10.1001/jamanetworkopen.2022.9553

4. Patchell RA, Tibbs PA, Regine WF, Dempsey RJ, Mohiuddin M, Kryscio RJ, et al. Postoperative radiotherapy in the treatment of single metastases to the BrainA randomized trial. *JAMA* (1998) 280:1485–9. doi: 10.1001/jama.280.17.1485

5. Schwarz SB, Thon N, Nikolajek K, Niyazi M, Tonn J-C, Belka C, et al. Iodine-125 brachytherapy for brain tumours - a review. *Radiat Oncol* (2012) 7:1–28. doi: 10.1186/1748-717X-7-30

6. Wang C, Xu Z, Wang S, Peng L, Zhang W, Li X, et al. Clinical importance of ADC in the prediction of (125)I in the treatment for gliomas. *J Cancer* (2021) 12:1945–51. doi: 10.7150/jca.50789

7. Wang C, Liu S, Peng L, Zhang K, Li W, Zhang H, et al. Permanent iodine-125 brachytherapy for patients with progressive or recurrent high-grade gliomas. *BMC Cancer* (2020) 20:1–8. doi: 10.1186/s12885-020-07086-8

8. Dale RG, Jones B. Radiobiological modelling in radiation oncology. *Br Inst Radiol* (2007). doi: 10.1259/9780905749839

9. Kawabe T, Phi JH, Yamamoto M, Kim DG, Barfod BE, Urakawa Y. Treatment of brain metastasis from lung. *Radiosurgery* (2012) 25:8. doi: 10.11606/T.5.2022.tde-19072022-182043

10. Smedby KE, Brandt L, Bäcklund ML, Blomqvist P. Brain metastases admissions in Sweden between 1987 and 2006. *Br J Cancer* (2009) 101:1919–24. doi: 10.1038/sj.bjc.6605373

11. Marwaha G, Macklis R, Singh AD, Wilkinson A. Brachytherapy. *Dev Ophthalmol* (2013) 52:29–35. doi: 10.1159/000351053

12. Nakagawa H, Miyawaki Y, Fujita T, Kubo S, Tokiyoshi K, Tsuruzono K, et al. Surgical treatment of brain metastases of lung cancer: retrospective analysis of 89 cases. *J Neurology Neurosurg Psychiatry* (1994) 57:950–6. doi: 10.1136/jnnp.57.8.950

13. Park DS, Gong IH, Choi DK, Hwang JH, Shin HS, Oh JJ. Radical prostatectomy versus high dose permanent prostate brachytherapy using iodine-125 seeds for patients with high risk prostate cancer: a matched cohort analysis. *World J Urol* (2013) 31:1511–7. doi: 10.1007/s00345-013-1086-3

14. Wang ZM, Lu J, Liu T, Chen KM, Huang G, Liu FJ. CT-guided interstitial brachytherapy of inoperable non-small cell lung cancer. *Lung Cancer* (2011) 74:253–7. doi: 10.1016/j.lungcan.2011.03.006

15. Wang JJ, Yuan HS, Li JN, Jiang WJ, Jiang YL, Tian SQ. Interstitial permanent implantation of 125I seeds as salvage therapy for re-recurrent rectal carcinoma. *Int J Colorectal Dis* (2009) 24:391–9. doi: 10.1007/s00384-008-0628-4

16. Liu Y, Jiang P, Zhang H, Wang J. Safety and efficacy of 3D-printed templates assisted CT-guided radioactive iodine-125 seed implantation for the treatment of recurrent cervical carcinoma after external beam radiotherapy. *J Gynecol Oncol* (2021) 32:e15. doi: 10.3802/jgo.2021.32.e15

17. Jiang Y-L, Meng N, Wang J-J, Ran W-Q, Yuan H-S, Qu A, et al. Percutaneous computed tomography/ultrasonography-guided permanent iodine-125 implantation as salvage therapy for recurrent squamous cell cancers of head and neck. *Cancer Biol Ther* (2014) 9:959–66. doi: 10.4161/cbt.9.12.11700

18. Chen L, Kan X, Sun T, Ren Y, Cao Y, Yan L, et al. Transarterial chemoembolization combined with iodine 125 seeds versus transarterial chemoembolization combined with radiofrequency ablation in the treatment of early- and intermediate-stage hepatocellular carcinoma. *BMC Gastroenterol* (2020) 20:205. doi: 10.1186/s12876-020-01355-3

19. Zou YP, Li WM, Zheng F, Li FC, Huang H, Du JD, et al. Intraoperative radiofrequency ablation combined with 125 iodine seed implantation for unresectable pancreatic cancer. *World J Gastroenterol* (2010) 16:5104–10. doi: 10.3748/wjg.v16.i40.5104

20. Le Rhun E, Dhermain F, Vogin G, Reyns N, Metellus P. Radionecrosis after stereotactic radiotherapy for brain metastases. *Expert Rev Neurother* (2016) 16:903–14. doi: 10.1080/14737175.2016.1184572

21. Milano MT, Grimm J, Niemierko A, Soltys SG, Moiseenko V, Redmond KJ, et al. Single- and multifraction stereotactic radiosurgery Dose/Volume tolerances of the brain. *Int J Radiat Oncol Biol Phys* (2021) 110:68–86. doi: 10.1016/j.ijrobp.2020.08.013

frontiers | Frontiers in Oncology

TYPE Review
PUBLISHED 15 December 2022
DOI 10.3389/fonc.2022.1085034

OPEN ACCESS

EDITED BY
Xingchun Gao,
Xi'an Medical University, China

REVIEWED BY
Chunming Cheng,
The Ohio State University,
United States
Xiangjun Tang,
Yale University, United States

*CORRESPONDENCE
Ayenachew Bezawork-Geleta
bezaworkgeleta.a@unimelb.edu.au

SPECIALTY SECTION
This article was submitted to Neuro-Oncology and Neurosurgical Oncology, a section of the journal Frontiers in Oncology

RECEIVED 31 October 2022
ACCEPTED 18 November 2022
PUBLISHED 15 December 2022

CITATION
Bezawork-Geleta A, Dimou J and Watt MJ (2022) Lipid droplets and ferroptosis as new players in brain cancer glioblastoma progression and therapeutic resistance.
Front. Oncol. 12:1085034.
doi: 10.3389/fonc.2022.1085034

Lipid droplets and ferroptosis as new players in brain cancer glioblastoma progression and therapeutic resistance

Ayenachew Bezawork-Geleta[1]*, James Dimou[2,3] and Matthew J. Watt[1]

[1]Department of Anatomy and Physiology, School of Biomedical Sciences, The University of Melbourne, Melbourne, VIC, Australia, [2]Department of Surgery, The University of Melbourne, Parkville, VIC, Australia, [3]Department of Neurosurgery, The Royal Melbourne Hospital, Parkville, VIC, Australia

A primary brain tumor glioblastoma is the most lethal of all cancers and remains an extremely challenging disease. Apparent oncogenic signaling in glioblastoma is genetically complex and raised at any stage of the disease's progression. Many clinical trials have shown that anticancer drugs for any specific oncogene aberrantly expressed in glioblastoma show very limited activity. Recent discoveries have highlighted that alterations in tumor metabolism also contribute to disease progression and resistance to current therapeutics for glioblastoma, implicating an alternative avenue to improve outcomes in glioblastoma patients. The roles of glucose, glutamine and tryptophan metabolism in glioblastoma pathogenesis have previously been described. This article provides an overview of the metabolic network and regulatory changes associated with lipid droplets that suppress ferroptosis. Ferroptosis is a newly discovered type of nonapoptotic programmed cell death induced by excessive lipid peroxidation. Although few studies have focused on potential correlations between tumor progression and lipid droplet abundance, there has recently been increasing interest in identifying key players in lipid droplet biology that suppress ferroptosis and whether these dependencies can be effectively exploited in cancer treatment. This article discusses how lipid droplet metabolism, including lipid synthesis, storage, and use modulates ferroptosis sensitivity or tolerance in different cancer models, focusing on glioblastoma.

KEYWORDS

brain cancer, metabolism, lipids, cell death, therapeutic vulnerabilities, glioma, lipid droplet (LD)

Introduction

Glioblastoma, designated as WHO grade 4, is the most common and most aggressive intra-axial brain tumor and has limited treatment options (1–3). The development of cancer therapies has improved outcomes for most malignancies, with the five-year survival of patients ranging from 25–95% (4–6). In contrast, glioblastoma remains overwhelmingly lethal, with only ~5% of patients alive five years after diagnosis (7).

The gold standard treatment of glioblastoma includes maximal safe surgical resection (8) combined with radiotherapy and temozolomide chemotherapy, which is referred to in neuro-oncology circles as the Stupp protocol (1, 2)**;** however, relapse remains inevitable. Temozolomide (chemical name 3-methyl-4-oxoimidazo[5,1-d](1–3, 5)tetrazine-8-carboxamide (9)) has several advantages, such as oral administration, a favorable side-effect profile, evidence of blood–brain barrier penetration, acidic environment stability, and limited drug interaction-related toxicity. The original randomized controlled trial published by Stupp et al. (1, 2) showed that adding postoperative adjuvant temozolomide chemotherapy to surgery and radiotherapy increased the median survival of glioblastoma patients from 12.1 months to 14.6 months. Bevacizumab, a monoclonal antibody targeted to vascular endothelial growth factor A (VEGF-A), has been shown to offer some progression-free survival benefits in patients who develop recurrent glioblastoma (10). Another study has shown that epigenetic silencing of the DNA repair gene O-6-methylguanine-DNA methyltransferase (MGMT) offers a superior response to chemoresistance tumors to temozolomide (11). However, it has limited therapeutic efficacy due to recurrence.

For three decades, other strategies have been pursued to improve the survival outcomes of glioblastoma patients (12, 13). Considerable efforts have been made to catalog genetic aberrations and associated disrupted signaling pathways in glioblastoma for the purpose of developing novel targeted therapies. The first genome atlas study by The Cancer Genome Atlas (TCGA) Research Network uncovered 453 validated missense somatic mutations in glioblastoma (14). Subsequent systematic analysis at the genomic and transcriptomic levels showed that 71 mutated genes as significant pathogenic factors (14, 15). Histological and molecular analysis further revealed a landscape of tumor heterogeneity, which led to efforts to differentiate glioblastoma into distinct molecular subtypes (16, 17). An early attempt at such molecular classification by Verhaak et al. distinguished glioblastoma into four molecular subtypes: proneural, mesenchymal, classical, and neural (18). The classical subtype was characterized by amplification of epidermal growth factor receptor (EGFR) and associated with the upregulation of retinoblastoma (RB), sonic hedgehog (SHH), and notch signaling-related pathway genes. The classical type typically lacks of TP53 mutation. Conversely, mesenchymal subtype glioblastomas were characterized by high expression of chitinase 3 like 1 (CHI3L1) and tyrosine-protein kinase Met (MET), a high frequency of neurofibromin 1 (NF1) mutation/deletion, and low NF1 gene expression. Key proneural subtype markers are TP53 aberrations and metabolic enzyme isocitrate dehydrogenase 1 (IDH1) mutation and platelet-derived growth factor receptor alpha (PDGFRA). The neural subtype expressed neurofilament light chain (NEFL), gamma-aminobutyric acid type A receptor subunit alpha1 (GABRA1), synaptotagmin 1 (SYT1), and solute carrier family 12 member 5 (SLC12A5). It has been proposed that these specific subtypes of glioblastoma develop due to promutagenic aberrations in distinct cells of origin (18). However, due to the inclusion of mRNA from glioblastoma-associated stroma (nonmalignant cells) along with tumor cells in the Verhaak et al. transcriptome study, these four pathological subtypes subjected to further interrogation. Accordingly, Wang et al. (19) used stringent criteria to distinguish specific mRNA from peripheral nonmalignant cells by comparing the transcriptome of core versus peripheral glioblastoma surgery specimens and mRNA profile from glioblastoma cell culture and revealed the presence of only three pathological subtypes (i.e., classical, proneural, and mesenschymal subtypes). Subsequent studies also classify glioblastoma into different prognostic subtypes (20–22) using different multi-omics signatures.

Recently, the integration of cross-platform analyses coupling metabolomic profiling with genomics and proteomics has provided an in-depth understanding of the metabolic programming that occurs during tumor growth. It has identified key metabolic nodes specific to glioblastoma and their molecular context. Notable findings of mutations in the metabolic enzyme IDH1, representing an early event in gliomagenesis (22, 23), have led to an in-depth study of metabolic status across all grades and subtypes of glioma. However, it must be stressed that the presence of IDH1 mutation now precludes the formal pathological diagnosis of glioblastoma, as it is now genetically defined as "IDH-wildtype" in the most recent edition of the WHO Classification of CNS Tumors (24).

Further, it has been found that glucose, glutamine, and tryptophan metabolism play roles in glioblastoma progression and recurrence following surgery and chemotherapy (25–28). Glutamine metabolism changes in glioblastoma have been incorporated into the clinical practice of noninvasive metabolic imaging strategies for stratifying patients, monitoring treatment response, and prognostication (29–32). Advances in metabolic imaging modalities, including magnetic resonance spectroscopy (MRS), positron emission tomography (PET), single-photon emission computerized tomography (SPECT), mass spectrometry imaging (MSI), and fluorescence imaging have given researchers and clinicians unprecedented opportunities for *in vivo* measurements of glutamine metabolism and clinical management of gliomas (29–32). In particular, PET using ^{11}C-glutamine allows noninvasive

visualization of glioma and various malignant tumors in multiple organs and for subsequent monitoring of responses to clinical treatments (29).

Unfortunately, our ever-improving understanding of the molecular basis of glioblastoma initiation and progression has not yet translated to therapeutic success (17). This requires the interrogation of novel molecular signaling mechanisms and metabolic processes in glioblastoma and their exploitation for therapeutic progress. To this end, lipid metabolism and ferroptosis have only recently been explored and identified as key regulators in the initiation and maintenance of glioblastoma (33–35) and other cancers (36–38). Notable related discoveries and translations include the recently developed and characterized selective, irreversible, and potent fatty acid synthase (FASN) inhibitor IPI-9119 (39), as well as the identification of druggable targets, including ATP-citrate lyase (ACLY) (40) and the plasma membrane lipid importer CD36 (41). This review examines recent studies showing lipid droplets' critical role in suppressing ferroptosis to promote tumorigenesis.

Features of ferroptosis

Ferroptosis is a recently discovered type of programmed cell death that exhibits unique morphological, biochemical and genetic features compared to previously characterized processes of cell death, including apoptosis, necrosis, and autophagy (42–44). Accordingly, ferroptosis does not depend on the mechanisms by which cancer cells frequently evade apoptosis, such as the activation of caspases. Apoptosis inhibitors (e.g., Z-VAD-FMK, BOC-D-FMK, wortmannin, and necrostatin-1) failed to protect cells from ferroptosis mediated cell death (42–44). Instead, ferroptosis is mainly embodied by accumulation iron, leading to lethal levels of lipid peroxidation. The typical cells in ferroptosis show extensive lipid peroxidative damage to biological membranes, shrunken mitochondria, and an increase in mitochondrial membrane density (45), indicating that execution of ferroptosis requires active mitochondrial function. Interestingly, the nucleus remains intact during ferroptosis, in contrast to other cell death mechanisms that lead to fragmented nuclei (43, 46, 47). Ferroptosis is also caused by a redox imbalance of cellular homeostasis, leading to the formation of a myriad of secondary byproducts, including breakdown products of lipid peroxides (e.g., malondialdehyde (MDA), 4-hydroxynonenal (4HNE), 4-hydroxyhexenal (4HHE), and 4-oxo-nonenal (4ONE)) and oxidized and modified proteins). This chain reaction may eventually lead to the breakdown of membrane integrity and the rupture of organelles and/or cell membranes and, ultimately, result in cell death (43–45, 48). In contrast, ferroptosis-mediated cell death can be modulated by the expression and activity of proteins that regulate the levels, transport, storage, and metabolism of iron, cystine, cysteine, GSH, glutamine, and selenium (43–45, 48). Antioxidant defense enzymes that repair oxidative damage to lipids, such as Glutathione peroxidase 4 (GPX4), are important inhibitors of ferroptosis (43–45, 48). Recently, it has been reported that Anti-TfR1 3B8 2A1 and anti-MDA 1F83 can be used to detect ferroptosis in both cell culture and xenograft tumor sections (49).

Although it was initially proposed to be the mechanism of neuronal death in many neurodegenerative diseases (43, 50, 51), emerging data indicate that ferroptosis plays an important role in cancer development and drug resistance (45). Therefore, inducing ferroptosis represents a potentially orthogonal approach to drug discovery to kill cancer cells that have developed resistance to apoptosis. Thus, a clearer understanding of ferroptosis in glioblastoma and its role in drug resistance may positively impact clinical practice (52, 53).

In and out of lipids: Lipid droplets as intracellular sources of fatty acids

Lipid droplets accumulate in cancers

Lipid droplets are fundamental in the storage and release of fatty acids. Lipid droplets are ubiquitously present organelles in many cells with a hydrophobic core surrounded by a single layer of phospholipids decorated with various sets of proteins. The hydrophobic core contains neutral lipids, including triacylglycerols, sterol esters, retinyl esters and 1-O-acylceramides (54–57). Emerging evidence indicated lipid droplet accumulation in several cancers (58, 59), especially in hypoxic cancer cells, and several studies have linked lipid droplet abundance with more aggressive tumor phenotype (34, 36, 58, 60). It has also shown lipid metabolism-dependent proliferation and survival of glioblastoma following radiation (61, 62), antiangiogenic (63) and ketone diet therapy (64). As such, they have recently been proposed to play direct roles in many cancers and considered a hallmark of fundamental tumor processes (58, 60, 65). The following sections discuss the possible roles of lipid droplet metabolism, including (1) fatty acid storage as neutral lipids, (2) lipolysis of neutral lipids, and (3) lipophagy in limiting or triggering ferroptosis.

De novo lipogenesis and ferroptosis

Lipogenesis (lipid acquisition) is an energy-expensive process of fatty acid synthesis and subsequent esterification to neutral lipids into lipid droplets. The primary process of synthesizing fatty acids from acetyl-CoA subunits that are produced most commonly from carbohydrate catabolism is called *de novo* lipogenesis (DNL) (66). Acetyl-coenzyme A (acetyl-CoA) is a key metabolite precursor in DNL, and its abundance is closely monitored by cellular adaptive

mechanisms. While glucose is the most common supplier of carbon units for DNL (Figure 1A), fructose is metabolized to glycerol and subsequently converted to a lipogenic substrate glycerol-3-phosphate (G3P) that can drive DNL.

Glutamine is another non-lipid metabolite that contributes carbon to lipogenic acetyl-CoA (Figure 1A) through two distinct pathways: Glutamine metabolism can produce citrate either through the tricarboxylic acid (TCA) cycle in mitochondria or by the reductive carboxylation of cytoplasmic α-ketoglutarate (αKG) to citrate by IDH1 (Figure 2) (67, 68). Interestingly, many cancer cells, including glioblastoma, generate 10–25% of their lipogenic acetyl-CoA from glutamine through reductively carboxylation (69), highlighting the general use of reductive carboxylation as the primary route to convert non-lipid carbon to lipids in cancer cells. In agreement with this, blood-borne glucose contribute minimal fraction to the acetyl-CoA pool of glioblastoma and brain metastases that originate from other tissues (70). In addition to a direct contribution of supplying a carbon unit, glucose and glutamine uptake promotes lipogenesis through transcriptional regulation in a sterol regulatory element-binding protein (SREBP) dependent manner in glioblastoma (71, 72).

Acetate, often dispensable for cells, has also been shown as a source of acetyl-CoA for DNL in cancer cells, especially primary glioblastomas and other cancer metastasis to brain (73, 74). In this case, three important processes need to be considered: acetate production, its intercellular import across the cell membrane, and the carbon fluxes from acetate to lipids. Imported acetate is converted to acetyl-CoA in a reaction catalyzed by acetyl-CoA synthetase 2 (ACSS2) (Figure 1A) (75). Thus, hypoxia-associated deficits in acetyl-CoA can be supplemented by increasing the use of free extracellular acetate (including plasma, interstitial fluid, and neighboring cells) and the intercellular pool of mainly acetate released from the deacetylation of histones and other cellular proteins (76). In line with acetate metabolism, apparent ACSS2 expression is associated with poor progenesis in glioblastoma patients (73, 74). Despite the fundamental importance of acetate and its vital roles to several intracellular and extracellular metabolism, little is known about the mechanisms and regulatory processes in acetate metabolism.

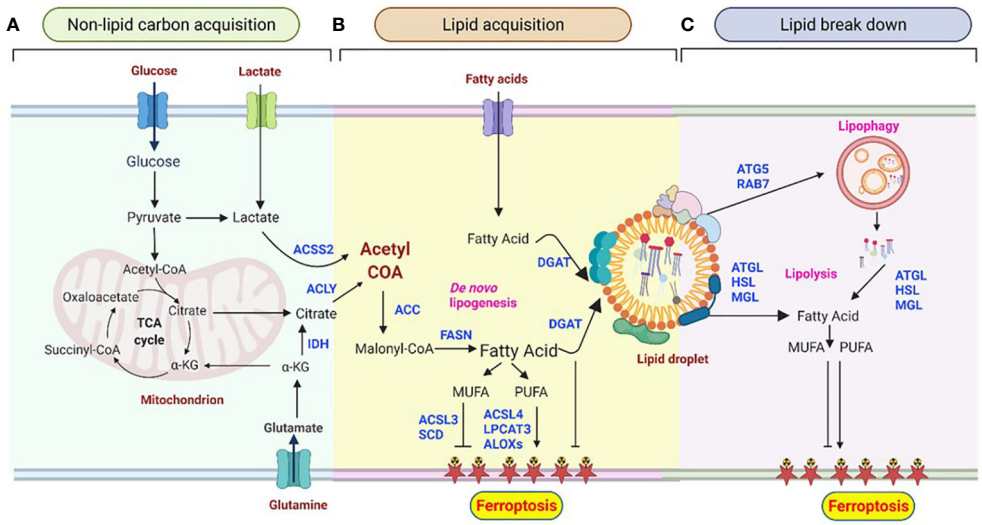

FIGURE 1
Lipid droplet metabolism is central to shaping the ferroptotic response. **(A)** Non-lipid carbon acquisition of carbon in cancer cells. Glucose- and glutamine-derived citrate, which results from increased glycolysis and glutaminolysis, is first converted to acetyl-coenzyme A (acetyl-CoA) by ATP-citrate lyase (ACLY). Acetyl-CoA can also be derived from acetate. **(B)** *De novo* lipogenesis (DNL) and esterification in ferroptosis. Acetyl-CoA is converted to malonyl-CoA by acetyl-CoA carboxylase (ACC) and condensed by fatty acid synthase (FAS). Acyl-CoA synthetase long-chain 4 (ACSL4) and lysophosphatidylcholine acyltransferase 3 (LPCAT3) mediate the production of polyunsaturated fatty acids (PUFAs), which are essential for the induction of ferroptosis. In contrast, acyl-CoA synthetase long-chain 3 (ACSL3) and stearoyl CoA desaturase (SCD) contribute to the synthesis of monounsaturated fatty acids (MUFAs), leading to ferroptosis resistance. Arachidonate lipoxygenases (ALOXs) catalyze the stereospecific insertion of oxygen into PUFAs, thereby promoting ferroptosis. Diacylglycerol acyltransferase (DGAT1/2)-mediated triglyceride synthesis and lipid droplet formation act as a sink for free fatty acids, thus preventing their peroxidation.**(C)** Lipid degradation in ferroptosis. The selective degradation of lipid droplets by member RAS oncogene family 7 (RAB7A)- and adipocyte triglyceride lipase (ATGL)-related lipophagy increases the production of free fatty acids for subsequent ferroptosis. Lipolysis may provide PUFAs, thus stimulating lipid peroxidation and sensitizing cells to ferroptosis. Lipases may also provide MUFAs that reduce the abundance of oxidizable PUFAs in membranes, thereby restricting lipid peroxidation and ferroptosis. Lipid droplets act as buffers of lipid flux and release, thereby emerging as master regulators of ferroptotic sensitivity.

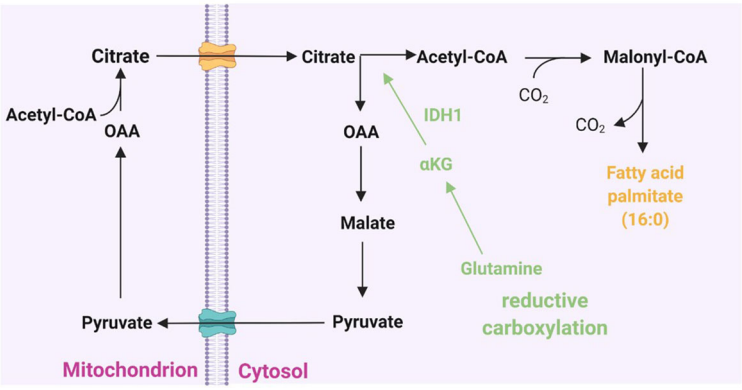

FIGURE 2
Cytoplasmic citrate pool and fatty acid synthesis. Acetyl-CoA couples with oxaloacetate (OAA) to form citrate at the beginning of the citric acid cycle. Citrate can then shuttle across the mitochondrial membrane to the cytoplasmic citrate pool. In the cytosol, citrate lyase splits citrate back into acetyl-CoA and OAA. The latter can then return to the mitochondrion. Acetyl-CoA is activated in the cytoplasm for incorporation into fatty acids by acetyl-CoA carboxylase to form malonyl-CoA and then to *de novo* fatty acid synthesis. Glutamine-derived α-ketoglutarate (α-KG) can add to the cytoplasmic citrate pool *via* reductive carboxylation to provide an alternative source of lipid synthesis.

Cytoplasmic acetyl-CoA is then carboxylated by acetyl-CoA carboxylase (ACC) to produce malonyl-CoA (Figure 1B), which is further used to synthesizes medium-and long-chain fatty acids. The key three proteins involved in the initial fatty acyl chain biosynthesis, ACLY, ACC, and FASN, are commonly upregulated and activated in many cancers (36, 60, 65), and they are in the frontline of pre-clinical target evaluations, drug discovery pipelines, and clinical trials. For instance, the therapeutic targeting of FASN is currently being explored in a phase 2 clinical trial in patients with glioblastoma using the FASN inhibitor TVB-2640 in combination with bevacizumab (NCT03032484) (28).

De novo synthesized fatty acids are then further esterified to neutral lipids and stored in their nontoxic (inert, neutral) form in lipid droplets (Figure 1B). Esterification starts with the acylation of glycerol-3-phosphate with two fatty acids to produce phosphatidic acid (PA), followed by dephosphorylation to yields diacylglycerol (DAG). DAG then serves as a precursor for the synthesis of both phospholipids and acylation to yield triacylglycerols (TAGs), which is catalyzed by diacylglycerol acyltransferase 1 and 2 (DGAT1 and DGAT2) (77, 78). TAG is stored in lipid droplets as energy reservoir, supplying the cell with energy when required.

Lipid droplets also store 1-O-acylceramides and cholesteryl ester. Although some studies indicated a minimal abundance of1-O-acylceramides in tissue (0.25-1.3 per mg of mice tissue), the indication of its level during Western diet consumption (79) warrants special attention, mainly its correlation with cancer progression in obese glioblastoma patients. Cholesteryl ester is another neutral lipid stored in lipid droplets. Acyl-CoA acyltransferase, also known as acyl-Coenzyme A or cholesterol acyltransferase (SOAT1 and SOAT2), catalyzes the formation of cholesteryl esters, using cholesterol and long-chain fatty acyl-CoA as substrates. Both isoforms of acyl-CoA acyltransferase (ACAT1 and ACAT2) are highly expressed and post-translationally regulated in glioblastomas and other cancers, and their expression and activation levels correlate with patient survival (79–81). *In vivo* studies showed that both genetic silencing of ACAT1 or blocking its activity using inhibitors suppresses tumor growth (80, 82, 83). These suggest that targeting ACAT1 and cholesteryl ester synthesis may be a promising anticancer strategy.

The *de novo* synthesis of fatty acids can be extended to the formation of either saturated or unsaturated fatty acids. Unsaturated fatty acids can be further classified into monounsaturated fatty acids [MUFAs, with only one double bond, e.g., oleic acid (18:1)] and polyunsaturated fatty acids [PUFAs, with at least two double bonds, e.g., linoleic acid (18:2 n-6) and α-linolenic (18:3 n-3)]. Unsaturated fatty acids can bind membrane phospholipids in differential degrees that subject tumor cells to oxidative stress. Studies have revealed that an increase in the MUFA/PUFA ratio results in fewer peroxidation-susceptible targets, ultimately reducing the susceptibility of cancer cells to ferroptosis (84). On the other hand, an increase in the synthesis of PUFAs can promote subsequent lipid peroxidation in cancer cells under oxidative stress conditions, suggesting that the formation of acetyl-CoA derivatives (*de novo* synthesis) of these PUFA is necessary for producing ferroptosis death signals (43, 45). Similarly, the esterification of fatty acids into neutral lipids has been shown to deplete the substrates for lipid peroxidation and increase the resistance of cancer cells to ferroptosis-mediated cell death (34, 36, 60, 85).

Lipid peroxidation normally occurs at a slow rate because PUFAs are required to react with the free radicals generated by iron acyl-CoA synthase long-chain family member 4 (ACSL4).

Using genetic ablation and pharmaceutical inhibition, it has been shown that ACSL4 is a rate-limiting enzyme to catalyze the conversion of long-chain PUFAs, such as arachidonic acid and eicosapentaenoic acid to PUFA-CoA, and ultimately this increases lipid peroxidation and decreases resistance to ferroptosis (86–88). Under oxidative or energetic stress, PUFAs, particularly arachidonoyl (AA, 20:4 n-6) and adrenic acid (AdA), are oxygenated by different classes of enzymes, including ACSL4, lysophosphatidylcholine acyltransferase (LPCAT), and 15-lipoxygenase (15-LOX/ALOX15), to generate PUFA-containing phospholipids and various bioactive lipids that modulate sensitivity to ferroptosis. In this regard, genetic or pharmacological inhibition of ACSL4 suppresses ferroptosis in glioblastoma (86). On the other hand, overexpression of ACSL4 was shown to increase the levels of ferroptosis markers, including 5-hydroxyeicosatetraenoic acid (HETE), 12-HETE, and 15-HETE (86), indicating a key role of ACSL4 in regulating ferroptosis and proliferation of glioma cells (89). Independent experimental evidence showed that suppressing miR-670-3p, which targets ACSL4, also modulates the sensitivity of glioblastoma cells to ferroptosis-mediated cell death (87, 90).

Esterification and ferroptosis

Blocking the esterification of fatty acyl-CoA prevents not only the formation of triglycerides but also modifies cell resistance to ferroptosis. It has been shown that in 3D tumor spheroids and *in vivo*, DGAT inhibition induces significant cytotoxic effects, especially when combined with dietary long-chain PUFAs (LC-PUFAs), implicating the combination of diet (LC-PUFAs) and DGAT inhibitor (DFATi) administration as a highly relevant therapeutic combination to induce ferroptosis (85). Mechanistically, DGATi administration inhibits lipid droplet formation resulting in the availability of more LC-PUFAs for peroxidation and ferroptotic cell death (85). In contrast, DGAT1 inhibition was recently reported to drive fatty acid-dependent oxidation in mitochondria generating high levels of reactive oxygen species, leading to apoptosis and significant growth inhibitory effects in glioblastoma (91). These contradictory reports are likely due to the difference in cell lineage, or a potential secondary effect associated with DGAT1 inhibition. Therefore, it will be relevant in the future to dissect the relative contributions of DGAT in different cancers, including glioblastoma, and the potential overlapping effects of DGAT inhibition on ferroptosis and apoptosis.

Lipolysis and lipophagy and their role in cell sensitivity to ferroptosis

Similar to lipid fluxes into lipid droplets that act as buffers, the release of fatty acids from storage controls the cancer cells' fate, including ferroptosis. Lipid droplet breakdown occurs *via* two major mechanisms-lipolysis, and lipophagy (Figure 1C), which provide a substrate for lipid peroxidation during ferroptosis. Unlike lipogenesis, the lipolysis process enables a highly regulated release of fatty acids from TAGs and is mediated by three essential lipases: adipocyte triglyceride lipase (ATGL), hormone-sensitive lipase (HSL), and monoacylglycerol lipase (MGL) (92–94). These three enzymes work together to promote the lipolysis of triglycerides and produce fatty acids and glycerol. ATGL catalyzes the first rate-limiting reaction whereby triglycerides are hydrolyzed to DAG. HSL then transforms DAG to monoacylglycerol (MAG), and MGL finally converts MAG to fatty acids and glycerol (93–96). However, the molecular regulation of the lipolysis of lipid droplet-containing triglycerides is complex. It involves a combination of subcellular localization, posttranslational modification (particularly phosphorylation), and protein-protein interactions (92, 97). For instance, hypoxia-induced lipid droplet-associated protein (HILPDA), also called hypoxia-induced gene-2 (HIG2), inhibits ATGL activity (98). Experimental evidence showed the correlation of the HIG2 expression with the glioma tumor grade and glioblastoma patient prognosis (34, 99).

Catabolism of lipid droplets also occur *via* lipophagy, a form of selective (macro)autophagy. Lipophagy is a process that tags specific lipid droplets and traffic whole lipid droplets to lysosomes for bulk degradation (Figure 1C). Lysosomal localized hydrolytic enzymes, such as triglycerides and cholesteryl ester hydrolase lysosomal acid lipase (LAL) (100), liberate neutral lipids stored in lipid droplet and generate free fatty acids and cholesterol in the cell. Although mechanistically lipolysis (the step-wise release of stored neutral lipids from lipid droplets) and lipophagy (a complete breakdown of lipid droplets) are distinct metabolic processes, it is not yet clear whether there is considerable crosstalk between the two processes and this may serve a distinct purpose in the cell (100, 101). It has been shown that perilipins (PLINs), lipid droplet surface proteins, act as gatekeepers to the lipophagy process and their degradation is a prerequisite for lipophagy. During starvation, perilipin 2 (PLIN2) and perilipin 3 (PLIN3) are proteolytically removed in parallel with the translocation of cytosolic ATGL and macroautophagy proteins onto lipid droplets (102). There is also evidence that PLIN2-mediated lipophagy regulation emerges as a key nodal point in modulating cellular sensitivity to ferroptosis. PLIN2 affects the proliferation of gastric carcinoma cells by modulating ferroptosis-related genes, including acyl-CoA synthetase long-chain family member 3 (ACL3), arachidonate 15-lipoxygenase (ALOXs), microtubule-associated protein 1 light chain 3 alpha (LC3), and the transcription factors pr/set domain 11 and importin 7 (IPO7) (103). Likewise, PLIN2 expression contributed to a decreased arachidonate 15-lipoxygenase (ALOX15) expression and arrested the occurrence of ferroptosis in gastric cancer. Conversely, PLIN2 knockdown

facilitated a higher ALOX15 expression and accelerated ferroptosis (103). In contrast, increased lipid storage by tumor protein D52 (TPD52), a PLIN2 interactor protein, diminished lipid peroxidation to trigger ferroptosis (104). Recently, PLIN2 was also shown to play a key role in glioblastoma pathology, although its role in ferroptosis has not been directly investigated (105).

It has also been shown that the knockdown of RAB7A (member RAS oncogene family 7A) and autophagy-associated gene 5 (ATG5), a cargo receptor of lipid droplets, can prevent induced lipid peroxidation and subsequent ferroptosis (104, 106). Mechanistically, RAB7A is an indispensable factor for docking lysosomes to the lipid droplet surface during lipophagy under nutrient deprivation (107). Moreover, RAB7A has been demonstrated to act as a tumor suppressor in glioblastoma and prostate cancer (108), unlike other cancers.

Although emerging evidence reinforces the idea that the amount of lipid and the localization of lipids in lipid droplets potentially affect the ability to induce ferroptosis in cancer cells, studies on the effect of lipolysis and lipophagy on sensitizing glioblastoma cells for ferroptosis are limited. There is limited information on how microenvironment and disease progression affect the biogenesis and breakdown of lipid droplets (101). There is a need for a better understanding of specific trafficking itinerary of lipophagy which may lead to new anticancer approaches, particularly against "lipid addicted tumors" like glioblastoma. Finally, the molecular regulators of 1-O-acylceramide hydrolysis and whether this process impacts tumorigenesis are unknown.

Summary

In the field of cancer metabolism reprogramming and plasticity, we have learned some fascinating lessons. One of the classical examples of metabolic reprogramming is the Warburg effect (109) which was reported almost 100 years ago and demonstrated a high glucose uptake and an increase in the glycolysis rate in cancer cells in an aerobic environment. In addition to high glucose consumption, glioblastoma has increased glutamine uptake rate to fuel proliferation compared with healthy cells. Emerging data have also shown that lipid metabolism provides an important energy substrate and carbon source for glioblastoma cells, affecting cancer cell plasticity and persistence during therapy (110, 111). Multiple lines of evidence also suggest that lipid droplets act as a central hub for lipid trafficking in glioblastoma, allowing lipids to move in and out of lipid droplets.

However, developing cancer treatments by targeting altered lipid metabolism is in its infancy. It remains challenging, primarily due to an incomplete understanding of the mechanisms that regulate lipid synthesis, esterification, lipolysis and lipophagy in cancer cells (34, 36, 58, 112, 113). In addition, our understanding of the pathways downstream of peroxidized phospholipids that execute ferroptosis remains extremely limited (Box 1). For instance, it is unclear whether peroxidized phospholipids are cytotoxic by themselves or when metabolized into products (e.g., electrophilic intermediates) that function as the primary drivers of ferroptosis or other adaptive metabolic reprogramming. The extent to which a physiological niche (cell/tissue function) alters lipid droplets contributions to ferroptosis and the unique context-dependent vulnerabilities that can be targeted in combinatorial approaches have also not been well explored. Moreover, metabolic byproducts accumulate in the tumor and its microenvironment, increasing the need for cancer cells to engage waste management and recycling pathways, as shown in the case of other metabolic byproducts such as acetate, ammonia, and free fatty acids (73–76, 114–116). However, the existence of waste management and the recycling of peroxidized phospholipids are not yet clear and require further study.

What is beyond question is the continued lack of life-prolonging treatment for glioblastoma patients despite significant advances in genetic and molecular characterization and almost twenty years since the introduction of temozolomide as the standard of care. This necessitates the discovery of nuanced avenues to understand glioblastoma formation to overcome therapeutic resistance. Ferroptosis and lipid

BOX 1 Unanswered questions.

Although monitoring the balance of PUFAs and MUFAs is known to predict the sensitivity of cells to ferroptosis, cellular sensing and the feedback mechanism that balances PUFAs/MUFAs remain to be investigated.

There is imputes to define the relationship between lipid droplets, fatty acid metabolism, and ferroptosis. However, key protein mediators of these biological processes remain to be discovered.

The most important factors for ferroptosis-dependent cell death are lipid peroxides that self-propagate along the plasma membrane and result in the accumulation of oxidatively damaged lipids. Our understanding of the downstream pathways of peroxidized phospholipids that execute ferroptosis and potentially contribute to tumorigenesis remains at a nascent phase. The question remains whether there is a repair or antagonism mechanism of peroxide lipids at damage loci in the cell membrane. Are oxidatively damaged membranes prone to recycling? Can this metabolic plasticity contribute to glioblastoma therapeutic resistance? How do these factors cooperate their functions in cancer microenvironments?

Many cancers, including glioblastoma, consist of both stem and nonstem cells; however, the degree to which these cells are resistant to ferroptosis remains mostly unknown.

metabolism offer some very early promise in this direction and are worthy of further exploration in this lethal cancer.

Author contributions

Conceptualization, AB-G. Writing-original draft preparation, AB-G, JD, and MW. Review and editing, AB-G, JD, and MW. Funding acquisition, AB-G. All authors have read and agreed to the published version of the manuscript.

Funding

This work was supported by grants from the Brian Foundation and Rebecca L Cooper Medical Research Foundation for AB-G.

Conflict of interest

The authors declare that the research was conducted in the absence of any commercial or financial relationships that could be construed as a potential conflict of interest.

Publisher's note

References

1. Stupp R, Mason WP, van den Bent MJ, Weller M, Fisher B, Taphoorn MJ, et al. Radiotherapy plus concomitant and adjuvant temozolomide for glioblastoma. *N Engl J Med* (2005) 352(10):987–96. doi: 10.1056/NEJMoa043330

2. Stupp R, Hegi ME, Mason WP, van den Bent MJ, Taphoorn MJ, Janzer RC, et al. Effects of radiotherapy with concomitant and adjuvant temozolomide versus radiotherapy alone on survival in glioblastoma in a randomised phase III study: 5-year analysis of the EORTC-NCIC trial. *Lancet Oncol* (2009) 10(5):459–66. doi: 10.1016/S1470-2045(09)70025-7

3. Park JK, Hodges T, Arko L, Shen M, Dello Iacono D, McNabb A, et al. Scale to predict survival after surgery for recurrent glioblastoma multiforme. *J Clin Oncol* (2010) 28(24):3838–43. doi: 10.1200/JCO.2010.30.0582

4. Ye X, Mahmud S, Skrabek P, Lix L, Johnston JB. Long-term time trends in incidence, survival and mortality of lymphomas by subtype among adults in Manitoba, Canada: A population-based study using cancer registry data. *BMJ Open* (2017) 7(7):e015106. doi: 10.1136/bmjopen-2016-015106

5. Siegel RL, Miller KD, Jemal A. Cancer statistics, 2020. *CA Cancer J Clin* (2020) 70(1):7–30. doi: 10.3322/caac.21590

6. Garon EB, Hellmann MD, Rizvi NA, Carcereny E, Leighl NB, Ahn MJ, et al. Five-year overall survival for patients with advanced NonSmall-cell lung cancer treated with pembrolizumab: Results from the phase I KEYNOTE-001 study. *J Clin Oncol* (2019) 37(28):2518–27. doi: 10.1200/JCO.19.00934

7. Krex D, Klink B, Hartmann C, von Deimling A, Pietsch T, Simon M, et al. Long-term survival with glioblastoma multiforme. *Brain* (2007) 130(Pt 10):2596–606. doi: 10.1093/brain/awm204

8. Stummer W, Reulen HJ, Meinel T, Pichlmeier U, Schumacher W, Tonn JC, et al. Extent of resection and survival in glioblastoma multiforme: Identification of and adjustment for bias. *Neurosurgery* (2008) 62(3):564–76. doi: 10.1227/01.neu.0000317304.31579.17

9. Stevens MF, Hickman JA, Langdon SP, Chubb D, Vickers L, Stone R, et al. Antitumor activity and pharmacokinetics in mice of 8-carbamoyl-3-methyl-imidazo[5,1-d]-1,2,3,5-tetrazin-4(3H)-one (CCRG 81045; m & b 39831), a novel drug with potential as an alternative to dacarbazine. *Cancer Res* (1987) 47 (22):5846–52.

10. Wick W, Gorlia T, Bendszus M, Taphoorn M, Sahm F, Harting I, et al. Lomustine and bevacizumab in progressive glioblastoma. *N Engl J Med* (2017) 377 (20):1954–63. doi: 10.1056/NEJMoa1707358

11. Hegi ME, Diserens AC, Gorlia T, Hamou MF, de Tribolet N, Weller M, et al. MGMT gene silencing and benefit from temozolomide in glioblastoma. *N Engl J Med* (2005) 352(10):997–1003. doi: 10.1056/NEJMoa043331

12. Weller M, Butowski N, Tran DD, Recht LD, Lim M, Hirte H, et al. Rindopepimut with temozolomide for patients with newly diagnosed, EGFRvIII-expressing glioblastoma (ACT IV): A randomised, double-blind, international phase 3 trial. *Lancet Oncol* (2017) 18(10):1373–85. doi: 10.1016/S1470-2045(17)30517-X

13. Chinot OL, Wick W, Mason W, Henriksson R, Saran F, Nishikawa R, et al. Bevacizumab plus radiotherapy-temozolomide for newly diagnosed glioblastoma. *N Engl J Med* (2014) 370(8):709–22. doi: 10.1056/NEJMoa1308345

14. Cancer Genome Atlas Research N. Comprehensive genomic characterization defines human glioblastoma genes and core pathways. *Nature* (2008) 455(7216):1061–8. doi: 10.1038/nature07385

15. Brennan CW, Verhaak RG, McKenna A, Campos B, Noushmehr H, Salama SR, et al. The somatic genomic landscape of glioblastoma. *Cell* (2013) 155(2):462–77. doi: 10.1016/j.cell.2013.09.034

16. Phillips HS, Kharbanda S, Chen R, Forrest WF, Soriano RH, Wu TD, et al. Molecular subclasses of high-grade glioma predict prognosis, delineate a pattern of disease progression, and resemble stages in neurogenesis. *Cancer Cell* (2006) 9 (3):157–73. doi: 10.1016/j.ccr.2006.02.019

17. Eckel-Passow JE, Lachance DH, Molinaro AM, Walsh KM, Decker PA, Sicotte H, et al. Glioma groups based on 1p/19q, IDH, and TERT promoter mutations in tumors. *N Engl J Med* (2015) 372(26):2499–508. doi: 10.1056/NEJMoa1407279

18. Verhaak RG, Hoadley KA, Purdom E, Wang V, Qi Y, Wilkerson MD, et al. Integrated genomic analysis identifies clinically relevant subtypes of glioblastoma characterized by abnormalities in PDGFRA, IDH1, EGFR, and NF1. *Cancer Cell* (2010) 17(1):98–110. doi: 10.1016/j.ccr.2009.12.020

19. Wang Q, Hu B, Hu X, Kim H, Squatrito M, Scarpace L, et al. Tumor evolution of glioma-intrinsic gene expression subtypes associates with immunological changes in the microenvironment. *Cancer Cell* (2017) 32(1):42–56.e6. doi: 10.1016/j.ccell.2017.06.003

20. Teo WY, Sekar K, Seshachalam P, Shen J, Chow WY, Lau CC, et al. Relevance of a TCGA-derived glioblastoma subtype gene-classifier among patient populations. *Sci Rep* (2019) 9(1):7442. doi: 10.1038/s41598-019-43173-y

21. Park J, Shim JK, Yoon SJ, Kim SH, Chang JH, Kang SG, et al. Transcriptome profiling-based identification of prognostic subtypes and multi-omics signatures of glioblastoma. *Sci Rep* (2019) 9(1):10555. doi: 10.1038/s41598-019-47066-y

22. Balss J, Meyer J, Mueller W, Korshunov A, Hartmann C, von Deimling A, et al. Analysis of the IDH1 codon 132 mutation in brain tumors. *Acta Neuropathol* (2008) 116(6):597–602. doi: 10.1007/s00401-008-0455-2

23. Yan H, Parsons DW, Jin G, McLendon R, Rasheed BA, Yuan W, et al. IDH1 and IDH2 mutations in gliomas. *N Engl J Med* (2009) 360(8):765–73. doi: 10.1056/NEJMoa0808710

24. Louis DN, Perry A, Wesseling P, Brat DJ, Cree IA, Figarella-Branger D, et al. The 2021 WHO classification of tumors of the central nervous system: A summary. *Neuro Oncol* (2021) 23(8):1231–51. doi: 10.1093/neuonc/noab106

25. Platten M, Wick W, Van den Eynde BJ. Tryptophan catabolism in cancer: Beyond IDO and tryptophan depletion. *Cancer Res* (2012) 72(21):5435–40. doi: 10.1158/0008-5472.CAN-12-0569

26. Ott M, Litzenburger UM, Rauschenbach KJ, Bunse L, Ochs K, Sahm F, et al. Suppression of TDO-mediated tryptophan catabolism in glioblastoma cells by a steroid-responsive FKBP52-dependent pathway. *Glia* (2015) 63(1):78–90. doi: 10.1002/glia.22734

27. Obara-Michlewska M, Szeliga M. Targeting glutamine addiction in gliomas. *Cancers (Basel)* (2020) 12(2):310. doi: 10.3390/cancers12020310

28. Badr CE, Silver DJ, Siebzehnrubl FA, Deleyrolle LP. Metabolic heterogeneity and adaptability in brain tumors. *Cell Mol Life Sci* (2020) 77(24):5101–19. doi: 10.1007/s00018-020-03569-w

29. Ekici S, Nye JA, Neill SG, Allen JW, Shu HK, Fleischer CC, et al. Glutamine imaging: A new avenue for glioma management. *AJNR Am J Neuroradiol* (2022) 43 (1):11–8. doi: 10.3174/ajnr.A7333

30. Cohen AS, Grudzinski J, Smith GT, Peterson TE, Whisenant JG, Hickman TL, et al. First-in-human PET imaging and estimated radiation dosimetry of l-[5-(11)C]-glutamine in patients with metastatic colorectal cancer. *J Nucl Med* (2021) 63(1):36–43. doi: 10.2967/jnumed.120.261594

31. Subramani E, Radoul M, Najac C, Batsios G, Molloy AR, Hong D, et al. Glutamate is a noninvasive metabolic biomarker of IDH1-mutant glioma response to temozolomide treatment. *Cancer Res* (2020) 80(22):5098–108. doi: 10.1158/0008-5472.CAN-20-1314

32. Venneti S, Dunphy MP, Zhang H, Pitter KL, Zanzonico P, Campos C, et al. Glutamine-based PET imaging facilitates enhanced metabolic evaluation of gliomas *in vivo*. *Sci Transl Med* (2015) 7(274):274ra17. doi: 10.1126/scitranslmed.aaa1009

33. Guo D, Bell EH, Chakravarti A. Lipid metabolism emerges as a promising target for malignant glioma therapy. *CNS Oncol* (2013) 2(3):289–99. doi: 10.2217/cns.13.20

34. Shakya S, Gromovsky AD, Hale JS, Knudsen AM, Prager B, Wallace LC, et al. Altered lipid metabolism marks glioblastoma stem and non-stem cells in separate tumor niches. *Acta Neuropathol Commun* (2021) 9(1):101. doi: 10.1186/s40478-021-01205-7

35. Tator CH, Evans JR, Olszewski J. Tracers for the detection of brain tumors. evaluation of radioiodinated human serum albumin and radioiodinated fatty acid. *Neurology* (1966) 16(7):650–61. doi: 10.1212/wnl.16.7.650

36. Bacci M, Lorito N, Smiriglia A, Morandi A. Fat and furious: Lipid metabolism in antitumoral therapy response and resistance. *Trends Cancer* (2021) 7(3):198–213. doi: 10.1016/j.trecan.2020.10.004

37. Ferraro GB, Ali A, Luengo A, Kodack DP, Deik A, Abbott KL, et al. Fatty acid synthesis is required for breast cancer brain metastasis. *Nat Cancer* (2021) 2 (4):414–28. doi: 10.1038/s43018-021-00183-y

38. Spector AA, Steinberg D. Relationship between fatty acid and glucose utilization in Ehrlich ascites tumor cells. *J Lipid Res* (1966) 7(5):657–63. doi: 10.1016/S0022-2275(20)39247-6

39. Zadra G, Ribeiro CF, Chetta P, Ho Y, Cacciatore S, Gao X, et al. Inhibition of *de novo* lipogenesis targets androgen receptor signaling in castration-resistant prostate cancer. *Proc Natl Acad Sci U S A.* (2019) 116(2):631–40. doi: 10.1073/pnas.1808834116

40. Wei J, Leit S, Kuai J, Therrien E, Rafi S, Harwood HJ Jr, et al. An allosteric mechanism for potent inhibition of human ATP-citrate lyase. *Nature* (2019) 568 (7753):566–70. doi: 10.1038/s41586-019-1094-6

41. Watt MJ, Clark AK, Selth LA, Haynes VR, Lister N, Rebello R, et al. Suppressing fatty acid uptake has therapeutic effects in preclinical models of prostate cancer. *Sci Transl Med* (2019) 11(478):eaau5758. doi: 10.1126/scitranslmed.aau5758

42. Dixon SJ, Lemberg KM, Lamprecht MR, Skouta R, Zaitsev EM, Gleason CE, et al. Ferroptosis: An iron-dependent form of nonapoptotic cell death. *Cell* (2012) 149(5):1060–72. doi: 10.1016/j.cell.2012.03.042

43. Jiang X, Stockwell BR, Conrad M. Ferroptosis: Mechanisms, biology and role in disease. *Nat Rev Mol Cell Biol* (2021) 22(4):266–82. doi: 10.1038/s41580-020-00324-8

44. Stockwell BR, Friedmann Angeli JP, Bayir H, Bush AI, Conrad M, Dixon SJ, et al. Ferroptosis: A regulated cell death nexus linking metabolism, redox biology, and disease. *Cell* (2017) 171(2):273–85. doi: 10.1016/j.cell.2017.09.021

45. Friedmann Angeli JP, Krysko DV, Conrad M. Ferroptosis at the crossroads of cancer-acquired drug resistance and immune evasion. *Nat Rev Cancer* (2019) 19 (7):405–14. doi: 10.1038/s41568-019-0149-1

46. Tang D, Chen X, Kang R, Kroemer G. Ferroptosis: molecular mechanisms and health implications. *Cell Res* (2021) 31(2):107–25. doi: 10.1038/s41422-020-00441-1

47. Dolma S, Lessnick SL, Hahn WC, Stockwell BR. Identification of genotype-selective antitumor agents using synthetic lethal chemical screening in engineered human tumor cells. *Cancer Cell* (2003) 3(3):285–96. doi: 10.1016/S1535-6108(03)00050-3

48. Bersuker K, Hendricks JM, Li Z, Magtanong L, Ford B, Tang PH, et al. The CoQ oxidoreductase FSP1 acts parallel to GPX4 to inhibit ferroptosis. *Nature* (2019) 575(7784):688–92. doi: 10.1038/s41586-019-1705-2

49. Feng H, Schorpp K, Jin J, Yozwiak CE, Hoffstrom BG, Decker AM, et al. Transferrin receptor is a specific ferroptosis marker. *Cell Rep* (2020) 30(10):3411–3423.e7. doi: 10.1016/j.celrep.2020.02.049

50. Turchi R, Faraonio R, Lettieri-Barbato D, Aquilano K. An overview of the ferroptosis hallmarks in friedreich's ataxia. *Biomolecules* (2020) 10(11):1489. doi: 10.3390/biom10111489

51. Mahoney-Sanchez L, Bouchaoui H, Ayton S, Devos D, Duce JA, Devedjian JC, et al. Ferroptosis and its potential role in the physiopathology of parkinson's disease. *Prog Neurobiol* (2021) 196:101890. doi: 10.1016/j.pneurobio.2020.101890

52. Gao X, Guo N, Xu H, Pan T, Lei H, Yan A, et al. Ibuprofen induces ferroptosis of glioblastoma cells *via* downregulation of nuclear factor erythroid 2-related factor 2 signaling pathway. *Anticancer Drugs* (2020) 31(1):27–34. doi: 10.1097/CAD.0000000000000825

53. Zhuo S, Chen Z, Yang Y, Zhang J, Tang J, Yang K, et al. Clinical and biological significances of a ferroptosis-related gene signature in glioma. *Front Oncol* (2020) 10:590861. doi: 10.3389/fonc.2020.590861

54. Olzmann JA, Carvalho P. Dynamics and functions of lipid droplets. *Nat Rev Mol Cell Biol* (2019) 20(3):137–55. doi: 10.1038/s41580-018-0085-z

55. Senkal CE, Salama MF, Snider AJ, Allopenna JJ, Rana NA, Koller A, et al. Ceramide is metabolized to acylceramide and stored in lipid droplets. *Cell Metab* (2017) 25(3):686–97. doi: 10.1016/j.cmet.2017.02.010

56. Chapman KD, Aziz M, Dyer JM, Mullen RT. Mechanisms of lipid droplet biogenesis. *Biochem J* (2019) 476(13):1929–42. doi: 10.1042/BCJ20180021

57. Walther TC, Chung J, Farese RVJr. Lipid droplet biogenesis. *Annu Rev Cell Dev Biol* (2017) 33:491–510. doi: 10.1146/annurev-cellbio-100616-060608

58. Petan T, Jarc E, Jusovic M. Lipid droplets in cancer: Guardians of fat in a stressful world. *Molecules* (2018) 23(8):1941. doi: 10.3390/molecules23081941

59. Klemm RW, Ikonen E. The cell biology of lipid droplets: More than just a phase. *Semin Cell Dev Biol* (2020) 108:1–3. doi: 10.1016/j.semcdb.2020.06.016

60. Munir R, Lisec J, Swinnen JV, Zaidi N. Lipid metabolism in cancer cells under metabolic stress. *Br J Cancer* (2019) 120(12):1090–8. doi: 10.1038/s41416-019-0451-4

61. De Martino M, Daviaud C, Minns H, Attarwala N, Chen Q, Dephoure N, et al. Radiation therapy promotes unsaturated fatty acids to maintain survival of glioblastoma. *bioRxiv* (2022). doi: 10.1101/2022.06.01.494338

62. Jiang N, Xie B, Xiao W, Fan M, Xu S, Duan Y, et al. Fatty acid oxidation fuels glioblastoma radioresistance with CD47-mediated immune evasion. *Nat Commun* (2022) 13(1):1511. doi: 10.1038/s41467-022-29137-3

63. Bensaad K, Favaro E, Lewis CA, Peck B, Lord S, Collins JM, et al. Fatty acid uptake and lipid storage induced by HIF-1alpha contribute to cell growth and survival after hypoxia-reoxygenation. *Cell Rep* (2014) 9(1):349–65. doi: 10.1016/j.celrep.2014.08.056

64. Sperry J, Condro MC, Guo L, Braas D, Vanderveer-Harris N, Kim KKO, et al. Glioblastoma utilizes fatty acids and ketone bodies for growth allowing progression during ketogenic diet therapy. *iScience* (2020) 23(9):101453. doi: 10.1016/j.isci.2020.101453

65. Cruz ALS, Barreto EA, Fazolini NPB, Viola JPB, Bozza PT, et al. Lipid droplets: Platforms with multiple functions in cancer hallmarks. *Cell Death Dis* (2020) 11(2):105. doi: 10.1038/s41419-020-2297-3

66. Ookhtens M, Kannan R, Lyon I, Baker N. Liver and adipose tissue contributions to newly formed fatty acids in an ascites tumor. *Am J Physiol* (1984) 247(1 Pt 2):R146–53. doi: 10.1152/ajpregu.1984.247.1.R146

67. DeBerardinis RJ, Mancuso A, Daikhin E, Nissim I, Yudkoff M, Wehrli S, et al. Beyond aerobic glycolysis: transformed cells can engage in glutamine metabolism that exceeds the requirement for protein and nucleotide synthesis. *Proc Natl Acad Sci U S A.* (2007) 104(49):19345–50. doi: 10.1073/pnas.0709747104

68. Yoo H, Antoniewicz MR, Stephanopoulos G, Kelleher JK. Quantifying reductive carboxylation flux of glutamine to lipid in a brown adipocyte cell line. *J Biol Chem* (2008) 283(30):20621–7. doi: 10.1074/jbc.M706494200

69. Metallo CM, Gameiro PA, Bell EL, Mattaini KR, Yang J, Hiller K, et al. Reductive glutamine metabolism by IDH1 mediates lipogenesis under hypoxia. *Nature* (2011) 481(7381):380–4.

70. Maher EA, Marin-Valencia I, Bachoo RM, Mashimo T, Raisanen J, Hatanpaa KJ, et al. Metabolism of [U-13 c]glucose in human brain tumors *in vivo*. *NMR Biomed* (2012) 25(11):1234–44. doi: 10.1002/nbm.2794

71. Cheng C, Ru P, Geng F, Liu J, Yoo JY, Wu X, et al. Glucose-mediated n-glycosylation of SCAP is essential for SREBP-1 activation and tumor growth. *Cancer Cell* (2015) 28(5):569–81. doi: 10.1016/j.ccell.2015.09.021

72. Cheng C, Geng F, Li Z, Zhong Y, Wang H, Cheng X, et al. Ammonia stimulates SCAP/Insig dissociation and SREBP-1 activation to promote lipogenesis and tumour growth. *Nat Metab* (2022) 4(5):575–88. doi: 10.1038/s42255-022-00568-y

73. Comerford SA, Huang Z, Du X, Wang Y, Cai L, Witkiewicz AK, et al. Acetate dependence of tumors. *Cell* (2014) 159(7):1591–602. doi: 10.1016/j.cell.2014.11.020

74. Mashimo T, Pichumani K, Vemireddy V, Hatanpaa KJ, Singh DK, Sirasanagandla S, et al. Acetate is a bioenergetic substrate for human glioblastoma and brain metastases. *Cell* (2014) 159(7):1603–14. doi: 10.1016/j.cell.2014.11.025

75. Schug ZT, Peck B, Jones DT, Zhang Q, Grosskurth S, Alam IS, et al. Acetyl-CoA synthetase 2 promotes acetate utilization and maintains cancer cell growth under metabolic stress. *Cancer Cell* (2015) 27(1):57–71. doi: 10.1016/j.ccell.2014.12.002

76. Gao X, Lin SH, Ren F, Li JT, Chen JJ, Yao CB, et al. Acetate functions as an epigenetic metabolite to promote lipid synthesis under hypoxia. *Nat Commun* (2016) 7:11960. doi: 10.1038/ncomms11960

77. Cases S, Smith SJ, Zheng YW, Myers HM, Lear SR, Sande E, et al. Identification of a gene encoding an acyl CoA:diacylglycerol acyltransferase, a key enzyme in triacylglycerol synthesis. *Proc Natl Acad Sci U S A.* (1998) 95 (22):13018–23. doi: 10.1073/pnas.95.22.13018

78. Cases S, Stone SJ, Zhou P, Yen E, Tow B, Lardizabal KD, et al. Cloning of DGAT2, a second mammalian diacylglycerol acyltransferase, and related family members. *J Biol Chem* (2001) 276(42):38870–6. doi: 10.1074/jbc.M106219200

79. Bayerle A, Marsching C, Rabionet M, Dworski S, Kamani MA, Chitraju C, et al. Endogenous levels of 1-o-acylceramides increase upon acidic ceramidase deficiency and decrease due to loss of Dgat1 in a tissue-dependent manner. *Biochim Biophys Acta Mol Cell Biol Lipids* (2020) 1865(9):158741. doi: 10.1016/j.bbalip.2020.158741

80. Bemlih S, Poirier MD, El Andaloussi A. Acyl-coenzyme a: Cholesterol acyltransferase inhibitor avasimibe affect survival and proliferation of glioma tumor cell lines. *Cancer Biol Ther* (2010) 9(12):1025–32. doi: 10.4161/cbt.9.12.11875

81. Nygren C, von Holst H, Mansson JE, Fredman P. Increased levels of cholesterol esters in glioma tissue and surrounding areas of human brain. *Br J Neurosurg* (1997) 11(3):216–20. doi: 10.1080/02688699746276

82. Ohmoto T, Nishitsuji K, Yoshitani N, Mizuguchi M, Yanagisawa Y, Saito H, et al. K604, a specific acylCoA: Cholesterol acyltransferase 1 inhibitor, suppresses proliferation of U251MG glioblastoma cells. *Mol Med Rep* (2015) 12(4):6037–42. doi: 10.3892/mmr.2015.4200

83. Liu JY, Fu WQ, Zheng XJ, Li W, Ren LW, Wang JH, et al. Avasimibe exerts anticancer effects on human glioblastoma cells *via* inducing cell apoptosis and cell cycle arrest. *Acta Pharmacol Sin* (2021) 42(1):97–107. doi: 10.1038/s41401-020-0404-8

84. Magtanong L, Ko PJ, To M, Cao JY, Forcina GC, Tarangelo A, et al. Exogenous monounsaturated fatty acids promote a ferroptosis-resistant cell state. *Cell Chem Biol* (2019) 26(3):420–432.e9. doi: 10.1016/j.chembiol.2018.11.016

85. Dierge E, Debock E, Guilbaud C, Corbet C, Mignolet E, Mignard L, et al. Peroxidation of n-3 and n-6 polyunsaturated fatty acids in the acidic tumor environment leads to ferroptosis-mediated anticancer effects. *Cell Metab* (2021) 33(8):1701–1715.e5. doi: 10.1016/j.cmet.2021.05.016

86. Kagan VE, Mao G, Qu F, Angeli JP, Doll S, Croix CS, et al. Oxidized arachidonic and adrenic PEs navigate cells to ferroptosis. *Nat Chem Biol* (2017) 13 (1):81–90. doi: 10.1038/nchembio.2238

87. Doll S, Proneth B, Tyurina YY, Panzilius E, Kobayashi S, Ingold I, et al. ACSL4 dictates ferroptosis sensitivity by shaping cellular lipid composition. *Nat Chem Biol* (2017) 13(1):91–8. doi: 10.1038/nchembio.2239

88. Yuan H, Li X, Zhang X, Kang R, Tang D, et al. Identification of ACSL4 as a biomarker and contributor of ferroptosis. *Biochem Biophys Res Commun* (2016) 478(3):1338–43. doi: 10.1016/j.bbrc.2016.08.124

89. Cheng J, Fan YQ, Liu BH, Zhou H, Wang JM, Chen QX, et al. ACSL4 suppresses glioma cells proliferation *via* activating ferroptosis. *Oncol Rep* (2020) 43 (1):147–58. doi: 10.3892/or.2019.7419

90. Bao C, Zhang J, Xian SY, Chen F. MicroRNA-670-3p suppresses ferroptosis of human glioblastoma cells through targeting ACSL4. *Free Radic Res* (2021) 55 (7):853–64. doi: 10.1080/10715762.2021.1962009

91. Cheng X, Geng F, Pan M, Wu X, Zhong Y, Wang C, et al. Targeting DGAT1 ameliorates glioblastoma by increasing fat catabolism and oxidative stress. *Cell Metab* (2020) 32(2):229–242.e8. doi: 10.1016/j.cmet.2020.06.002

92. Wang H, Bell M, Sreenivasan U, Hu H, Liu J, et al. Unique regulation of adipose triglyceride lipase (ATGL) by perilipin 5, a lipid droplet-associated protein. *J Biol Chem* (2011) 286(18):15707–15. doi: 10.1074/jbc.M110.207779

93. Lass A, Zimmermann R, Oberer M, Zechner R. Lipolysis - a highly regulated multi-enzyme complex mediates the catabolism of cellular fat stores. *Prog Lipid Res* (2011) 50(1):14–27. doi: 10.1016/j.plipres.2010.10.004

94. Zimmermann R, Strauss JG, Haemmerle G, Schoiswohl G, Birner-Gruenberger R, Riederer M, et al. Fat mobilization in adipose tissue is promoted by adipose triglyceride lipase. *Science* (2004) 306(5700):1383–6. doi: 10.1126/science.1100747

95. Taschler U, Radner FP, Heier C, Schreiber R, Schweiger M, Schoiswohl G, et al. Monoglyceride lipase deficiency in mice impairs lipolysis and attenuates diet-induced insulin resistance. *J Biol Chem* (2011) 286(20):17467–77. doi: 10.1074/jbc.M110.215434

96. Haemmerle G, Zimmermann R, Strauss JG, Kratky D, Riederer M, Knipping G, et al. Hormone-sensitive lipase deficiency in mice changes the plasma lipid profile by affecting the tissue-specific expression pattern of lipoprotein lipase in adipose tissue and muscle. *J Biol Chem* (2002) 277(15):12946–52. doi: 10.1074/jbc.M108640200

97. Keenan SN, De Nardo W, Lou J, Schittenhelm RB, Montgomery MK, Granneman JG, et al. Perilipin 5 S155 phosphorylation by PKA is required for the control of hepatic lipid metabolism and glycemic control. *J Lipid Res* (2021) 62:100016. doi: 10.1194/jlr.RA120001126

98. Gimm T, Wiese M, Teschemacher B, Deggerich A, Schodel J, Knaup KX, et al. Hypoxia-inducible protein 2 is a novel lipid droplet protein and a specific target gene of hypoxia-inducible factor-1. *FASEB J* (2010) 24(11):4443–58. doi: 10.1096/fj.10-159806

99. Mao XG, Wang C, Liu DY, Zhang X, Wang L, Yan M, et al. Hypoxia upregulates HIG2 expression and contributes to bevacizumab resistance in glioblastoma. *Oncotarget* (2016) 7(30):47808–20. doi: 10.18632/oncotarget.10029

100. Zechner R, Madeo F, Kratky D. Cytosolic lipolysis and lipophagy: Two sides of the same coin. *Nat Rev Mol Cell Biol* (2017) 18(11):671–84. doi: 10.1038/nrm.2017.76

101. Ogasawara Y, Tsuji T, Fujimoto T. Multifarious roles of lipid droplets in autophagy - target, product, and what else? *Semin Cell Dev Biol* (2020) 108:47–54. doi: 10.1016/j.semcdb.2020.02.013

102. Kaushik S, Cuervo AM. Degradation of lipid droplet-associated proteins by chaperone-mediated autophagy facilitates lipolysis. *Nat Cell Biol* (2015) 17(6):759–70. doi: 10.1038/ncb3166

103. Sun X, Yang S, Feng X, Zhou J, Wang H, et al. The modification of ferroptosis and abnormal lipometabolism through overexpression and knockdown of potential prognostic biomarker perilipin2 in gastric carcinoma. *Gastric Cancer* (2020) 23(2):241–59. doi: 10.1007/s10120-019-01004-z

104. Bai Y, Meng L, Han L, Jia Y, Zhao Y, Gao H, et al. Lipid storage and lipophagy regulates ferroptosis. *Biochem Biophys Res Commun* (2019) 508(4):997–1003. doi: 10.1016/j.bbrc.2018.12.039

105. Liu R, Lee JH, Li J, Yu R, Tan L, Xia Y, et al. Choline kinase alpha 2 acts as a protein kinase to promote lipolysis of lipid droplets. *Mol Cell* (2021) 81(13):2722–2735.e9. doi: 10.1016/j.molcel.2021.05.005

106. Hou W, Xie Y, Song X, Sun X, Lotze MT, Zeh HJ 3rd, et al. Autophagy promotes ferroptosis by degradation of ferritin. *Autophagy* (2016) 12(8):1425–8. doi: 10.1080/15548627.2016.1187366

107. Schroeder B, Schulze RJ, Weller SG, Sletten AC, Casey CA, McNiven MA, et al. The small GTPase Rab7 as a central regulator of hepatocellular lipophagy. *Hepatology* (2015) 61(6):1896–907. doi: 10.1002/hep.27667

108. Wang W, Zhang H, Liu S, Kim CK, Xu Y, Hurley LA, et al. Internalized CD44s splice isoform attenuates EGFR degradation by targeting Rab7A. *Proc Natl Acad Sci U S A.* (2017) 114(31):8366–71. doi: 10.1073/pnas.1701289114

109. Warburg O, Wind F, Negelein E. The metabolism of tumors in the body. *J Gen Physiol* (1927) 8(6):519–30. doi: 10.1085/jgp.8.6.519

110. Cheng C, Geng F, Cheng X, Guo D. Lipid metabolism reprogramming and its potential targets in cancer. *Cancer Commun (Lond)* (2018) 38(1):27. doi: 10.1186/s40880-018-0301-4

111. Jones SF, Infante JR. Molecular pathways: Fatty acid synthase. *Clin Cancer Res* (2015) 21(24):5434–8. doi: 10.1158/1078-0432.CCR-15-0126

112. Wu X, Geng F, Cheng X, Guo Q, Zhong Y, Cloughesy TF, et al. Lipid droplets maintain energy homeostasis and glioblastoma growth *via* autophagic release of stored fatty acids. *iScience* (2020) 23(10):101569. doi: 10.1016/j.isci.2020.101569

113. Choi YK, Park KG. Targeting glutamine metabolism for cancer treatment. *Biomol Ther (Seoul)* (2018) 26(1):19–28. doi: 10.4062/biomolther.2017.178

114. Lyssiotis CA, Kimmelman AC. Metabolic interactions in the tumor microenvironment. *Trends Cell Biol* (2017) 27(11):863–75. doi: 10.1016/j.tcb.2017.06.003

115. Spinelli JB, Yoon H, Ringel AE, Jeanfavre S, Clish CB, Haigis MC, et al. Metabolic recycling of ammonia *via* glutamate dehydrogenase supports breast cancer biomass. *Science* (2017) 358(6365):941–6. doi: 10.1038/s41556-018-0124-1

116. Li Y, Zong WX, Ding WX. Recycling the danger *via* lipid droplet biogenesis after autophagy. *Autophagy* (2017) 13(11):1995–7. doi: 10.1080/15548627.2017.1371394

frontiers | Frontiers in Oncology

TYPE Review
PUBLISHED 17 January 2023
DOI 10.3389/fonc.2022.1075559

OPEN ACCESS

EDITED BY
Michela Buglione,
University and ASST Spedali Civili, Brescia, Italy

REVIEWED BY
Hong-My Nguyen,
Texas Tech University Health Sciences Center, Abilene, United States
Hao Zhang,
Second Affiliated Hospital, Chongqing Medical University, China

*CORRESPONDENCE
Daniel Ebner
daniel.ebner@ndm.ox.ac.uk

†These authors have contributed equally to this work and share first authorship

SPECIALTY SECTION
This article was submitted to Neuro-Oncology and Neurosurgical Oncology, a section of the journal Frontiers in Oncology

RECEIVED 20 October 2022
ACCEPTED 28 December 2022
PUBLISHED 17 January 2023

CITATION
Johanssen T, McVeigh L, Erridge S, Higgins G, Straehla J, Frame M, Aittokallio T, Carragher NO and Ebner D (2023) Glioblastoma and the search for non-hypothesis driven combination therapeutics in academia.
Front. Oncol. 12:1075559.
doi: 10.3389/fonc.2022.1075559

Glioblastoma and the search for non-hypothesis driven combination therapeutics in academia

Timothy Johanssen[1†], Laura McVeigh[2†], Sara Erridge[3], Geoffrey Higgins[4], Joelle Straehla[5], Margaret Frame[2], Tero Aittokallio[6,7,8], Neil O. Carragher[2] and Daniel Ebner[1,4*]

[1]Target Discovery Institute, Nuffield Department of Medicine, University of Oxford, Oxford, United Kingdom, [2]Cancer Research UK Scotland Centre, Institute of Genetics and Cancer, University of Edinburgh, Edinburgh, United Kingdom, [3]Edinburgh Cancer Centre, Western General Hospital, Edinburgh, United Kingdom, [4]Department of Oncology, University of Oxford, Oxford, United Kingdom, [5]Koch Institute for Integrative Cancer Research, Massachusetts Institute of Technology, Cambridge, Department of Pediatric Oncology, Dana-Farber Cancer Institute, Division of Pediatric Hematology/Oncology, Boston Children's Hospital, Boston, MA, United States, [6]Institute for Molecular Medicine Finland (FIMM), HiLIFE, University of Helsinki, Helsinki, Finland, [7]Institute for Cancer Research, Department of Cancer Genetics, Oslo University Hospital, Oslo, Norway, [8]Centre for Biostatistics and Epidemiology (OCBE), Faculty of Medicine, University of Oslo, Oslo, Norway

Glioblastoma (GBM) remains a cancer of high unmet clinical need. Current standard of care for GBM, consisting of maximal surgical resection, followed by ionisation radiation (IR) plus concomitant and adjuvant temozolomide (TMZ), provides less than 15-month survival benefit. Efforts by conventional drug discovery to improve overall survival have failed to overcome challenges presented by inherent tumor heterogeneity, therapeutic resistance attributed to GBM stem cells, and tumor niches supporting self-renewal. In this review we describe the steps academic researchers are taking to address these limitations in high throughput screening programs to identify novel GBM combinatorial targets. We detail how they are implementing more physiologically relevant phenotypic assays which better recapitulate key areas of disease biology coupled with more focussed libraries of small compounds, such as drug repurposing, target discovery, pharmacologically active and novel, more comprehensive anti-cancer target-annotated compound libraries. Herein, we discuss the rationale for current GBM combination trials and the need for more systematic and transparent strategies for identification, validation and prioritisation of combinations that lead to clinical trials. Finally, we make specific recommendations to the preclinical, small compound screening paradigm that could increase the likelihood of identifying tractable, combinatorial, small molecule inhibitors and better drug targets specific to GBM.

KEYWORDS

glioblastoma, glioblastoma stem cell, drug target combination, temozolamide, radiotherapy, hypoxia, high throughput screening (HTS)

Introduction

Glioblastoma remains a cancer of high unmet clinical need. Since 2005, the standard of care (SOC) treatment for younger, more physically fit patients has been surgery followed by radiotherapy and chemotherapy with TMZ. Unfortunately, surgical intervention is unable to prevent GBM progress due to the difficulty in obtaining the maximal resection of all tumour material whilst minimising surgical morbidity of essential brain regions. There is some evidence that the higher the level of tumor resection, aided by the development of image-guided surgical applications such as 5-aminolevulinic acid (5-ALA) or BLZ-100 to more readily define the tumour/brain tissue border, thus improving the amount of tumour surgically removed (1, 2), the better the resulting patient outcome (3). Coupled with surgical treatment is chemoradiation that combines six weeks of IR, delivering 60 Gy in 30 fractions to residual disease with daily TMZ (4), followed by six months of adjuvant TMZ using a 5-day over 28-day schedule (5). This standard therapeutic combination has not changed for almost 20 years but inevitably tumour recurrence occurs with a median survival for paitents treated with this schedule of under two years (6, 7).

Since the adoption of TMZ, there have been considerable efforts to broaden the number and range of therapeutics available to treat GBM (Table 1). However, the vast majority of systemic treatments, including all trials involving small molecules and biologics, have failed to improve patient outcomes. There are several factors prevalent in GBM driving this poor record of drug development and, consequently, the absence of improvement in patient outcomes; these include the striking range of molecular and cellular heterogeneity found in GBM tumours, the presence of both

TABLE 1 Summary of Phase II-III Randomized Clinical Trials for Drug Combinations in GBM and their outcome.

Reference	Clinical Stage	# of patients	Clinical Benefit	Therapy	Disease state	Clinical trial identifier
Omuro et al., 2022 (8)	Phase III	560	Not met	Nivolumab + TMZ + RT *vs* TMZ + RT	Newly diagnosed GBM, unmethylated MGMT	NCT02617589
Lim et al., 2022 (9)	Phase III	716	Not met	Nivolumab + TMZ + RT *vs* TMZ + RT	Newly diagnosed GBM, methylated MGMT	NCT02667587
Sim et al., 2021 (10)	Phase II	125	Not met	RT+ Velaparib + TMZ *vs* RT + TMZ	Newly diagnosed GBM, unmethylated MGMT	ACTRN12615000407594
Nayak et al., 2021 (11)	Phase II	80	Not met	Pembrolizumab + Bevacizumab *vs* Pembrolizumab Alone	rGBM	NCT02337491
Peereboom et al., 2021 (12)	Phase II	47	Not met	RO4929097 (gamma secretase inhibitor)	rGBM	NCT01122901
Wen et al., 2021 (13)	Phase II	33	Positive	Dabrafenib + Trametinib	rGBM	NCT02034110
Cloughesy et al., 2020 (14)	Phase II/ III	403	Not met	Vocimagene amiretrorepvec + flucytosine (retroviral replicating fector + prodrug) *vs* standard of care	Surgically resectable rGBM	NCT02414165
Natsume et al., 2020 (15)	Phase II	122	Not met	Interferonβ + TMZ *vs* TMZ alone	Newly diagnosed GBM	JCOG0911
Reardon et al., 2020 (16)	Phase II	73	Positive	BEV with either rindopepimut or a control injection of keyhole limpet hemocyanin	Relapsed EGFRvIII-expressing GBM	NCT01498328
Puduvalli et al., 2020 (17)	Phase II	90	Not met	BEV alone or with vorinostat	rGBM after RT with no prior BEV or HDAC inhibitors	NCT01266031
Lee et al., 2020 (18)	Phase II	115	Not met	BEV with and without trebananib	rGBM or gliosarcoma	NCT01609790
Cloughesy et al., 2020 (19)	Phase III	256	Not met	Ofranergene obadenovec (VB-111 viral therapy) + BEV *vs* BEV monotherapy	rGBM	NCT02511405
Rosenthal et al., 2020 (20)	Phase Ib/ II	35	Not met	Buparlisib (pan PI3K inhibitor) + carboplatin or lomustine (compared with historical single agent data)	rGBM	NCT01934361
Galanis et al., 2019 (21)	Phase I/II	121	Not met	BEV + dasatinib or BEV + placebo	rGBM	NCT00892177
Cloughesy et al., 2019 (22)		35	Positive	Neo-adjuvant PD-1 blockade + surgery + adjuvant PD-1 blockade *vs* surgery + adjuvant PD-1 blockade	Surgically resectable rGBM	
Van den Bent et al., 2020 (23)	Phase II	260	Positive	Depatux-M (antibody-drug-conjugate) *vs* TMZ + Depatux-M	EGFR amplified rGBM	NCT02343406

(Continued)

TABLE 1 Continued

Reference	Clinical Stage	# of patients	Clinical Benefit	Therapy	Disease state	Clinical trial identifier
Herrlinger et al., 2019 (24)	Phase III	141	Positive	TMZ *vs* CCNU-TMZ	Newly diagnosed GBM with methylated MGMT promoter	NCT01149109
Wakabayashi et al., 2018 (25)	Phase II	122	Not met	TMZ + interferonβ + RT *vs* TMZ + RT	Newly diagnosed GBM	JCOG0911
Wakabayashi et al., 2018 (26)	Phase II	170	Positive	BEV/IRI + RT *vs* TMZ + RT	Newly diagnosed, MGMT-nonmethylated GBM	NCT00967330
Chinnaiyan et al., 2018 (27)	Phase II	176	Not met	RT + TMZ + everolimus *vs* RT + TMZ	Newly diagnosed GBM	NCT01062399
Duerinck et al., 2018 (28)	Phase II	101	Not met	Axitinib monotherapy *vs* axitinib + CCNU	rGBM	NCT01562197
Wick et al., 2017 (29)	Phase III	437	Not met	CCNU + BEV *vs* CCNU alone	Progressive GBM	NCT01290939
Capper et al., 2017 (30)	Phase II	158	Not met	Galunisertib *vs* CCNU *vs* galunisertib + CCNU	rGBM	NCT01582269
Capper et al., 2017 (31)	Phase III	180	Not met	CIK cell immunotherapy + standard TMZ *vs* standard TMZ alone	Newly diagnosed GBM	NCT 00807027
Weller et al., 2017 (32)	Phase III	745	Not met	Rindopepimut + TMZ *vs* control injection of keyhole limpet hemocyanin	Newly diagnosed EGFRvIII expressing GBM	NCT01480479
Cloughesy et al., 2017 (33)	Phase II	129	Not met	Onartuzumab + BEV *vs* placebo + BEV	rGBM	NCT01632228
Gilbert et al., 2017 (34)	Phase II	117	Positive	BEV + IRI *vs* BEV + TMZ	rGBM	
Weathers et al., 2016 (35)	Phase II	71	Not met	Low dose BEV + CCNU *vs* standard dose BEV	rGBM	
Brandes et al., 2016a (36)	Phase II	91	Not met	RT/TMZ therapy and BEV or fotemustine	rGBM	NCT01474239
Brandes et al., 2016b (37)	Phase II	158	Not met	Galunisertib + CCNU or galunisertib monotherapy compared with CCNU + placebo	Relapsed or progressed GBM	NCT01582269
Brown et al., 2016 (38)	Phase II	38	Not met	Cediranib + gefitinib *vs* cediranib + placebo	First relapse/first progression of GBM following surgery +chemoradiotherapy	NCT01310855
Herrlinger et al., 2016 (39)	Phase II	182	Not met	BEV during RT followed by maintenance BEV + IRI or TMZ during RT followed by TMZ	Newly diagnosed GBM harbouring an unmethylated MGMT promoter	NCT00967330
Balana et al., 2016 (40)	Phase II	93	Not met	BEV + TMZ *vs* TMZ alone (neoadjuvant)	Unresected GBM	NCT01102595
Erdem-Eraslan et al., 2016 (41)	Phase II	114	Subtype benefits	CCNU, BEV or a combination of CCNU + BEV	First recurrence of GBM after TMZ + RT treatment	NCT01290939
Robins et al., 2016 (42)	Phase I/II	225	Not met	ABT-888 (velparib) in combination with TMZ	Recurrent TMZ resistant GBM	NCT01026493
Robins et al., 2016 (43)	Phase II	122	Not met	Carboplatin + BEV *vs* BEV monotherapy	rGBM	ACTRN12610000915055
Lee et al., 2016 (44)	Phase II	106	Not met	RT + TMZ with or without vandetanib	Newly diagnosed GBM or gliosarcoma	NCT00441142
(Blumenthal et al., 2015 (45)	Phase III	183	Not met	RT and O^6-benzylguanine + BCNU *vs* RT and BCNU alone	Newly diagnosed GBM or gliosarcoma	NCT00017147

(Continued)

TABLE 1 Continued

Reference	Clinical Stage	# of patients	Clinical Benefit	Therapy	Disease state	Clinical trial identifier
(Blumenthal et al., 2015 (46)	Phase II	138	Positive (HRQoL)	CCNU or BEV *vs* CCNU + BEV	rGBM	NCT01290939
(Blumenthal et al., 2015 (47)	Phase II	265	Failed	Standard and intensive cilengitide dose regimens in combination with TMZ/RT	Newly diagnosed GBM + unmethylated MGMT promoter	NCT00813943
Westphal et al., 2015 (47)	Phase III	149	Not met	Nimotuzumab + standard radiochemotherapy *vs* standard radiochemotherapy alone	Newly diagnosed GBM	NCT00753246
Schiff et al., 2015 (48)	Phase II	63	Not met	CT-322 with or without IRI	rGBM	NCT00562419
Penas-Prado et al., 2015 (49)	Phase II	155	Not met	Dose-dense TMZ in combination with isotretinoin, celecoxib, and/or thalidomide	Newly diagnosed GBM	NCT00112502
Penas-Prado et al., 2015 (50)	Phase II	25	Not met	Paclitaxel poliglumex (dose escalation) + TMZ + RT	Newly diagnosed GBM	NCT01402063
Stupp et al., 2014 (51)	Phase III	545	Not met	Cilengitide + TMZ/RT *vs* TMZ/RT alone	Newly diagnosed GBM + methylated MGMT promoter	NCT00689221
Taal et al., 2014 (52)	Phase II	140	Not met/ uncertain	BEV alone *vs* CCNU alone *vs* BEV + CCNU	rGBM	NTR1929
Gilbert et al., 2014 (53)	Phase III	637	Not met	BEV + RT + TMZ *vs* placebo + RT + TMZ (BEV during RT, crossover allowed at progression)	Newly diagnosed GBM	NCT00884741
Hofland et al., 2014 (54)	Phase II	63	Not met	Neoadjuvant BEV + irinotecan *vs* BEV + TMZ (before, during and after RT)	Newly diagnosed GBM	NCT-00817284
Chauffert et al., 2014 (55)	Phase II	120	Not met	IRI + BEV as neo-adjuvant and adjuvant to TMZ-based chemoradiation *vs* TMZ-chemoradiation	Unresected GBM	NCT01022918
Batchelor et al., 2013 (56)	Phase III	325	Not met	Cediranib monotherapy *vs* cediranib + CCNU *vs* CCNU + placebo	rGBM	NCT00777153
Stragliotto et al., 2013 (57)	Phase I/II	42	Not met	Valganciclovir *vs* placebo (in addition to standard therapy)	rGBM	NCT00400322
Stragliotto et al., 2013 (58)	Phase III	250	Not met	Intraoperative perilesional injection of sitimagene ceradenovec followed by ganciclovir in addition to standard care or resection and standard care alone	Newly diagnosed GBM amenable to complete resection	2004-000464-28
Shibui et al., 2013 (59)	Phase II/ III	111	Not met	Nimustine hydrochloride + procarbazine + RT *vs* procarbazine alone + RT	Newly diagnosed anaplastic astrocytoma (n=30) and GBM (n=81)	UMIN-CTR C000000108
Nabors et al., 2012 (60)	Phase II	112	Positive	Cilengitide (either 500 mg or 2000 mg) + standard RT/TMZ	Newly diagnosed GBM	EORTC 26981
Nabors et al., 2012 (61)	Phase II	68	Positive	BEV and everolimus + standard RT/TMZ	Newly diagnosed GBM	
Kim et al., 2011 (62)	Phase III	168	Not met	RT followed by adjuvant TMZ with or without neoadjuvant nimustine-cisplatin chemotherapy	Newly diagnosed GBM	
Dresemann et al., 2010 (63)	Phase III	240	Not met	Imatinib and hydroxyurea *vs* hydroxyurea monotherapy	rGBM after resection, RT and first-line chemotherapy (preferably TMZ)	NCT00154375
Friedman et al., 2009 (64)	Phase II	167	Positive	BEV alone and in combination with IRI with or without concomitant enzyme-inducing antiepileptic drugs	rGBM	NCT00345163
Buckner et al., 2006 (65)	Phase III	401	Not met	Carmustine + cisplatin compared with carmustine alone + standard RT or accelerated RT	Newly diagnosed GBM	

(Continued)

TABLE 1 Continued

Reference	Clinical Stage	# of patients	Clinical Benefit	Therapy	Disease state	Clinical trial identifier
Sotelo, Briceño & López-González, 2006 (66)	Phase III	30	Small sample size	Adding chloroquine to conventional therapy	Histologically confirmed GBM in first or second recurrence or relapse	NCT00224978
Stupp et al., 2005 (7)	Phase III	573	Positive	RT + TMZ	Newly diagnosed GBM	NCT

BEV, bevacizumab; RT, radiotherapy, TMZ, temozolomide; IRI, irinotecan; BCNU, 1,3-bis(2-chloroethyl)-1-nitrosourea; PCV, procarbazine, lomustine, and vincristine; CCNU, lomustine; ACNU, 1-(4-amino-2-methyl-5-pyrimidinyl)methyl-3- (2-chloroethyl)-3-nitrosourea hydrochloride; 5-FU, 5-fluorouracil; VM-26, teniposide; PCNU, nitrosourea analogue; CT-322, VEGFR2 antagonist; DTIC, dacarbazine; rGBM, recurrent glioblastoma.

chemotherapeutic and radioresistant sub-populations of glioblastoma stem cells (GSC) in the tumour, the development and existence of protectant tumour microenvironments (TME) and of course, the existence of the blood-brain barrier which impedes the movement of small molecule and biologic therapeutics into brain tissue.

In this article, we summarize the current state of clinical trials in GBM and highlight the fact that poor clinical translation of potential GBM therapeutics could, in part, be attributed to the failure of drug development campaigns to incorporate many of the key pathophysiological features and sources of heterogeneity of human GBM into the earliest stages of the drug development pipeline. We review the steps academic research scientists are taking to address these failures and argue that high throughput screening to identify novel GBM combinatorial targets for drug development must incorporate the use of a diverse set of patient-derived GSC lines from as wide a cross-section of the GBM disease spectrum as possible, should include chemotherapeutic and radio-resistant cells, and be screened in physiologically relevant conditions including hypoxia in combination with radiotherapy +/- TMZ. Next, we discuss the rationale for current GBM combination trials is not always clear and we wish to emphasise the need for more systematic and transparent strategies for identification, validation and prioritization of combinations that lead to clinical trials. Finally, we make some specific recommendations to the preclinical, small compound screening paradigm that we feel could increase the likelihood of identifying tractable, combinatorial, small molecule inhibitors and better drug targets specific to GBM.

GBM intra/inter heterogeneity as a driver of resistance

The degree of intra-/inter-heterogeneity of GBM tumor profiles is particularly extensive (Figure 1) and has proven to be an important factor in determining long term cancer survival (67). Whole-genome sequencing of tumours has revealed extensive molecular heterogeneity within (68) and between (69, 70) patients, presenting substantial challenges to the identification and prediction of targeted

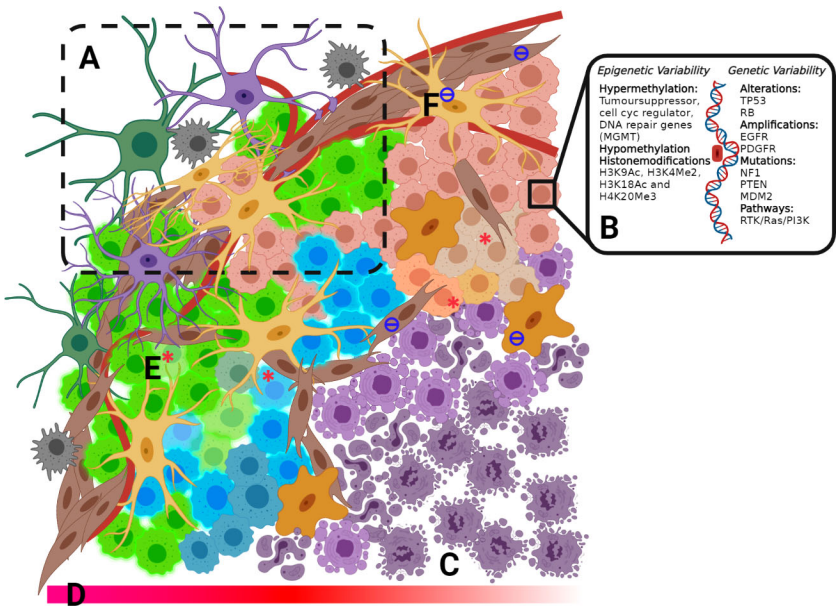

FIGURE 1
(A) Invasive Zone includes a mixture of cell types, including fibroblasts, oligodendrocytes, macrophages, microglia, astrocytes and GBM tumour cells. **(B)** Epigenetic and genetic variability **(C)** Necrotic core **(D)** Decreasing O_2 concentration into the tumour core **(E)** GSC from each of the 4-subtypes: Classical, pro-Neura, Neural and Mesenchimal within microenvironmental niches **(F)** Tumour-associated fibroblast and macrophages.

(precision) therapeutic strategies. Tumours exhibit many somatic mutations in both coding (69) and non-coding regions (71) affecting both gene copy number and coding mutations, as well as regulatory elements for specific genes. However, clearly not all are driver mutations. Instead, the majority are 'passenger' mutations that may confer additional survival advantages under the selective pressures of drug or radiation treatment and promote clonal evolution during therapy, providing opportunities for drug resistance to occur (67).

Tumour heterogeneity and the implications of mutations on GBM pathology are seen at the genomic level when the WHO re-classification of GBM based on the mutational status of isocitrate dehydrogenase (IDH) (72) and recently completed a further re-classification to include one additional feature such as of loss chr 10 or gain chr 7, EGFR ampli, or TERT (73). IDH mutant status in GBM has a significant impact on prognosis. Although IDH-mutated glioma generally exhibit a better disease outcome (74), the incidence of IDH mutations in secondary tumour suggests that lower-grade glioma with IDH mutation often recur after having undergone malignant transformation to a higher grade. In addition, IDH-mutated glioma is more likely to develop a hypermutation phenotype (75). Ongoing research has generated a growing list of molecular and protein differences found in GBM tumours (Figure 1) relating to treatment response and patient outcome (76). These mutations have been well catalogued with strong correlation across testing platforms (69, 77, 78).

An example of tumour heterogeneity at the epigenetic level occurs with the methylation status of O6-methylguanine-DNA methyltransferase (MGMT). When MGMT is silenced through methylation, it is unable to repair the DNA damage induced by TMZ (79) which has been associated with improved survival. Protein arginine methyltransferase 5 (PRMT5) gene expression in GBM is inversely correlated with survival (80). Recent studies show that pharmacological inhibition of PRMT5 suppresses the growth of GSC cultures and significantly prolongs the survival of mice with orthotopic patient-derived GBM xenografts (81). These emerging studies, together with observations that mutations in genes linked to chromatin organisation, are a common feature of GBM (69), implying that epigenetic processes may be a common driver of GBM across heterogeneous subtypes.

Another confounding factor in the resistance of GBM to chemotherapeutics is the developmental state of GBM cells within the tumour. GBM hijacks mechanisms of neural development to produce subcompartments of GSCs that exhibit resistance to radiotherapy and chemotherapies contributing to tumour-propagating potential and recurrence following treatment (82–85). In a recent study, an integrative approach incorporating single-cell RNA-sequencing, bulk genetic and expression analysis of multiple patient tumours, functional assays and single-cell lineage tracing was employed to derive a unified model of cellular states and genetic diversity in GBM (86). The authors postulate that malignant cells in GBM exist in four main cellular states that recapitulate distinct neural cell type features; Astrocyte like, Oligodendrocyte precursor cells, Neural progenitor cells, and Mesenchymal like.

Along with genetic/epigenetic inputs and GSC, the TME drives cellular heterogeneity and subsequently treatment outcomes in GBM. A major structural component of the TME is established by a complex mixture of >15 glycosylated extracellular matrix (ECM) proteins, which establishes a physical and biochemical niche which impacts the interactions between tumour cells and the ECM, including regulation of cell fate, differentiation and migration (87) and are critical to the invasiveness and malignancy of GBM. Importantly, the TME in GBM helps to create avascular regions within the tumour, which leads to decreased tumour O_2 tension and the development of a necrotic core in the tumour, a hallmark of GBM. These hypoxic conditions play a crucial role in protection against chemotherapy and radiation, likely through low O_2 content in the tumour as radiation treatment relies on O_2 and upregulation of numerous proliferative and metastatic pathways attributed to the hypoxia-inducible factors (HIF1α and HIF2α) (88). HIF has been implicated in the dedifferentiation of GBM cells driving the proneural-to-mesenchymal transition, believed to be a hallmark of resistance in recurrent tumours. Another important characteristic of the GBM microenvironment is the significant infiltration of resident microglia and peripheral macrophages. Recent research has implicated these tumour-associated microglia and macrophages in central aspects of tumour development in GBM, including proliferation, angiogenesis and immunosuppression (89), which contributes to the chemoradiation resistance and rapid progression of the disease.

Glioblastomas stem cells and the rationale for combinations

The need for a combination strategy can be rationalized by the well-established cellular heterogeneity of brain tumours. There is evidence to suggest that brain tumours may arise from a stem cell origin (90). The proportion of stem cells in tumours, and the proteins they express (such as CD133 and Ki67), often determine the aggressiveness of recurrent GBM and can inversely correlate with patient outcomes (91, 92). Additionally, from a collection of experimental approaches (68, 86, 93), this stem cell origin gives rise to a proliferative hierarchy in primary GBM, leading to the presence of a range of cell states, from stem cell to differentiated cells within a tumour. Developmental and lineage subtypes invariably generate therapy-resistant populations due to higher cellular entropy (94), providing various genetic and epigenetic mechanisms stem cells use to evade death from radiation and chemotherapy treatment (95, 96).

Stem cells are increasingly becoming the target cell for further research into understanding GBM and treatment responses. The variable responses of tumour cell populations to standard GBM treatment implies that it is sensible to consider the combination of more than one drug; one of these may target stem cells and the other target non-stem cells in the bulk tumour. Data increasingly show the importance of targeting both subpopulations. For example, using patient-derived cells from biopsies, it has been reported that for greatest patient benefit, both stem cells and 'tumour bulk' cells need to be killed by >40% and >55%, respectively (97). Additional evidence that stem cells and bulk cell populations respond differently to drugs has been gathered from the development of a chemotherapeutics assay termed ChemoID (97). The assay involves culturing GBM stem cells and tumour bulk cells from patient biopsy material and assessing the *in vitro* killing ability of a panel of chemotherapeutic drugs. Significant differences in sensitivity to TMZ between stem cells and bulk cells within the same patient tumour sample (Figure 2) have been observed.

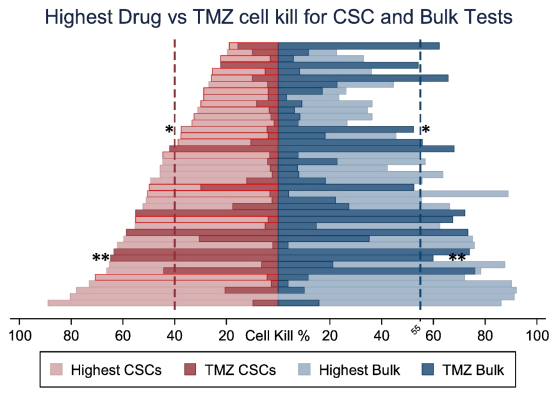

FIGURE 2
Percent cell death for the most cytotoxic drug and TMZ for each patient comparing Cancer Stem cell (CSC) *vs* bulk of tumour cell sensitivity to TMZ. Optimal therapies with highest cell death shown in light colours and cell detah by TMZ in dark. CSC results outlined in red show patients whose optimal therapy differs from the optimal therapy identified by the bulk of tumour cells test * p <0.05, ** p < 0.01. Adapted from Howard C.M., et al., 2017 (97).

In the majority of samples tested, bulk cells were more sensitive to TMZ than stem cells; thus, TMZ-treatment will not likely have significantly killed the stem cell population. Although not the ideal chemotherapeutic drug, due to insensitivity in a large proportion of patients, TMZ may be of greater value for use against bulk tumour cells, opening up the possibility of using TMZ combined with additional drugs to attack the heterogeneous tumour cell complement within the tumour mass.

Hypothesis-driven drug additions to the standard-of-care regimen of TMZ and IR

The treatment regimen of surgery followed by TMZ and IR can slow the progression of GBM tumours, but it is not generally curative. The simplest solution to increasing the effectiveness of treatment would be to incorporate an additional therapeutic agent into the SOC treatment regimen to target one or more specific GBM tumour cell survival pathways to yield a combinatorial or synergistic effect. An example of a hypothesis-driven combinatorial approach has been to target tumour angiogenesis, increased tumour vascularisation supports GBM growth and survival in the face of radiochemotherapy. Vascular Endothelial Growth Factor (VEGF) is over-expressed in a variety of metastatic tumours and bevacizumab (Avastin), an anti-VEGF antibody, was first approved for treatment in metastatic colorectal cancer in 2004 (98) and later for GBM treatment in 2009 (6). Trials in in newly diagnosed GBM, such as the Avaglio trial or RTOG 0825 trial (53, 99) showed no increase in overall survival although progression-free survival times were extended by 3-4 months with bevacizumab (53, 100). To date, it remains the only approved (not in EU) antibody treatment for recurrent GBM (101). The difficulty in obtaining significant clinical benefits for anti-angiogenic therapies in newly diagnosed GBM has been summarized in retrospective meta-analyses reviews (102, 103).

Another promising approach that has had significant success in many advanced malignancies is the use of immune checkpoint inhibitors (ICI) targeting key checkpoint pathways including the cytotoxic T-lymphocyte-associated antigen 4 (CTLA-4)/B7 and programmed death 1 (PD-1)/programmed cell death ligand 1 (PD-L1), reviewed by Zhang et al., 2021 (104). Despite their successes, ICIs are yet to improve survival in GBM. By addressing the restrictive nature of the TME, the timing of checkpoint inhibition and employing novel combinatorial strategies of ICIs this strategy could still provide effective therapeutic options in the future for GBM (105).

Additional small molecules have been tested as potential treatments based on GBM driver pathways. A recent review listed 90 clinical trials with 85 different compounds either as monotherapy or in combination with standard treatment, the majority are tyrosine kinase inhibitors (6), and alternative alkylating agents (Clinicaltrials.gov). Unfortunately, so far, none of these has delivered a beneficial treatment (Table 1).

Data and clinical trials from hypothesis-driven multiple drug combination therapies are less well documented than those seen for single or double additions to SOC treatment. Here, the strategy is to target multiple molecules or pathways implicated in tumour development and survival. One such hypothesis is the Co-ordinated Undermining of Survival Pathways (CUSP9) in GBM, which utilizes nine clinically approved growth-factor inhibiting drugs alongside TMZ treatment for recurrent GBM. (now called CUSP9 with slightly altered panel composition - Table 2) (131).

A recent study in patient-derived GSC based on the CUSP9 drug panel, highlights individually these drugs have little effect, but in combination the tumour killing effect can become significant (Figures 3A, B) (132).

Figure 3: CUSP9 with TMZ. **A**, **B** Individually, the drugs in the CUSP9 or TMZ did not reduce cell survival, evaluated by the cell viability or cytotoxicity assay; a significant effect was observed when applied as a drug combination in CPCs (both $p < 0.0001$, one-way ANOVA). **C** Percentage of growth inhibition of human GAMG cells following the addition of temozolomide (TMZ), ritonavir (RITON) and aprepitant (APREP) in monotherapy; temozolomide + ritonavir, temozolomide + aprepitant and aprepitant + ritonavir in combination therapy. Adapted from Kast RE,. et al., 2015 (131) and Skaga E., et al., 2019 (132)

A further study highlights two of the CUSP9 drugs, aprepitant and ritonavir (133), tumour cell killing is either poor (aprepitant 6%) or equivalent to TMZ alone (ritonavir 14%). However, when used in combination, aprepitant and ritonavir show significantly increased synergistic inhibition which was increased when TMZ was also added for a triple combination (Figure 3). The CUSP idea and initial promising results using tumour cell lines imply that successful combination therapies for GBM may well require more than two or even three drugs.

Non-hypothesis driven drug additions to the SOC regiment of TMZ and IR

With the failure of clinical trials resulting from hypothesis-driven drug combination studies, non-hypothesis driven, high throughput

TABLE 2 List of CUSP9 drugs and their expected benefit in treating GBM. Adapted from Kast R.E., 2013 (106).

DRUG	EXPECTED BENEFIT	REF.
aprepitant	Nausea reduction, inhibit growth by blocking NK-IR.	(107, 108)
artesunate	Increases ROS, empirical anti-glioma effects, survivin inhibition	(109, 110)
sertraline	Empirical longer OS, improved mood, documented anti-proliferation effects in glioma cells.	(111–113)
captopril	Empirical longer OS, MMP-2 & MMP-9 inhibition, prevents AT-2 stimulation, lowers IL-18, stimulated VEGF, TNF & IL-8.	(114–117)
auranofin	Thioredoxin reductase inhibition, cathepsin B inhibition i.e. ROS, empirical [& potentially dangerous] synergy with artesunate.	(118, 119)
nelfinavir	HSP90 inhibition, MMP-2 & MMP-9 inhibition, decreased signaling at multiple receptors, i.e. TGF-β, increased ROS, decreased AKT activation, lower VEGF, IL-8, ICE inhibition.	(120–122)
temozolomide	A common and accepted treatment for recurrent GBM	(79)
disulfiram	ALDH inhibition, glutathione inhibition, increases ROS, lowers IL-18, stimulated VEGF, TNF, & IL-8, MMP-2 & MMP-9 inhibition, proteasome inhibition, SOD inhibition, P-glycoprotein inactivation, MGMT inhibition.	(123–128)
Cu gluconate	Adequate Cu may be a requirement for disulfiram activity.	(129)
ketoconazole	Drug efflux inhibitor at BBB, permits higher brain ritonavir (or nelfinavir) concentrations, 5-lipoxygenase inhibitor, thromboxane synthase inhibitor, empirical anti-glioma effect.	(121, 130)

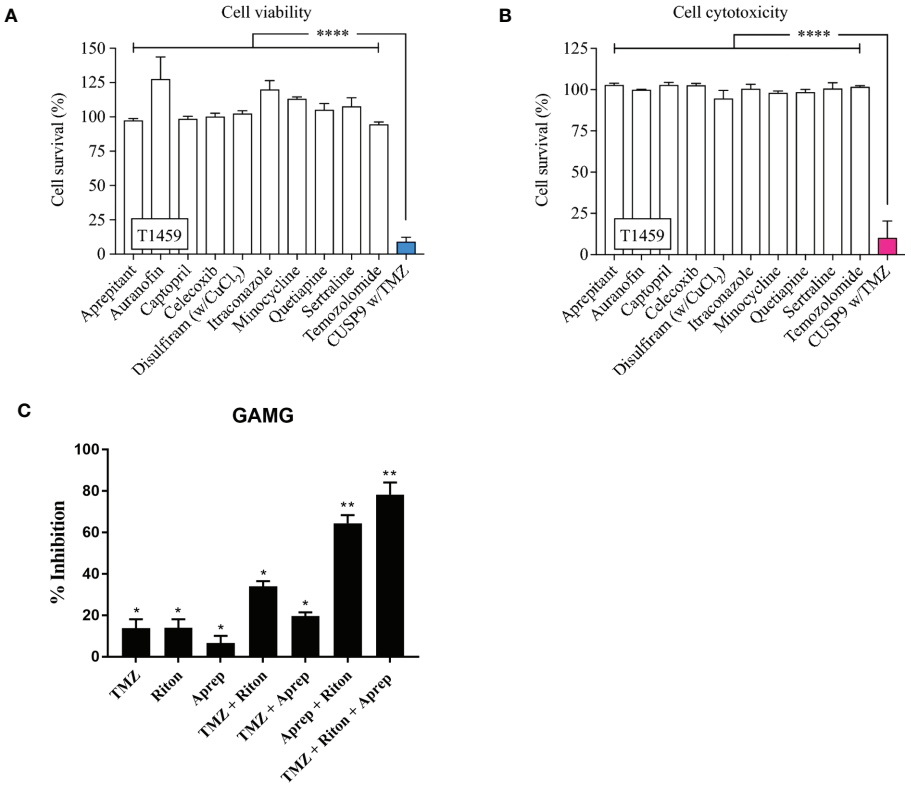

FIGURE 3
CUSP9 with TMZ. **(A, B)** Individually, the drugs in the CUSP9 or TMZ did not reduce cell survival, evaluated by the cell viability or cytotoxicity assay; a significant effect was observed when applied as a drug combination in CPCs (**** $p < 0.0001$, one-way ANOVA). **(C)** Percentage of growth inhibition of human GAMG cells following the addition of temozolomide (TMZ), ritonavir (Riton) and aprepitant (Aprep) in monotherapy; temozolomide + ritonavir, temozolomide + aprepitant and aprepitant + ritonavir in combination therapy (* $p < 0.05$, ** $p < 0.01$). Adapted from Skaga E., et al., 2019 (132) and Kast R.E., et al., 2016 (105).

screening (HTS) strategies are now coming to the forefront of academic and pharmaceutical industry research (Table 3).

Traditionally in HTS, very large collections of small compound libraries with diverse chemical structures have been employed by the pharmaceutical industry to identify starting compounds for drug development programs. However, this process is generally less successful at the academic level due to the prohibitive infrastructural costs required to develop and produce larger screens, as well as the cost to develop a small compound hit into a clinical drug candidate. As a result, many academic screening facilities have instead focussed on developing more physiologically relevant phenotypic assays which better recapitulate key areas of disease biology (145) and then screen smaller, focussed libraries such as "drug repurposing" (146–148), probes for target discovery (149–151) or pharmacologically active small compound sets (152). This focussed approach has the advantage of providing a better understanding of the molecular basis of the disease while simultaneously providing the opportunity to exploit existing therapeutics and compounds with known safety profiles, small compounds that possess drug-like properties and compounds with known protein targets, and can provide a more direct path to clinical translation (153).

Academic drug screens have proven to be successful at identifying novel repurposing opportunities in a variety of other cancers (154), so are good candidates as potential additions for GBM therapy (137, 155, 156). While a number of HTS and drug repurposing screens have been performed recently in GBM, with several hits being tested in early-phase clinical trials (Table 3), such screening hits have yet to translate into robust randomized phase II/III testing (Table 1).

Screens using smaller but diverse small molecule libraries are also becoming more commonplace, including uncharacterized molecules that could lead to a novel therapeutic discovery program rather than just a repurposing opportunity. One example study using

TABLE 3 Non-hypothesis driven HTS campaigns to identify novel targets, drug-combinations or small compounds for the treatment of GBM.

Reference	Cell type	Assay format	Assay endpoint	Screen size	No. of hits
Skaga et al., 2019 (134)	GBM biopsies from 12 patients were used to establish cell cultures.	Cells were plated at 5000 cells/well in a 96-well plate under sphere conditions, cultured for 24 h before the addition of drugs and further incubated for 72 h.	Viability was assessed using Cell Proliferation Kit II XTT (Roche) solution incubated for 24 h before analysis.	The oncology drug collection consisted of 461 FDA/EMA-approved anti-cancer drugs and investigational compounds with a broad range of molecular targets.	All drugs have (i) been tested in clinical trials of GBM (nintedanib, paclitaxel, topotecan), (ii) are currently in clinical trials of GBM (belinostat (NCT02137759), sapanisertib and selinexor (clinicaltrials.gov) or (iii) represent drugs within a class that are being investigated in GBM (carfilzomib; proteasome inhibitors, idasanutlin; mdm2 inhibitors, clinicaltrials.gov).
Lucki et al., 2019 (135)	Patient-derived GBM CSC cultures	uHTS Luciferase-based survival assay (~10^6 molecules) followed by high content imaging-based selective toxicity assay (~8000 molecules) then a caspase 3/7 activation assay (~200 molecules)	Induction of apoptosis	~10^6 small molecules	Identified a small molecule, RIPGBM, that selectively induces apoptosis in GBM CSCs *in vitro* and significantly decreases tumour size *in vivo* in a physiologically relevant, patient-derived intracranial xenograft mouse model.
Wilson et al., 2019 (136)	Two spheroid cell lines, JHH-136 and JHH-520,	High-throughput drug screen using an 11-point dose response. Drug combination screening of 30 compounds (435 combinations) using 5 concentrations of one and 5 concentrations of a second compound. Follow up drug screen of 46 drug combinations.	Cell viability or apoptosis	The Mechanism Interrogation PlatE (MIPE) 4.0 is a collection of 1912 small molecules that target signalling pathway components that are altered in many different cancers.	Drug mechanisms that were cytotoxic in both cell lines were Hsp90 and proteasome inhibitors. JHH-136 was uniquely sensitive to topoisomerase 1 inhibitors, while JHH-520 was uniquely sensitive to Mek inhibitors. Drug combination screening revealed that PI3 kinase inhibitors (GDC-0941) combined with Mek (PD0325901) or proteasome inhibitors (marizomib) were synergistic. *In vivo* revealed that Mek inhibition alone was superior to the combination treatments.
Quereda et al., 2018 (137)	Patient-Derived Glioma Stem Cells	1536-well spheroid-based proliferation assay using 3300 approved drugs.	3-D Cell proliferation was assessed after another 72-hour incubation using CellTiter Glo reagent	A collection of 3,291 clinically approved drugs assembled at the Scripps Research Institute Molecular Screening Center (SRIMSC).	Bortezomib was observed to be more potent against GBM6 GSCs (GBM6 spheroids or in laminin) than against the differentiated GBM6 (bulk tumour) or the U87 cell line, suggesting Bortezomib may specifically affect the master regulators of the GSCs.
Yu et al., 2018 (138)	7 patient derived cancer stem cell lines: 5 GBM: 1 Gliosarcoma:	High content screening assay, two 384-well plate formats performed in tandem in serum-free conditions: 1. Adherent monolayer on	HCI DRAQ7 and Hoechst 33342 to identify compounds for cell death and proliferation. Triage in 3D neurospheres. *In vivo* validation of hits in orthotopic model following	83 chemotherapy drugs with and without irradiation	Drug hits demonstrating significant reduction of tumour growth *in vivo* include: Mitoantrone; Bortezomib, Actinomycin D and Paclitaxel. Only paclitaxel (in a form that was linked to a biodegradable, water-soluble polyglutamate polymer) was

(Continued)

TABLE 3 Continued

Reference	Cell type	Assay format	Assay endpoint	Screen size	No. of hits
	1 Gliomatosis cerebri	laminin-coated plates. 2. 3D neurospheres Each compound screened as a 5-point dose-response	stereotactic injection of cells into the right striatum of NOD-SCID Gamma Null (NSG) mice.		evaluated in a phase II trial Paclitaxel poliglumex (dose escalation) + TMZ + RT Newly diagnosed GBM (NCT01402063).
Lee et al., 2017 (139)	NHA-astrocyte AGM and four patient-derived GBM cells from four GBM patients	3D cell-based high-throughput screening method reflecting the microenvironments using a micropillar and microwell chip platform	Cell viability or a high-dose heat map of the cytotoxicity and efficacy of 70 compounds	70 compounds	Among the 70 compounds tested, cediranib (a potent inhibitor of vascular endothelial growth factor (VEGF) receptor tyrosine kinases) exhibited the lowest cytotoxicity to astrocytes and high efficacy to GBM cells in a high-dose heat map model.
Lun et al., 2016 (140)	13 independent genetically distinct patient-derived brain tumour-initiating cell lines	HTS was performed using 96-well microplates and two drug concentrations. Secondary validation was performed on a subset of BTICs using 8-point, 3-fold serial dilutions of compounds.	72h Alamar blue – proliferation assay	NIH clinical drug library that contains 446 compounds that have been used in human clinical trials, and a ToolKit library (OICR, Canada) containing 160 compounds	Montelukast, clioquinol & disulfiram. Disulfiram, an off-patent drug previously used to treat alcoholism, in the presence of a copper supplement, showed low nanomolar efficacy (including those resistant to TMZ and the highly infiltrative quiescent stem-like population). Validated *in vivo*, prolonged survival in patient-derived BTIC models established from both newly diagnosed and recurrent tumours.
Denicolaï et al., 2014 (141)	GBM6 and GBM9 stem-like cell lines and on U87-MG and U251-MG cell lines	Scratch assay and flash-cytometer acquisitions (drug treatment for 3 days)	Inhibitory efficacy on cell migration and proliferation	Prestwick chemical library® of 1120 molecules (all approved drugs)	Proscillaridin A, a cardiac glycoside inhibitor of the Na+/K+ ATPase pump. Also selected: emetine dihydrochloride and strophantidin.
Hothi et al., 2012 (142)	Glioma stem cell cultures were established from freshly resected tumour tissues	HTS was performed on five patient-derived cultures (384-well plates, 8-point dose-response curves). Further ToxCount cell viability assays, proteasomal chymotrypsin-like activity assays, aldefluor analysis and flow cytometry.	CellTiter-Glo was added to individual wells and, following 20 minutes incubation on an orbital shaker, luminescence was measured, and percentage cell viability was calculated.	Chemical library of 2,000 compounds.	Identified disulfiram (tetraethylthiuram disulfide, Antabuse®, DSF), a clinically approved drug for the treatment of alcoholism, as a potent inhibitor of multiple patient-derived GSCs.
Wang et al., 2012 (143)	Human GBM cell lines U87MG and U251MG	An HTS assay for cell growth and invasion followed by traditional cell growth and invasion assays.	Cell growth and invasion.	LOPAC1280 pharmacologically active compounds that influence most cellular processes and cover all major drug target classes.	Ten validated active compounds were obtained, of which six have been previously reported and four newly identified compounds 6-nitroso- 1,2-benzopyrone, S-(p-azidophenacyl) glutathione, phenoxybenzamine hydrochloride and SCH-28080
Visnyei et al., 2011 (144)	Patient-derived GBM stem cells	Multiple screening strategies. The HTS was done in a 384-well plate format at concentrations recommended by the manufacturers	(1) Cell viability GSC derived from one tumour. (2) differential effect between any of the two samples (3) repeat (2) on a panel of serum- and sphere-derived GBM samples (4) evaluate for their GSC selectivity and gene-target specific qRT-PCR–based screens to determine their inhibitory effect on key GBM regulator genes.	31,624 small molecules from 7 chemical libraries.	Highest priority compounds validated *in vivo*. Compounds #5560509, #5256360, OLDA, and emetine inhibited tumour formation in immunosuppressed animals.

approximately 31,000 small molecules identified 8 compounds showing greater inhibitory effect in GSC cultures compared with non-stem cell-enriched GBM cultures (144). In addition, another two compounds inhibited four GBM hub genes ASPM, MELK, FOXM1b and TOP2a. From these xenotransplants of GSC enriched tumour cells pre-treated with four candidate compounds (Emetine, #5560509, #5256360 or OLDA) displayed significantly reduced tumour mass volume suggesting a targeted effect on the tumour initiating stem cells. However, no further studies have been done on these compounds.

For larger cancer focussed HTS employing pharmacologically active compound libraries (157) or collections of probe libraries

targeting, for example, kinases (158) or epigenetic modifiers (159), the size of some of the available drug libraries is in the hundreds/thousands, resulting in an exponentially increasing the number of possible drug combinations. Therefore, screening all possible pairwise or higher-order combinations would be a huge task. For time and financial reasons, combinatorial drug screening will, therefore, realistically need to be constrained. If it is likely that one or more drugs would be required in addition to TMZ, what are the criteria that would identify a sole molecule as advantageous to use in combination? This may be an important consideration in the light of, for example, the CUSP9 data showing little activity as sole agents but significant effect in combination. The simplest and quickest screening format would be to identify candidates that already show a significant amount of tumour killing ability by themselves, and the studies described above show that potential drugs can be selected. In contrast, however, that format would not have selected any of the CUSP9 drugs which look potentially promising.

Non-hypothesis (screening) combinatorial studies from CRISPR screens

The development of clustered, regularly interspaced short palindromic repeats (CRISPR)/Cas gene-editing technologies can be deployed in the earliest stages of drug development to enable unbiased identification of new molecular targets through genome-wide CRISPR screens in cells or small model organism-based models of disease (160–162). A study using genome-wide pooled CRISPR screening across a panel of patient-derived GCS cultures was recently reported to define the molecular determinants governing GSC growth and survival (163). The screen was performed in the presence of a lethal dose of TMZ to identify genes modulating TMZ sensitivity revealing mechanisms of therapeutic resistance and new strategies for combinatorial therapy, including GSC self-renewal, GSC stemness and proliferation, as well as regulators of Cell Stress Response Pathways which all appear essential for GSC viability and fitness. Positive selection screens performed in two patient-derived GBM cell cultures treated with a lethal dose of TMZ revealed core members of the mismatch repair (MMR) pathway. To identify mechanisms of intrinsic resistance of the GSC population to TMZ, the authors performed negative selection screens in the presence of a sublethal dose of TMZ. These studies identified the Fanconi anemia pathway' (163)

Other CRISPR-Cas9 screenings have identified further potential targets that sensitize GBM cells to TMZ, including suppressing the NF-κB/E2F6 signalling axis (164). In another study, the authors applied a pooled CRISPR-Cas9 screening approach to the U138 human glioma line in a transwell invasion assay (165). Isolation and sequencing of cells that display accelerated invasion through the transwell filter identified inhibition of mitogen-activated protein kinase 4 (MAP4K4) as a potential therapeutic target for GBM invasion (165). A further study used CRISPR interference (CRISPRi) to screen 5689 Long non-coding RNAs (lncRNAs) loci in human GBM cells, identified 467 hits that modify cell growth in the presence of clinically relevant doses of fractionated radiation and 33 of these lncRNA hits sensitize GBM cells to radiation (166). Follow up studies demonstrated that antisense oligonucleotides targeting lncGRS-1 selectively decrease tumour growth and sensitize glioma cells to radiation therapy (166). The evolution of CRISPR/Cas 9 screening, including arrayed screening strategies across more definitive GBM phenotypic assay endpoints and pooled screens to identify sensitizers of additional drug classes are well placed to identify further therapeutic targets and drug combination hypotheses in GBM.

The role of hypoxia, tumor-microenvironment, and non-neoplastic cells for IR and drug resistance in GSC

Tumour heterogeneity and the presence of GSC alone does not explain the lack of successful clinical translation of promising preclinical discoveries in GBM (Table 1) and may in fact be due to experimental reasons; chief among them is the growing realisation that currently, the *in vitro* and *in vivo* models of GBM used in preclinical drug discovery do not completely recapitulate tumour biology within patients. GBM cells and their progenitor GSC dynamically respond to their local microenvironment through a multitude of bidirectional communications resulting in the permissive conditions for tumour growth and invasion. *In vitro* models employed to date have sought to encompass, to varying degrees, some of this environmental complexity in the high throughput setting.

In initial experiments isolating and characterising GSCs, a neurosphere culture paradigm was used successfully with GSCs (167, 168). Further advances have seen the field introduce adherent culture grown on different base layer coatings of ECM components, including collagen and laminin. These methods, previously established for fetal and human neural stem cells, overcame limitations of neurospheres, whilst generating pure and expandable populations of GSCs, are (169) readily amenable to an HTS format and have been extensively used in drug discovery for GBM since their establishment (144, 170).

A major hallmark of GBM and a vital component of the TME that has not featured in drug discovery efforts to date is the hypoxic core of tumours. These regions result from increased cell proliferation overcoming oxygen supply (171), in turn generating an environment that supports tumour progression through GSC maintenance, proliferation, and drug resistance (172–174). In current GBM research the majority of *in vitro* cell models do not account for the effects of the hypoxic TME with cells cultured in atmospheric oxygen with a partial oxygen pressure of 159 mmHg. Studies quantitating pO_2 in gliomas recorded a highly significant number of pO_2 readings in patients with GBM less than 2.5 mmHg (175, 176), levels known to reduce the efficacy of radiotherapy where cellular sensitivity is halved when pO_2 is below 3 mmHg (177). Recent research generated a novel 3D *in vitro* model with common GBM cell lines, U87, U251, and SNB19, to study hypoxic effects in the context of TMZ resistance (178), highlighting the significant role of hypoxia on drug resistance.

The role of non-neoplastic cells in GBM is another vital consideration when attempting to model TME conditions *in vitro*. These consist of immune cells, including invading macrophages and resident microglia, stromal cells including astrocytes, vascular endothelial cells and pericytes (88). Microglia and astrocytes, both of which are found in abundance in the brain, accounting for approximately 30-50% and 50% of the volumes in the tumour and brain tissue, respectively (89, 179) have been implicated in glioma invasion and survival (88) highlighting the importance of their inclusion in comprehensive studies of the effects of TME on GBM. For a more indepth review refer to Decordova et al., 2020 (180). Throughput is a significant limitation on the extent to which the effects of microglia and astrocytes can be utilized; however, several academic laboratories have generated 3D co-culture models to elucidate the roles of these cell types that offer potential for adaption to a higher throughput format. One such study has generated luciferase reporter GBM cell lines with a cell viability readout on 3D floating co-culture spheroids of bioluminescent GBM tumour cells and non-luminescent rat astrocytic cells. The research demonstrated an astrocyte-mediated increase in TMZ resistance in four of a panel of six GBM tumour cell lines (181). This *in vitro* model was also successfully employed along with stem cells and *in vivo* models to demonstrate growth-supportive effects of astrocytes (182). The protective effects of astrocytes in co-culture against the main chemotherapeutics, TMZ and vincristine, have also been observed in subsequent research in 2D and 3D co-culture and demonstrated to be contact-dependent (183, 184) where drug resistance might be due to the transfer of mitochondria through tunnelling nanotubes connecting with and rescuing the tumour cells (183). Colleagues from this laboratory utilized the same 3D HA-based model with co-cultured microglia to demonstrate chemoresistance that was not present in monocultures of GBM cell lines (185).

When designing an optimized platform for high throughput combinatorial screening, balancing the need for larger screening libraries to generate novel drug candidates and physiologically relevant models to better predict drug response is crucial. In order to better model tissue-like features and cellular interactions of the TME, recent HTS efforts have utilized 3D *in vitro* models of GBM. High content screening against a panel of 83 chemotherapeutics in both 2D and 3D cultures in the U87 cell line highlighted shortcomings in the former's ability to detect drug sensitivities with only those resulting from 3D cultures aligning with *in vivo* results (138). These findings are also supported by an independent study demonstrating TMZ sensitivity is decreased in 3D cultures of the common GBM cell lines, U87, U251, and SNB19, when compared with its 2D counterpart (178) Others have employed a 3D *in vitro* model with cell lines cultured in a HA-gelatin based hydrogel to model the ECM in 3D cultures, with chondroitin sulphate, chitosan and collagen/gelatine have also been utilized (186). Increased drug resistance was attributed to the co-cultured microglia and astrocytes.

Finding the appropriate balance in a GBM model between the complexity of the TME and the practical considerations of HTS is a challenge that has to be addressed for more successful translation of hits in drug discovery. In recent research, this balance may well have been achieved (187) in a study of 461 mostly FDA-approved drugs in 12 patient-derived GSCs, that incorporated both a 2D culture model in the primary HTS followed by a secondary 3D model for hit validations experiments. Results from this study demonstrate significant differences in sensitivity to hits representing multiple drug classes across patient-derived GSC models.

The implications of rational combinatorial small compound drug screening in GSC

In complex heterogeneous tumours, no single molecular event drives continued proliferation and tumour progression, and redundancy in signalling pathways limits the efficacy of therapies targeting single pathways (188). Network and pathway switching permit rapid tumour evolution and therapeutic evasion; this requires a holistic approach to understand cancer cell signalling networks, 'driver' pathways, and how best to collapse the robustness of such networks to address therapeutic resistance. Thus the complexity of GBM has been likened to the "three lock problem", describing that a door with three locks will not open any better even if keys are found to one or two locks (106). With so many different signalling pathways and cellular heterogeneity involved in tumour growth, combinations of targeted agents may well be most effective in treating rapidly evolving heterogeneous tumours, provided we can identify the network changes that permit cancer cells to subvert single agents.

In addition to the importance of the disease model and optimal drug combination delivery, equally relevant questions are; what is the rationale behind choosing specific drugs for potential combination therapies? How many drugs will be most beneficial to patients? What is the quickest and most successful way to identify these combinations? The rationale behind many drug combinations strategies tested in clinical trials studies is often unclear, and to date, unsuccessful. Even with the automated HTS instruments, exhaustive screening of drug combinations becomes quickly impractical, both in terms of time and cells required, as the number of potential drug and dose combinations increases exponentially with the number of tested drug components and dose levels. This combinatorial explosion requires intelligent computational-experimental strategies to guide the discovery of the most potent and less toxic combinations to be prioritized for further preclinical development before entering into lengthy and costly animal or clinical studies (189).

For rational combinatorial screening, there is a need for computationally efficient and experimentally feasible approaches that can (i) reduce combinatorial search space of potential combinations, (ii) and to identify both synergistic and safe combinatorial therapies for each individual patient and cell-context. For cancer-selectivity, it is important to guarantee that the combinations target stem cells and bulk tumour cells in GBM, while avoiding co-inhibition of non-malignant cells, to avoid treatment resistance and severe toxic effects. Ianevski et al. demonstrated recently the feasibility of using XGBoost machine learning (ML) algorithm together with ex vivo single-agent responses and single-cell transcriptomic profiling to identify patient-specific and cancer-selective pairwise combinations for treatment-refractory AML patients, each with different molecular backgrounds and synergy mechanisms (190). Using flow cytometry

drug assay, they demonstrated that the predicted combinations resulted not only in synergistic cancer cell co-inhibition, but were also capable of targeting specific AML cell subpopulations that emerge in differing stages of disease pathogenesis or treatment regimens. Such patient- and cell subpopulation-specific combinatorial approaches may avoid overlapping toxic effects through co-inhibiting mainly malignant cell types, therefore increasing their likelihood for clinical success.

There are many experimental and computational challenges that need to be solved to implement similar translational approaches for GBM combinatorial screening. Machine learning algorithms could help in predicting full dose-response matrices using a minimal number of combinatorial experiments, thereby enabling more cost-effective, yet systematic combinatorial screens (191). Computationally, one needs to consider also higher-order combinations of more than two drugs to facilitate the current paradigm shift from the traditional 'two drugs in combination' to more complex 'multi-drug cocktails' (192). While there are a number of machine learning models for prediction of pairwise drug-dose combinations (193), accurate prediction of higher-order combination effects with more than two drugs remains an unsolved problem. A tensor learning model that enables the accurate prediction of pairwise dose-response combinations for each cancer cell line (194) has been recently developed. Higher-order tensor learning may enable generalising and learning from the currently still rather limited combination data to explore and score in an iterative manner so-far untested massive drug spaces of higher-order combinations (195), hence enabling adaptive learning of best combinations for each cell context or patient individually.

Outlook and conclusions

At the time of writing, a search for the terms 'glioblastoma' and 'combination' on the clinicaltrials.gov website returns 604 separate clinical trials; 29 not yet recruiting, 123 recruiting, 65 active but not recruiting, 102 suspended, terminated or withdrawn, 40 with status unknown and 242 completed. Despite the many successes of modern drug discovery strategies across several cancers, such approaches have yet to provide significant benefit for the majority of GBM patients (196). As detailed in this review, this failure can be attributed to several factors, including remarkable heterogeneity of GBM between and within individual patients, multiple redundant and adaptive pathway signalling mechanisms allowing GBM to escape from any substantial consequence of individual target perturbation, poor preclinical models, which fail to recapitulate the complex microenvironment and pathophysiology of clinical GBM. Below we outline some of the key technological advancements which are well placed to address past failures and maximize future opportunities of targeted therapies and their combinations in GBM.

Improving GBM high throughput screening

To date, hypothesis-driven or targeted drug discovery such as efforts to inhibit the receptor tyrosine kinase (RTK) signalling pathways have been largely disappointing. Overexpression or mutations of EGFR occur in ~50% of GBM, yet clinical trials targeting this RTK in combination with standard care or other therapies have proven ineffective for GBM treatment (197). If this is to be overcome, future drug discovery programs must include combined targeted phenotypic approaches with comprehensive screening strategies incorporating phenotypic readouts as the primary HTS and target-based secondary and tertiary assays.

GBM cell lines have been integral to many HTS efforts in the past but are subject to significant genetic drift. Analysis of one widely used line, U87MG, has demonstrated that following 50 years of culture, it no longer reflects the phenotype of its tumour of origin (198). By employing GSC isolated from primary human tissue samples and maintained at low passage numbers, phenotypic screening can provide a more accurate representation of the tumour cell physiology than observed in cell lines (199). In addition, high throughput screens can incorporate the genetic diversity of GBM tumours by utilising GSCs from the main tumour-intrinsic transcriptional subtypes: Classical, Mesenchymal and Proneural as defined by aberrations and gene expression of EGFR, NF1, and PDGFRA/IDH1 (70).

GSC are highly resistant to chemotherapy and radiation (200). The acquisition of resistance to the SOC treatment in GBM is one of, if not the most significant hindrance to any new therapeutic and must be addressed in any cell models of GBM to be used for drug discovery. In primary high throughput screens, the rapid reformation of highly resistant tumours following surgical resection can be modelled by generating both chemotherapeutic and radioresistant GSC lines. As we have suggested, the most likely advances in GBM treatment will originate from the combination of additional therapeutic drugs with the existing SOC, so investigating new combinations of treatments/drugs in screening paradigms including irradiation and TMZ is absolutely critical to success.

Additionally, the hypoxic microenvironment plays a central role in the malignancy of GBM, acting on gene expression (201), promoting angiogenesis (202) and is implicated in tumour metastasis (203). The hypoxic environment presents further obstacles to the success of HTS by the generation of chemoresistance through various means, including activation of HIF1α and inducing radioresistance by preventing the formation of reactive oxygen species, the primary mechanisms of ionising radiation (204). The majority of drug discovery efforts in GBM have not factored in the significant contributions this environment plays on therapy resistance. Research in a 3D *in vitro* model has demonstrated the potentiation of TMZ resistance due to hypoxic conditions in GBM cell lines (178). However, unlike their 3D counterparts, 2D *in vitro* cell models are unable to foster an oxygen-deprived TME. This limitation can be overcome in future HTS programs by employing GSC cultures that are maintained, concurrently, in normoxia and hypoxia, through the use of standard incubators and physiological cell culture workstations, respectively.

Finally, the significant financial implications of running large HTS programs as is the norm in the pharmaceutical industry make these strategies not feasible for non-profit organisations in academic research. Rather, to achieve the same outcomes, anti-cancer targeted small molecule libraries and repurposed drugs can be utilized. This focused approach has the combined advantages of providing a more direct path to clinical translation by using existing compounds with

known safety profiles and by providing molecular detail on the aetiology of the disease.

Application of more predictive preclinical models in the GBM screening cascade

In vivo models of GBM are used in the advanced stages of drug discovery; they are expensive and not feasible for high-throughput testing of candidate drugs and drug combinations. Genetically engineered mouse models have a low incidence rate and long latency, while implanted tumours grow expansively due to high proliferative rates, with minimal diffuse local invasion when compared to clinical GBM. For this reason, there is a need for more relevant preclinical models which recapitulate the TME and can be incorporated downstream of high throughput screens to validate hit compounds. Due to the complexity of GBM, cell response and behaviour are vastly different when comparing a 3D microenvironment with traditional 2D monolayer cell culture models. This is particularly important when considering mechanisms of tumour cell invasion, which is a major cause of treatment failure in GBM, contributing to poor prognosis. Therefore, we suggest that a combination of complementary 3D assays be used to collectively assess the cell-ECM interaction and invasion types (into astrocyte rich stroma and along blood vessels/white matter tracts), which are observed *in vivo*.

3D tumour spheroid-based functional assays which aim to mimic the *in vivo* like invasion patterns, preferentially migrating along basement membranes (blood vessels and white matter tracks). While it is not possible to replicate all aspects, 3D assays may be used to recapitulate the defining aspects of GBM invasion/migration (205, 206). To mimic 3D invasion, spheroids submerged in a reconstituted basement membrane matrix, such as growth factor reduced Matrigel, can be used to determine the invasive potential of a cell line and support screening for compounds and/or drug combinations that may inhibit invasion (207). While Matrigel is a viable matrix, it is important to note the high percentage of collagen and reproducibility issues with batch-to-batch variability. Radial migration of spheroids placed onto a basement membrane such as laminin or Matrigel with media substituted with hyaluronan may be used to recapitulate perivascular glioma cell migration. Typically, GBM invasion/migration occurs along a basement membrane rather than through one, such as with the Boyden chamber membrane assay.

Recapitulating all aspects of the brain microenvironment is difficult *in vitro*. Therefore, ex vivo brain slice assays are used to maintain the complexities of the extracellular matrix and brain architecture and preserve *in vivo* morphology on which to grow tumour cells or spheroids and monitor cell behaviour in response to treatment (208–210). It has been shown that GBM stem cell motility decreases compared to 2D culture when maintained in this way, presumably due to additional barriers such as the extracellular matrix and the need for extracellular matrix remodelling (211). GBM cells also proliferate and differentiate differently depending on which region of the coronal brain slice the cells are injected (212). Surgically resected human tumour slices may also be used for ex vivo drug screening to personalize cancer therapy (213). The analysis of tissue slices is often by histochemistry, but recently, whole transcriptome sequencing of resected human GBM tumour slices has been performed to determine gene expression differences after drug treatment (214). Further advances in automated high-content confocal imaging enable systematic testing of candidate drugs and drug combinations on phenotypic markers in advanced 3D *in vitro* and ex-vivo model systems. Organotypic brain/tumour slice assays may play a useful role in bridging the gap between existing *in vitro* and *in vivo* assays, especially when investigating tumour cell migration, invasion and growth to evaluate novel therapeutic strategies.

Cost-effective and transparent AI-guided prediction of drug combinations

Large-scale multi-dose combinatorial screening requires extensive resources and instrumentation beyond the capability of most academic laboratories. Testing of thousands of drug-dose combinations is also impossible in limited numbers of primary cells from patients. The development of transparent and robust experimental and computational strategies is expected to lead to effective prioritisation and validation of optimal drug combination and dose ratios toward next-generation preclinical and clinical testing platforms. The predictive models, based on both physiologically relevant GBM conditions and practically feasible ML models, are therefore expected to lead to both cost- and time-efficacy in academic cancer research. Using such strategies, the drug screening efforts can be targeted to verifying the most promising drug combinations, with maximal cancer-selectivity, thereby significantly accelerating the future design and testing of combination therapies, as well as increasing the likelihood of their success in preclinical and clinical studies with the aim to improve both combination efficacy and tolerability (215).

Many of the most accurate ML or artificial intelligence (AI) models are not transparent for humans, e.g., those based on deep learning or tensor learning algorithms, and they may rely on an overly large set of input features for cost-efficient implementation. For widespread adoption among experimental researchers, the learning algorithms need to be transparent and explainable to experimental researchers, including a clear description of the optimisation objectives (synergy, efficacy and/or toxicity) and quantitative performance and confidence evaluation (e.g. using conformal prediction), which help the experimentalists to decide when and how to use the algorithms to obtain valid results (216). For experimental feasibility, there is also a need to implement effective computational approaches that make use of partial measurements of the full drug-dose spaces to predict the most potent higher-order combinations and to provide high-resolution information of response landscapes across various dose combinations, critical for clinical translation (e.g. low dose and less toxic synergies).

The increased understanding of disease heterogeneity and new emerging methodologies described in this review article enable modern non-reductionist and more evidence-led discovery strategies which embrace the complexity of GBM. We believe such approaches will facilitate a more systematic and transparent approach to the identification and prioritisation of new drug combinations which can contribute to improved treatments for GBM patients.

Author contributions

DE conceived the review, wrote the manuscript and is the corresponding author. TJ is first author and wrote the manuscript. LM compiled the clinical trials tables and wrote the manuscript. JS compiled the clinical trials data. SE, GH and MF contributed to writing the manuscript and provided critical editing. TA and NC wrote the manuscript. All authors contributed to the article and approved the submitted version.

Funding

This work was supported by a joint Cancer Research UK (A28596) and The Brain Tumour Charity award (GN-000676) to D.E.,N.C and M.F. TA was supported by the Academy of Finland (grant 344698), the Cancer Society of Finland, and the Norwegian Cancer Society (grant 216104).

Conflict of interest

The authors declare that the research was conducted in the absence of any commercial or financial relationships that could be construed as a potential conflict of interest.

Publisher's note

References

1. Butte PV, Mamelak A, Parrish-Novak J, Drazin D, Shweikeh F, Gangalum PR, et al. Near-infrared imaging of brain tumors using the tumor paint BLZ-100 to achieve near-complete resection of brain tumors. *Neurosurgical focus.* (2014) 36(2):E1. doi: 10.3171/2013.11.FOCUS13497

2. Patil CG, Walker DG, Miller DM, Butte P, Morrison B, Kittle DS, et al. Phase 1 safety, pharmacokinetics, and fluorescence imaging study of tozuleristide (BLZ-100) in adults with newly diagnosed or recurrent gliomas. *Neurosurgery* (2019) 85(4):E641–9. doi: 10.1093/neuros/nyz125

3. Hardesty DA, Sanai N. The value of glioma extent of resection in the modern neurosurgical era. *Front Neurol* (2012) 3:140. doi: 10.3389/fneur.2012.00140

4. Davis ME. Glioblastoma: Overview of disease and treatment. *Clin J Oncol Nurs.* (2016) 20(5 Suppl):S2–8. doi: 10.1188/16.CJON.S1.2-8

5. Gilbert MR, Wang M, Aldape KD, Stupp R, Hegi ME, Jaeckle KA, et al. Dose-dense temozolomide for newly diagnosed glioblastoma: a randomized phase III clinical trial. *J Clin Oncol* (2013) 31(32):4085–91. doi: 10.1200/JCO.2013.49.6968

6. Shergalis A, Bankhead A3rd, Luesakul U, Muangsin N, Neamati N. Current challenges and opportunities in treating glioblastoma. *Pharmacol Rev* (2018) 70(3):412–45. doi: 10.1124/pr.117.014944

7. Stupp R, Mason WP, van den Bent MJ, Weller M, Fisher B, Taphoorn MJ, et al. Radiotherapy plus concomitant and adjuvant temozolomide for glioblastoma. *N Engl J Med* (2005) 352(10):987–96. doi: 10.1056/NEJMoa043330

8. Omuro A, Brandes AA, Carpentier AF, Idbaih A, Reardon DA, Cloughesy T, et al. Radiotherapy combined with nivolumab or temozolomide for newly diagnosed glioblastoma with unmethylated MGMT promoter: An international randomized phase 3 trial. *Neuro Oncol* (2022) 25(1):123–34. doi: 10.1093/neuonc/noac099

9. Lim M, Weller M, Idbaih A, Steinbach J, Finocchiaro G, Raval RR, et al. Phase 3 trial of chemoradiotherapy with temozolomide plus nivolumab or placebo for newly diagnosed glioblastoma with methylated MGMT promoter. *Neuro Oncol* (2022) 24(11):1935–49. doi: 10.1093/neuonc/noac116

10. Sim HW, McDonald KL, Lwin Z, Barnes EH, Rosenthal M, Foote MC, et al. A randomized phase II trial of veliparib, radiotherapy, and temozolomide in patients with unmethylated MGMT glioblastoma: the VERTU study. *Neuro Oncol* (2021) 23(10):1736–49. doi: 10.1093/neuonc/noab111

11. Nayak L, Molinaro AM, Peters K, Clarke JL, Jordan JT, de Groot J, et al. Randomized phase II and biomarker study of pembrolizumab plus bevacizumab versus pembrolizumab alone for patients with recurrent glioblastoma. *Clin Cancer Res* (2021) 27 (4):1048–57. doi: 10.1158/1078-0432.CCR-20-2500

12. Peereboom DM, Ye X, Mikkelsen T, Lesser GJ, Lieberman FS, Robins HI, et al. A phase II and pharmacodynamic trial of RO4929097 for patients with Recurrent/Progressive glioblastoma. *Neurosurgery* (2021) 88(2):246–51. doi: 10.1093/neuros/nyaa412

13. Wen PY, Stein A, van den Bent M, De Greve J, Wick A, de Vos F, et al. Dabrafenib plus trametinib in patients with BRAF(V600E)-mutant low-grade and high-grade glioma (ROAR): a multicentre, open-label, single-arm, phase 2, basket trial. *Lancet Oncol* (2022) 23(1):53–64. doi: 10.1016/S1470-2045(21)00578-7

14. Cloughesy TF, Petrecca K, Walbert T, Butowski N, Salacz M, Perry J, et al. Effect of vocimagene amiretrorepvec in combination with flucytosine vs standard of care on survival following tumor resection in patients with recurrent high-grade glioma: A randomized clinical trial. *JAMA Oncol* (2020) 6(12):1939–46. doi: 10.1001/jamaoncol.2020.3161

15. Natsume A, Aoki K, Ohka F, Maeda S, Hirano M, Adilijiang A, et al. Genetic analysis in patients with newly diagnosed glioblastomas treated with interferon-beta plus temozolomide in comparison with temozolomide alone. *J Neuro-Oncology.* (2020) 148:17–27. doi: 10.1007/s11060-020-03505-9

16. Reardon DA, Desjardins A, Vredenburgh JJ, O'Rourke DM, Tran DD, Fink KL, et al. Rindopepimut with bevacizumab for patients with relapsed EGFRvIII-expressing glioblastoma (ReACT): Results of a double-blind randomized phase II trial. *Clin Cancer Res* (2020) 26:1586–94. doi: 10.1158/1078-0432.CCR-18-1140

17. Puduvalli VK, Wu J, Yuan Y, Armstrong TS, Vera E, Wu J, et al. A Bayesian adaptive randomized phase II multicenter trial of bevacizumab with or without vorinostat in adults with recurrent glioblastoma. *Neuro-Oncology* (2020) 14;22(10):1505–15. doi: 10.1093/neuonc/noaa062

18. Lee EQ, Zhang P, Wen PY, Gerstner ER, Reardon DA, Aldape KD, et al. NRG/RTOG 1122: A phase 2, double-blinded, placebo-controlled study of bevacizumab with and without trebananib in patients with recurrent glioblastoma or gliosarcoma. *Cancer* (2020) 126:2821–8. doi: 10.1002/cncr.32811

19. Cloughesy TF, Brenner A, de Groot JF, Butowski NA, Zach L, Campian JL, et al. A randomized controlled phase III study of VB-111 combined with bevacizumab vs bevacizumab monotherapy in patients with recurrent glioblastoma (GLOBE). *Neuro Oncol* (2020) 22(5):705–17. doi: 10.1093/neuonc/noz232

20. Rosenthal M, Clement PM, Campone M, Gil-Gil MJ, DeGroot J, Chinot O, et al. Buparlisib plus carboplatin or lomustine in patients with recurrent glioblastoma: a phase Ib/II, open-label, multicentre, randomised study. *ESMO Open* (2020) 5(4):e000672. doi: 10.1136/esmoopen-2020-000672

21. Galanis E, Anderson SK, Twohy EL, Carrero XW, Dixon JG, Tran DD, et al. A phase 1 and randomized, placebo-controlled phase 2 trial of bevacizumab plus dasatinib in patients with recurrent glioblastoma: Alliance/North central cancer treatment group N0872. *Cancer* (2019) 125:3790–800. doi: 10.1002/cncr.32340

22. Cloughesy TF, Mochizuki AY, Orpilla JR, Hugo W, Lee AH, Davidson TB, et al. Neoadjuvant anti-PD-1 immunotherapy promotes a survival benefit with intratumoral and systemic immune responses in recurrent glioblastoma. *Nat Med* (2019) 25(3):477–86. doi: 10.1038/s41591-018-0337-7

23. van den Bent M, Eoli M, Sepulveda JM, Smits M, Walenkamp A, Frenel J-S, et al. INTELLANCE 2/EORTC 1410 randomized phase II study of depatux-m alone and with temozolomide vs temozolomide or lomustine in recurrent EGFR amplified glioblastoma. *Neuro-Oncology* (2020) 22:684–93. doi: 10.1093/neuonc/noz222

24. Herrlinger U, Tzaridis T, Mack F, Steinbach JP, Schlegel U, Sabel M, et al. Lomustine-temozolomide combination therapy versus standard temozolomide therapy in patients with newly diagnosed glioblastoma with methylated MGMT promoter (CeTeG/NOA–09): a randomised, open-label, phase 3 trial. *Lancet* (2019) 393:678–88. doi: 10.1016/S0140-6736(18)31791-4

25. Wakabayashi T, Natsume A, Mizusawa J, Katayama H, Fukuda H, Sumi M, et al. JCOG0911 INTEGRA study: a randomized screening phase II trial of interferonβ plus temozolomide in comparison with temozolomide alone for newly diagnosed glioblastoma. *J Neuro-Oncology.* (2018) 138:627–36. doi: 10.1007/s11060-018-2831-7

26. Schäfer N, Proescholdt M, Steinbach JP, Weyerbrock A, Hau P, Grauer O, et al. Quality of life in the GLARIUS trial randomizing bevacizumab/irinotecan versus temozolomide in newly diagnosed, MGMT-nonmethylated glioblastoma. *Neuro-Oncology* (2018) 20:975–85. doi: 10.1093/neuonc/nox204

27. Chinnaiyan P, Won M, Wen PY, Rojiani AM, Werner-Wasik M, Shih HA, et al. A randomized phase II study of everolimus in combination with chemoradiation in newly

diagnosed glioblastoma: results of NRG oncology RTOG 0913. *Neuro-Oncology* (2018) 20:666–73. doi: 10.1093/neuonc/nox209

28. Duerinck J, Du Four S, Bouttens F, Andre C, Verschaeve V, Van Fraeyenhove F, et al. Randomized phase II trial comparing axitinib with the combination of axitinib and lomustine in patients with recurrent glioblastoma. *J Neuro-Oncology.* (2018) 136:115–25. doi: 10.1007/s11060-017-2629-z

29. Wick W, Gorlia T, Bendszus M, Taphoorn M, Sahm F, Harting I, et al. Lomustine and bevacizumab in progressive glioblastoma. *New Engl J Med* (2017) 377:1954–63. doi: 10.1056/NEJMoa1707358

30. Capper D, von Deimling A, Brandes A, Carpentier A, Kesari S, Sepulveda-Sanchez J, et al. Biomarker and histopathology evaluation of patients with recurrent glioblastoma treated with galunisertib, lomustine, or the combination of galunisertib and lomustine. *Int J Mol Sci* (2017) 18:995. doi: 10.3390/ijms18050995

31. Kong D-S, Nam D-H, Kang S-H, Lee JW, Chang J-H, Kim J-H, et al. Phase III randomized trial of autologous cytokine-induced killer cell immunotherapy for newly diagnosed glioblastoma in korea. *Oncotarget* (2017) 8:7003–13. doi: 10.18632/oncotarget.12273

32. Weller M, Butowski N, Tran DD, Recht LD, Lim M, Hirte H, et al. Rindopepimut with temozolomide for patients with newly diagnosed, EGFRvIII-expressing glioblastoma (ACT IV): a randomised, double-blind, international phase 3 trial. *Lancet Oncol* (2017) 18 (10):1373–85. doi: 10.1016/S1470-2045(17)30517-X

33. Cloughesy T, Finocchiaro G, Belda-Iniesta C, Recht L, Brandes AA, Pineda E, et al. Randomized, double-blind, placebo-controlled, multicenter phase II study of onartuzumab plus bevacizumab versus placebo plus bevacizumab in patients with recurrent glioblastoma: Efficacy, safety, and hepatocyte growth factor and O 6 -Methylguanine–DNA met. *J Clin Oncol* (2017) 35:343–51. doi: 10.1200/JCO.2015.64.7685

34. Gilbert MR, Pugh SL, Aldape K, Sorensen AG, Mikkelsen T, Penas-Prado M, et al. NRG oncology RTOG 0625: a randomized phase II trial of bevacizumab with either irinotecan or dose-dense temozolomide in recurrent glioblastoma. *J Neuro-Oncology.* (2017) 131:193–9. doi: 10.1007/s11060-016-2288-5

35. Weathers S-P, Han X, Liu DD, Conrad CA, Gilbert MR, Loghin ME, et al. A randomized phase II trial of standard dose bevacizumab versus low dose bevacizumab plus lomustine (CCNU) in adults with recurrent glioblastoma. *J Neuro-Oncology.* (2016) 129:487–94. doi: 10.1007/s11060-016-2195-9

36. Brandes AA, Finocchiaro G, Zagonel V, Reni M, Caserta C, Fabi A, et al. AVAREG: a phase II, randomized, noncomparative study of fotemustine or bevacizumab for patients with recurrent glioblastoma. *Neuro-Oncology* (2016) 18:1304–12. doi: 10.1093/neuonc/now035

37. Brandes AA, Carpentier AF, Kesari S, Sepulveda-Sanchez JM, Wheeler HR, Chinot O, et al. A phase II randomized study of galunisertib monotherapy or galunisertib plus lomustine compared with lomustine monotherapy in patients with recurrent glioblastoma. *Neuro-Oncology* (2016) 18:1146–56. doi: 10.1093/neuonc/now009

38. Brown N, McBain C, Nash S, Hopkins K, Sanghera P, Saran F, et al. Multi-center randomized phase II study comparing cediranib plus gefitinib with cediranib plus placebo in subjects with Recurrent/Progressive glioblastoma. *PloS One* (2016) 11:e0156369. doi: 10.1371/journal.pone.0156369

39. Herrlinger U, Schäfer N, Steinbach JP, Weyerbrock A, Hau P, Goldbrunner R, et al. Bevacizumab plus irinotecan versus temozolomide in newly diagnosed O 6 -Methylguanine–DNA methyltransferase nonmethylated glioblastoma: The randomized GLARIUS trial. *J Clin Oncol* (2016) 34:1611–9. doi: 10.1200/JCO.2015.63.4691

40. Balana C, De Las Penas R, Sepúlveda JM, Gil-Gil MJ, Luque R, Gallego O, et al. Bevacizumab and temozolomide versus temozolomide alone as neoadjuvant treatment in unresected glioblastoma: the GENOM 009 randomized phase II trial. *J Neuro-Oncology.* (2016) 127:569–79. doi: 10.1007/s11060-016-2065-5

41. Erdem-Eraslan L, van den Bent MJ, Hoogstrate Y, Naz-Khan H, Stubbs A, van der Spek P, et al. Identification of patients with recurrent glioblastoma who may benefit from combined bevacizumab and CCNU therapy: A report from the BELOB trial. *Cancer Res* (2016) 76:525–34. doi: 10.1158/0008-5472.CAN-15-0776

42. Robins HI, Zhang P, Gilbert MR, Chakravarti A, de Groot JF, Grimm SA, et al. A randomized phase I/II study of ABT-888 in combination with temozolomide in recurrent temozolomide resistant glioblastoma: an NRG oncology RTOG group study. *J Neuro-Oncology.* (2016) 126:309–16. doi: 10.1007/s11060-015-1966-z

43. Field KM, Simes J, Nowak AK, Cher L, Wheeler H, Hovey EJ, et al. Randomized phase 2 study of carboplatin and bevacizumab in recurrent glioblastoma. *Neuro-Oncology* (2015) 17:1504–13. doi: 10.1093/neuonc/nov104

44. Lee EQ, Kaley TJ, Duda DG, Schiff D, Lassman AB, Wong ET, et al. A multicenter, phase II, randomized, noncomparative clinical trial of radiation and temozolomide with or without vandetanib in newly diagnosed glioblastoma patients. *Clin Cancer Res* (2015) 21:3610–8. doi: 10.1158/1078-0432.CCR-14-3220

45. Blumenthal DT, Rankin C, Stelzer KJ, Spence AM, Sloan AE, Moore DF, et al. A phase III study of radiation therapy (RT) and O6-benzylguanine + BCNU versus RT and BCNU alone and methylation status in newly diagnosed glioblastoma and gliosarcoma: Southwest oncology group (SWOG) study S0001. *Int J Clin Oncol* (2015) 20:650–8. doi: 10.1007/s10147-014-0769-0

46. Dirven L, van den Bent MJ, Bottomley A, van der Meer N, van der Holt B, Vos MJ, et al. The impact of bevacizumab on health-related quality of life in patients treated for recurrent glioblastoma: Results of the randomised controlled phase 2 BELOB trial. *Eur J Cancer.* (2015) 51:1321–30. doi: 10.1016/j.ejca.2015.03.025

47. Nabors LB, Fink KL, Mikkelsen T, Grujicic D, Tarnawski R, Nam DH, et al. Two cilengitide regimens in combination with standard treatment for patients with newly diagnosed glioblastoma and unmethylated MGMT gene promoter: results of the open-label, controlled, randomized phase II CORE study. *Neuro-Oncology* (2015) 17:708–17. doi: 10.1093/neuonc/nou356

48. Schiff D, Kesari S, de Groot J, Mikkelsen T, Drappatz J, Coyle T, et al. Phase 2 study of CT-322, a targeted biologic inhibitor of VEGFR-2 based on a domain of human fibronectin, in recurrent glioblastoma. *Investigational New Drugs* (2015) 33:247–53. doi: 10.1007/s10637-014-0186-2

49. Penas-Prado M, Hess KR, Fisch MJ, Lagrone LW, Groves MD, Levin VA, et al. Randomized phase II adjuvant factorial study of dose-dense temozolomide alone and in combination with isotretinoin, celecoxib, and/or thalidomide for glioblastoma. *Neuro-Oncology* (2015) 17:266–73. doi: 10.1093/neuonc/nou155

50. Jeyapalan S, Boxerman J, Donahue J, Goldman M, Kinsella T, Dipetrillo T, et al. Paclitaxel poliglumex, temozolomide, and radiation for newly diagnosed high-grade glioma. *Am J Clin Oncol* (2014) 37:444–9. doi: 10.1097/COC.0b013e31827de92b

51. Stupp R, Hegi ME, Gorlia T, Erridge SC, Perry J, Hong Y-K, et al. Cilengitide combined with standard treatment for patients with newly diagnosed glioblastoma with methylated MGMT promoter (CENTRIC EORTC 26071-22072 study): a multicentre, randomised, open-label, phase 3 trial. *Lancet Oncol* (2014) 15:1100–8. doi: 10.1016/S1470-2045(14)70379-1

52. Taal W, Oosterkamp HM, Walenkamp AME, Dubbink HJ, Beerepoot LV, Hanse MCJ, et al. Single-agent bevacizumab or lomustine versus a combination of bevacizumab plus lomustine in patients with recurrent glioblastoma (BELOB trial): a randomised controlled phase 2 trial. *Lancet Oncol* (2014) 15:943–53. doi: 10.1016/S1470-2045(14)70314-6

53. Gilbert MR, Dignam JJ, Armstrong TS, Wefel JS, Blumenthal DT, Vogelbaum MA, et al. A randomized trial of bevacizumab for newly diagnosed glioblastoma. *N Engl J Med* (2014) 370(8):699–708. doi: 10.1056/NEJMoa1308573

54. Hofland KF, Hansen S, Sorensen M, Engelholm S, Schultz HP, Muhic A, et al. Neoadjuvant bevacizumab and irinotecan versus bevacizumab and temozolomide followed by concomitant chemoradiotherapy in newly diagnosed glioblastoma multiforme: A randomized phase II study. *Acta Oncol* (2014) 53:939–44. doi: 10.3109/0284186X.2013.879607

55. Chauffert B, Feuvret L, Bonnetain F, Taillandier L, Frappaz D, Taillia H, et al. Randomized phase II trial of irinotecan and bevacizumab as neo-adjuvant and adjuvant to temozolomide-based chemoradiation compared with temozolomide-chemoradiation for unresectable glioblastoma: final results of the TEMAVIR study from ANOCEF. *Ann Oncol* (2014) 25:1442–7. doi: 10.1093/annonc/mdu148

56. Batchelor TT, Mulholland P, Neyns B, Nabors LB, Campone M, Wick A, et al. Phase III randomized trial comparing the efficacy of cediranib as monotherapy, and in combination with lomustine, versus lomustine alone in patients with recurrent glioblastoma. *J Clin Oncol* (2013) 31:3212–8. doi: 10.1200/JCO.2012.47.2464

57. Stragliotto G, Rahbar A, Solberg NW, Lilja A, Taher C, Orrego A, et al. Effects of valganciclovir as an add-on therapy in patients with cytomegalovirus-positive glioblastoma: A randomized, double-blind, hypothesis-generating study. *Int J Cancer.* (2013) 133:1204–13. doi: 10.1002/ijc.28111

58. Westphal M, Ylä-Herttuala S, Martin J, Warnke P, Menei P, Eckland D, et al. Adenovirus-mediated gene therapy with sitimagene ceradenovec followed by intravenous ganciclovir for patients with operable high-grade glioma (ASPECT): a randomised, open-label, phase 3 trial. *Lancet Oncol* (2013) 14(9):823–33. doi: 10.1016/S1470-2045(13)70274-2

59. Shibui S, Narita Y, Mizusawa J, Beppu T, Ogasawara K, Sawamura Y, et al. Randomized trial of chemoradiotherapy and adjuvant chemotherapy with nimustine (ACNU) versus nimustine plus procarbazine for newly diagnosed anaplastic astrocytoma and glioblastoma (JCOG0305). *Cancer Chemother Pharmacol* (2013) 71:511–21. doi: 10.1007/s00280-012-2041-5

60. Nabors LB, Mikkelsen T, Hegi ME, Ye X, Batchelor T, Lesser G, et al. A safety run-in and randomized phase 2 study of cilengitide combined with chemoradiation for newly diagnosed glioblastoma (NABTT 0306). *Cancer* (2012) 118:5601–7. doi: 10.1002/cncr.27585

61. Hainsworth J, Shih K, Shepard G, Tillinghast G, Brinker B, Spigel D. Phase II study of concurrent radiation therapy, temozolomide, and bevacizumab followed by bevacizumab/everolimus as first-line treatment for patients with glioblastoma. *Clin Adv Hematol Oncol* (2012) 10:240–6.

62. Kim IH, Park C-K, Heo DS, Kim C-Y, Rhee CH, Nam D-H, et al. Radiotherapy followed by adjuvant temozolomide with or without neoadjuvant ACNU-CDDP chemotherapy in newly diagnosed glioblastomas: a prospective randomized controlled multicenter phase III trial. *J Neuro-Oncology.* (2011) 103:595–602. doi: 10.1007/s11060-010-0427-y

63. Dresemann G, Weller M, Rosenthal MA, Wedding U, Wagner W, Engel E, et al. Imatinib in combination with hydroxyurea versus hydroxyurea alone as oral therapy in patients with progressive pretreated glioblastoma resistant to standard dose temozolomide. *J Neuro-Oncology.* (2010) 96:393–402. doi: 10.1007/s11060-009-9976-3

64. Friedman HS, Prados MD, Wen PY, Mikkelsen T, Schiff D, Abrey LE, et al. Bevacizumab alone and in combination with irinotecan in recurrent glioblastoma. *J Clin Oncol* (2009) 27:4733–40. doi: 10.1200/JCO.2008.19.8721

65. Buckner JC, Ballman KV, Michalak JC, Burton GV, Cascino TL, Schomberg PJ, et al. Phase III trial of carmustine and cisplatin compared with carmustine alone and standard radiation therapy or accelerated radiation therapy in patients with glioblastoma multiforme: North central cancer treatment group 93-72-52 and southwest oncology group. *J Clin Oncol* (2006) 24:3871–9. doi: 10.1200/JCO.2005.04.6979

66. Sotelo J, Briceño E, López-González MA. Adding chloroquine to conventional treatment for glioblastoma multiforme. *Ann Internal Med* (2006) 144:337. doi: 10.7326/0003-4819-144-5-200603070-00008

67. Kruglyak KM, Lin E, Ong FS. Next-generation sequencing in precision oncology: challenges and opportunities. *Expert Rev Mol Diagn.* (2014) 14(6):635–7. doi: 10.1586/14737159.2014.916213

68. Patel AP, Tirosh I, Trombetta JJ, Shalek AK, Gillespie SM, Wakimoto H, et al. Single-cell RNA-seq highlights intratumoral heterogeneity in primary glioblastoma. *Science* (2014) 344(6190):1396–401. doi: 10.1126/science.1254257

69. Brennan CW, Verhaak RGW, McKenna A, Campos B, Noushmehr H, Salama SR, et al. The somatic genomic landscape of glioblastoma. *Cell* (2013) 155(2):462–77. doi: 10.1016/j.cell.2013.09.034

70. Verhaak RG, Hoadley KA, Purdom E, Wang V, Qi Y, Wilkerson MD, et al. Integrated genomic analysis identifies clinically relevant subtypes of glioblastoma characterized by abnormalities in PDGFRA, IDH1, EGFR, and NF1. *Cancer Cell* (2010) 17(1):98–110. doi: 10.1016/j.ccr.2009.12.020

71. Sakthikumar S, Roy A, Haseeb L, Pettersson ME, Sundström E, Marinescu VD, et al. Whole-genome sequencing of glioblastoma reveals enrichment of non-coding constraint mutations in known and novel genes. *Genome Biol* (2020) 21(1):127. doi: 10.1186/s13059-020-02035-x

72. Nobusawa S, Watanabe T, Kleihues P, Ohgaki H. IDH1 mutations as molecular signature and predictive factor of secondary glioblastomas. *Clin Cancer Res* (2009) 15 (19):6002–7. doi: 10.1158/1078-0432.CCR-09-0715

73. Rushing EJ. WHO classification of tumors of the nervous system: preview of the upcoming 5th edition. *memo - Magazine Eur Med Oncol* (2021) 14(2):188–91. doi: 10.1007/s12254-021-00680-x

74. Yan H, Parsons DW, Jin G, McLendon R, Rasheed BA, Yuan W, et al. IDH1 and IDH2 mutations in gliomas. *N Engl J Med* (2009) 360(8):765–73. doi: 10.1056/NEJMoa0808710

75. Choi S, Yu Y, Grimmer MR, Wahl M, Chang SM, Costello JF. Temozolomide-associated hypermutation in gliomas. *Neuro Oncol* (2018) 20(10):1300–9. doi: 10.1093/neuonc/noy016

76. Pan YB, Wang S, Yang B, Jiang Z, Lenahan C, Wang J, et al. Transcriptome analyses reveal molecular mechanisms underlying phenotypic differences among transcriptional subtypes of glioblastoma. *J Cell Mol Med* (2020) 24(7):3901–16. doi: 10.1111/jcmm.14976

77. McLendon R, Friedman A, Bigner D, Van Meir EG, Brat DJ, Mastrogianakis GM, et al. Comprehensive genomic characterization defines human glioblastoma genes and core pathways. *Nature* (2008) 455(7216):1061–8. doi: 10.1038/nature07385

78. Parsons DW, Jones S, Zhang X, Lin JC-H, Leary RJ, Angenendt P, et al. An integrated genomic analysis of human glioblastoma multiforme. *Science* (2008) 321 (5897):1807. doi: 10.1126/science.1164382

79. Hegi ME, Diserens AC, Gorlia T, Hamou MF, de Tribolet N, Weller M, et al. MGMT gene silencing and benefit from temozolomide in glioblastoma. *N Engl J Med* (2005) 352(10):997–1003. doi: 10.1056/NEJMoa043331

80. Yan F, Alinari L, Lustberg ME, Katherine Martin L, Cordero-Nieves HM, Banasavadi-Siddegowda Y, et al. Genetic validation of the protein arginine methyltransferase PRMT5 as a candidate therapeutic target in glioblastoma. *Cancer Res* (2014) 74(6):1752. doi: 10.1158/0008-5472.CAN-13-0884

81. Sachamitr P, Ho JC, Ciamponi FE, Ba-Alawi W, Coutinho FJ, Guilhamon P, et al. PRMT5 inhibition disrupts splicing and stemness in glioblastoma. *Nat Commun* (2021) 12(1):979. doi: 10.1038/s41467-021-21204-5

82. Bao S, Wu Q, McLendon RE, Hao Y, Shi Q, Hjelmeland AB, et al. Glioma stem cells promote radioresistance by preferential activation of the DNA damage response. *Nature* (2006) 444(7120):756–60. doi: 10.1038/nature05236

83. Chen J, Li Y, Yu TS, McKay RM, Burns DK, Kernie SG, et al. A restricted cell population propagates glioblastoma growth after chemotherapy. *Nature* (2012) 488 (7412):522–6. doi: 10.1038/nature11287

84. Lathia JD, Mack SC, Mulkearns-Hubert EE, Valentim CL, Rich JN. Cancer stem cells in glioblastoma. *Genes Dev* (2015) 29(12):1203–17. doi: 10.1101/gad.261982.115

85. Parada LF, Dirks PB, Wechsler-Reya RJ. Brain tumor stem cells remain in play. *J Clin Oncol* (2017) 35(21):2428–31. doi: 10.1200/JCO.2017.73.9540

86. Neftel C, Laffy J, Filbin MG, Hara T, Shore ME, Rahme GJ, et al. An integrative model of cellular states, plasticity, and genetics for glioblastoma. *Cell* (2019) 178(4):835–849.e821. doi: 10.1016/j.cell.2019.06.024

87. Frantz C, Stewart KM, Weaver VM. The extracellular matrix at a glance. *J Cell Science.* (2010) 123(24):4195. doi: 10.1242/jcs.023820

88. Hambardzumyan D, Gutmann DH, Kettenmann H. The role of microglia and macrophages in glioma maintenance and progression. *Nat Neurosci* (2016) 19(1):20–7. doi: 10.1038/nn.4185

89. Morantz RA, Wood GW, Foster M, Clark M, Gollahon K. Macrophages in experimental and human brain tumors. part 2: studies of the macrophage content of human brain tumors. *J neurosurgery.* (1979) 50(3):305–11. doi: 10.3171/jns.1979.50.3.0305

90. Dirks PB. Brain tumor stem cells: the cancer stem cell hypothesis writ large. *Mol Oncol* (2010) 4(5):420–30. doi: 10.1016/j.molonc.2010.08.001

91. Pallini R, Ricci-Vitiani L, Banna GL, Signore M, Lombardi D, Todaro M, et al. Cancer stem cell analysis and clinical outcome in patients with glioblastoma multiforme. *Clin Cancer Res* (2008) 14(24):8205–12. doi: 10.1158/1078-0432.CCR-08-0644

92. Zeppernick F, Ahmadi R, Campos B, Dictus C, Helmke BM, Becker N, et al. Stem cell marker CD133 affects clinical outcome in glioma patients. *Clin Cancer Res* (2008) 14 (1):123–9. doi: 10.1158/1078-0432.CCR-07-0932

93. Lan X, Jörg DJ, Cavalli FMG, Richards LM, Nguyen LV, Vanner RJ, et al. Fate mapping of human glioblastoma reveals an invariant stem cell hierarchy. *Nature* (2017) 549(7671):227–32. doi: 10.1038/nature23666

94. Prager BC, Bhargava S, Mahadev V, Hubert CG, Rich JN. Glioblastoma stem cells: Driving resilience through chaos. *Trends Cancer.* (2020) 6(3):223–35. doi: 10.1016/j.trecan.2020.01.009

95. Arnold CR, Mangesius J, Skvortsova II, Ganswindt U. The role of cancer stem cells in radiation resistance. *Front Oncol* (2020) 10:164. doi: 10.3389/fonc.2020.00164

96. Malik B, Nie D. Cancer stem cells and resistance to chemo and radio therapy. *Front Biosci (Elite Ed).* (2012) 4:2142–9. doi: 10.2741/e531

97. Howard CM, Valluri J, Alberico A, Julien T, Mazagri R, Marsh R, et al. Analysis of chemopredictive assay for targeting cancer stem cells in glioblastoma patients. *Transl Oncol* (2017) 10(2):241–54. doi: 10.1016/j.tranon.2017.01.008

98. Pavlidis ET, Pavlidis TE. Role of bevacizumab in colorectal cancer growth and its adverse effects: a review. *World J Gastroenterol* (2013) 19(31):5051–60. doi: 10.3748/wjg.v19.i31.5051

99. Chinot OL, de la Motte Rouge T, Moore N, Zeaiter A, Das A, Phillips H, et al. AVAglio: Phase 3 trial of bevacizumab plus temozolomide and radiotherapy in newly diagnosed glioblastoma multiforme. *Adv Ther* (2011) 28(4):334–40. doi: 10.1007/s12325-011-0007-3

100. Chinot OL, Wick W, Mason W, Henriksson R, Saran F, Nishikawa R, et al. Bevacizumab plus radiotherapy-temozolomide for newly diagnosed glioblastoma. *N Engl J Med* (2014) 370(8):709–22. doi: 10.1056/NEJMoa1308345

101. Diaz RJ, Ali S, Qadir MG, de la Fuente MI, Ivan ME, Komotar RJ. The role of bevacizumab in the treatment of glioblastoma. *J Neurooncol.* (2017) 133(3):455–67. doi: 10.1007/s11060-017-2477-x

102. Ameratunga M, Pavlakis N, Wheeler H, Grant R, Simes J, Khasraw M. Anti-angiogenic therapy for high-grade glioma. *Cochrane Database Syst Rev* (2018) 11: CD008218. doi: 10.1002/14651858.CD008218.pub4

103. Wang WL, Aru N, Liu Z, Shen X, Ding YM, Wu SJ, et al. Prognosis of patients with newly diagnosed glioblastoma treated with molecularly targeted drugs combined with radiotherapy vs temozolomide monotherapy: A meta-analysis. *Med (Baltimore).* (2019) 98(45):e17759. doi: 10.1097/MD.0000000000017759

104. Zhang H, Dai Z, Wu W, Wang Z, Zhang N, Zhang L, et al. Regulatory mechanisms of immune checkpoints PD-L1 and CTLA-4 in cancer. *J Exp Clin Cancer Res* (2021) 40(1):184. doi: 10.1158/1557-3265.ADI21-IA-18

105. Persico P, Lorenzi E, Dipasquale A, Pessina F, Navarria P, Politi LS, et al. Checkpoint inhibitors as high-grade gliomas treatment: State of the art and future perspectives. *J Clin Med* (2021) 10(7):1367. doi: 10.3390/jcm10071367

106. Kast RE, Boockvar JA, Brüning A, Cappello F, Chang WW, Cvek B, et al. A conceptually new treatment approach for relapsed glioblastoma: coordinated undermining of survival paths with nine repurposed drugs (CUSP9) by the international initiative for accelerated improvement of glioblastoma care. *Oncotarget* (2013) 4(4):502–30. doi: 10.18632/oncotarget.969

107. Ruhlmann CH, Herrstedt J. Safety evaluation of aprepitant for the prevention of chemotherapy-induced nausea and vomiting. *Expert Opin Drug Saf.* (2011) 10(3):449–62. doi: 10.1517/14740338.2011.563235

108. Chrisp P. Aprepitant: the evidence for its place in the prevention of chemotherapy-induced nausea and vomiting. *Core Evid.* (2007) 2(1):15–30. doi: 10.2147/CE.S7420

109. Efferth T, Briehl MM, Tome ME. Role of antioxidant genes for the activity of artesunate against tumor cells. *Int J Oncol* (2003) 23(4):1231–5. doi: 10.3892/ijo.23.4.1231

110. Reichert S, Reinboldt V, Hehlgans S, Efferth T, Rödel C, Rödel F. A radiosensitizing effect of artesunate in glioblastoma cells is associated with a diminished expression of the inhibitor of apoptosis protein survivin. *Radiother Oncol* (2012) 103(3):394–401. doi: 10.1016/j.radonc.2012.03.018

111. McRae AL, Brady KT. Review of sertraline and its clinical applications in psychiatric disorders. *Expert Opin Pharmacother.* (2001) 2(5):883–92. doi: 10.1517/14656566.2.5.883

112. Caudill JS, Brown PD, Cerhan JH, Rummans TA. Selective serotonin reuptake inhibitors, glioblastoma multiforme, and impact on toxicities and overall survival: the mayo clinic experience. *Am J Clin Oncol* (2011) 34(4):385–7. doi: 10.1097/COC.0b013e3181e8461a

113. Tzadok S, Beery E, Israeli M, Uziel O, Lahav M, Fenig E, et al. *In vitro* novel combinations of psychotropics and anti-cancer modalities in U87 human glioblastoma cells. *Int J Oncol* (2010) 37(4):1043–51. doi: 10.3892/ijo_00000756

114. Nakagawa T, Kubota T, Kabuto M, Kodera T. Captopril inhibits glioma cell invasion in vitro: involvement of matrix metalloproteinases. *Anticancer Res* (1995) 15 (5b):1985–9.

115. Tolman EL, Fuller BL. Inhibition of thromboxane synthesis in guinea pig lung and human platelets by clotrimazole and other imidazole antifungals. *Biochem Pharmacol* (1983) 32(22):3488–90. doi: 10.1016/0006-2952(83)90383-0

116. Arrieta O, Pineda-Olvera B, Guevara-Salazar P, Hernandez-Pedro N, Morales-Espinosa D, Ceron-Lizarraga TL, et al. Expression of AT1 and AT2 angiotensin receptors in astrocytomas is associated with poor prognosis. *Br J Cancer.* (2008) 99(1):160–6. doi: 10.1038/sj.bjc.6604431

117. Arrieta O, Guevara P, Escobar E, García-Navarrete R, Pineda B, Sotelo J. Blockage of angiotensin II type I receptor decreases the synthesis of growth factors and induces

apoptosis in C6 cultured cells and C6 rat glioma. *Br J Cancer*. (2005) 92(7):1247–52. doi: 10.1038/sj.bjc.6602483

118. Becker K, Gromer S, Schirmer RH, Müller S. Thioredoxin reductase as a pathophysiological factor and drug target. *Eur J Biochem* (2000) 267(20):6118–25. doi: 10.1046/j.1432-1327.2000.01703.x

119. Pore N, Gupta AK, Cerniglia GJ, Jiang Z, Bernhard EJ, Evans SM, et al. Nelfinavir down-regulates hypoxia-inducible factor 1alpha and VEGF expression and increases tumor oxygenation: implications for radiotherapy. *Cancer Res* (2006) 66(18):9252–9. doi: 10.1158/0008-5472.CAN-06-1239

120. Kast RE, Halatsch ME. Matrix metalloproteinase-2 and -9 in glioblastoma: a trio of old drugs-captopril, disulfiram and nelfinavir-are inhibitors with potential as adjunctive treatments in glioblastoma. *Arch Med Res* (2012) 43(3):243–7. doi: 10.1016/j.arcmed.2012.04.005

121. Khaliq Y, Gallicano K, Venance S, Kravcik S, Cameron DW. Effect of ketoconazole on ritonavir and saquinavir concentrations in plasma and cerebrospinal fluid from patients infected with human immunodeficiency virus. *Clin Pharmacol Ther* (2000) 68(6):637–46. doi: 10.1067/mcp.2000.112363

122. Shim JS, Rao R, Beebe K, Neckers L, Han I, Nahta R, et al. Selective inhibition of HER2-positive breast cancer cells by the HIV protease inhibitor nelfinavir. *J Natl Cancer Inst* (2012) 104(20):1576–90. doi: 10.1093/jnci/djs396

123. Liu P, Brown S, Goktug T, Channathodiyil P, Kannappan V, Hugnot JP, et al. Cytotoxic effect of disulfiram/copper on human glioblastoma cell lines and ALDH-positive cancer-stem-like cells. *Br J Cancer*. (2012) 107(9):1488–97. doi: 10.1038/bjc.2012.442

124. Liu P, Brown S, Channathodiyil P, Kannappan V, Armesilla AL, Darling JL, et al. Reply: Cytotoxic effect of disulfiram/copper on human glioblastoma cell lines and ALDH-positive cancer-stem-like cells. *Br J Cancer*. (2013) 108(4):994–4. doi: 10.1038/bjc.2013.19

125. Yip NC, Fombon IS, Liu P, Brown S, Kannappan V, Armesilla AL, et al. Disulfiram modulated ROS-MAPK and NFκB pathways and targeted breast cancer cells with cancer stem cell-like properties. *Br J Cancer*. (2011) 104(10):1564–74. doi: 10.1038/bjc.2011.126

126. Loo TW, Bartlett MC, Clarke DM. Disulfiram metabolites permanently inactivate the human multidrug resistance p-glycoprotein. *Mol Pharm* (2004) 1(6):426–33. doi: 10.1021/mp049917l

127. Niture SK, Velu CS, Smith QR, Bhat GJ, Srivenugopal KS. Increased expression of the MGMT repair protein mediated by cysteine prodrugs and chemopreventative natural products in human lymphocytes and tumor cell lines. *Carcinogenesis* (2007) 28(2):378–89. doi: 10.1093/carcin/bgl155

128. Lehmann K, Rickenbacher A, Jang JH, Oberkofler CE, Vonlanthen R, von Boehmer L, et al. New insight into hyperthermic intraperitoneal chemotherapy: induction of oxidative stress dramatically enhanced tumor killing in *in vitro* and *in vivo* models. *Ann Surg* (2012) 256(5):730–737; discussion 737-738. doi: 10.1097/SLA.0b013e3182737517

129. Morrison BW, Doudican NA, Patel KR, Orlow SJ. Disulfiram induces copper-dependent stimulation of reactive oxygen species and activation of the extrinsic apoptotic pathway in melanoma. *Melanoma Res* (2010) 20(1):11–20. doi: 10.1097/CMR.0b013e328334131d

130. Nardone PA, Slotman GJ, Vezeridis MP. Ketoconazole: a thromboxane synthetase and 5-lipoxygenase inhibitor with antimetastatic activity in B16-F10 melanoma. *J Surg Res* (1988) 44(4):425–9. doi: 10.1016/0022-4804(88)90185-0

131. Kast RE, Karpel-Massler G, Halatsch ME. CUSP9* treatment protocol for recurrent glioblastoma: aprepitant, artesunate, auranofin, captopril, celecoxib, disulfiram, itraconazole, ritonavir, sertraline augmenting continuous low dose temozolomide. *Oncotarget* (2014) 5(18):8052–82. doi: 10.18632/oncotarget.2408

132. Skaga E, Skaga I, Grieg Z, Sandberg CJ, Langmoen IA, Vik-Mo EO. The efficacy of a coordinated pharmacological blockade in glioblastoma stem cells with nine repurposed drugs using the CUSP9 strategy. *J Cancer Res Clin Oncol* (2019) 145(6):1495–507. doi: 10.1007/s00432-019-02920-4

133. Kast RE, Ramiro S, Llado S, Toro S, Covenas R, Munoz M. Antitumor action of temozolomide, ritonavir and aprepitant against human glioma cells. *J Neurooncol*. (2016) 126(3):425–31. doi: 10.1007/s11060-015-1996-6

134. Skaga E, Kulesskiy E, Brynjulvsen M, Sandberg CJ, Potdar S, Langmoen IA, et al. Feasibility study of using high-throughput drug sensitivity testing to target recurrent glioblastoma stem cells for individualized treatment. *Clin Transl Med* (2019) 8(1):33. doi: 10.1186/s40169-019-0253-6

135. Lucki NC, Villa GR, Vergani N, Bollong MJ, Beyer BA, Lee JW, et al. A cell type-selective apoptosis-inducing small molecule for the treatment of brain cancer. *Proc Natl Acad Sci United States America*. (2019) 116:6435–40. doi: 10.1073/pnas.1816626116

136. Wilson KM, Mathews-Griner LA, Williamson T, Guha R, Chen L, Shinn P, et al. Mutation profiles in glioblastoma 3D oncospheres modulate drug efficacy. *SLAS Technol* (2019) 24:28–40. doi: 10.1177/2472630318803749

137. Quereda V, Hou S, Madoux F, Scampavia L, Spicer TP, Duckett D. A cytotoxic three-Dimensional-Spheroid, high-throughput assay using patient-derived glioma stem cells. *SLAS discovery: advancing Life Sci R D*. (2018) 23(8):842–9. doi: 10.1177/2472555218775055

138. Yu KK, Taylor JT, Pathmanaban ON, Youshani AS, Beyit D, Dutko-Gwozdz J, et al. High content screening of patient-derived cell lines highlights the potential of non-standard chemotherapeutic agents for the treatment of glioblastoma. *PloS One* (2018) 13(3):e0193694. doi: 10.1371/journal.pone.0193694

139. Lee DW, Lee SY, Doh I, Ryu GH, Nam DH. High-dose compound heat map for 3D-cultured glioblastoma multiforme cells in a micropillar and microwell chip platform. *BioMed Res Int* (2017) 2017:7218707. doi: 10.1155/2017/7218707

140. Lun X, Wells JC, Grinshtein N, King JC, Hao X, Dang NH, et al. Disulfiram when combined with copper enhances the therapeutic effects of temozolomide for the treatment of glioblastoma. *Clin Cancer Res* (2016) 22:3860–75. doi: 10.1158/1078-0432.CCR-15-1798

141. Denicolaï E, Baeza-Kallee N, Tchoghandjian A, Carré M, Colin C, Jiglaire CJ, et al. Proscillaridin a is cytotoxic for glioblastoma cell lines and controls tumor xenograft growth *in vivo*. *Oncotarget* (2014) 5:10934–48. doi: 10.18632/oncotarget.2541

142. Hothi P, Martins TJ, Chen LP, Deleyrolle L, Yoon JG, Reynolds B, et al. High-throughput chemical screens identify disulfiram as an inhibitor of human glioblastoma stem cells. *Oncotarget* (2012) 3:1124–36. doi: 10.18632/oncotarget.707

143. Wang L, Zhao H, Cui K, Yao L, Ren M, Hao A, et al. Identification of novel small-molecule inhibitors of glioblastoma cell growth and invasion by high-throughput screening. *BioScience Trends*. (2012) 6:192–200. doi: 10.5582/bst.2012.v6.4.192

144. Visnyei K, Onodera H, Damoiseaux R, Saigusa K, Petrosyan S, De Vries D, et al. A molecular screening approach to identify and characterize inhibitors of glioblastoma stem cells. *Mol Cancer Ther* (2011) 10:1818–28. doi: 10.1158/1535-7163.MCT-11-0268

145. Horvath P, Aulner N, Bickle M, Davies AM, Nery ED, Ebner D, et al. Screening out irrelevant cell-based models of disease. *Nat Rev Drug discovery*. (2016) 15(11):751–69. doi: 10.1038/nrd.2016.175

146. Janes J, Young ME, Chen E, Rogers NH, Burgstaller-Muehlbacher S, Hughes LD, et al. The ReFRAME library as a comprehensive drug repurposing library and its application to the treatment of cryptosporidiosis. *Proc Natl Acad Sci* (2018) 115(42):10750. doi: 10.1073/pnas.1810137115

147. Allison M. NCATS launches drug repurposing program. *Nat Biotechnol* (2012) 30(7):571–2. doi: 10.1038/nbt0712-571a

148. Corsello SM, Bittker JA, Liu Z, Gould J, McCarren P, Hirschman JE, et al. The drug repurposing hub: a next-generation drug library and information resource. *Nat Med* (2017) 23(4):405–8. doi: 10.1038/nm.4306

149. Skuta C, Popr M, Muller T, Jindrich J, Kahle M, Sedlak D, et al. Probes & drugs portal: an interactive, open data resource for chemical biology. *Nat Methods* (2017) 14(8):759–60. doi: 10.1038/nmeth.4365

150. Tang J, Tanoli Z.-U.-R., Ravikumar B, Alam Z, Rebane A, Vähä-Koskela M, et al. Drug target commons: A community effort to build a consensus knowledge base for drug-target interactions. *Cell Chem Biol* (2018) 25(2):224–229.e222. doi: 10.1016/j.chembiol.2017.11.009

151. Athanasiadis P, Ravikumar B, Carragher NO, Clemons PA, Johanssen T, Ebner D, et al. Optimized chemogenomic library design strategies for precision oncology. *bioRxiv* (2020). doi: 10.1101/2020.11.30.403329

152. . *Merck_KGaA. LOPAC®1280 – the library of pharmacologically active compounds. web site - LOPAC®1280 – the library of pharmacologically active compounds.*

153. Science USDoHaHS-N-NCfAT. *Repurposing drugs* (2020). Available at: https://ncats.nih.gov/preclinical/repurpose (Accessed Feb 10, 2021).

154. Zhang Z, Zhou L, Xie N, Nice EC, Zhang T, Cui Y, et al. Overcoming cancer therapeutic bottleneck by drug repurposing. *Signal Transduction Targeted Ther* (2020) 5(1):113. doi: 10.1038/s41392-020-00213-8

155. Teng J, Hejazi S, Hiddingh L, Carvalho L, de Gooijer MC, Wakimoto H, et al. Recycling drug screen repurposes hydroxyurea as a sensitizer of glioblastomas to temozolomide targeting *de novo* DNA synthesis, irrespective of molecular subtype. *Neuro Oncol* (2018) 20(5):642–54. doi: 10.1093/neuonc/nox198

156. Sleire L, Førde HE, Netland IA, Leiss L, Skeie BS, Enger PØ. Drug repurposing in cancer. *Pharmacol Res* (2017) 124:74–91. doi: 10.1016/j.phrs.2017.07.013

157. Patel A, Seraia E, Ebner D, Ryan AJ. Adefovir dipivoxil induces DNA replication stress and augments ATR inhibitor-related cytotoxicity. *Int J Cancer*. (2020) 147(5):1474–84. doi: 10.1002/ijc.32966

158. Buti L, Ruiz-Puig C, Sangberg D, Leissing TM, Brewer RC, Owen RP, et al. CagA–ASPP2 complex mediates loss of cell polarity and favors <em<H. pylori</em< colonization of human gastric organoids. *Proc Natl Acad Sci* (2020) 117(5):2645. doi: 10.1073/pnas.1908787117

159. Montenegro RC, Clark PGK, Howarth A, Wan X, Ceroni A, Siejka P, et al. BET inhibition as a new strategy for the treatment of gastric cancer. *Oncotarget* (2016) 7(28):43997–4012. doi: 10.18632/oncotarget.9766

160. Hart T, Chandrashekhar M, Aregger M, Steinhart Z, Brown KR, MacLeod G, et al. High-resolution CRISPR screens reveal fitness genes and genotype-specific cancer liabilities. *Cell* (2015) 163(6):1515–26. doi: 10.1016/j.cell.2015.11.015

161. Munoz DM, Cassiani PJ, Li L, Billy E, Korn JM, Jones MD, et al. CRISPR screens provide a comprehensive assessment of cancer vulnerabilities but generate false-positive hits for highly amplified genomic regions. *Cancer Discovery* (2016) 6(8):900–13. doi: 10.1158/2159-8290.CD-16-0178

162. Toledo CM, Ding Y, Hoellerbauer P, Davis RJ, Basom R, Girard EJ, et al. Genome-wide CRISPR-Cas9 screens reveal loss of redundancy between PKMYT1 and WEE1 in glioblastoma stem-like cells. *Cell Rep* (2015) 13(11):2425–39. doi: 10.1016/j.celrep.2015.11.021

163. MacLeod G, Bozek DA, Rajakulendran N, Monteiro V, Ahmadi M, Steinhart Z, et al. Genome-wide CRISPR-Cas9 screens expose genetic vulnerabilities and mechanisms of temozolomide sensitivity in glioblastoma stem cells. *Cell Rep* (2019) 27(3):971–986.e979. doi: 10.1016/j.celrep.2019.03.047

164. Huang K, Liu X, Li Y, Wang Q, Zhou J, Wang Y, et al. Genome-wide CRISPR-Cas9 screening identifies NF-kappaB/E2F6 responsible for EGFRvIII-associated

temozolomide resistance in glioblastoma. *Adv Sci (Weinh).* (2019) 6(17):1900782. doi: 10.1002/advs.201900782

165. Prolo LM, Li A, Owen SF, Parker JJ, Foshay K, Nitta RT, et al. Targeted genomic CRISPR-Cas9 screen identifies MAP4K4 as essential for glioblastoma invasion. *Sci Rep* (2019) 9(1):14020. doi: 10.1038/s41598-019-50160-w

166. Liu SJ, Malatesta M, Lien BV, Saha P, Thombare SS, Hong SJ, et al. CRISPRi-based radiation modifier screen identifies long non-coding RNA therapeutic targets in glioma. *Genome Biol* (2020) 21(1):83. doi: 10.1186/s13059-020-01995-4

167. Galli R, Binda E, Orfanelli U, Cipelletti B, Gritti A, De Vitis S, et al. Isolation and characterization of tumorigenic, stem-like neural precursors from human glioblastoma. *Cancer Res* (2004) 64(19):7011–21. doi: 10.1158/0008-5472.CAN-04-1364

168. Yuan X, Curtin J, Xiong Y, Liu G, Waschsmann-Hogiu S, Farkas DL, et al. Isolation of cancer stem cells from adult glioblastoma multiforme. *Oncogene* (2004) 23 (58):9392–400. doi: 10.1038/sj.onc.1208311

169. Pollard SM, Yoshikawa K, Clarke ID, Danovi D, Stricker S, Russell R, et al. Glioma stem cell lines expanded in adherent culture have tumor-specific phenotypes and are suitable for chemical and genetic screens. *Cell Stem Cell* (2009) 4(6):568–80. doi: 10.1016/j.stem.2009.03.014

170. Dao Trong P, Jungwirth G, Yu T, Pusch S, Unterberg A, Herold-Mende C, et al. Large-Scale drug screening in patient-derived IDHmut glioma stem cells identifies several efficient drugs among FDA-approved antineoplastic agents. *Cells* (2020) 9(6):1389. doi: 10.3390/cells9061389

171. Gao T, Li J-Z, Lu Y, Zhang C-Y, Li Q, Mao J, et al. The mechanism between epithelial mesenchymal transition in breast cancer and hypoxia microenvironment. *Biomedicine Pharmacotherapy.* (2016) 80:393–405. doi: 10.1016/j.biopha.2016.02.044

172. Teicher BA. Hypoxia and drug resistance. *Cancer Metastasis Rev* (1994) 13 (2):139–68. doi: 10.1007/BF00689633

173. Heddleston JM, Li Z, McLendon RE, Hjelmeland AB, Rich JN. The hypoxic microenvironment maintains glioblastoma stem cells and promotes reprogramming towards a cancer stem cell phenotype. *Cell Cycle* (2009) 8(20):3274–84. doi: 10.4161/cc.8.20.9701

174. Wilson WR, Hay MP. Targeting hypoxia in cancer therapy. *Nat Rev Cancer.* (2011) 11(6):393–410. doi: 10.1038/nrc3064

175. Ortiz-Prado E, Dunn JF, Vasconez J, Castillo D. Viscor g. partial pressure of oxygen in the human body: a general review. *Am J Blood Res* (2019) 9(1):1–14.

176. Collingridge DR, Piepmeier JM, Rockwell S, Knisely JP. Polarographic measurements of oxygen tension in human glioma and surrounding peritumoural brain tissue. *Radiotherapy oncology: J Eur Soc Ther Radiol Oncol* (1999) 53(2):127–31. doi: 10.1016/S0167-8140(99)00121-8

177. Gray LH, Conger AD, Ebert M, Hornsey S, Scott OCA. The concentration of oxygen dissolved in tissues at the time of irradiation as a factor in radiotherapy. *Br J Radiology.* (1953) 26(312):638–48. doi: 10.1259/0007-1285-26-312-638

178. Musah-Eroje A, Watson S. A novel 3D *in vitro* model of glioblastoma reveals resistance to temozolomide which was potentiated by hypoxia. *J neuro-oncology.* (2019) 142(2):231–40. doi: 10.1007/s11060-019-03107-0

179. Abbott NJ, Rönnbäck L, Hansson E. Astrocyte–endothelial interactions at the blood–brain barrier. *Nat Rev Neurosci* (2006) 7(1):41–53. doi: 10.1038/nrn1824

180. DeCordova S, Shastri A, Tsolaki AG, Yasmin H, Klein L, Singh SK, et al. Molecular heterogeneity and immunosuppressive microenvironment in glioblastoma. *Front Immunol* (2020) 11:1402. doi: 10.3389/fimmu.2020.01402

181. Yang N, Yan T, Zhu H, Liang X, Leiss L, Sakariassen P, et al. A co-culture model with brain tumor-specific bioluminescence demonstrates astrocyte-induced drug resistance in glioblastoma. *J Trans Med* (2014) 12:278. doi: 10.1186/s12967-014-0278-y

182. Mega A, Hartmark Nilsen M, Leiss LW, Tobin NP, Miletic H, Sleire L, et al. Astrocytes enhance glioblastoma growth. *Glia* (2020) 68(2):316–27. doi: 10.1002/glia.23718

183. Civita P, Leite D M, Pilkington GJ. Pre-clinical drug testing in 2D and 3D human *In vitro* models of glioblastoma incorporating non-neoplastic astrocytes: Tunneling nano tubules and mitochondrial transfer modulates cell behavior and therapeutic respons. *Int J Mol Sci* (2019) 20(23):6017. doi: 10.3390/ijms20236017

184. Chen W, Wang D, Du X, He Y, Chen S, Shao Q, et al. Glioma cells escaped from cytotoxicity of temozolomide and vincristine by communicating with human astrocytes. *Med Oncol* (2015) 32(3):43. doi: 10.1007/s12032-015-0487-0

185. Leite DM, Zvar Baskovic B, Civita P, Neto C, Gumbleton M, Pilkington GJ. A human co-culture cell model incorporating microglia supports glioblastoma growth and migration, and confers resistance to cytotoxics. *FASEB J* (2020) 34(1):1710–27. doi: 10.1096/fj.201901858RR

186. Manini I, Caponnetto F, Bartolini A, Ius T, Mariuzzi L, Di Loreto C, et al. Role of microenvironment in glioma invasion: What we learned from in vitro models. *Int J Mol Sci* (2018) 19(1):147–78. doi: 10.3390/ijms19010147

187. Skaga E, Kulesskiy E, Fayzullin A, Sandberg CJ, Potdar S, Kyttälä A, et al. Intertumoral heterogeneity in patient-specific drug sensitivities in treatment-naïve glioblastoma. *BMC cancer.* (2019) 19:1–14. doi: 10.1186/s12885-019-5861-4

188. Stommel JM, Kimmelman AC, Ying H, Nabioullin R, Ponugoti AH, Wiedemeyer R, et al. Coactivation of receptor tyrosine kinases affects the response of tumor cells to targeted therapies. *Science* (2007) 318(5848):287–90. doi: 10.1126/science.1142946

189. Ianevski A, Timonen S, Kononov A, Aittokallio T, Giri AK. SynToxProfiler: An interactive analysis of drug combination synergy, toxicity and efficacy. *PloS Comput Biol* (2020) 16(2):e1007604. doi: 10.1371/journal.pcbi.1007604

190. Ianevski A, Lahtela J, Javarappa KK, Sergeev P, Ghimire BR, Gautam P, et al. Patient-tailored design for selective co-inhibition of leukemic cell subpopulations. *Sci advances.* (2021) 7(8):eabe4038. doi: 10.1126/sciadv.abe4038

191. Ianevski A, Giri AK, Gautam P, Kononov A, Potdar S, Saarela J, et al. Prediction of drug combination effects with a minimal set of experiments. *Nat Mach intelligence.* (2019) 1(12):568–77. doi: 10.1038/s42256-019-0122-4

192. Sicklick JK, Kato S, Okamura R, Schwaederle M, Hahn ME, Williams CB, et al. Molecular profiling of cancer patients enables personalized combination therapy: the I-PREDICT study. *Nat Med* (2019) 25(5):744–50. doi: 10.1038/s41591-019-0407-5

193. Menden MP, Wang D, Mason MJ, Szalai B, Bulusu KC, Guan Y, et al. Community assessment to advance computational prediction of cancer drug combinations in a pharmacogenomic screen. *Nat Commun* (2019) 10(1):2674. doi: 10.1038/s41467-019-09799-2

194. Julkunen H, Cichonska A, Gautam P, Szedmak S, Douat J, Pahikkala T, et al. Leveraging multi-way interactions for systematic prediction of pre-clinical drug combination effects. *Nat Commun* (2020) 11(1):6136. doi: 10.1038/s41467-020-19950-z

195. Ianevski A, Giri AK, Aittokallio T. SynergyFinder 2.0: visual analytics of multi-drug combination synergies. *Nucleic Acids Res* (2020) 48(W1):W488–w493. doi: 10.1093/nar/gkaa216

196. Smith-Cohn MA, Celiku O, Gilbert MR. Molecularly targeted clinical trials. *Neurosurg Clinics North America.* (2021) 32(2):191–210. doi: 10.1016/j.nec.2020.12.002

197. Gao X, Xia X, Li F, Zhang M, Zhou H, Wu X, et al. Circular RNA-encoded oncogenic e-cadherin variant promotes glioblastoma tumorigenicity through activation of EGFR-STAT3 signalling. *Nat Cell Biol* (2021) 23(3):278–91. doi: 10.1038/s41556-021-00639-4

198. Allen M, Bjerke M, Edlund H, Nelander S, Westermark B. Origin of the U87MG glioma cell line: Good news and bad news. *Sci Transl Med* (2016) 8(354):354re353. doi: 10.1126/scitranslmed.aaf6853

199. Seidel S, Garvalov BK, Acker T. Isolation and culture of primary glioblastoma cells from human tumor specimens. *Methods Mol Biol* (2015) 1235:263–75. doi: 10.1007/978-1-4939-1785-3_19

200. Bischof J, Westhoff MA, Wagner JE, Halatsch ME, Trentmann S, Knippschild U, et al. Cancer stem cells: The potential role of autophagy, proteolysis, and cathepsins in glioblastoma stem cells. *Tumour biology: J Int Soc Oncodevelopmental Biol Med* (2017) 39 (3):1010428317692227. doi: 10.1177/1010428317692227

201. Chi JT, Wang Z, Nuyten DS, Rodriguez EH, Schaner ME, Salim A, et al. Gene expression programs in response to hypoxia: cell type specificity and prognostic significance in human cancers. *PloS Med* (2006) 3(3):e47. doi: 10.1371/journal.pmed.0030047

202. Klimkiewicz K, Weglarczyk K, Collet G, Paprocka M, Guichard A, Sarna M, et al. A 3D model of tumour angiogenic microenvironment to monitor hypoxia effects on cell interactions and cancer stem cell selection. *Cancer letters.* (2017) 396:10–20. doi: 10.1016/j.canlet.2017.03.006

203. Nobre AR, Entenberg D, Wang Y, Condeelis J, Aguirre-Ghiso JA. The different routes to metastasis *via* hypoxia-regulated programs. *Trends Cell Biol* (2018) 28(11):941–56. doi: 10.1016/j.tcb.2018.06.008

204. Rockwell S, Dobrucki IT, Kim EY, Marrison ST, Vu VT. Hypoxia and radiation therapy: past history, ongoing research, and future promise. *Curr Mol Med* (2009) 9 (4):442–58. doi: 10.2174/156652409788167087

205. Gritsenko P, Leenders W, Friedl P. Recapitulating *in vivo*-like plasticity of glioma cell invasion along blood vessels and in astrocyte-rich stroma. *Histochem Cell Biol* (2017) 148(4):395–406. doi: 10.1007/s00418-017-1604-2

206. Rape A, Ananthanarayanan B, Kumar S. Engineering strategies to mimic the glioblastoma microenvironment. *Advanced Drug delivery Rev* (2014) 79-80:172–83. doi: 10.1016/j.addr.2014.08.012

207. Oraiopoulou ME, Tzamali E, Tzedakis G, Liapis E, Zacharakis G, Vakis A, et al. Integrating *in vitro* experiments with in silico approaches for glioblastoma invasion: the role of cell-to-cell adhesion heterogeneity. *Sci Rep* (2018) 8(1):16200. doi: 10.1038/s41598-018-34521-5

208. Ravi VM, Joseph K, Wurm J, Behringer S, Garrelfs N, d'Errico P, et al. Human organotypic brain slice culture: a novel framework for environmental research in neuro-oncology. *Life Sci Alliance.* (2019) 2(4):e201900305. doi: 10.26508/lsa.201900305

209. Eisemann T, Costa B, Strelau J, Mittelbronn M, Angel P, Peterziel H. An advanced glioma cell invasion assay based on organotypic brain slice cultures. *BMC cancer.* (2018) 18(1):103. doi: 10.1186/s12885-018-4007-4

210. Sidorcenco V, Krahnen L, Schulz M, Remy J, Kögel D, Temme A, et al. Glioblastoma tissue slice tandem-cultures for quantitative evaluation of inhibitory effects on invasion and growth. *Cancers* (2020) 12(9):2707–21. doi: 10.3390/cancers12092707

211. Birch JL, Strathdee K, Gilmour L, Vallatos A, McDonald L, Kouzeli A, et al. A novel small-molecule inhibitor of MRCK prevents radiation-driven invasion in glioblastoma. *Cancer Res* (2018) 78(22):6509–22. doi: 10.1158/0008-5472.CAN-18-1697

212. Marques-Torrejon MA, Gangoso E, Pollard SM. Modelling glioblastoma tumour-host cell interactions using adult brain organotypic slice co-culture. *Dis Models mechanisms.* (2018) 11(2):dmm031435. doi: 10.1242/dmm.031435

213. Merz F, Gaunitz F, Dehghani F, Renner C, Meixensberger J, Gutenberg A, et al. Organotypic slice cultures of human glioblastoma reveal different susceptibilities to treatments. *Neuro-oncology* (2013) 15(6):670–81. doi: 10.1093/neuonc/not003

214. Haehnel S, Reiche K, Loeffler D, Horn A, Blumert C, Puppel S-H, et al. Deep sequencing and automated histochemistry of human tissue slice cultures improve their usability as preclinical model for cancer research. *Sci Rep* (2019) 9(1):19961. doi: 10.1038/s41598-019-56509-5

215. Aittokallio T. What are the current challenges for machine learning in drug discovery and repurposing? *Expert Opin Drug Discovery* (2022) 17(5):423–5. doi: 10.1080/17460441.2022.2050694

216. Goecks J, Jalili V, Heiser LM, Gray JW. How machine learning will transform biomedicine. *Cell* (2020) 181(1):92–101. doi: 10.1016/j.cell.2020.03.022

frontiers | Frontiers in Oncology

TYPE Original Research
PUBLISHED 18 January 2023
DOI 10.3389/fonc.2022.1100350

OPEN ACCESS

EDITED BY
Andrea Ciarmiello,
Sant'Andrea University Hospital, Italy

REVIEWED BY
Min-Ying Lydia Su,
University of California,
Irvine, United States
Tommaso Sciortino,
Galeazzi Orthopedic Institute (IRCCS),
Italy

*CORRESPONDENCE
Liangping Luo
tluolp@jnu.edu.cn

†These authors have contributed equally to this work

SPECIALTY SECTION
This article was submitted to Cancer Imaging and Image-directed Interventions, a section of the journal Frontiers in Oncology

RECEIVED 16 November 2022
ACCEPTED 27 December 2022
PUBLISHED 18 January 2023

CITATION
Jiang J, Yu J, Liu X, Deng K, Zhuang K, Lin F and Luo L (2023) The efficacy of preoperative MRI features in the diagnosis of meningioma WHO grade and brain invasion.
Front. Oncol. 12:1100350.
doi: 10.3389/fonc.2022.1100350

The efficacy of preoperative MRI features in the diagnosis of meningioma WHO grade and brain invasion

Jun Jiang[1†], Juan Yu[1†], Xiajing Liu[1], Kan Deng[2], Kaichao Zhuang[1], Fan Lin[1] and Liangping Luo[3*]

[1]Department of Radiology, Health Science Center, Shenzhen Second People's Hospital, The First Affiliated Hospital of Shenzhen University, Shenzhen, China, [2]Philips Healthcare, China International Center, Guangzhou, China, [3]Medical Imaging Center, The First Affiliated Hospital of Jinan University, Guangzhou, China

Objective: The preoperative MRI scans of meningiomas were analyzed based on the 2021 World Health Organization (WHO) Central Nervous System (CNS) Guidelines, and the efficacy of MRI features in diagnosing WHO grades and brain invasion was analyzed.

Materials and methods: The data of 675 patients with meningioma who underwent MRI in our hospital from 2006 to 2022, including 108 with brain invasion, were retrospectively analyzed. Referring to the WHO Guidelines for the Classification of Central Nervous System Tumors (Fifth Edition 2021), 17 features were analyzed, with age, sex and meningioma MRI features as risk factors for evaluating WHO grade and brain invasion. The risk factors were identified through multivariable logistic regression analysis, and their receiver operating characteristic (ROC) curves for predicting WHO grades and brain invasion were generated, and the area under the curve (AUC), sensitivity and specificity were calculated.

Results: Univariate analysis showed that sex, tumor size, lobulated sign, peritumoral edema, vascular flow void, bone invasion, tumor-brain interface, finger-like protrusion and mushroom sign were significant for diagnosing meningioma WHO grades, while these features and ADC value were significant for predicting brain invasion ($P < 0.05$). Multivariable logistic regression analysis showed that the lobulated sign, tumor-brain interface, finger-like protrusion, mushroom sign and bone invasion were independent risk factors for diagnosing meningioma WHO grades, while the above features, tumor size and ADC value were independent risk factors for diagnosing brain invasion ($P < 0.05$). The tumor-brain interface had the highest efficacy in evaluating WHO grade and brain invasion, with AUCs of 0.779 and 0.860, respectively. Combined, the variables had AUCs of 0.834 and 0.935 for determining WHO grade and brain invasion, respectively.

Conclusion: Preoperative MRI has excellent performance in diagnosing meningioma WHO grade and brain invasion, while the tumor-brain interface serves as a key factor. The preoperative MRI characteristics of meningioma can help predict WHO grade and brain invasion, thus facilitating complete lesion resection and improving patient prognosis.

KEYWORDS

brain invasion, WHO grade, meningioma, MRI, diagnosis

Introduction

Meningioma is one of the most common brain tumors, representing 37.6% of primary intracranial tumors (1). Although the 2021 WHO Guidelines for the Classification of Tumors (5th Edition) propose a greater reliance on genetic testing for grading, morphological classification remains divided into 15 pathological subtypes and grades 1, 2 and 3 (2). The tumors are diverse in biological characteristics in terms of different pathological subtypes and grades, and the tumor recurrence rate is closely related to the WHO grade and completeness of surgical resection. WHO grade 1 meningiomas have a very low recurrence rate after total resection, but there is a higher tendency for recurrence as the WHO meningioma grade increases. The five-year recurrence rates after total resection for meningiomas have been reported to be 7%~23% for WHO grade 1, 50%~55% for WHO grade 2, and 72%~78% for WHO grade 3; subtotally resected tumors usually have poor prognosis (3). The 2016 4th edition of the WHO CNS guidelines included brain invasion as a diagnostic criterion for WHO grade 2 meningiomas and modified WHO grade 1 meningiomas with brain invasion to atypical meningiomas, increasing the incidence rate of WHO grade 2 meningiomas by 1% to 10% (4). With regard to the analysis of data collected from 2016 and 2022, WHO grade 2 meningiomas accounted for 1/5 to 1/3 of all meningiomas (5). Notably, in comparison with meningiomas without brain invasion, meningiomas with brain invasion exhibit aggressive behaviors, an increased recurrence rate (6), three times more bleeding intraoperatively, and an increased risk of postoperative seizures as well as postoperative bleeding (7).

However, there is a gross underestimation of meningioma brain invasion (7). Due to incomplete surgical resection and incomplete sampling, the incidence of brain invasion is underestimated, and the postoperative recurrence rate is high (8). Because of a lack of attention and emphasis on preoperative imaging assessments, the specific imaging signs of brain invasion are still unclear (9), with very few previous imaging studies including brain invasion as an independent factor (10–15).

Therefore, based on the 2021 edition of the Central Nervous System (CNS) WHO guidelines, this paper discusses the diagnostic value of clinical and MRI-specific features for WHO grade and brain invasion in meningioma to provide adequate information for preoperative preparations, improve the resection efficacy for the tumor and invaded brain tissue, and reduce recurrence and mortality rates while improving patient prognosis.

Materials and methods

Subjects

The research proposal has been reviewed and approved by the ethics committee of our hospital, with the approval number 20190910. All data from meningiomas resected in our hospital from 2006 to 2022 were analyzed retrospectively. The inclusion criteria were as follows: (1) preoperative MRI examination performed; and (2) meningioma confirmed through routine pathology and immunohistochemistry of surgically resected lesion tissue. The exclusion criteria were as follows: (1) pathological findings that diagnosed brain invasion in meningioma but did not describe the specimen as containing brain tissue; (2) preoperative treatment; and (3) previous surgical resection for the same tumor. A total of 675 meningioma cases were included in the study.

Magnetic resonance imaging

A 3.0T (Siemens MAGNETOM Prisma) or 1.5T (Siemens MAGNETOM Avanto) MRI scanner was used, with 20- or 8-channel head coils. The sequences and scanning parameters were as follows: T1-weighted imaging (T1WI) (3T: repetition time (TR) 500 ms, echo time (TE) 7.4 ms, field of view (FOV) 320 mm×240 mm, slice thickness (ST) 6 mm; 1.5 T: TR 388 ms, TE 13 ms, FOV 199 mm×220 mm, ST 6 mm); T2-weighted imaging (T2WI) (3T: TR 5000 ms, TE 117 ms, FOV 220

mm×220 mm, ST 6 mm; 1.5 T: TR 4000 ms, TE 95 ms, FOV 220 mm×220 mm, ST 6 mm); fluid-attenuated inversion recovery (FLAIR) (3T: TR 9000 ms, TE 81 ms, FOV 220 mm×220 mm, ST 6 mm; 1.5 T: TR 8650 ms, TE 96 ms, FOV 220 mm×220 mm, ST 6 mm); diffusion-weighted imaging (DWI) (3T: TR 2900 ms, TE 98 ms, FOV 230 mm×230 mm, ST 6 mm; 1.5 T: TR 2900 ms, TE 97 ms, FOV 220 mm×220 mm, ST 6 mm); and T1-weighted postcontrast (T1C) (contrast agent: gadolinium borate; 3T: TR 600 ms, TE 7.6 ms, FOV 320 mm×240 mm, ST 1.5 mm; 1.5 T: TR 350 ms, TE 9.6 ms, FOV 199 mm×220 mm, ST 1.5 mm).

Radiological data

An associate senior neuroimaging specialist (11 years of experience) and a senior specialist (16 years of experience) evaluated the images on the PACS workstation without knowing the pathological results, and any differences were resolved through discussion. The MRI scans were evaluated for meningioma features (T1WI signal intensity (SI), T2WI SI, degree and homogeneity of T1C, tumor size, lobulated sign, peritumoral edema, ADC value, vascular flow-void sign, dural tail sign, venous sinus invasion, bone invasion, tumor-brain interface, finger-like protrusions, and mushroom sign) (Figure 1).

The MRI signal was scored according to the Elster criteria (16): T1WI SI: 1 point: the signal is significantly lower than that of the cerebral gray matter and is close to that of the cerebrospinal fluid; 2 points: the signal is slightly below the cerebral gray matter signal; 3 points: the signal is close to the gray matter signal; 4 points: the signal is lightly higher than the gray matter signal; and 5 points: the signal is significantly higher than the gray matter signal and close to the fat signal. T2WI SI: 1 point: the signal is significantly lower than that of the gray matter and close to that of the bone cortex; 2 points: the signal is slightly lower than the gray matter signal; 3 points: the signal is close to the gray matter signal; 4 points: the signal is slightly higher than the gray matter signal; and 5 points: the signal is significantly higher than the gray matter signal and close to the cerebrospinal fluid signal. T1C enhancement degree: 1 point: significantly enhanced, enhanced SI close to that of fat; 2 points: moderately enhanced, enhanced SI slightly lower than that of fat; 3 points: mildly enhanced, enhanced SI lower than that of fat but higher than the gray matter signal.

The tumor size(volume) was measured by the software on PACS. The lobulated sign refers to an uneven, curved depression

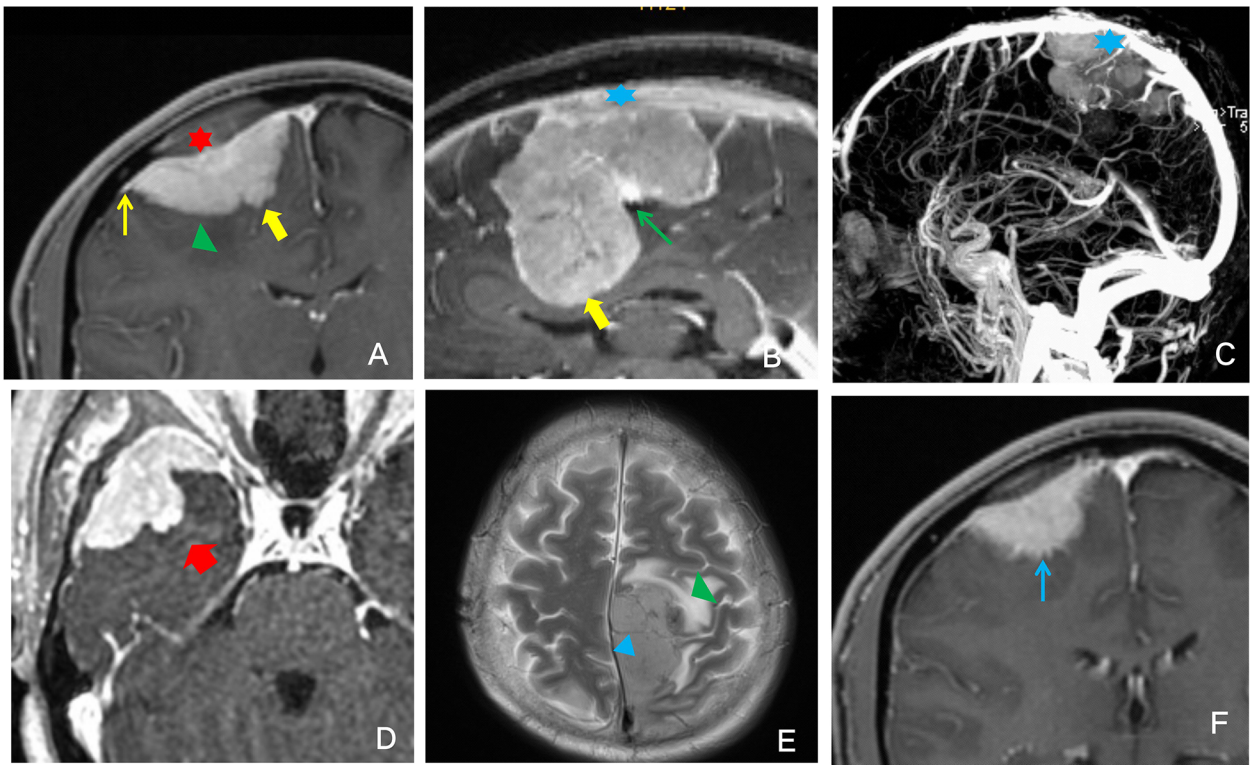

FIGURE 1
Illustrative example of the description of the analyzed imaging features. **(A)** Red star: bone invasion; green triangle: peritumoral edema; thin yellow arrow: dural tail sign; thick yellow arrow: finger-like protrusion. **(B)** Blue star: venous sinus invasion; thin green arrow: lobulated sign; thick yellow arrow: finger-like protrusion. **(C)** Blue star: venous sinus invasion. **(D)** The thick red arrow points to the enhanced signal as the mushroom sign. **(E)** Green triangle: peritumoral edema; blue triangle: vascular flow void. **(F)** Thin blue arrow: unclear tumor-brain surface.

or convex change in the tumor surface margin. The vascular flow void sign referred to tumor vessels in which MRI could not collect blood flow signal, showing a low signal in the shape of a cord on T1WI and T2WI sequences. The dural tail sign manifested as tumor-adjacent meningeal enhancement, thickening, and distal thinning. Venous sinus invasion was evaluated on T2WI and T1C and observed as tumor adhesion to the venous sinus, invasion of the venous sinus, or complete occlusion of the venous sinus. Bone invasion could be clearly seen on T1C as an enhanced signal at the site of invasion. The tumor-brain interface refers to the tumor boundary. When tumor progression did not reach a certain degree, the tumor was separated from the brain tissue by the cerebrospinal fluid-vascular gap and arachnoid interface, and a low signal ring was present on T1C. When the low signal ring disappeared, the tumor-brain interface was considered unclear. Finger-like protrusions could be clearly shown on T1C, and the tumor border could be clearly observed with tumor tissue protruding in a finger-like pattern into the adjacent brain parenchyma. The mushroom sign was observed on T1C as an enhancing band of spherical tumor invading peripherally along the dural attachment; this sign is more distant, thicker and longer than the commonly seen dural tail sign, and the proximal cerebral surface is often more irregular and uneven.

Histopathological data

All pathological findings were reinterpreted by two neuropathologists referring to the 2021 CNS WHO guidelines, and the morphological diagnosis was made using the "933" grading model (2, 4, 5), i.e., 9 WHO grade 1, 3 WHO grade 2 and 3 WHO grade 3, to determine the pathological grade of meningiomas and to diagnose cases of brain invasion (Table 1). Based on the latest 2021 5th guidelines, brain invasion otherwise benign meningiomas (BIOB) were classified as WHO grade 2 in this study. The diagnostic criteria for brain invasion were as follows (15) (1): HE-stained slides of the tumor-brain interface revealed irregular, tongue-like invasion into the brain parenchyma without soft meningeal involvement; (2) glial cell proliferation and neuronal degradation in the invaded brain tissue; and (3) positive immunohistochemical staining for GFAP

TABLE 1 Histopathological classification of meningioma [N(%)].

Histopathological classification	N(%)	Brain invasion	
		yes	no
WHO grade 1/BIOB	**610(90.4)**	**67(11.0)**	**543(89.0)**
Meningothelial meningioma	147(24.1)	23(34.3)	124(22.8)
Fibrous meningioma	127(20.8)	9(13.4)	118(21.7)
Transitional meningioma	249(41.8)	26(38.8)	223(41.0)
Psammomatous meningioma	41(6.7)	4(5.9)	37(6.8)
Angiomatous meningioma	29(4.8)	2(2.9)	27(4.9)
Microcystic meningioma	11(1.8)	2(1.4)	9(1.6)
Secretory meningioma	4(0.6)	1(1.4)	3(0.5)
Metaplastic meningioma	1(0.1)	0(0.0)	1(0.1)
Lymphoplasmacyte-rich meningioma	1(0.1)	0(0.0)	1(0.1)
WHO grade 2	**56(8.3)**	**32(57.2)**	**24(42.8)**
Atypical meningioma	49(87.5)	30(93.1)	19(79.1)
Chordoid meningioma	4(7.1)	1(3.1)	3(12.5)
Clear cell meningioma	3(5.3)	1(3.1)	2(8.3)
WHO grade 3	**9(1.3)**	**9(100.0)**	**0(0.0)**
Anaplastic meningioma	7(77.8)	7(77.8)	0(0.0)
Rhabdoid meningioma	1(11.1)	1(11.1)	0(0.0)
Papillary meningioma	1(11.1)	1(11.1)	0(0.0)
Total	**675**	**108(16.0)**	**567(84.0)**

WHO, World health organization; BIOB, Brain invasion otherwise benign meningiomas.

in paraffin sections; brain invasion from the tumor was considered if any of the above criteria were met. In this study, the pathology report description of each case was required to include brain tissue; otherwise, the case was excluded from the study.

Statistical analysis

SPSS software (v.26.0, IBM, USA) was used for statistical analysis, and Medcalc software (v.20.0.22, Solvusoft, USA) was used to generate the receiver operating characteristic (ROC) curves. Descriptive statistics were applied for age, sex, and meningioma MRI features using the results of the evaluation performed by the senior specialist, with continuous variables expressed as the mean ± standard deviation and categorical variables expressed as frequency distributions. All the characteristic parameters were analyzed in univariate logistic regression as factors for meningioma WHO grade and brain invasion, and the meaningful parameters were selected for multivariate logistic regression analysis. ROC curves of the selected parameters for the diagnosis of WHO grade and brain invasion were generated, and AUC, sensitivity and specificity were calculated. P value < 0.05 was considered statistically significant.

Results

Among the 675 meningiomas cases, 543 (80.4%) were WHO grade 1, 123 (18.2%) were WHO grade 2, and 9 (1.3%) were WHO grade 3; 567 (84.0%) cases were meningiomas without brain invasion, and 108 (16.0%) were meningiomas with brain invasion. A consistency test was carried out on the data evaluated by the two neuroradiology experts, and the correlation coefficient ranged from 0.848 to 0.997, indicating good consistency between the two experts.

Association of WHO grades with findings on radiological imaging

The clinical data and MRI features were compared between WHO grade 1 and WHO grade 2/3 lesions. Univariate logistic regression showed that age (P=0.258), T1WI (P=0.615), T2WI (P=0.617), degree of T1C (P=0.754), T1C enhancement homogeneity (P=0.869), ADC value (P=0.780), dural tail sign (P=0.384), and venous sinus invasion (P=0.062) were not associated with WHO grade. However, the male/female ratio was 56/76 for WHO grade 2/3 and 154/409 for WHO grade 1 (P=0.002). The mean size of WHO grade 2/3 tumors was larger than that of WHO grade 1 tumors (P=0.000). In addition, the lobulated sign, peritumoral edema, vascular flow void, bone invasion, unclear tumor-brain interface, finger-like protrusion, and mushroom sign were more common in WHO grade 2/3 tumors than in WHO grade 1 tumors (P<0.05; Table 2).

Multivariate logistic regression analysis revealed that the lobulated sign (OR 0.528; 95% CI 0.307~0.909; P=0.021), tumor-brain interface (OR 7.946; 95% CI 4.427~14.262; P=0.000), finger-like protrusion (OR 4.845; 95% CI 2.076~11.310; P=0.000), mushroom sign (OR 9.346; 95% CI 2.014~43.376; P=0.004), and bone invasion (OR 2.311; 95% CI 1.315~4.061; P=0.004) were independent risk factors for the diagnosis of meningioma WHO grade.

ROC curves were generated for the five independent risk factors for WHO grade: lobulated sign, tumor-brain interface, finger-like protrusion, mushroom sign, and bone invasion (Figure 2). The results showed that the tumor-brain interface had the highest diagnostic accuracy for WHO grade (AUC 0.779; 95% CI 0.746~0.810; sensitivity 0.742; specificity 0.816). Finally, a ROC curve was created for the fitted variable for WHO grade obtained by multivariate logistic regression (AUC 0.834; 95% CI 0.832-0.885; sensitivity 0.727; specificity 0.858), reflecting a strong diagnostic efficacy.

Association of brain invasion with findings on radiological imaging

Table 3 summarizes the associations among of age, sex, 15 imaging features and brain invasion. Univariate logistic regression analysis showed that age (P=0.331), T1WI (P=0.656), T2WI (P=0.933), degree of T1C (P=0.687), enhancement homogeneity (P=0.682), dural tail sign (P=0.773), and venous sinus invasion (P=0.077) were not associated with brain invasion. However, the male/female ratio was higher among meningiomas with brain invasion (48/60) than among meningiomas without brain invasion (162/405) (P=0.001). The meningiomas with brain invasion had a significantly larger mean size than the noninvasive meningiomas (P=0.000). The mean ADC values were lower for meningiomas with brain invasion than for meningiomas without brain invasion (P=0.008). In addition, the lobulated sign, peritumoral edema, vascular flow void, bone invasion, unclear tumor-brain interface, finger-like protrusion, and mushroom sign were more common in meningiomas with brain invasion than in meningiomas without brain invasion (P < 0.05; Table 3).

Multivariate logistic regression analysis revealed that tumor size (OR 1.270; 95% CI 1.020~1.582; P=0.033), ADC value (OR 0.998; 95% CI 0.996~1.000; P=0.043), lobulated sign (OR 0.309; 95% CI 0.150~0.633; P=0.001), tumor-brain interface (OR 36.307; 95% CI 15.438~85.390; P=0.000), finger-like protrusion (OR 6.011; 95% CI 2.448~14.760; P=0.000), mushroom sign (OR 12.392; 95% CI 2.451~62.644; P=0.002), and bone invasion (OR 3.272; 95% CI 1.664~6.436; P=0.001) were independent risk factors for brain invasion in meningioma.

10.3389/fonc.2022.1100350

TABLE 2 Univariate analysis of features associated with WHO grades [N(%)].

Features		WHO 1	WHO 2/3	Exp(B)	P-value
N		543	132		
Age (years)		51.1 ± 12.7	49.6 ± 15.0	0.992	0.258
Sex	Male	154 (28.3)	56 (42.4)	0.537	0.002
	Female	389 (71.6)	76 (57.6)		
T1WI	1	11 (2.0)	4 (3.0)	0.911	0.615
	2	110 (20.2)	30 (22.7)		
	3	413 (76.0)	93 (70.4)		
	4	8 (1.4)	5 (3.7)		
	5	1 (0.1)	0 (0.0)		
T2WI	1	11 (2.0)	3 (2.2)	1.139	0.617
	2	40 (7.3)	10 (7.5)		
	3	302 (55.6)	68 (51.5)		
	4	169 (31.1)	45 (34.0)		
	5	21 (3.8)	6 (4.5)		
T1C	1	397 (73.1)	96 (72.7)	1.058	0.754
	2	128 (23.5)	30 (22.7)		
	3	18 (3.4)	6 (4.5)		
Enhancement homogeneity	heterog-eneous	362 (66.7)	87 (66.0)	0.967	0.869
	homog-eneous	181 (33.3)	45 (34.0)		
Tumor size (cm^3)		26.0 ± 2.1	47.1 ± 2.6	1.822	0.000
Lobulated sign	yes	230 (42.4)	71 (53.8)	1.584	0.018
	no	313 (57.6)	61 (46.2)		
Peritumoral edema	yes	196 (36.1)	84 (63.7)	3.098	0.000
	no	347 (63.9)	48 (36.3)		
ADC value ($/\times10^{-5}$ $mm^2 \cdot s^{-1}$)		908.4 ± 165.8	877.7 ± 208.7	1.000	0.780
Vascular flow void	yes	95 (17.5)	39 (29.6)	1.978	0.002
	no	448 (82.5)	93 (70.4)		
Dural tail sign	yes	470 (86.5)	118 (89.3)	1.309	0.384
	no	73 (13.5)	14 (10.7)		
Venous sinus invasion	yes	191 (35.2)	58 (43.9)	1.444	0.062
	no	352 (64.8)	74 (56.1)		
Bone invasion	yes	63 (11.6)	50 (37.8)	4.646	0.000
	no	480 (88.4)	82 (62.2)		
Tumor-brain surface	clear	443 (81.5)	34 (25.8)	12.769	0.000
	unclear	100 (18.5)	98 (74.2)		
Finger-like protrusion	yes	10 (1.9)	38 (28.7)	21.547	0.000

(Continued)

TABLE 2 Continued

Features		WHO 1	WHO 2/3	Exp(B)	P-value
	no	533 (98.1)	94 (71.3)		
Mushroom sign	yes	2 (0.4)	25 (18.9)	63.201	0.000
	no	541 (99.6)	107 (81.1)		

WHO, World Health Organization; T1WI, T1-weighted imaging; T2WI, T2-weighted imaging; T1C, T1-weighted postcontrast.

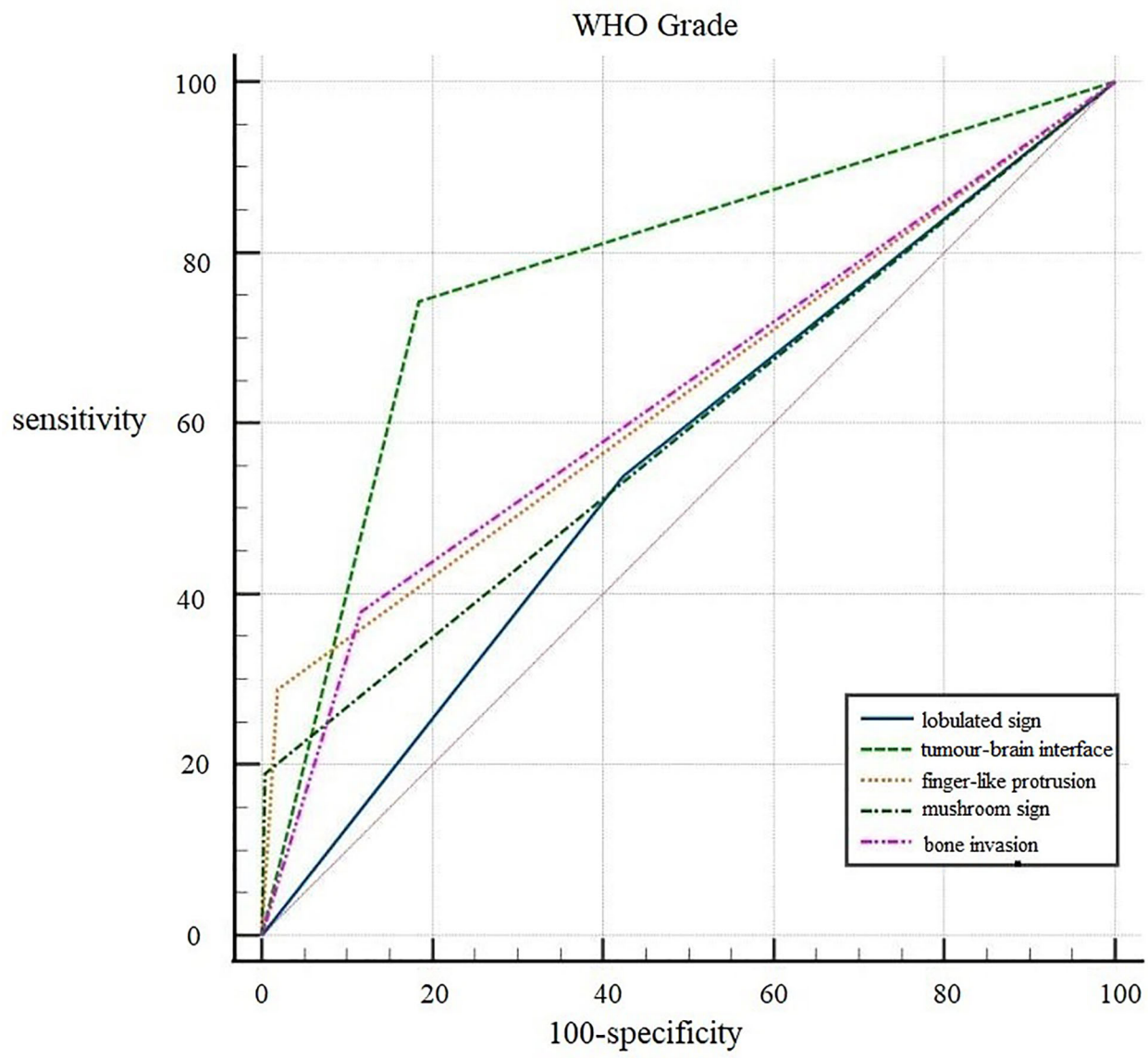

FIGURE 2
ROC curves of independent risk factors for WHO grade.

10.3389/fonc.2022.1100350

TABLE 3 Univariate analysis of features associated with brain invasion [N(%)].

Features		Brain invasion	Non-brain-invasion	Exp(B)	P-value
N		108 (16.0)	567 (84.0)		
Age (years)		49.9 ± 14.4	51.2 ± 13.0	0.992	0.331
Sex	male	48 (44.4)	162 (28.6)	0.500	0.001
	female	60 (55.6)	405 (71.4)		
T1WI	1	4 (3.7)	11 (1.9)	0.915	0.656
	2	22 (20.4)	118 (20.8)		
	3	79 (73.2)	427 (75.3)		
	4	4 (2.7)	10 (1.7)		
	5	0 (0.0)	1 (0.1)		
T2WI	1	3 (2.7)	11 (1.9)	1.012	0.933
	2	7 (6.4)	43 (7.5)		
	3	59 (54.6)	311 (54.8)		
	4	34 (31.4)	180 (31.7)		
	5	5 (4.6)	22 (3.8)		
T1C	1	78 (72.2)	415 (73.1)	1.081	0.687
	2	25 (23.1)	133 (23.4)		
	3	5 (4.6)	19 (3.3)		
Enhancement homogeneity	heterog-eneous	70 (64.8)	379 (66.9)	0.914	0.682
	homog-eneous	38 (35.1)	188 (33.1)		
Tumor size (cm^3)		54.3 ± 2.5	25.6 ± 2.1	1.980	0.000
Lobulated sign	yes	62 (57.4)	239 (42.1)	1.850	0.004
	no	46 (42.6)	328 (57.8)		
Peritumoral edema	yes	73 (67.5)	207 (36.6)	3.627	0.000
	no	35 (32.4)	360 (63.4)		
ADC value ($/\times10^{-5}$ mm^2 $-s^{-1}$)		862.9 ± 165.8	910.2 ± 176.3	0.998	0.001
Vascular flow void	yes	35 (32.5)	99 (17.4)	2.267	0.000
	no	73 (67.5)	468 (82.6)		
Dural tail sign	yes	95 (87.9)	493 (86.9)	1.097	0.773
	no	13 (12.1)	74 (13.1)		
Venous sinus invasion	yes	48 (44.4)	201 (35.4)	1.457	0.077
	no	60 (55.6)	366 (64.6)		
Bone invasion	yes	49 (45.3)	64 (11.2)	6.527	0.000
	no	59 (54.6)	503 (88.8)		
Tumor-brain surface	clear	11 (10.1)	466 (82.2)	40.686	0.000
	unclear	97 (89.9)	101 (17.8)		
Finger-like protrusion	yes	38 (35.1)	10 (1.7)	30.237	0.000

(Continued)

TABLE 3 Continued

Features		Brain invasion	Non-brain-invasion	Exp(B)	P-value
	no	70 (64.9)	557 (98.3)		
Mushroom sign	yes	25 (23.1)	2 (0.3)	80.090	0.000
	no	83 (76.9)	565 (99.7)		

T1WI, T1-weighted imaging; T2WI, T2-weighted imaging; T1C, T1-weighted postcontrast.

ROC curves of the seven independent risk factors for diagnosing brain invasion, including tumor size, ADC value, lobulated sign, tumor-brain interface, finger-like protrusion, mushroom sign and bone invasion, were generated (Figure 3). The results showed that the tumor-brain interface had the highest diagnostic accuracy for brain invasion in meningioma (AUC 0.860; 95% CI 0.832~0.885; sensitivity 0.898; specificity 0.822). Finally, the ROC curve of the fitted variable obtained by multivariate logistic regression for diagnosing brain invasion in meningioma was created (AUC 0.935; 95% CI 0.910~0.959; sensitivity 0.935; specificity 0.817), indicating good diagnostic efficiency (Figure 3).

Discussion

MRI is one of the most reliable imaging methods recommended by the WHO Guidelines for the Classification of CNS Tumors (Fifth Edition 2021) for meningioma diagnosis, follow-up, and recurrence detection. MRI has high soft tissue resolution, and the sensitivity and specificity of MRI can reach 75.0% and 93.5%, respectively, for evaluating tissue conditions in and around the tumor (5). Previous literature reports have mostly focused on MRI-based predictions of meningioma WHO classification, and there have been very few independent studies regarding brain invasion in meningioma (10–15). This lack of attention to the potential assessment value of preoperative imaging for brain invasion in meningiomas tends to result in incomplete clinical surgical resection and specimen retrieval, leading to increased recurrence and mortality rates in patients after surgery, and the pathological diagnosis of brain invasion is severely underestimated as a result (9). Therefore, it is necessary to set up imaging criteria for brain invasion based on known pathological findings to distinguish whether the meningioma has invaded into the adjacent brain parenchyma. Previous brain invasion studies have included very limited MRI features and have not analyzed the diagnostic efficacy of each feature. In this study, the MRI features of meningiomas were

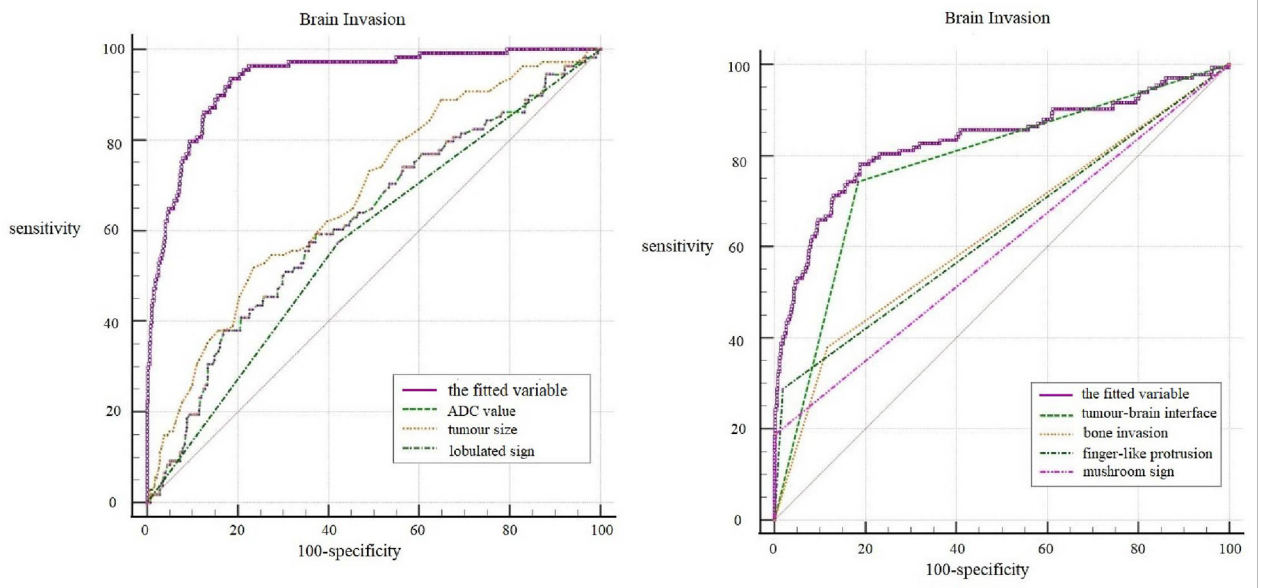

FIGURE 3
ROC curves of independent risk factors for brain invasion.

comprehensively analyzed, and WHO grade and brain invasion were analyzed as outcomes, aiming to identify features that could predict WHO grade and brain invasion.

In our study, the male/female ratio was higher in malignant meningiomas and brain invasion than in benign meningiomas and meningiomas without brain invasion, but the incidence in males was still lower than the incidence in females, which is different from a previous report that the incidence of brain invasion in meningiomas is higher in males than in females (17). Age and T1WI and T2WI SI were not directly correlated with WHO grade and brain invasion in meningiomas, consistent with previous reports (17, 18). Adeli et al. (14)concluded that the proportion of meningiomas with brain invasion showing heterogeneous enhancement was higher than that of tumors without brain invasion, without considering their WHO grades. However, this study showed that the degree and homogeneity of enhancement cannot be used to distinguish features between benign and malignant tumors or to predict brain invasion in meningioma; we suggest that the degree and homogeneity of enhancement is related to the blood supply of the of meningioma and its composition (19). This study found that the dural tail sign and venous sinus invasion were not related to WHO grade and brain invasion, but according to Maiuri et al. (20), venous sinus invasion may be related to the location of tumor growth.

According to a previous literature report, WHO grade 3 meningiomas are larger than grade 1 and grade 2 meningiomas, with a cutoff value of 5 cm (21). Univariate regression analysis in this study also showed that the higher the WHO grade was, the larger the tumor; meningiomas with brain invasion were larger than those without brain invasion. Multivariate regression analysis showed that tumor size was also an independent risk factor for brain invasion, but the diagnostic efficacy was not high (AUC: 0.677). In this study, vascular flow void and peritumoral edema were found to be associated with WHO grade and brain invasion, and both were more common in meningiomas with brain invasion than in meningiomas without brain invasion, but multivariate regression analysis showed that neither of these features were independent risk factors for WHO grade and brain invasion. In previous studies, some scholars believed that perineural edema was predictive of brain invasion (10, 14). They suggested that perineural edema is due to the erosion of brain parenchyma by tumor tissue following destruction of the tumor-brain interface and is therefore more pronounced in those with brain invasion than in those without. It is possible that edema was an effective factor but not an independent predictor in our study because we did not calculate edema volume, and the presence or absence of edema alone may not have predicted the meningioma WHO grade and brain invasion.

Reviewing previous literature, the lobulated sign is more common in meningiomas with higher WHO grades, with the proportion of lobulated signs in anaplastic meningiomas reaching up to 100% (21). The present study showed that the lobulated sign was an influential factor for WHO grade and brain invasion in meningioma and an independent risk factor for brain invasion, a finding consistent with Adeli's study (14). However, the efficacy of the lobulated sign in diagnosing both WHO grade and brain invasion was low (AUC: 0.557 and 0.576, respectively). Finger-like protrusion and the mushroom sign have also been reported by many scholars as characteristics of malignant meningioma, and the pathological basis of the mushroom sign is caused by tumor invasion of the adjacent dura mater, arachnoid membrane, subarachnoid space, pia mater and brain (22). We found that finger-like protrusion, the mushroom sign and bone invasion were all independent risk factors for predicting WHO grade and brain invasion in meningiomas. Although single factors had a low diagnostic efficacy, the specificity was good, so these factors could basically be considered characteristic imaging findings of brain invasion in malignant tumors.

In the histopathological diagnosis of brain invasion in meningioma, the hematoxylin and eosin (HE) staining specimens need to contain the tumor-brain interface, and the diagnosis can only be confirmed when the tumor cells are found to be irregular and tongue-like, invading into the brain parenchyma without pia matter involvement. Therefore, it is very important to obtain specimens during the operation. In recent years, researchers have paid attention to the visualization of the tumor-brain interface in imaging studies. Adeli et al. believed that the tumor-brain interface was not correlated with brain invasion (14), while Joo et al. believed that the tumor-brain interface was important for the diagnosis of brain invasion (10, 12, 13). This study concluded that the tumor-brain interface was the most meaningful MRI feature, an independent risk factor for WHO grade and brain invasion, with the best diagnostic efficacy among all single variables (Figure 4). The tumor-brain interface had an AUC of 0.779 (0.746-0.810), a sensitivity of 0.742 and a specificity of 0.816 for predicting WHO grade and an AUC of 0.860 (0.832-0.885), a sensitivity of 0.898 and a specificity of 0.822 for predicting brain invasion. MRI showed excellent diagnostic efficacy overall for WHO grade and brain invasion in meningioma (AUC: 0.834/0.935). In recent years, Kandemirli et al. (11) showed an AUC of 0.74 for the diagnosis of brain invasion, and Li et al. (13) concluded that the efficacy of MRI based on clinical semantics and radiomics models had an AUC of 0.895 for predicting brain invasion. The diagnostic efficiency of MRI in the above studies is lower than that in this study, which may be because most of their studies adopted artificial intelligence computer-aided diagnosis and did not include all MRI features in the study; additionally, the number of cases was small. Moreover, some studies only included WHO grade 2 tumors, resulting in a limited reference value.

Brain invasion of meningioma is closely related to recurrence and prognosis. Perry found that the recurrence and mortality rates of benign meningiomas with brain invasion are very similar to those of atypical meningiomas, and brain

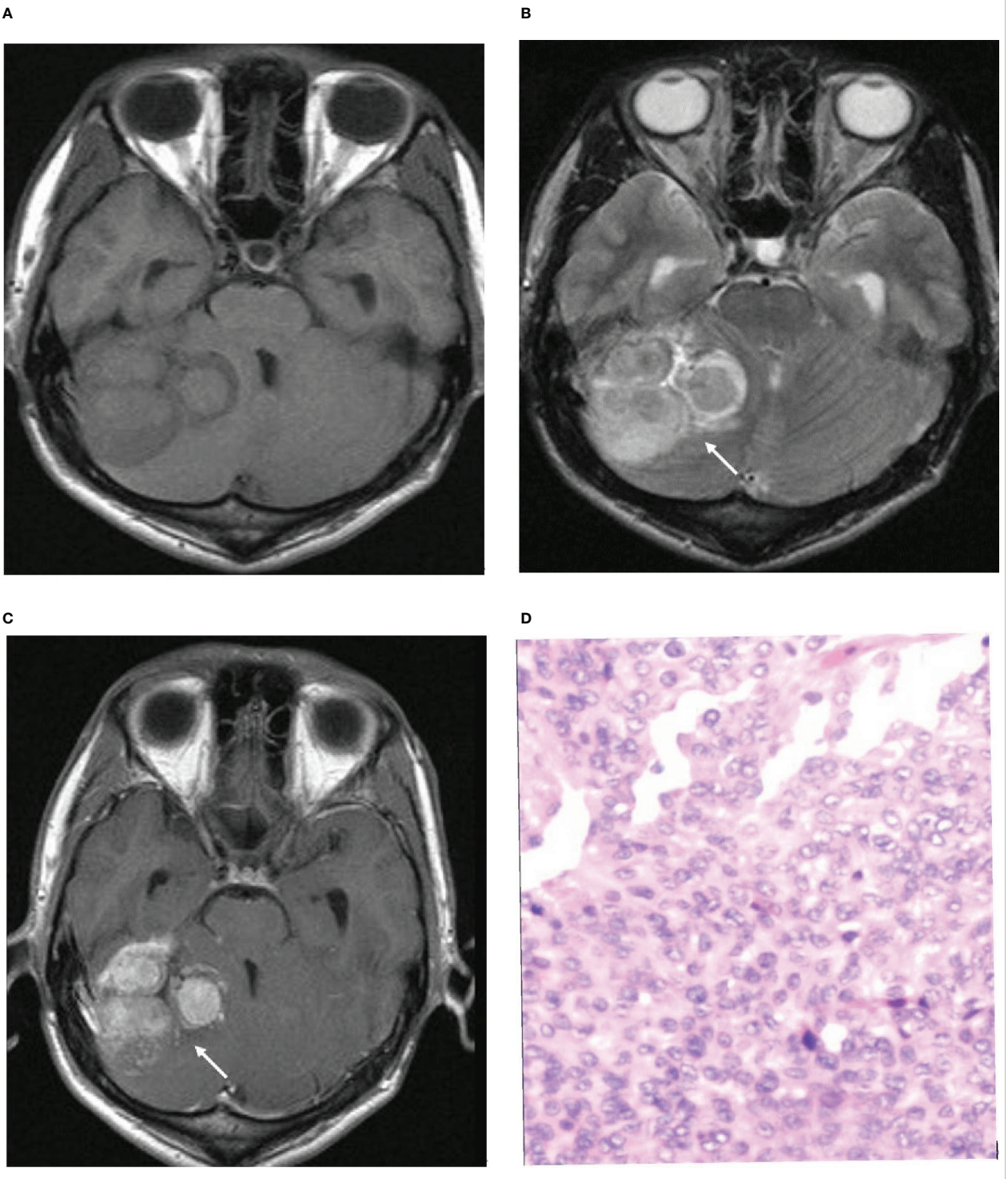

FIGURE 4
Illustrative example of the analyzed MRI variables. **(A)** Axial T1-weighted image. **(B)** Axial T2-weighted image. **(C)** Axial T1-weighted postcontrast image. **(D)** Pathological section. **(B, C)** Arrows show an unclear tumor-brain interface. **(D)**. Pathological examination confirmed brain invasion.

invasion affects the prognosis of benign meningiomas (23). The recurrence rate of brain invasion meningioma is closely related to the degree of tumor resection. The recurrence rate of total resection is lower than that of subtotal resection and incomplete surgical resection is a direct factor of the high recurrence rate (24, 25). However, surgery requires both complete resection of the lesion and the preservation of as much normal brain tissue surrounding the tumor as possible. Therefore, preoperative imaging assessment of brain invasion is particularly important. The results of this study show that the presence or absence of brain invasion of meningiomas can be predicted preoperatively by the "tumor-brain interface", thus allowing a fuller assessment of meningiomas with brain invasion, especially BIOB, for which complete resection is attempted during surgery, and helping to reduce their recurrence rate. In our medical center, we conducted multidisciplinary discussions on the preoperative cases suspected to be BIOB by MRI, made precise surgical plans, and removed the tumor tissue and the brain parenchyma as far as possible. After surgery, we determined whether the patients needed radiotherapy or not according to the results of intraoperative findings, pathology, immunohistochemistry and genetic testing.

In conclusion, several features of preoperative MRI are reliable in diagnosing meningioma WHO grade and predicting brain invasion, as an unclear tumor-brain interface on preoperative MRI indicates a higher WHO grade of meningiomas and a higher likelihood of brain invasion. In clinical practice, a preliminary estimate of WHO grade can be made based on the MRI features of meningiomas to predict the presence of brain invasion in advance, which helps facilitate the complete removal of lesions, guide specimen sampling, improve the accuracy of the pathological diagnosis of brain invasion, and improve patient prognosis.

Data availability statement

The original contributions presented in the study are included in the article/supplementary material. Further inquiries can be directed to the corresponding author.

Ethics statement

The studies involving human participants were reviewed and approved by Ethics Committee of Shenzhen Second People's Hospital. Written informed consent to participate in this study was provided by the participants' legal guardian/next of kin. Written informed consent was obtained from the individual(s), and minor(s)' legal guardian/next of kin, for the publication of any potentially identifiable images or data included in this article.

Author contributions

Conceptualization: JJ, JY, and LL. Data curation: JJ, JY, LL, KD, KZ, and FL. Formal analysis: JJ, JY, XL, and LL. Investigation: JJ, JY, XL, and LL. Methodology: JJ, JY, XL, and LL. Project administration: JJ, JY, and LL. Resources: JY and LL. Supervision: LL. Validation: all authors. Writing-original draft: JJ and JY. Writing-review & editing: LL. All authors contributed to the article and approved the submitted version.

Funding

This study was supported by Shenzhen Basic Research Project (Natural Science Foundation) (Grant No. 20220527092639003).

Conflict of interest

The authors declare that the research was conducted in the absence of any commercial or financial relationships that could be construed as a potential conflict of interest.

Publisher's note

References

1. Euskirchen P, Peyre M. Management of meningioma. *Presse medicale (Paris France 1983).* (2018) 47(11-12 Pt 2):e245–52. doi: 10.1016/j.lpm.2018.05.016

2. Louis DN, Perry A, Wesseling P, Brat DJ, Cree IA, Figarella-Branger D, et al. The 2021 WHO classification of tumors of the central nervous system: A summary. *Neuro-oncology* (2021) 23(8):1231–51. doi: 10.1093/neuonc/noab106

3. Huntoon K, Toland AMS, Dahiya S. Meningioma: A review of clinicopathological and molecular aspects. *Front Oncol* (2020) 10:579599. doi: 10.3389/fonc.2020.579599

4. Louis DN, Perry A, Reifenberger G, von Deimling A, Figarella-Branger D, Cavenee WK, et al. The 2016 world health organization classification of tumors of

the central nervous system: a summary. *Acta Neuropathol.* (2016) 131(6):803–20. doi: 10.1007/s00401-016-1545-1

5. Gritsch S, Batchelor TT, Gonzalez Castro LN. Diagnostic, therapeutic, and prognostic implications of the 2021 world health organization classification of tumors of the central nervous system. *Cancer* (2022) 128(1):47–58. doi: 10.1002/cncr.33918

6. Bulleid LS, James Z, Lammie A, Hayhurst C, Leach PA. The effect of the revised WHO classification on the incidence of grade II meningioma. *Br J neurosurgery.* (2020) 34(5):584–6. doi: 10.1080/02688697.2019.1639616

7. Hess K, Spille DC, Adeli A, Sporns PB, Brokinkel C, Grauer O, et al. Brain invasion and the risk of seizures in patients with meningioma. *J Neurosurg* (2018) 130(3):789–96. doi: 10.3171/2017.11.JNS172265

8. Nakasu S, Nakasu Y. Prognostic significance of brain invasion in meningiomas: systematic review and meta-analysis. *Brain Tumor Pathol* (2021) 38(2):81–95. doi: 10.1007/s10014-020-00390-y

9. Behling F, Fodi C, Gepfner-Tuma I, Machetanz K, Renovanz M, Skardelly M, et al. CNS invasion in meningioma-how the intraoperative assessment can improve the prognostic evaluation of tumor recurrence. *Cancers* (2020) 12(12):3620. doi: 10.3390/cancers12123620

10. Joo L, Park JE, Park SY, Nam SJ, Kim YH, Kim JH, et al. Extensive peritumoral edema and brain-to-tumor interface MRI features enable prediction of brain invasion in meningioma: development and validation. *Neuro-oncology* (2021) 23(2):324–33. doi: 10.1093/neuonc/noaa190

11. Kandemirli SG, Chopra S, Priya S, Ward C, Locke T, Soni N, et al. Presurgical detection of brain invasion status in meningiomas based on first-order histogram based texture analysis of contrast enhanced imaging. *Clin Neurol neurosurgery.* (2020) 198:106205. doi: 10.1016/j.clineuro.2020.106205

12. Xiao D, Zhao Z, Liu J, Wang X, Fu P, Le Grange JM, et al. Diagnosis of invasive meningioma based on brain-tumor interface radiomics features on brain MR images: A multicenter study. *Front Oncol* (2021) 11:708040. doi: 10.3389/fonc.2021.708040

13. Li N, Mo Y, Huang C, Han K, He M, Wang X, et al. A clinical semantic and radiomics nomogram for predicting brain invasion in WHO grade II meningioma based on tumor and tumor-to-Brain interface features. *Front Oncol* (2021) 11:752158. doi: 10.3389/fonc.2021.752158

14. Adeli A, Hess K, Mawrin C, Streckert EMS, Stummer W, Paulus W, et al. Prediction of brain invasion in patients with meningiomas using preoperative magnetic resonance imaging. *Oncotarget* (2018) 9(89):35974–82. doi: 10.18632/oncotarget.26313

15. Zhang J, Yao K, Liu P, Liu Z, Han T, Zhao Z, et al. A radiomics model for preoperative prediction of brain invasion in meningioma non-invasively based on MRI: A multicentre study. *EBioMedicine* (2020) 58:102933. doi: 10.1016/j.ebiom.2020.102933

16. Zhu Y, Man C, Gong L, Dong D, Yu X, Wang S, et al. A deep learning radiomics model for preoperative grading in meningioma. *Eur J Radiol* (2019) 116:128–34. doi: 10.1016/j.ejrad.2019.04.022

17. Yun S, Koh JM, Lee KS, Seo AN, Nam KH, Choe G. Expression of c-MET in invasive meningioma. *J Pathol Trans Med* (2015) 49(1):44–51. doi: 10.4132/jptm.2014.10.13

18. Butts AM, Weigand S, Brown PD, Petersen RC, Jack CRJr., Machulda MM, et al. Neurocognition in individuals with incidentally-identified meningioma. *J Neuro-Oncol* (2017) 134(1):125–32. doi: 10.1007/s11060-017-2495-8

19. Krivoshapkin AL, Sergeev GS, Kalneus LE, Gaytan AS, Murtazin VI, Kurbatov VP, et al. New software for preoperative diagnostics of meningeal tumor histologic types. *World Neurosurg* (2016) 90:123–32. doi: 10.1016/j.wneu.2016.02.084

20. Maiuri F, Donzelli R, Pagano S, Mariniello G. The management of the venous sinuses during surgery for posterior fossa meningiomas. *World neurosurgery.* (2019) 125:357–63. doi: 10.1016/j.wneu.2019.02.032

21. Lemée JM, Joswig H, Da Broi M, Corniola MV, Scheie D, Schaller K, et al. WHO grade I meningiomas: Classification-tree for prognostic factors of survival. *Neurosurgical review.* (2020) 43(2):749–58. doi: 10.1007/s10143-019-01117-0

22. Zwirner K, Paulsen F, Schittenhelm J, Gepfner-Tuma I, Tabatabai G, Behling F, et al. Integrative assessment of brain and bone invasion in meningioma patients. *Radiat Oncol (London England).* (2019) 14(1):132. doi: 10.1186/s13014-019-1341-x

23. Perry A, Stafford SL, Scheithauer BW, Suman VJ, Lohse CM. Meningioma grading: An analysis of histologic parameters. *Am J Surg Pathol* (1997) 21 (12):1455–65. doi: 10.1097/00000478-199712000-00008

24. Hwang WL, Marciscano AE, Niemierko A, Kim DW, Stemmer-Rachamimov AO, Curry WT, et al. Imaging and extent of surgical resection predict risk of meningioma recurrence better than WHO histopathological grade. *Neuro-oncology* (2016) 18(6):863–72. doi: 10.1093/neuonc/nov285

25. Slot KM, Verbaan D, Bosscher L, Sanchez E, Vandertop WP, Peerdeman SM. Agreement between extent of meningioma resection based on surgical Simpson grade and based on postoperative magnetic resonance imaging findings. *World Neurosurg* (2018) 111:e856–e62. doi: 10.1016/j.wneu.2017.12.178

frontiers | Frontiers in Oncology

TYPE Review
PUBLISHED 02 May 2023
DOI 10.3389/fonc.2023.1144184

OPEN ACCESS

EDITED BY
Briana Prager,
Massachusetts General Hospital,
Harvard Medical School,
United States

REVIEWED BY
Ye Wang,
Qingdao University, The Affiliated Qingdao Central Hospital of Qingdao University, China
Aram S. Modrek,
Grossman School of Medicine, New York University, United States

*CORRESPONDENCE
Albert H. Kim
alberthkim@wustl.edu

†These authors have contributed equally to this work and share first authorship

RECEIVED 13 January 2023
ACCEPTED 29 March 2023
PUBLISHED 02 May 2023

CITATION
McCornack C, Woodiwiss T, Hardi A, Yano H and Kim AH (2023) The function of histone methylation and acetylation regulators in GBM pathophysiology. *Front. Oncol.* 13:1144184. doi: 10.3389/fonc.2023.1144184

The function of histone methylation and acetylation regulators in GBM pathophysiology

Colin McCornack[1†], Timothy Woodiwiss[2,3†], Angela Hardi[4], Hiroko Yano[2,5] and Albert H. Kim[2,5*]

[1]Medical Scientist Training Program, Washington University School of Medicine, St. Louis, MO, United States, [2]Department of Neurological Surgery, Washington University School of Medicine, St. Louis, MO, United States, [3]Department of Neurosurgery, University of Iowa Carver College of Medicine, Iowa, IA, United States, [4]Bernard Becker Medical Library, Washington University School of Medicine, St. Louis, MO, United States, [5]The Brain Tumor Center, Siteman Cancer Center, Washington University School of Medicine, St. Louis, MO, United States

Glioblastoma (GBM) is the most common and lethal primary brain malignancy and is characterized by a high degree of intra and intertumor cellular heterogeneity, a starkly immunosuppressive tumor microenvironment, and nearly universal recurrence. The application of various genomic approaches has allowed us to understand the core molecular signatures, transcriptional states, and DNA methylation patterns that define GBM. Histone posttranslational modifications (PTMs) have been shown to influence oncogenesis in a variety of malignancies, including other forms of glioma, yet comparatively less effort has been placed on understanding the transcriptional impact and regulation of histone PTMs in the context of GBM. In this review we discuss work that investigates the role of histone acetylating and methylating enzymes in GBM pathogenesis, as well as the effects of targeted inhibition of these enzymes. We then synthesize broader genomic and epigenomic approaches to understand the influence of histone PTMs on chromatin architecture and transcription within GBM and finally, explore the limitations of current research in this field before proposing future directions for this area of research.

KEYWORDS

glioblastoma, histone postranslational modifications, histone post translational modifications, histone acetylation, histone methylation, glioblastoma epigenomics

1 Introduction

Glioblastoma (GBM) is the most common primary malignant brain tumor of the central nervous system with discouraging patient survival despite extensive research and clinical efforts to better understand and treat this malignancy. The median survival of 17-20 months in newly diagnosed GBM patients treated with standard of care has changed only modestly since the advent of the Stupp protocol published nearly two decades ago (1, 2). Although

numerous clinical trials have been undertaken to improve outcomes in this disease, the standard of care for newly diagnosed disease—a combination of maximally safe resection, radiation therapy, and chemotherapy—has remained relatively unchanged for many years (2–4). Challenges to clinical progress include an incomplete understanding of cancer biology, a heterogeneous genetic and cellular environment, an immunosuppressive tumor microenvironment, and a delicate and difficult to access host organ system (5, 6). Extensive efforts have led to better characterization of the genetic and transcriptomic alterations in this cancer, but our understanding of the epigenetic regulation of this disease remains incomplete. Posttranslational modifications of histones play an important role in influencing transcription. Histone post-translational modifications (PTMs) have proven important in other forms of glioma, such as diffuse midline glioma, which commonly contain mutations in H3-K27M leading to global reduction in H3K27 methylation and increased PRC2-mediated repression of neurodevelopmental genes, potentially leading to lineage restriction and a preponderance of oligodendrocytic precursor like cells (7, 8). Similarly, the presence of IDH mutations in lower grade astrocytoma impacts the function of DNA methyltransferases and histone methyltransferases, leading to alterations in levels of activating and repressive histone post-translational modifications, as reviewed elsewhere (9). Methylation of the O6-Methylguanine-DNA methyltransferase (MGMT) promoter, which is associated with improved chemotherapy response, is a widely recognized epigenetic determinant in GBM, yet beyond DNA methylation, there is now a greater appreciation for the complex role that histone post-translational modifying enzymes play in regulating GBM pathophysiology (10, 11). This diverse group of enzymes carry out their effects *via* the modification of histone and non-histone substrates to control the ability of GBM cells to proliferate, invade surrounding tissue, and modulate the host immune response (12–14).

Epigenetics refers to heritable phenotypic changes that are independent of changes to underlying DNA sequences. These changes typically involve alterations in chromatin, a complex of the double-stranded DNA and an octamer containing two copies of the histone proteins H2A, H2B, H3, and H4. There are numerous PTMs that can be applied to the N-terminal tails and the core globular domains of these histone proteins, including, among other modifications, acetylation, methylation, and phosphorylation. Histone tail PTMs have varying impacts on the histone protein–DNA interaction, creating regions of transcriptionally-accessible chromatin (euchromatin) and transcriptionally-inaccessible chromatin (heterochromatin), which ultimately regulate functions such as transcription, DNA repair, and recombination. Importantly, recent efforts have suggested the ability of heterochromatin domains to persist through cellular division, thus representing a heritable aspect of information independent of DNA sequence identity (15, 16). Individual histone PTMs are associated with different states of transcriptional activation and repression and play a significant role in the broader landscape of the transcriptional machinery of a cell. Given the importance of transcriptional regulation, there are a variety of enzymes involved in regulating the modification of histone tails, including histone acetyltransferases (HATs/KATs), deacetylases (HDACs), methyltransferases (HMTs/KMTs), demethylases (HDMs/KDMs), ubiquitinases (ubiquitin ligases)/deubiquitinases, and protein kinases/phosphatases, which dynamically regulate the histone PTM landscape. In addition to their role in histone modification, many of these enzymes can modify non-histone substrates, including p53 demethylation *via* KDM1A, PRMT5-mediated arginine methylation of components of the ribonucleoprotein-assembling Survival of Motor Neurons (SMN) complex, and EZH2-mediated methylation and activation of STAT3 (17–19). Due to the diversity and complexity of these enzyme families, it has become increasingly important to understand their respective functions in the context of normal physiology and the impact of their dysregulation in human disease.

Histone PTMs at the global and local levels are frequently dysregulated in cancer, and the enzymes involved in histone modification have therefore become viable therapeutic targets. Large-scale genomic sequencing efforts have illuminated recurrent mutations of histone modifying genes in many distinct forms of cancer (20). These include *MLL*, *EP300*, and *CREBBP* in small cell lung cancer, *EHMT1* and *KDM6A* in medulloblastoma, and *EZH2* in diffuse large B cell lymphoma and follicular lymphoma (21–23). In addition to somatic mutations, histone modifying genes are often found to be over- or underexpressed in the context of cancer, such as EZH2 overexpression in prostate, bladder, ovarian, and breast cancer, MLL1 overexpression in colon cancer, and SIRT1 overexpression in prostate and colon cancer and downregulation in breast cancer and hepatic cell carcinoma (24–29). Although much of the research in GBM epigenetics and epigenomics has focused on DNA methylation, parallel research has shown alterations in the expression of histone modifying enzymes and the landscape of histone PTMs in primary GBM tumors (5, 30). Moreover, the well-established presence of GBM stem cells (GSCs) within primary tumors, along with the substantial transcriptional heterogeneity and plasticity found within GBM, raises a number of questions regarding whether histone PTMs and chromatin architecture play a role in regulating transcription and degree of differentiation, as exemplified by the role of specific histone demethylases in treatment escape in GSCs exposed to prolonged receptor tyrosine kinase inhibition (6, 31–36). In this review, we will discuss the current landscape of research into the role of histone modifying enzymes in GBM pathophysiology, highlighting research into histone tail acetylation and methylation enzymes, broader genomic characterizations of the histone landscape, and identifying the challenges and opportunities within this field of research.

2 Histone acetylation

The addition of acetyl groups to histone N-terminal domain lysine residues is catalyzed by the action of lysine acetyltransferases/histone acetyltransferases (KATs/HATs) whereas the removal of acetyl groups is catalyzed by histone deacetylases (HDACs). The HAT family of enzymes can be divided into subgroups based on structural and sequence homology — the Gcn5-related N-acetyl transferase (GNAT) family, the MOZ, Ybf2-Sas3, Sas2, and Tip60 (MYST) family, and the CBP/p300 family (37). These subgroups vary in specificity and roles outside of histone acetylation, such as the catalysis of p53 acetylation mediated by CBP/p300 and GCN5/

PCAF or introduction of histone acetylation to regulate the binding of 53BP1 and influence DNA damage repair pathway selection (38, 39). HDACs are divided into four classes (Classes I–IV) based on similarity to yeast orthologs: Class I, comprised of HDAC1, HDAC2, HDAC3, and HDAC8; Class IIA, comprised of HDAC4, HDAC5, HDAC7, and HDAC9; Class IIB, comprised of HDAC6 and HDAC10; Class III, comprised of the Sirtuins 1-7; and Class IV, comprised solely of HDAC11 (40, 41). Of these, Classes I, II, and IV are Zn^{2+}-dependent, whereas Class III/Sirtuins are NAD^{+}-dependent. Like HATs, the enzymatic role of HDACs is not confined to histone deacetylation, with high levels of substrate promiscuity in the Sirtuin class of enzymes (40). Histone tail acetylation weakens the DNA-histone interaction by neutralizing the basic charge of the lysine residue, leading to decreased nucleosome occupancy and increased accessibility for RNA polymerase II binding and is often enriched at enhancers and promoters and correlated with transcriptional activity (42, 43). While this supports the view of HATs being associated with active genes and HDACs associated with inactive genes, genome-wide characterizations of HAT and HDAC activity reveal a more dynamic and nuanced picture, with HDACs serving roles in regulating active transcription as well as potentiating genes for future transcription (44). Given their functional role in both transcriptional regulation and modifications of non-histone substrates, HATs and HDACs have been implicated in many different disease states, including inflammatory diseases due to HAT-mediated post-translational modification of NF-κB, HAT-mediated acetylation of tau and concomitant increased expression of phosphorylated tau in Alzheimer's disease, as well as overexpression, underexpression, and/or mutation of both HATs and HDACs in many different forms of cancer, as reviewed elsewhere (20, 40, 45–49). As diametrically opposed regulators of histone acetylation, the diverse families of HATs and HDACs play an important role in influencing the interaction between DNA and histones and consequently are significant actors in disease pathophysiology when this process becomes dysregulated.

2.1 Histone deacetylases and histone acetyltransferases in GBM

Like many other forms of cancer, the expression of HATs and HDACs is altered in GBM. Though comparatively less work has been done on the role of lysine acetyltransferases in GBM, expression of the lysine acetyltransferase KAT6A is upregulated in GBM, and its acetyltransferase activity promotes tumorigenesis through the regulation of *PIK3CA* expression and PI3K/AKT pathway activation (50). Early gene profiling experiments into the expression of HDACs and Sirtuins in GBM found significant decreases in *HDAC5* and *HDAC11* expression and significant increases in *HDAC6*, *HDAC7*, and *HDAC10* expression when compared to normal brain tissue (51). Further investigation of individual HDACs has begun to shed light on the role and function they play in the pathophysiology of GBM, and a catalog of this information can be found in Table 1. HDAC1 expression is elevated in GBM tumor tissue as compared to normal surrounding brain tissue, and early gene expression profiling experiments in GBM revealed TCGA subtype exclusivity in the activity of histone acetyltransferase and deacetylase pathways, with proneural tumors having increased activation of HDAC1 and mesenchymal tumors having increased activation of HDAC4 and SIRT1 pathways (51–53, 55). Further research into the functional consequences of HDAC1 knockdown in GBM cell lines revealed increased apoptosis and decreased cellular migration upon HDAC1 knockdown *in vitro*, alongside concomitant decreased levels of active AKT and ERK, highlighting a potential relationship between HDAC1 and the PI3K/AKT and Ras/ERK signaling pathways in GBM (53, 54). Additionally, selective inhibition of HDAC1 and HDAC3, enzymes whose expression in tumors is associated with significant decreases in overall survival of human GBM patients, leads to increased temozolomide (TMZ)-induced cell death *in vitro* through the hyperacetylation of the NF-κB subunit p65 and inhibition of its interaction with NF-κB coactivators KAT2B and KAT3B and increased interaction with ING4, a tumor suppressor (51, 56). In addition to its correlated pathway activation in mesenchymal tumors, HDAC4 overexpression led to increased cell proliferation, decreased reactive oxygen species (ROS) production, and increased invasiveness of U251 cells *in vitro*, and HDAC4 knockdown in U87 cells *in vitro* induced the expression of $p21^{WAF1/Cip1}$, a cyclin-dependent kinase inhibitor and tumor suppressor involved in cell cycle regulation (55, 57, 58). Moreover, HDAC4 knockdown in U87 and U251 GBM cell lines led to radiation-induced senescence mediated by $p21^{WAF1/CIP1}$ in addition to reducing neurosphere formation and the frequency of $CD133^{+}$ and $Nestin^{+}$ (stem) cells (59). A multivariate retrospective immunohistochemical analysis of GBM tumor tissue for HDAC4 and HDAC6 expression found that at the mean of the covariates, high expression of either or both HDACs is associated with decreased overall survival, conflicting with the findings of the cohort in a study by Dali-Youcef et al. (51, 59) Alongside these findings, HDAC6 knockdown was found to increase apoptotic cell death and autophagy in U251 GBM cells *in vitro*, with another investigation showing impaired EGFR pathway activation in HDAC6 knockdown U87 cells (60). A similar pathway dependency was found following knockdown of HDAC9, which led to reduced proliferation of U87 cells *in vitro*, potentially through downregulation of the EGFR/AKT/ERK pathway (61). Within the Sirtuin family of deacetylases, SIRT1 has been found to be associated with tumorigenesis and stemness in NSCs and GSCs, respectively, with selective inhibition of SIRT1 leading to increased p53-dependent transcriptional activity, acetylation, and apoptosis in NSCs but not in U87 cells (62). Additionally, SIRT1 expression decreases during differentiation of GSCs, along with their susceptibility to apoptosis *via* SIRT1 inhibition (62). There is conflicting evidence regarding the role and expression of SIRT2 in GBM. Early proteomic-based analysis found decreased SIRT2 expression in GBM tissue samples, and overexpression in GBM cell lines suppressed cell growth and induced changes in microtubule localization in one of the cell lines studied (63). Treatment with the polyphenol resveratrol led to SIRT2-mediated decreases in GSC proliferation. However, SIRT2 was also found to be expressed in GSCs but not NSCs (64). SIRT3, which is localized in mitochondria,

TABLE 1 The function of histone acetyltransferases & histone deacetylases in GBM.

Enzyme	Associated role in GBM	Cell lines/model system used	References
KAT6A	Promotion of H3K23 acetylation through interaction with TRIM24, leading to PI3K/AKT pathway upregulation	U87, LN229	(50)
HDAC1	Elevated expression in GBM; increased apoptosis, decreased cellular migration, and decreased MAPK signaling upon knockdown *in vitro*	Patient-derived cell cultures (52); U251, T98G (53); U87 (54)	(51–55)
HDAC3	Overexpression associated with decreased overall survival; inhibition leads to increased TMZ-induced cell death		(51, 56)
HDAC4	Overexpression associated with increased cell proliferation/invasiveness and decreased ROS production, knockdown associated with p21WAF/Cip1-mediated radiation-induced senescence and decreased stem marker expression	U87, U251	(55, 57–59)
HDAC6	Conflicting associations between expression in tumors and overall survival, knockdown impairs EGFR pathway and increases apoptosis and autophagy *in vitro*	U87, U251	(51, 59, 60)
HDAC9	Knockdown leads to reduced proliferation and downregulation of EGFR signaling pathway	U87	(61)
SIRT1	Selective inhibition leads to apoptosis in engineered NSCs and GSCs but not U87 cells, and reduced expression of stem markers in GSCs	U87, engineered NSCs, GSCs	(62)
SIRT1	Conflicting evidence – research on primary tumor tissue showed decreased protein expression and that overexpression in GBM cell lines suppressed cell growth, while contrasting research showed SIRT2 essentiality in mediating decreased cellular proliferation in GSCs upon treatment with resveratrol	Glioma cell lines (unspecified), GSCs, NSCs	(63, 64)
SIRT3	Overexpressed in GSCs, interacts with TRAP1 to activate SOD2 and prevent ROS overproduction. Knockdown leads to increased ROS production and loss of stemness	GSCs	(65)
SIRT6	Overexpression leads to apoptosis and JAK-STAT pathway downregulation *in vitro*, conflicting evidence about expression in GBM	T98G	(51, 66–68)

A summary of the functions of individual histone deacetylase and acetyltransferase enzymes in GBM pathophysiology, and the corresponding model system(s) used and reference to the original publication(s).

is overexpressed in GSCs and plays an important role in GSC stemness and survival through its direct interaction with TRAP1, which together contribute to regulation of ROS primarily through the deacetylation of SOD2 (65). SIRT6 overexpression in T98G cells led to apoptosis and downregulation of the JAK2/STAT3 signaling pathway *in vitro*, though its influence on oncogenesis is cell-context dependent, and evidence regarding the relative expression of *SIRT6* in GBM is inconsistent (51, 66–68). While the role and dysregulation of HATs in GBM still requires targeted investigation, the altered expression of histone deacetylases in GBM has been found to have important functional consequences on stemness, tumorgenicity, and cell signaling, and thus these enzymes represent potential targets for treatment.

2.2 Histone deacetylase inhibition in GBM

In addition to targeted approaches assessing the role of histone acetylation-modifying enzymes in GBM, there has been increasing interest in the use of existing histone deacetylase inhibitors to treat GBM. A catalog of the inhibitors presented here can be found in Table 2. In addition to its anticonvulsant properties, valproic acid inhibits the activity of class I and II HDACs and has been demonstrated to augment radiation therapy in anti-cancer treatment (69, 80, 81). GBM-specific investigations have shown valproic acid treatment *in vitro* causes increased $p21^{WAF1/Cip1}$ expression in multiple cell lines and sensitization to TMZ treatment in GBM cell lines but not in primary GSC cultures derived from

TABLE 2 The effect of select HDAC inhibitors in GBM pathophysiology.

Treatment/Drug	Effect	Cell model(s) used	References
Valproic acid	*In vitro* radiosensitization of GBM cells, increased p21 expression in GBM model cells but not patient-derived cell lines	U87, T98G, TP365MG, U118MG, U251MG, U373MG, patient derived GSC lines	(69–71)
Suberanilohydroxamic acid (SAHA, vorinostat)	*In vitro* radiosensitization (compounded with concomitant Bcl-2 inhibition), leads to cell cycle arrest in G0/G1, shifts transcriptional phenotype away from proneural and classical transcriptional signatures	U87, GSCs	(72–75)
Trichostatin A	*In vitro* radiosensitization, shifts transcriptional phenotype away from proneural and classical transcriptional signatures, upregulates DIRAS-1 expression	U87, U373, U251, Hs683	(75–77)
Panobinostat	*In vitro* radiosensitization, apoptosis and necroptosis in neurospheres with concomitant KLF9 overexpression, metabolic shift to oxidative phosphorylation	GSCs/neurospheres, NCH644, NCH421k, U87	(69, 78, 79)

A summary of the impact of select HDAC inhibitors on GBM pathophysiology, and the corresponding model system(s) used and reference to the original publication(s).

human tumors (70, 71). Vorinostat (suberoylanilide hydroxamic acid, SAHA), a selective inhibitor of HDACs 1, 2, 3, and 6, has been used to treat certain types of cutaneous T cell lymphoma and has demonstrated similar ability to radiosensitize patient-derived GBM cell cultures *in vitro*, with this effect acting synergistically with a Bcl-2 pathway inhibitor, obatoclax (72–75). U87 cells treated with vorinostat exhibited cell cycle arrest in G_0/G_1 and reduced cell motility, whereas other studies have reported conflicting results for these phenotypes in patient-derived GBM cell lines (75, 76). In addition to these phenotypic changes, treatment with vorinostat was found to significantly alter the transcriptomic landscape of patient-derived GBM cell lines, with gene expression profiling revealing a shift away from TCGA proneural and classical molecular signatures towards a neural signature, though the existence of this particular molecular subtype has been questioned in more recent work (76, 82, 83). Trichostatin A, a class I and II HDAC inhibitor, has shown a similar ability to radiosensitize U87 and U373 cells *in vitro* and triggers similar transcriptional shifts away from TCGA proneural and classical expressional signatures in patient-derived cell lines *in vitro* (76, 77). Trichostatin A treatment of U251 and Hs683 cell lines *in vitro* has also been shown to upregulate mRNA expression of DIRAS-1, a small Ras GTPase and potential tumor suppressor in various solid tumors (84). Panobinostat, a nonselective HDAC inhibitor that has been explored as a potential therapeutic agent in a variety of cancers, has been shown to impact GBM cells in a manner similar to other HDAC inhibitors. Panobinostat radiosensitizes patient-derived GBM cell lines *in vitro*, with a greater effect on cell lines with *MGMT* promoter methylation (73). Panobinostat treatment in KLF9-overexpressing primary GBM neurospheres led to induction of apoptosis and necroptosis pathways *in vitro* (78). While the mechanism behind reduced cellular viability with treatment is undoubtedly multifactorial, *in vitro* and *in vivo* work by Nguyen et al. established a partial role for panobinostat-mediated disruption of c-Myc and subsequent metabolic shift to oxidative phosphorylation (79). Although HDACs represent a wide variety of enzymes with diverse downstream effectors, selective and broad inhibition of their function results in varying anti-tumor effects in GBM, including radiosensitization, sensitization to TMZ, and induction of cell death pathways. While the current preclinical evidence regarding HDAC inhibition in GBM is encouraging, clinical trials with the current generation of HDAC inhibitors have shown a mixture of outcomes with modest benefit in some trials and disappointing results in others due to unanticipated toxicity or failure to fill study arms (85). With newer therapeutic agents continually being generated, HDAC inhibition will undoubtedly continue to serve as a salient target for clinical trials for GBM (86–89).

3 Histone methylation

Histone tails are methylated through the action of histone methyltransferases, which catalyze the donation of methyl groups from S-adenosylmethionine to basic residues of the histone tail, whereas the removal of this modification is catalyzed by histone demethylases. Histone methylation most commonly occurs on lysine and arginine residues; lysine can be mono-, di-, or trimethylated, and arginine can be mono- or dimethylated, with dimethylation occurring either symmetrically or asymmetrically (90). Histone methyltransferases can be divided into three groups: SET-domain proteins and DOT1-like proteins (KMTs) which methylate lysine, and arginine *N*-methyltransferase proteins (PRMTs) which methylate arginine. Histone lysine demethylation is catalyzed by amine oxidase domain-containing proteins and Jumonji C (JmjC)-domain containing proteins, whereas the identification of selective arginine demethylases has proved elusive, with recent evidence suggesting dual lysine/arginine demethylase activity of certain lysine demethylase enzymes *in vitro* (91–93). Despite a few exceptions, these enzymes typically have higher substrate specificity compared to acetyltransferases, with specificity for unique methylation locations and degree of methylation (93–95). Unlike histone acetylation, the addition of methyl groups to histone tails does not result in charge neutralization of the target residue, instead altering the hydrophobicity and hydrogen bonding radius in the case of methyl-lysine, and thus the binding properties of these sites (96). Histone lysine methylation has a variety of correlations with transcriptional regulation and chromatin structure, depending on the location and degree of methylation. This includes associations of H3K4me1 with enhancer regions, H3K4me2 and H3K4me3 with promoter regions and transcription start sites, H3K27me3 with repressed transcriptional regions, and H3K36me3 in gene bodies of actively transcribed genes (44, 97, 98). Histone arginine methylation has been demonstrated to play a similarly important role in regulating transcription and chromatin architecture. Examples of this include the association of H3R2 symmetric dimethylation (H3R2me2s) with euchromatic promoters and H3K4me3 modifications, asymmetric H3R2 dimethylation (H3R2me2a) with promoter heterochromatinization, H4R3me2s with transcriptional repression and recruitment of DNMT3A, and CARM1 mediated methylation of H3R17 and H3R26 with transcriptional activation (99–103). However, histone methylation is context-dependent, as in the case of H3K4 methylation, where the plant homeodomain (PHD)-containing proteins recruited by this modification have varying functions in transcriptional activation and repression (96). Moreover, the colocalization of different methylation marks can lead to unique functions, as in the case of "bivalent" chromatin domains, such as embryonic stem cell transcription start sites marked by both H3K4me3 and H3K27me3, with loss of the repressive or activating mark during differentiation dependent on expression of the corresponding gene (104).

3.1 Histone demethylases in GBM

Research into the KDM (lysine-specific demethylase) family in GBM has provided insights into how these enzymes affect tumorigenicity through their dual role in demethylation of histone and non-histone substrates, a comprehensive summary of which can be found in Table 3. KDM1A (LSD1) is a H3K4/H3K9 demethylase that is overexpressed in GBM, which is consistent with similar

TABLE 3 The function of histone demethylases in GBM.

Enzyme	Associated role in GBM	Cell lines/ model system used	References
KDM1A	Overexpressed in GBM, particularly in stem-like cells. Constant inhibition decreases proliferation, colony formation, and tumorgenicity, and sensitizes cells to HDAC inhibitors, while transient inhibition increases stem gene expression. Stabilized by GSK3β-mediated phosphorylation,	GSCs, U251, U87, SNB-19, LN-18	(105–109)
KDM2A	Knockdown associated with reduced proliferation, migration, and invasiveness	A172, U251, T98G	(110)
KDM2B	Knockdown associated with reductions in cellular viability and self-renewal, increased sensitization to CCNU, and increased susceptibility to TRAIL-induced apoptosis	Patient-derived cultures, U87, T98G	(111, 112)
KDM4A	Upregulated in TMZ-resistant GSCs, knockdown results in reduced mTOR pathway activation, reduced invasiveness, and autophagy-dependent apoptosis	A172, U87MG, T98G, U251	(113–115)
KDM4C	Knockdown leads to reduced cellular viability, KDM4C acts as a p53 demethylase to inhibit initiation of apoptotic pathways	GSCs, U87, U251	(116, 117)
KDM5A	Upregulated in TMZ-resistant GSCs, overexpression inhibits TMZ-induced apoptosis in GBM cell lines, inhibition in TMZ-resistant subclones leads to decreased cellular viability	A172, U251, CAS1, DBTRG, U87, GSCs	(113, 118)
KDM5B	Higher expression in tumor tissue than surrounding brain, expression inversely correlated with overall survival post-resection	SW1783, U-87, LN-18, Hs683, and T98G	(119)
KDM6B	Conflicting evidence: Upregulated in TMZ-resistant GSCs, inhibition has been shown to induce apoptosis in both TMZ-naïve and TMZ-resistant cells. Overexpression has been shown to inhibit neurosphere formation *in vitro* and *in vivo*, and STAT3-mediated repression causes normal neurosphere formation	A172, U251, DBTRG, GSCs, NSCs.	(113, 120, 121)

A summary of the functions of individual histone demethylase enzymes in GBM pathophysiology, and the corresponding model system(s) used and reference to the original publication(s).

overexpression in bladder, lung, and colorectal cancer (122). In GBM, expression in isolated GSCs is inversely correlated with degree of differentiation (105). Initial research on the function of KDM1A in GBM focused on the similarities in the catalytic domain between KDM1A and monoamine oxidases (MAOs), finding that inhibition of KDM1A with the MAO inhibitor tranylcypromine rendered GBM cell lines more sensitive to treatment with HDAC inhibitors, but this synergistic effect was not observed in immortalized human astrocytes (106). In addition, selective inhibition of KDM1A through small molecule inhibitors or shRNA has been shown to decrease cellular proliferation, colony formation, and *in vivo* tumor progression. In tandem with these changes, expression of stem cell-associated genes decreased, and expression of genes involved in the unfolded protein response pathway increased, partially mediated by increases in H3K4me2 at associated loci (105, 107). However, the work of Kozono et al. complicated the conclusion that KDM1A promotes tumorigenicity. Instead, their findings suggested a dose-dependent influence of KDM1A on tumorigenicity as partial inhibition was associated with increased H3K4me3 at the MYC locus, increased MYC expression, and increased downstream expression of stem cell-associated genes, whereas complete inhibition led to decreased MYC expression and consequent cell death (108). Subsequent work described a mechanism by which GSK3β increases KDM1A stability *via* phosphorylation, allowing for downstream increases in USP22-mediated deubiquitylation and H3K4 demethylation activity of KDM1A. In turn, increased KDM1A binding to BMP2, CDKN1A, and GATA6 promoters repressed transcription of these genes, while increasing the expression of stem cell-related genes (109). Loss of either of the H3K36 demethylases KDM2A or KDM2B resulted in dysregulation of several GBM cellular phenotypes. Knockdown of KDM2A, a target of the microRNA miR-366 which is downregulated in GBM, resulted in reduced cellular proliferation, migration, and invasiveness (110). Alongside similar reductions in cellular viability, KDM2B knockdown reduced GSC self-renewal and increased sensitization to chemotherapy treatment with the alkylating agent lomustine, alongside increased susceptibility to TRAIL-induced apoptosis (111, 112). In addition to upregulation of mean expression in primary GBM tumor samples, the H3K9/H3K36 demethylase KDM4A has been shown to be upregulated in TMZ-resistant GSCs (113). KDM4A knockdown in GBM cell lines *in vitro* led to increased apoptosis and reductions in cellular viability and invasiveness, and these effects were ameliorated by the suppression of autophagy (114). A separate investigation suggested a connection between KDM4A and the mTOR pathway, a negative regulator of autophagy, with KDM4A overexpression and knockdown leading to increased and decreased activation of the mTOR pathway, respectively (115). Knockdown of the H3K9/H3K36 demethylase KDM4C led to a reduction in $CD133^+$ GSCs and reduced cellular viability, potentially mediated by a link between KDM4C and c-Myc/p53, in which KDM4C demethylates p53 and inhibits its roles in transcriptional activation and initiation of apoptotic pathways (116, 117). KDM5A, a H3K4 demethylase, has been shown to be markedly elevated in TMZ-resistant GSCs, a finding that is consistent with similar overexpression seen in drug-resistant non-small cell lung cancer (123). Exogenous KDM5A overexpression inhibited TMZ-induced apoptosis in GBM cell lines (113). This finding was further supported by work showing significant decreases in cellular

viability in TMZ-resistant subclones treated with the selective KDM5A inhibitor CPI 455 (118). Fellow H3K4 demethylase KDM5B has been found to have higher expression in GBM tumor tissue than normal surrounding brain tissue and has an inverse correlation with overall survival post-resection (119). Expression of H3K27 demethylase KDM6B is upregulated in TMZ-resistant GSCs, and selective inhibition of this enzyme *via* the drug GSK J4 led to reduction of cell cycle transition to G2 and induction of apoptosis, though these phenotypes did not differ between TMZ-naïve and TMZ-resistant populations (113, 120). However, the expression of KDM6B in human GBM tumors is variable and heterogeneous, and contrasting research has suggested that overexpression of this enzyme inhibits neurosphere formation *in vitro* and tumor formation *in vivo* and further that STAT3-mediated repression of KDM6B expression is essential for neurosphere formation and cellular proliferation (121). With some exceptions, the function of histone demethylases primarily acts to promote tumorigenicity, thus serving as a potential therapeutic target to abrogate proliferative and anti-apoptotic functions in GBM.

3.2 Histone methyltransferases in GBM

Trimethylation of H3K27 is a ubiquitous repressive mark found in large stretches of heterochromatic DNA and is associated with transcriptional repression. The introduction of this modification is catalyzed by Polycomb Repressive Complex 2 (PRC2), a multiprotein complex that carries out methyltransferase enzymatic function *via* the enhancer of zeste homolog 2 (EZH2) subunit (124). Adding complexity to its regulatory role, EZH2 can methylate non-histone substrates within the nucleus or the cytosol (125). Aberrant EZH2 expression is a hallmark of many cancers and elevated expression in the context of malignancy can be a marker of poor prognosis and advanced disease (126). EZH2 expression has been shown to be elevated in GBM, and its expression is similarly correlated with a poorer prognosis (12, 127–129). Due to the importance of H3K27me3 in transcriptional regulation and chromatin architecture, extensive efforts have been made to understand the role of EZH2 in promoting GBM tumorigenicity. EZH2 has been shown to exert diverse regulatory roles in GBM, modulating pathways in tumor initiation/self-renewal, differentiation, cell cycle progression, metabolism, immunogenicity, and invasiveness. Early work by Suvà et al. showed that EZH2 is necessary for tumor formation and self-renewal in patient-derived GSCs, with further research highlighting the importance of an AKT-mediated interaction between EZH2 and STAT3 in GSC self-renewal (19, 32, 130–133). There is evidence that EZH2 mediates both pro- and inhibitory differentiation signals. One mode of inhibition of GSC differentiation occurs through hypermethylation of the BMPR1B promoter, thought to be mediated by EZH2 recruitment of DNMT1, allowing for clonal expansion *via* inhibition of differentiation (134). In contrast, differentiation is induced *via* H3K27me3-mediated suppression of Nanog (131). Investigations using a transgenic high-grade glioma mouse model demonstrated that FZD8, a G protein-coupled receptor involved in Wnt signaling, undergoes H3K27me3-mediated suppression during tumorigenesis and that this could be an early disruptor of normal differentiation pathways during gliomagenesis (135). Fitting with this theme, Mortimer et al. provided compelling evidence for redistribution of EZH2 binding sites across the genome following malignant transformation, most significantly at *HOX* genes (136). EZH2 inhibition has been shown to impact cell cycle progression, with inhibition leading to apoptosis and block of cell cycle progression in a p16, p21, and p27-mediated manner (12, 137–139). Alterations in metabolic pathways is a hallmark of cancer, and EZH2 has been shown to upregulate glycolysis *via* increased HIF1α expression, a known transcription factor important for activism of metabolism-related genes. EZH2 promotes the glycolysis pathway *via* binding to the promoter of a known HIF1α repressor EAF2, resulting in H3K27me3-mediated repression (128). A role for EZH2 in the regulation of fatty acid metabolism has been suggested by *in vitro* and *in vivo* knockdown of EZH2, which correlated with decreased lipid metabolism and decreased expression of PGC-1a, FASN, and SREBP-1. Interestingly, TERT appears to be a co-regulator of EZH2 in this pathway, demonstrating an ability to restrict the repair of DNA damage *via* downregulation of phospho-ATM, providing fitness/adaptation benefits through increased genomic instability (140). Further adding intrigue to EZH2 modulation of DNA damage repair, De Vries et al. showed that prolonged EZH2 inhibition in a syngeneic mouse model leads to enhanced tumor growth after an initial 3 week period of inhibited growth. This reversion to the pre-inhibited tumor growth state appears to be due to enhanced DNA damage repair within tumor cells (141). EZH2 also contributes to the immunosuppressive microenvironment of GBM by triggering specific cytokine expression, maintaining expression of interferon-stimulated genes that promote a M2 microglial phenotype in an iNOS and TGF-β2-dependent manner. Evasion of NK cell immune surveillance occurs *via* a circular EZH2 encoded protein (EZH2-92aa) that directly binds the promoters of genes (MICA/B, ULBP) necessary for the expression of NK group 2D ligands in GSCs, leading to decreased transcription and ultimately decreased NK cell-mediated tumor cell death (14, 139, 142, 143). The role of EZH2 in promoting GBM invasiveness *via* regulation of AXL in a histone modification-independent manner has been demonstrated *in vitro* with EZH2 knockdown (127). Expanding upon this work, another group showed that EZH2 inhibitors decrease invasiveness by downregulating VEGF, matrix metalloproteinases, and cell surface adhesion markers (E-cadherin and N-cadherin) (139). Several non-coding RNAs have been shown to be important in EZH2-mediated invasiveness. The lncRNA NEAT1, which is upregulated by EGFR, forms a scaffold with EZH2, which together augment invasion by increasing nuclear β-catenin. (144) This activation of β-catenin also appears to feedback on EZH2 activity by increasing expression of USP1, a deubiquitinase that stabilizes EZH2 (145). The microRNA, miR-490-3p, undergoes EZH2-mediated H3K27me3 silencing, resulting in increased colony formation and transwell migration *in vitro* (13). It is evident that EZH2 plays a broad and diverse role in the regulation of tumorigenicity in GBM tumor cells, highlighting its significant clinical potential as a therapeutic target.

The family of H3K9 methyltransferases has been shown to be similarly important in GBM tumorgenicity. Euchromatic histone lysine methyltransferase 2 (EHMT2), also known as G9a, mediates repressive mono- and dimethylation of H3K9 and its expression is associated with improved survival in grade II oligodendrogliomas. Contrasted with a protective role in oligodendrogliomas, early work on the role of EHMT2 in GBM tumorigenicity was mixed, but with

more recent evidence supporting a pro-tumorigenic role (146, 147). *In vitro* studies have shown that inhibition of EHMT2 in established GBM cell lines promoted GBM cell growth and increased expression of stem cell markers, and direct methylation of HIF-1α by EHMT2 inhibits hypoxia adaptation and cellular invasion (148, 149). Conflicting evidence demonstrates that EHMT2 contributes to tumorigenicity in GBM. *In vitro* assays in established GBM lines show that EHMT2 is required for proliferation, migration, and invasion in a c-Myc dependent manner and that inhibition of EHMT2 leads to reduced global H3K9me2 and to increased apoptosis, autophagy markers, and differentiation in human primary GSCs (150, 151). Further work revealed EHMT2-mediated evasion of IFNγ-directed apoptosis and increased survival with EHMT2 knockdown in GSCs in an orthotopic nude mouse model (150, 152). Similar to EHMT2, Suv39H1 and SETDB1 decrease gene expression through their H3K9 methyltransferase activity (153, 154). Studies evaluating their role in the setting of GBM have found increased expression of both genes compared to normal brain, and decreased cell proliferation, increased apoptosis, reduced migration, and reduced colony formation upon shRNA knockdown of SETDB1 or inhibition of Suv39H1 with chaetocin in established GBM cell lines (155, 156). Interestingly, there appears to be a relationship between poor survival and increased cytoplasmic Suv39H1 that does not exist for nuclear Suv39H1, suggesting a histone independent mechanism of pathogenesis. Thus, there is a compelling role for EHMT2 in the promotion of GBM proliferative and invasion, which is consistent with its pro-malignancy role in numerous other cancers, yet further work in needed to fully understand its role in GBM (157). Similarly, further work is needed to characterize the mechanisms by which SETDB1 and Suv39H1 mediate the observed phenotypic changes as well as their impact on chromatin architecture and organization in GBM.

Due to the role of arginine methyltransferases enzymes in AML, melanoma, and lung cancer recent efforts have been made to characterize their role in GBM pathogenesis (133, 158–160). The arginine methyltransferase PRMT3, PRMT5, and PRMT6 have elevated expression in GBM tissue, and their expression is associated with decreased survival (161–163). In contrast to the pro-tumorigenic effect of these enzymes, PRMT1 plays an antiproliferative role by counteracting the effect of EHMT2 in the presence of IFNγ (152). PRMT3 appears to regulate multiple metabolic pathways in GBM with a specific role in preventing ubiquitination of HIF1α, thereby promoting glycolysis (163). PRMT3 knockdown in GSCs induced cell cycle arrest and apoptosis, and its inhibition led to decreased tumor growth in a nude mouse flank model (163). *In vitro* knockdown of PRMT5 reduced colony formation, migratory activity, and led to increased cell cycle arrest and apoptosis (161, 164, 165). Further work showed that PRMT5 downregulates PTEN *via* promoter binding and ultimately leads to increased active ERK and AKT (164). PRMT5 is also used by GBM cells to evade mTOR inhibition, and PRMT5 inhibition causes widespread disruption of mRNA splicing, especially in cell cycle related genes (166, 167). Adding validity to this *in vitro* work, inhibition of PRMT5 *in vivo* increased animal survival (164, 166, 167). Inhibition of PRMT6 limits RCC1 driven mitotic activity, leading to decreased tumor growth and increased radiation sensitivity *in vivo* (162). Overall, these studies provide an initial characterization of the function of arginine methyltransferases in GBM, but more work is needed to clarify their influence on genomic architecture and transcriptional regulation.

Much less is known about the various other human histone methyltransferases in the context of GBM. H3K4 methyltransferase KMT2A (MLL1) expression increases in GBM in the setting of hypoxia in a HIF-dependent manner, with knockdown leading to decreased self-renewal *in vitro* and decreased tumor formation *in vivo* (168). Although KMT2E (MLL5) has no catalytically active histone methylation domain, its expression is anticorrelated with H3K4me3 levels in primary GBM cultures, and knockout reduced self-renewal capacity (94, 169). DPY30 is the catalytic subdomain of the MLL/SET1 family of proteins, and recent work explored its role in GBM based on an RNAi screen demonstrating that DPY30 knockdown decreases cell viability *in vivo*. Interestingly, *in vitro* inhibition had no effect, which is consistent with the demonstrated pro-tumorigenic mechanism of DPY30 in GBM cells where it improves hypoxia adaptation and activates angiogenesis pathways (170). A subset of low-grade glioma and GBM patients harbor an inhibitory mutation in *SETD2*, and decreased SETD2 expression is associated with poor prognosis in GBM. Higher secretion of TGF-β1 in GBM cells derived from patients carrying the *SETD2* mutation led to an increase in activated tumor-associated microglia which fueled tumor progression (171). Additional work has shown that EGFR-mediated suppression of SETD2 results in decreased DNA damage repair, resulting in an accumulation of DNA damage in established GBM cells lines, leading to increased mutagenesis and subsequent selective adaptation (172). Stabilization of SETD2 with Palmostatin-B, a drug the prevents de-palmitoylation, led to decreased proliferation of established GBM cell lines and decreased tumor growth in a nude mouse model, consistent with an antiproliferative role for SETD2 in GBM (172). Comparison of periventricular human GBM to normal subventricular zone NSCs obtained from non-human primates suggested a potential role for the H4K20 methyltransferases KMT5B and KMT5C (Suv420H1/2) in GBM tumorigenesis, showing that 21-31% of genes repressed by the H4K20me3 mark in NSCs are upregulated in GBM cells (173). Finally, one study has shown that SMYD3, a member of the SMYD lysine methylase family, promotes proliferation and tumorigenicity in established GBM cell lines *in vitro* and *in vivo* (94, 119, 174). Despite the important role that the MLL/SET1 family of enzymes play in other cancers, less is known about these enzymes in the context of GBM and more work is needed to better elucidate their role in regulating and promoting tumorigenesis through their modifications of histone and non-histone substrates (175). A comprehensive summary of the functions of the methyltransferase enzymes described herein can be found in Table 4.

3.3 Inhibition of histone demethylases and methyltransferases in GBM

Numerous inhibitors have been used in the laboratory to better understand the role of histone methyltransferases and demethylases in GBM pathophysiology, with many shown to have anti-proliferative

TABLE 4 The function of histone methyltransferases in GBM.

Enzyme	Associated role in GBM	Cell lines/model system used	References
EZH2	Overexpressed in GBM. Increases cell cycle progression, invasiveness, tumorigenicity, and tumor growth. Modulates metabolism, differentiation, and immune signaling.	A172, BCRC 60380, BCRC 60163, GL261, H4, LN18, LN229, N33, T98G, U87MG, U251, patient-derived GSCs, patient-derived neurospheres, nude mouse model, syngeneic mouse model	(12–14, 19, 32, 127, 128, 130, 132, 134–145, 176–186)
EHMT2	Promotes proliferation, migration, and invasion. Reduces differentiation, apoptosis, and autophagy.	A172, LN18, LN229, U87MG, U251MG, patient derived GBM cell cultures, patient derived GSCs, nude mouse model	(148–152, 187)
Suv39H1	Overexpressed in GBM. Promotes proliferation, migration, and colony formation.	T98G, U87MG	(155, 156)
SETDB1	Overexpressed in GBM. Promotes proliferation, migration, and colony formation.	T98G, U87MG	(155, 156)
PRMT1	Decreases GBM cell viability in a counter-regulatory fashion to EHMT2	A172, U87MG	(152)
PRMT3	Overexpressed in GBM. Regulates glycolysis and inhibition increases apoptosis, inhibitors cell cycle progression, decreases tumor growth	U87, U251, patient derived GSCs, nude mouse flank model	(163)
PRMT5	Overexpressed in GBM. Promotes colony formation, migration, and cell cycle progression.	LN229, U87EGFRvIII, patient derived GBM cell cultures, patient derived neurospheres, patient derived GSCs, zebrafish GBM model, nude mouse model	(161, 164, 166, 167)
PRMT6	Overexpressed in GBM. Promotes cell proliferation.	T98G, U87, patient derived GBM cells, nude mouse model	(162)
MLL1	Promotes self-renewal and tumor formation.	Patient derived GSCs, nude mouse model	(168)
MLL5	Promotes self-renewal	Patient derived GBM cell lines, nude mouse model	(169)
SMYD3	Promotes cell proliferation and tumorigenicity	HEB, LN18, T98G, U87, U373, nude mouse flank model	(188)
DPY30	Promotes cell viability through regulation of hypoxia and angiogenesis	Patient derived GBM cell lines, patient derived GSCs, nude mouse model	(170, 189)
SETD2	Antiproliferative effects are neutralized in GBM through mutation or EGFR suppression	Patient derived GBM cell lines, patient derived GSCs, nude mouse model	(171, 172)
KMT5B/5C	Dysregulation implicated in gliomagenesis	Baboon and mouse-derived NSCs	(173)

A summary of the functions of individual histone methytransferase enzymes in GBM pathophysiology, the associated histone post-translational modification, and the corresponding model system(s) used and reference to the original publication(s).

effects. A summary of these inhibitors can be found in Table 5. Inhibitors that target KDMs range from broad class inhibition to individual enzyme specificity. Examples of KDM inhibitors with broad enzymatic targets include dimethyloxaloglycine (DMOG), GSK-14, and JIB-04. DMOG has been shown to induce DNA damage and apoptosis in GSCs through targeting of the Jumonji (JMJ) family of demethylases (KDM2-KDM7) (116). Although GSK-14 is a broad KDM class inhibitor, its antiproliferative effects in GCSs appear to operate through inhibition of KDM2B (111). JIB-04 is another broad inhibitor of KDMs with some specificity for KDM5A and has been shown to activate autophagy and apoptosis in established GBM cells lines *in vitro* (118). Additional work demonstrated a synergistic effect when JIB-04 is combined with GSKJ4, a KDM6B inhibitor, in TMZ resistant cells *in vitro* (120). Several targeted inhibitors of KDM1A, KDM4C, and KDM6B have been investigated in GBM. The tricyclic antidepressant tranylcypromine, which also functions as a KDM1A inhibitor, caused apoptosis in established GBM cells lines when combined with vorinostat (106). NCL-1 and NCD-38 are small molecule inhibitors that target KDM1A and preferentially affect GSCs, leading to apoptosis *in vitro* and increased survival *in vivo*, without notable effects on differentiated cells (105). Similarly, selective inhibition of KMD4C by SD70 decreased cell viability *in vitro* in established GBM cell lines (117). In GSCs, inhibition of KDM6B *via* GSKJ4 inhibited cell growth through activation of apoptosis pathways (36, 120).

The majority of the work on HMT inhibitors has focused on EZH2 and to a lesser extent EHMT2, with more recent work focusing on arginine methyltransferases. The most studied inhibitor of EZH2 is 3-deazanoplanocin A (DZNep), with numerous studies demonstrating its ability to decrease GBM cell self-renewal and viability *in vitro* and decrease tumor growth *in vivo* (14, 19, 131, 132, 190, 192). *In vitro* and *in vivo* work in a murine flank tumor model demonstrated that AC1Q3QWB, a small molecule inhibitor of EZH2's interaction with the lncRNA HOTAIR, increases cell death and decreases tumor growth (184). Similarly, the small molecule inhibitor EPZ6438 has been used to inhibit EZH2 in GSCs and murine GBM models, leading to increased apoptosis *in vitro* and increased survival *in vivo* (135, 181). EPZ6438 has also been shown to accumulate intracranially in murine tumors (181). In contrast, although targeting EZH2 with UNC1999 decreased GSC viability and self-renewal *in vitro*, *in vivo* studies did not show benefit in orthotopic xenografts despite decreased growth in flank models, suggesting low brain penetration. Further *in vitro* studies demonstrated reduced cell

TABLE 5 The effect of select histone methyltransferase and histone demethylase inhibitors in GBM pathophysiology.

Treatment/ Drug	Target	Effect	Cell model(s) used	References
Tranylcypromine	KDM1A	Increased cell death in combination with vorinostat	LN-18, U87	(106)
NCL-1 & NCD-38	KDM1A	Reduced viability and increased survival	GSCs, U251, murine mouse model	(105)
GSK-14	KDM class/ KDM2B	Decreased cell viability	GSCs	(111)
SD70	KDM4C	Decreased cell viability	U251, U87	(117)
JIB-04	KDM class/ KDM5A	Activated autophagy and apoptosis	A172, U251, GSCs	(118, 120)
GSKJ4	KDM6B	Decreased cell growth and increased apoptosis	U251, GSCs	(36, 120)
DMOG	KDMs 2-7	Induced DNA damage and apoptosis	GSCs	(116)
AC1Q3QWB	EZH2	Increased cell death and decreases tumor growth when combined with DZNep	N5, N33, murine flank model	(184)
DZNep	EZH2	Decreased self-renewal and tumor growth	U87, U251, LN229, D54, GSCs, murine mouse models	(12, 19, 131, 132, 181, 190)
GSK126	EZH2	Decreased pSTAT3	GSCs	(19)
PCI-24781	EZH2	Reduced proliferation and induced cell cycle arrest and apoptosis	LN18, LN229, U87	(137)
UNC1999	EZH2	Decrease cell viability, induced autophagy, reduce flank tumor growth	GSCs, murine mouse model	(179)
EPZ6438	EZH2	Increased apoptosis and survival	GSCs, murine mouse model	(135, 181)
MC4040 & MC4041	EZH2	Cell cycle arrest, decreased invasiveness	U87, patient derived cell cultures	(139)
BIX01294	EHMT2	Decreased self-renewal and cell viability, activation of autophagy, reduced tumor growth	U87, U251, LN18, LN229, D54, GSCs, murine mouse model	(148, 150, 151, 187, 190, 191)
Chaetocin	SUV39H1	Reduced proliferation and clongenic ability	T98G	(156)
SGC707	PRMT3	Inhibited cell growth and glycolysis, Inhibited tumor growth	U87, U251, patient derived GSCs, nude mouse flank model	(163)
HLCL65, CMP12	PRMT5	Increased cell death, improved survival	Patient derived cell cultures, zebrafish GBM model	(165)
CMP5	PRMT5	Inhibits self-renewal and cell cycle progression, increased apoptosis and survival, long term survivors	Patient derived cell cultures, zebrafish GBM model	(165)
GSK591 & LLY-283	PRMT5	Inhibits proliferation and sphere formation, increases apoptosis and survival, crosses BBB	GSCs, murine mouse model	(167)
EPZ020411	PRMT6	Induces cell cycle arrest, decreases sphere formation, increased survival	GSCs, murine mouse model	(162)

A summary of the impact of select histone methyltransferase and histone demethylase inhibitors on GBM pathophysiology, and the corresponding model system(s) used and reference to the original publication(s).

viability and increased apoptosis *via* inhibition of EZH2 with the small molecule inhibitors PCI-2478, MC4040, and MC4041 (137, 139, 179). Multiple studies have evaluated the role of BIX01294 as an EHMT2 inhibitor in GBM. *In vitro* experiments demonstrated decreased GBM cell viability *via* apoptosis and autophagy and increased GSC differentiation, in line with *in vivo* experiments which showed reduced tumorigenicity (62, 148, 150, 151, 187, 190). Finally, one study utilized chaetocin to inhibit SUV39H1, which reduced GBM cell clonogenic potential and migratory ability (156).

Multiple inhibitors of arginine methyltransferase enzymes PRMT3, PRMT5, and PRMT6 have shown promising results in recent years. Work in patient-derived GSCs and a nude mouse flank model demonstrated decreased glycolysis, cell growth, and tumor growth with SGC707, a small molecule PRMT3 inhibitor (163). A zebrafish GBM model was used to identify numerous inhibitors of PRMT5 with anti-proliferative effects. Three compounds (HLCL65, CMP12, CMP5) were identified, all of which provided *in vitro* cytotoxicity and increased survival *in vivo*, although CMP5 appeared most promising as treatment led to a significant number of long-term survivors (165). Further work targeting PRMT5 in GSCs showed that the compounds GSK591 and LLY-283 decreased *in vitro* proliferation and sphere-forming capacity with evidence of blood-brain barrier (BBB) drug penetration by

LLY-283, leading to increased survival *in vivo* (167). The PRMT5 inhibitor, EPZ01566, in concert with mTOR inhibitors provided anti-proliferative effects *in vitro* and increased survival *in vivo* (166). A sole PRMT6 inhibitor (EPZ020411) has been shown in GSCs to induce differentiation and cell cycle arrest, and increased *in vivo* survival was most pronounced when combined with ionizing radiation (162). Overall, these numerous studies demonstrate the utility of using small molecule inhibitors to target histone modifying enzymes in GBM, but work investigating the brain penetration of these drugs or opportunities to combine these drugs with BBB modulating technologies, as well as studies characterizing their impact on non-GBM cells in the tumor micro-environment (TME) are needed.

4 Genomic landscape of GBM

The potential functional impact of the diverse enzymes with roles in histone PTMs can be seen through the presence and location of these various alterations across the genome. A summary of selected modifications can be seen above in Figure 1. Early work in this area explored the conversion of GSCs to more terminally-differentiated brain tumor cells, a process dependent on PRC2-mediated H3K27me3 at the BMP5 locus and a concordant loss of this modification at the Wnt1 promoter (131). The essentiality of Wnt signaling in GSC maintenance was further underscored by the dual observation of increased expression of Wnt-pathway activator ASCL1 in GSCs and ASCL1 binding to a H3K4me1-marked poised enhancer of Wnt signaling inhibitor DKK1, preventing its expression (193). However, further research into the role of ASCL1 in promoting stemness or differentiation suggested that its role may be context-dependent, as separate work suggested that ASCL1 can independently direct GSCs to a neuronal fate, downregulate cell cycle genes *in vivo*, and act as a potential pioneer factor for neuronal target genes (194, 195). Loss of stem-like properties in GSC populations is also associated with global chromatin changes in H3K4me3/H3K27me3 ("bivalent") histone modifications. Genome-wide profiling of H3K4me3 and H3K27me3 in eight GSC lines in comparison to human astrocytes revealed unique bivalent modifications at loci for a variety of gene families, including HOX family genes, Wnt pathway genes, Hedgehog signaling, and solute carrier family genes (196, 197). In comparison to fetal neural stem cells (fNSCs), roughly 37% of H3K4me3/H3K27me3 marks at promoter regions were found to be unique to GSCs, with 137 promoter regions containing this bivalent modification in fNSCs but only the H3K4me3 modification in GSCs, and 191 promoter regions containing both modifications in fNSCs but only the H3K27me3 modification in GSCs (198). A similar comparison of chromatin states between fNSCs and GSCs revealed that GSCs had lost brain-specific H3K4me1-marked active enhancers, as well as transitioning to poised or active enhancer marks in other tissue-specific enhancers. Additionally, GSC specific regions with colocalized H3K4me1 and H3K27ac marks were enriched for gene ontology terms related to angiogenesis and DNA damage response pathways (199). Upon repression of stem cell-like properties in GSCs, genes with histone mark changes from H3K4me3 to H3K27me3 included Wnt-signaling pathway mediator *LEF1*, and *ARNT2*, a mediator of the hypoxia response pathway involved in promoting the expression of stem cell markers *OLIG2*, *POU3F2*, and *SOX9* (200). Expanding upon the observation that primary GBM tumors contain only a small fraction of cycling cells, Liau et al. used receptor tyrosine kinase inhibitors to induce a similar, slowly cycling quiescent state within a GSC population. This change from proliferation to quiescence was accompanied by changes in H3K27ac and H3K27me3 marks, with H3K27ac-associated motifs specific to the quiescent population being marked with H3K27me3 in the untreated/

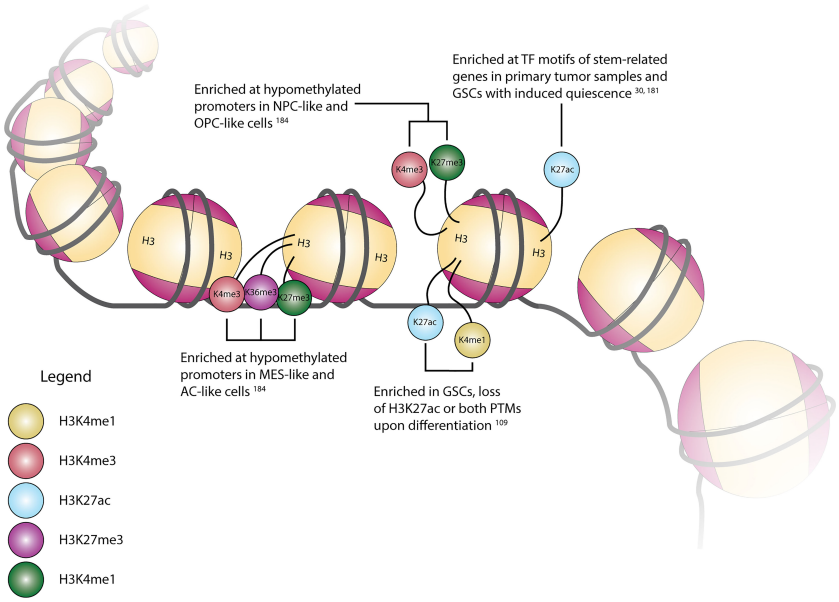

FIGURE 1
Cartoon depiction of common histone H3 modification locations and their associated modifications, transcriptional state associations, and/or regulation in GBM.

RTK-naïve population, and motifs related to neural stem cell development becoming enriched in H3K27ac marks in the quiescent population (36). Separate research integrated this mark of active enhancer regions with gene expression and DNA methylation data to define the enhancer landscape within GBM, finding many of the concordant loci located at genes with important functions in stem cell maintenance, such as *SOX2*, *EGFR*, *POU3F2*, and *SALL3*. Further profiling of the H3K27ac landscape in primary tumor tissue samples revealed SOX2 to be a shared TF among all GBM subtypes and normal brain tissue, while POU3F2 was preferentially found in proneural tumor samples (201). Mapping of enhancer regions from H3K27ac ChIP-seq data to high resolution fetal brain Hi-C data identified 116 enhancer-promoter pairs with significant contact frequency, corresponding to 96 total genes of which 17 were differentially expressed in GBM as compared to lower grade glioma and pilocytic astrocytoma. This list included ANXA2R, which encodes the receptor for annexin 2, a gene overexpressed in GBM and other malignancies, which is thought to contribute to cellular migration and growth (202, 203). Similar research investigating broader changes in histone lysine PTMs upon GSC differentiation observed alterations in the active enhancer regions, finding regions with both H3K27ac and H3K4me1 modifications in GSCs losing the H3K27ac modification upon differentiation, as well as increases in larger (3-50 kb) domains containing repressive H3K9me3 and H3K27me3 modifications (116). Unsurprisingly, in addition to correlations with varying degrees of GSC differentiation, there are correlations between transcriptional state and promoter histone PTMs. By superimposing paired multiplexed single cell reduced representation bisulfite sequencing and scRNA-seq onto existing ChIP-seq data, Chaligne et al. found connections between these three modalities, specifically that hypomethylated promoters in astrocyte-like and mesenchymal-like cells primarily contained H3K4me3, H3K27ac, and H3K36me3 modifications, which are associated with active transcription (204). Similarly, hypomethylated promoters in neural progenitor-like and oligodendrocyte progenitor-like cells primarily had H3K4me3 and H3K27me3 (bivalent) modifications, recapitulating the observed change from bivalent to single histone modifications during differentiation given that progenitor-like cells are less terminally-differentiated than MES- and AC-like cells (35, 204). As methods to simultaneously profile histone PTMs and gene expression at single-cell resolution become more accessible, our understanding of the correlations between the epigenetic and transcriptional landscape of GBM will increase, allowing us to better grasp the interplay between individual histone modifications, and histone modifications and downstream gene expression.

5 Challenges and knowledge gaps

Work on the role of EZH2 in GBM pathophysiology has revealed the more general concept that the effects of canonical histone modifying enzymes may in fact be mediated by both histone and non-histone substrates. For instance, enrichment of H3K27me3 at the *PTEN* promoter decreased gene expression, allowing for increased AKT/mTOR signaling (185). But in contrast to a histone remodeling mechanism, EZH2 also exerts a direct activating effect on STAT3 *via* methylation of lysine residue 180 (K180) (19). As highlighted by these EZH2-dependent mechanisms, there is a comparative lack of clarity surrounding the mechanism of action of many histone modifying enzymes in GBM pathophysiology. Furthermore, many of the studies that modulate the expression of individual histone modifying enzymes in GBM have used phenotypic changes as an endpoint. This results in ambiguity as to the effector(s) of these phenotypes, as they could be the result of either genomic and transcriptional dysregulation, or alterations in the function of non-histone substrates. Incorporating epigenomic profiling methods such as ChIPseq, CUT&RUN, CUT&Tag, Hi-C, and their single-cell variants would allow observation of the genomic consequences of these alterations, whereas coimmunoprecipitation, affinity purification with mass spectrometry, and similar protein-based assays could point to similar implications of altering histone PTM enzymes on non-histone substrates. Additionally, the degree to which established immortalized GBM cell lines replicate the transcriptional landscape of primary tumors has been brought into question, and recapitulating the effects of single or multi-target inhibition in multiple model systems as well as both *in vitro* and *in vivo* has become increasingly important, as previous screening between these environments has showcased a vast difference in environment-specific gene dependencies (189, 205, 206). While there have been several studies investigating the impact of single-target perturbations in GBM, many of these have relied on immortalized cell line cultures *in vitro*. This presents both a limitation of the existing work as well as an opportunity for future research in model systems and environments which better mimic that of GBM. In recent years, organoid-based model systems and embryonic stem cell-derived model systems have been validated in their ability to reflect characteristics of GBM biology (207, 208). Application of epigenetic and biochemical profiling techniques to these model systems, as well as model systems mimicking the current standard of care or *in vivo* systems could help illuminate the functional dependency of tumor cells on specific epigenetic states or enzymatic actions.

Perturbations at the DNA or RNA levels and small molecule inhibitors are powerful tools for unraveling the biological function of a gene product and have been used extensively to elucidate the role of histone modifying enzymes in GBM. Inhibition of these enzymes also holds promise in clinical therapies when found to preferentially target cancer-dependent pathways. Most human clinical trials have focused on the use of HDAC inhibitors in GBM and a recent systematic review was published supporting the use of valproic acid to increase overall survival in GBM, although prospective randomized control trials are needed to confirm these findings (209). In contrast to valproic acid, vorinostat and panobinostat have demonstrated less promising data with vorinostat leading to toxicities or failing to show benefit, and similar lack of benefit in panobinostat (85). Another challenge for HDACi trials has been difficulty with recruiting patients. It is likely that the anti-epileptic role of valproic acid has increased its use and subsequent study in glioblastoma patients. Outside of histone acetylation, there has been little clinical investigation of methylation inhibitors with a currently recruiting phase II clinical trial for the EZH2 inhibitor EPZ6438, but in

pediatric gliomas. An active, but no longer recruiting phase I clinical trial is investigation PRT811, a PRMT5 inhibitor, but again without a glioblastoma focus as the trial is treating all high grade gliomas (clinicaltrials.gov). A challenge in using some of the drugs listed in this review is an inability to penetrate the BBB. This challenge can be better managed moving forward with the emergence of BBB modulating therapies such as laser interstitial thermal therapy and focused ultrasound (210, 211).

As inhibitors of histone modifying enzymes are being translated to the clinical setting, it is imperative to understand the role that these inhibitors play not just on the cancer cells but also on the tumor microenvironment, including blood and lymph vessels and tumor infiltrating immune cells. Thus, although the use of immunodeficient mice to mimic an *in vivo* environment has improved our understanding of human cancer biology, these environments lack the adaptive immune component of the human tumor microenvironment. As the number of successful immunotherapies across human malignancies grows and with increasing appreciation for the role of adaptive and innate immunity in GBM treatment resistance, the need for more complex models is needed. Multiple syngeneic mouse tumor lines have been developed to model GBM in the setting of an intact immune system. Due to the differences between human and mouse tumor biology and it is imperative that newly developed mouse tumor cell lines recapitulate the starkly immunosuppressive microenvironment of glioblastoma to ensure clinical utility. GL261 is an examples of a syngeneic mouse tumor line that possesses significant mutation burden and expresses elevated MHC1 levels, leading to a favorable immune response that arguably does not capture the full complexity of human disease (212). In contrast, the SB28 model demonstrates a greater resistance to immune checkpoint blockade, more faithfully recapitulating human glioblastoma immune characteristics (213). A recent review highlighting the importance of diverse cellular and extracellular components that contribute to the TME found in human glioblastoma adds salience to the need for more robust pre-clinical models (214, 215). Additional examples supporting the need for immunocompetent mouse models include, as mentioned earlier, prolonged inhibition of EZH2 leading to a reversion back to a pro-growth state (141). Further work in immunocompetent models has shown the role of macrophages in supporting an immunosuppressive TME partially through immune-induced changes in DNA methylation in GSCs (216). Orthogonal work in immune cells and blood cancers has shown that HDAC inhibitors affect the immune microenvironment in multiple ways. Although HDAC inhibitors appear to downregulate the primary immune response and increase the expression of PD-L1 in cancer cells, these inhibitors can also increase the adaptive immune response (217–221). Further work is clearly needed to understand the global impact of histone modifying enzyme inhibition in the GBM tumor ecosystem.

6 Conclusion

Encouraging efforts across the GBM research community are increasing our understanding of the roles that histone modifying enzymes play in GBM pathophysiology. Our work here summarizes these efforts and provides a framework for improvements in the field moving forward. Given the dysregulated expression of enzymes involved in histone acetylation and methylation within GBM, it is important to understand how this aspect of epigenetics potentially influences tumorigenicity and transcriptional plasticity. Furthermore, the subtype-specific correlation of histone PTMs with gene expression and methylation, as well as the reversibility of histone PTMs in response to selective inhibition, highlight the link between these epigenetic modifications and our current understanding of transcriptional heterogeneity and plasticity in GBM. Inhibition of these numerous enzymes thus holds promise as a clinical target to improve GBM patient outcomes. Although numerous clinical trials using HDAC and HMT inhibitors are underway, there remains the need for greater efforts in understanding how altering enzymatic activity of histone PTM modifying enzymes impacts genomic architecture, non-histone substrates and their respective pathways, and the complex tumor microenvironment. Our understanding of the core molecular pathways, genetic aberrations, and transcriptional states that define GBM have progressed immensely since the clinical trials that define the current standard of care, yet these advancements have unfortunately not yet led to similar transformations in the clinic. By incorporating this existing knowledge with further studies into the targetability and pathophysiology of histone PTMs with orthogonal research on the immune microenvironment, metabolome, and neuronal and glial interactions, we can provide the best scientific foundation for the success of future clinical trials and improved care for patients with GBM.

Author contributions

CM, TW, HY, and AHK prepared the manuscript, tables, and figures. AH guided literature search strategy. AHK oversaw the project. All authors contributed to the article and approved the submitted version.

Funding

This work was supported by the Alvin J. Siteman Cancer Center (to AHK); the Christopher Davidson and Knight Family Fund (to AHK); and the Duesenberg Research Fund (to AHK).

Conflict of interest

Author AHK is a consultant for Monteris Medical and has received research grants from Monteris Medical for a mouse laser therapy study as well as from Stryker and Collagen Matrix for clinical outcomes studies about a dural substitute, which have no direct relation to this study.

The remaining authors declare that the research was conducted in the absence of any commercial or financial relationships that could be construed as a potential conflict of interest.

Publisher's note

References

1. Bjorland LS, Fluge O, Gilje B, Mahesparan R, Farbu E. Treatment approach and survival from glioblastoma: results from a population-based retrospective cohort study from Western Norway. *BMJ Open* (2021) 11:e043208. doi: 10.1136/bmjopen-2020-043208

2. Stupp R, Taillibert S, Kanner A, Read W, Steinberg DM, Lhermitte B, et al. Effect of tumor-treating fields plus maintenance temozolomide vs maintenance temozolomide alone on survival in patients with glioblastoma: A randomized clinical trial. *JAMA* (2017) 318:2306–16. doi: 10.1001/jama.2017.18718

3. Stupp R, Mason WP, van den Bent MJ, Weller M, Fisher B, Taphoorn MJB, et al. Radiotherapy plus concomitant and adjuvant temozolomide for glioblastoma. *N Engl J Med* (2005) 352:987–96. doi: 10.1056/NEJMoa043330

4. Liau LM, Ashkan K, Tran DD, Campian JL, Trusheim JE, Cobbs CS, et al. First results on survival from a large phase 3 clinical trial of an autologous dendritic cell vaccine in newly diagnosed glioblastoma. *J Transl Med* (2018) 16:142. doi: 10.1186/s12967-018-1507-6

5. Brennan CW, Verhaak RGW, McKenna A, Campos B, Noushmehr H, Salama SR, et al. The somatic genomic landscape of glioblastoma. *Cell* (2013) 155:462. doi: 10.1016/j.cell.2013.09.034

6. Patel AP, Tirosh I, Trombetta JJ, Shalek AK, Gillespie SM, Wakimoto H, et al. Single-cell RNA-seq highlights intratumoral heterogeneity in primary glioblastoma. *Science* (2014) 344:1396–401. doi: 10.1126/science.1254257

7. Brien GL, Bressan RB, Monger C, Gannon D, Lagan E, Doherty AM, et al. Simultaneous disruption of PRC2 and enhancer function underlies histone H3.3-K27M oncogenic activity in human hindbrain neural stem cells. *Nat Genet* (2021) 53:1221–32. doi: 10.1038/s41588-021-00897-w

8. Liu I, Jiang L, Samuelsson ER, Marco Salas S, Beck A, Hack OA, et al. The landscape of tumor cell states and spatial organization in H3-K27M mutant diffuse midline glioma across age and location. *Nat Genet* (2022) 54:1881–94. doi: 10.1038/s41588-022-01236-3

9. Pirozzi CJ, Yan H. The implications of IDH mutations for cancer development and therapy. *Nat Rev Clin Oncol* (2021) 18:645–61. doi: 10.1038/s41571-021-00521-0

10. Chinot OL, Barrié M, Fuentes S, Eudes N, Lancelot S, Metellus P, et al. Correlation between O6-Methylguanine-DNA methyltransferase and survival in inoperable newly diagnosed glioblastoma patients treated with neoadjuvant temozolomide. *J Clin Oncol* (2007) 25:1470–5. doi: 10.1200/JCO.2006.07.4807

11. Wu Q, Berglund AE, Etame AB. The impact of epigenetic modifications on adaptive resistance evolution in glioblastoma. *Int J Mol Sci* (2021) 22:8234. doi: 10.3390/ijms22158324

12. Zhang J, Chen L, Han L, Shi Z, Zhang J, Pu P, et al. EZH2 is a negative prognostic factor and exhibits pro-oncogenic activity in glioblastoma. *Cancer Lett* (2015) 356:929–36. doi: 10.1016/j.canlet.2014.11.003

13. Vinchure OS, Sharma V, Tabasum S, Ghosh S, Singh RP, Sarkar C, et al. Polycomb complex mediated epigenetic reprogramming alters TGF-β signaling *via* a novel EZH2/miR-490/TGIF2 axis thereby inducing migration and EMT potential in glioblastomas. *Int J Cancer* (2019) 145:1254–69. doi: 10.1002/ijc.32360

14. Yin Y, Qiu S, Li X, Huang B, Xu Y, Peng Y, et al. EZH2 suppression in glioblastoma shifts microglia toward M1 phenotype in tumor microenvironment. *J Neuroinflamm* (2017) 14:220. doi: 10.1186/s12974-017-0993-4

15. Escobar TM, Loyola A, Reinberg D. Parental nucleosome segregation and the inheritance of cellular identity. *Nat Rev Genet* (2021) 22:379–92. doi: 10.1038/s41576-020-00312-w

16. Allshire RC, Madhani HD. Ten principles of heterochromatin formation and function. *Nat Rev Mol Cell Biol* (2018) 19:229–44. doi: 10.1038/nrm.2017.119

17. Huang J, Sengupta R, Espejo AB, Lee MG, Dorsey JA, Richter M, et al. p53 is regulated by the lysine demethylase LSD1. *Nature* (2007) 449:105–8. doi: 10.1038/nature06092

18. Battle DJ, Kasim M, Yong J, Lotti F, Lau C-K, Mouaikel J, et al. The SMN complex: An assembly machine for RNPs. *Cold Spring Harb. Symp Quant. Biol* (2006) 71:313–20. doi: 10.1101/sqb.2006.71.001

19. Kim E, Kim M, Woo D-H, Shin Y, Shin J, Chang N, et al. Phosphorylation of EZH2 activates STAT3 signaling *via* STAT3 methylation and promotes tumorigenicity of glioblastoma stem-like cells. *Cancer Cell* (2013) 23:839–52. doi: 10.1016/j.ccr.2013.04.008

20. Dawson MA, Kouzarides T. Cancer epigenetics: From mechanism to therapy. *Cell* (2012) 150:12–27. doi: 10.1016/j.cell.2012.06.013

21. Peifer M, Fernández-Cuesta L, Sos ML, George J, Seidel D, Kasper LH, et al. Integrative genome analyses identify key somatic driver mutations of small-cell lung cancer. *Nat Genet* (2012) 44:1104–10. doi: 10.1038/ng.2396

22. Northcott PA, Shih DJH, Peacock J, Garzia L, Sorana Morrissy A, Zichner T, et al. Subgroup-specific structural variation across 1,000 medulloblastoma genomes. *Nature* (2012) 488:49–56. doi: 10.1038/nature11327

23. Roy DM, Walsh LA, Chan TA. Driver mutations of cancer epigenomes. *Protein Cell* (2014) 5:265–96. doi: 10.1007/s13238-014-0031-6

24. Varambally S, Dhanasekaran SM, Zhou M, Barrette TR, Kumar-Sinha C, Sanda MG, et al. The polycomb group protein EZH2 is involved in progression of prostate cancer. *Nature* (2002) 419:624–9. doi: 10.1038/nature01075

25. Weikert S, Christoph F, Köllermann J, Müller M, Schrader M, Miller K, et al. Expression levels of the EZH2 polycomb transcriptional repressor correlate with aggressiveness and invasive potential of bladder carcinomas. *Int J Mol Med* (2005) 16:349–53. doi: 10.3892/ijmm.16.2.349

26. Lu C, Han HD, Mangala LS, Ali-Fehmi R, Newton CS, Ozbun L, et al. Regulation of tumor angiogenesis by EZH2. *Cancer Cell* (2010) 18:185–97. doi: 10.1016/j.ccr.2010.06.016

27. Chang C-J, Yang J-Y, Xia W, Chen C-T, Xie X, Chao C-H, et al. EZH2 promotes expansion of breast tumor initiating cells through activation of RAF1-β-Catenin signaling. *Cancer Cell* (2011) 19:86–100. doi: 10.1016/j.ccr.2010.10.035

28. Grinat J, Heuberger J, Vidal RO, Goveas N, Kosel F, Berenguer-Llergo A, et al. The epigenetic regulator Mll1 is required for wnt-driven intestinal tumorigenesis and cancer stemness. *Nat Commun* (2020) 11:6422. doi: 10.1038/s41467-020-20222-z

29. Alves-Fernandes DK, Jasiulionis MG. The role of SIRT1 on DNA damage response and epigenetic alterations in cancer. *Int J Mol Sci* (2019) 20:3153. doi: 10.3390/ijms20133153

30. Hegi ME, Diserens A-C, Gorlia T, Hamou M-F, de Tribolet N, Weller M, et al. MGMT gene silencing and benefit from temozolomide in glioblastoma. *N Engl J Med* (2005) 352:997–1003. doi: 10.1056/NEJMoa043331

31. Bao S, Wu Q, McLendon RE, Hao Y, Shi Q, Hjelmeland AB, et al. Glioma stem cells promote radioresistance by preferential activation of the DNA damage response. *Nature* (2006) 444:756–60. doi: 10.1038/nature05236

32. Suvà M-L, Riggi N, Janiszewska M, Radovanovic I, Provero P, Stehle J-C, et al. EZH2 is essential for glioblastoma cancer stem cell maintenance. *Cancer Res* (2009) 69:9211–8. doi: 10.1158/0008-5472.CAN-09-1622

33. Nakano I. Stem cell signature in glioblastoma: Therapeutic development for a moving target. *J Neurosurg* (2015) 122:324–30. doi: 10.3171/2014.9.JNS132253

34. Gimple RC, Bhargava S, Dixit D, Rich JN. Glioblastoma stem cells: lessons from the tumor hierarchy in a lethal cancer. *Genes & Development* (2019) 33:591–609. doi: 10.1101/gad.324301

35. Neftel C, Laffy J, Filbin MG, Hara T, Shore ME, Rahme GJ, et al. An integrative model of cellular states, plasticity, and genetics for glioblastoma. *Cell* (2019) 178:835–849.e21. doi: 10.1016/j.cell.2019.06.024

36. Liau BB, Sievers C, Donohue LK, Gillespie SM, Flavahan WA, Miller TE, et al. Adaptive chromatin remodeling drives glioblastoma stem cell plasticity and drug tolerance. *Cell Stem Cell* (2017) 20:233–246.e7. doi: 10.1016/j.stem.2016.11.003

37. Lee KK, Workman JL. Histone acetyltransferase complexes: one size doesn't fit all. *Nat Rev Mol Cell Biol* (2007) 8:284–95. doi: 10.1038/nrm2145

38. Barlev NA, Liu L, Chehab NH, Mansfield K, Harris KG, Halazonetis TD, et al. Acetylation of p53 activates transcription through recruitment of Coactivators/Histone acetyltransferases. *Mol Cell* (2001) 8:1243–54. doi: 10.1016/S1097-2765(01)00414-2

39. Panier S, Boulton SJ. Double-strand break repair: 53BP1 comes into focus. *Nat Rev Mol Cell Biol* (2014) 15:7–18. doi: 10.1038/nrm3719

40. Audia JE, Campbell RM. Histone modifications and cancer. *Cold Spring Harb. Perspect Biol* (2016) 8:a019521.

41. Haberland M, Montgomery RL, Olson EN. The many roles of histone deacetylases in development and physiology: implications for disease and therapy. *Nat Rev Genet* (2009) 10:32–42. doi: 10.1038/nrg2485

42. Kouzarides T. Chromatin modifications and their function. *Cell* (2007) 128:693–705. doi: 10.1016/j.cell.2007.02.005

43. Millán-Zambrano G, Burton A, Bannister AJ, Schneider R. Histone post-translational modifications — cause and consequence of genome function. *Nat Rev Genet* (2022) 23:563–80. doi: 10.1038/s41576-022-00468-7

44. Wang Z, Zang C, Cui K, Schones DE, Barski A, Peng W, et al. Genome-wide mapping of HATs and HDACs reveals distinct functions in active and inactive genes. *Cell* (2009) 138:1019–31. doi: 10.1016/j.cell.2009.06.049

45. Wapenaar H, Dekker FJ. Histone acetyltransferases: challenges in targeting bi-substrate enzymes. *Clin Epigenet* (2016) 8:59. doi: 10.1186/s13148-016-0225-2

46. Dekker FJ, van den Bosch T, Martin NI. Small molecule inhibitors of histone acetyltransferases and deacetylases are potential drugs for inflammatory diseases. *Drug Discovery Today* (2014) 19:654–60. doi: 10.1016/j.drudis.2013.11.012

47. Falkenberg KJ, Johnstone RW. Histone deacetylases and their inhibitors in cancer, neurological diseases and immune disorders. *Nat Rev Drug Discovery* (2014) 13:673–91. doi: 10.1038/nrd4360

48. Hyun K, Jeon J, Park K, Kim J. Writing, erasing and reading histone lysine methylations. *Exp Mol Med* (2017) 49:e324–4. doi: 10.1038/emm.2017.11

49. Yang Y, Bedford MT. Protein arginine methyltransferases and cancer. *Nat Rev Cancer* (2013) 13:37–50. doi: 10.1038/nrc3409

50. Lv D, Jia F, Hou Y, Sang Y, Alvarez AA, Zhang W, et al. Histone acetyltransferase KAT6A upregulates PI3K/AKT signaling through TRIM24 binding. *Cancer Res* (2017) 77:6190–201. doi: 10.1158/0008-5472.CAN-17-1388

51. Dali-Youcef N, Froelich S, Moussallieh F-M, Chibbaro S, Noël G, Namer IJ, et al. Gene expression mapping of histone deacetylases and Co-factors and correlation with survival time and 1H-HRMAS metabolomic profile in human gliomas. *Sci Rep* (2015) 5:9087. doi: 10.1038/srep09087

52. Rasmussen RD, Gajjar MK, Jensen KE, Hamerlik P. Enhanced efficacy of combined HDAC and PARP targeting in glioblastoma. *Mol Oncol* (2016) 10:751–63. doi: 10.1016/j.molonc.2015.12.014

53. Wang X-Q, Bai H-M, Li S-T, Sun H, Min L-Z, Tao B-B, et al. Knockdown of HDAC1 expression suppresses invasion and induces apoptosis in glioma cells. *Oncotarget* (2017) 8:48027–40. doi: 10.18632/oncotarget.18227

54. Li S, Chen X, Mao L, Zahid KR, Wen J, Zhang L, et al. Histone deacetylase 1 promotes glioblastoma cell proliferation and invasion *via* activation of PI3K/AKT and MEK/ERK signaling pathways. *Brain Res* (2018) 1692:154–62. doi: 10.1016/j.brainres.2018.05.023

55. Cohen AL, Piccolo SR, Cheng L, Soldi R, Han B, Johnson WE, et al. Genomic pathway analysis reveals that EZH2 and HDAC4 represent mutually exclusive epigenetic pathways across human cancers. *BMC Med Genomics* (2013) 6:35. doi: 10.1186/1755-8794-6-35

56. Li Z, Li Q, Chen L, Chen B, Wang B, Zhang X, et al. Histone deacetylase inhibitor RGFP109 overcomes temozolomide resistance by blocking NF-κB-Dependent transcription in glioblastoma cell lines. *Neurochem Res* (2016) 41:3192–205. doi: 10.1007/s11064-016-2043-5

57. Cai J-Y, Xu T-T, Wang Y, Chang J-J, Li J, Chen X-Y, et al. Histone deacetylase HDAC4 promotes the proliferation and invasion of glioma cells. *Int J Oncol* (2018) 53:2758–68. doi: 10.3892/ijo.2018.4564

58. Mottet D, Pirotte S, Lamour V, Hagedorn M, Javerzat S, Bikfalvi A, et al. HDAC4 represses p21WAF1/Cip1 expression in human cancer cells through a Sp1-dependent, p53-independent mechanism. *Oncogene* (2009) 28:243–56. doi: 10.1038/onc.2008.371

59. Marampon F, Megiorni F, Camero S, Crescioli C, McDowell HP, Sferra R, et al. HDAC4 and HDAC6 sustain DNA double strand break repair and stem-like phenotype by promoting radioresistance in glioblastoma cells. *Cancer Lett* (2017) 397:1–11. doi: 10.1016/j.canlet.2017.03.028

60. Wang Z, Hu P, Tang F, Lian H, Chen X, Zhang Y, et al. HDAC6 promotes cell proliferation and confers resistance to temozolomide in glioblastoma. *Cancer Lett* (2016) 379:134–42. doi: 10.1016/j.canlet.2016.06.001

61. Yang R, Wu Y, Wang M, Sun Z, Zou J, Zhang Y, et al. HDAC9 promotes glioblastoma growth *via* TAZ-mediated EGFR pathway activation. *Oncotarget* (2015) 6:7644–56. doi: 10.18632/oncotarget.3223

62. Lee J-S, Park J-R, Kwon O-S, Lee T-H, Nakano I, Miyoshi H, et al. SIRT1 is required for oncogenic transformation of neural stem cells and for the survival of 'cancer cells with neural stemness' in a p53-dependent manner. *Neuro-Oncol* (2015) 17:95–106. doi: 10.1093/neuonc/nou145

63. Hiratsuka M, Inoue T, Toda T, Kimura N, Shirayoshi Y, Kamitani H, et al. Proteomics-based identification of differentially expressed genes in human gliomas: down-regulation of SIRT2 gene. *Biochem Biophys Res Commun* (2003) 309:558–66. doi: 10.1016/j.bbrc.2003.08.029

64. Sayd S, Thirant C, El-Habr EA, Lipecka J, Dubois LG, Bogeas A, et al. Sirtuin-2 activity is required for glioma stem cell proliferation arrest but not necrosis induced by resveratrol. *Stem Cell Rev Rep* (2014) 10:103–13. doi: 10.1007/s12015-013-9465-0

65. Park H-K, Hong J-H, Oh YT, Kim SS, Yin J, Lee A-J, et al. Interplay between TRAP1 and sirtuin-3 modulates mitochondrial respiration and oxidative stress to maintain stemness of glioma stem cells. *Cancer Res* (2019) 79:1369–82. doi: 10.1158/0008-5472.CAN-18-2558

66. Feng J, Yan P-F, Zhao H-Y, Zhang F-C, Zhao W-H, Feng M, et al. SIRT6 suppresses glioma cell growth *via* induction of apoptosis, inhibition of oxidative stress and suppression of JAK2/STAT3 signaling pathway activation. *Oncol Rep* (2016) 35:1395–402. doi: 10.3892/or.2015.4477

67. Li Y, Jin J, Wang Y. SIRT6 widely regulates aging, immunity, and cancer. *Front Oncol* (2022) 12. doi: 10.3389/fonc.2022.861334

68. Chen X, Hao B, Liu Y, Dai D, Han G, Li Y, et al. The histone deacetylase SIRT6 suppresses the expression of the RNA-binding protein PCBP2 in glioma. *Biochem Biophys Res Commun* (2014) 446:364–9. doi: 10.1016/j.bbrc.2014.02.116

69. Chie EK, Shin JH, Kim JH, Kim HJ, Kim IA, Kim IH, et al. *In vitro* and *In vivo* radiosensitizing effect of valproic acid on fractionated irradiation. *Cancer Res Treat* (2014) 47:527–33. doi: 10.4143/crt.2014.026

70. Hoja S, Schulze M, Rehli M, Proescholdt M, Herold-Mende C, Hau P, et al. Molecular dissection of the valproic acid effects on glioma cells. *Oncotarget* (2016) 7:62989–3002. doi: 10.18632/oncotarget.11379

71. Riva G, Butta V, Cilibrasi C, Baronchelli S, Redaelli S, Dalprà L, et al. Epigenetic targeting of glioma stem cells: Short-term and long-term treatments with valproic acid modulate DNA methylation and differentiation behavior, but not temozolomide sensitivity. *Oncol Rep* (2016) 35:2811–24. doi: 10.3892/or.2016.4665

72. Olsen EA, Kim YH, Kuzel TM, Pacheco TR, Foss FM, Parker S, et al. Phase IIb multicenter trial of vorinostat in patients with persistent, progressive, or treatment refractory cutaneous T-cell lymphoma. *J Clin Oncol Off J Am Soc Clin Oncol* (2007) 25:3109–15. doi: 10.1200/JCO.2006.10.2434

73. Pont LMEB, Naipal K, Kloezeman JJ, Venkatesan S, van den Bent M, van Gent DC, et al. DNA Damage response and anti-apoptotic proteins predict radiosensitization efficacy of HDAC inhibitors SAHA and LBH589 in patient-derived glioblastoma cells. *Cancer Lett* (2015) 356:525–35. doi: 10.1016/j.canlet.2014.09.049

74. Berghauser Pont LME, Spoor JKH, Venkatesan S, Swagemakers S, Kloezeman JJ, Dirven CMF, et al. The bcl-2 inhibitor obatoclax overcomes resistance to histone deacetylase inhibitors SAHA and LBH589 as radiosensitizers in patient-derived glioblastoma stem-like cells. *Genes Cancer* (2014) 5:445–59. doi: 10.18632/genesandcancer.42

75. Menezes A, Dos Reis GH, Oliveira-Nunes MC, Mariath F, Cabanel M, Pontes B, et al. Live cell imaging supports a key role for histone deacetylase as a molecular target during glioblastoma malignancy downgrade through tumor competence modulation. *J Oncol* (2019) 2019:9043675. doi: 10.1155/2019/9043675

76. Rampazzo E, Manfreda L, Bresolin S, Cani A, Mariotto E, Bortolozzi R, et al. Histone deacetylase inhibitors impair glioblastoma cell motility and proliferation. *Cancers* (2022) 14:1897. doi: 10.3390/cancers14081897

77. Kim JH, Shin JH, Kim IH. Susceptibility and radiosensitization of human glioblastoma cells to trichostatin a, a histone deacetylase inhibitor. *Int J Radiat. Oncol* (2004) 59:1174–80. doi: 10.1016/j.ijrobp.2004.03.001

78. Tung B, Ma D, Wang S, Oyinlade O, Laterra J, Ying M, et al. Krüppel-like factor 9 and histone deacetylase inhibitors synergistically induce cell death in glioblastoma stem-like cells. *BMC Cancer* (2018) 18:1025. doi: 10.1186/s12885-018-4874-8

79. Nguyen TTT, Zhang Y, Shang E, Shu C, Torrini C, Zhao J, et al. HDAC inhibitors elicit metabolic reprogramming by targeting super-enhancers in glioblastoma models. *J Clin Invest.* (2020) 130:3699–716. doi: 10.1172/JCI129049

80. Richens A, Ahmad S. Controlled trial of sodium valproate in severe epilepsy. *Br Med J* (1975) 4:255–6. doi: 10.1136/bmj.4.5991.255

81. Gurvich N, Tsygankova OM, Meinkoth JL, Klein PS. Histone deacetylase is a target of valproic acid-mediated cellular differentiation. *Cancer Res* (2004) 64:1079–86.

82. Wang Q, Hu B, Hu X, Kim H, Squatrito M, Scarpace L, et al. Tumor evolution of glioma-intrinsic gene expression subtypes associates with immunological changes in the microenvironment. *Cancer Cell* (2017) 32:42–56.e6. doi: 10.1016/j.ccell.2017.06.003

83. Sidaway P. Glioblastoma subtypes revisited. *Nat Rev Clin Oncol* (2017) 14:587–7.

84. Rothhammer-Hampl T, Liesenberg F, Hansen N, Hoja S, Delic S, Reifenberger G, et al. Frequent epigenetic inactivation of DIRAS-1 and DIRAS-2 contributes to chemo-resistance in gliomas. *Cancers* (2021) 13:5113. doi: 10.3390/cancers13205113

85. Everix L, Seane EN, Ebenhan T, Goethals I, Bolcaen J. Introducing HDAC-targeting radiopharmaceuticals for glioblastoma imaging and therapy. *Pharmaceuticals* (2023) 16:227. doi: 10.3390/ph16020227

86. Galanis E, et al. Phase I/II trial of vorinostat combined with temozolomide and radiation therapy for newly diagnosed glioblastoma: Results of alliance N0874/ABTC 02. *Neuro-Oncol* (2018) 20:546–56. doi: 10.1093/neuonc/nox161

87. Barker CA, Bishop AJ, Chang M, Beal K, Chan TA. Valproic acid use during radiation therapy for glioblastoma associated with improved survival. *Int J Radiat. Oncol Biol Phys* (2013) 86:504–9. doi: 10.1016/j.ijrobp.2013.02.012

88. Krauze AV, Megan M, Theresa C-Z, Peter M, Shih JH, Tofilon PJ, et al. The addition of valproic acid to concurrent radiation therapy and temozolomide improves patient outcome: a correlative analysis of RTOG 0525, SEER and a phase II NCI trial. *Cancer Stud Ther* (2020) 5:1–8. doi: 10.31038/CST.2020511

89. Puduvalli VK, Wu J, Yuan Y, Armstrong TS, Vera E, Wu J, et al. A Bayesian adaptive randomized phase II multicenter trial of bevacizumab with or without vorinostat in adults with recurrent glioblastoma. *Neuro-Oncol* (2020) 22:1505–15. doi: 10.1093/neuonc/noaa062

90. Guccione E, Richard S. The regulation, functions and clinical relevance of arginine methylation. *Nat Rev Mol Cell Biol* (2019) 20:642–57. doi: 10.1038/s41580-019-0155-x

91. Shi Y, Whetstine JR. Dynamic regulation of histone lysine methylation by demethylases. *Mol Cell* (2007) 25:1–14. doi: 10.1016/j.molcel.2006.12.010

92. Blanc RS, Richard S. Arginine methylation: The coming of age. *Mol Cell* (2017) 65:8–24. doi: 10.1016/j.molcel.2016.11.003

93. Walport LJ, Hopkinson RJ, Chowdhury R, Schiller R, Ge W, Kawamura A, et al. Arginine demethylation is catalysed by a subset of JmjC histone lysine demethylases. *Nat Commun* (2016) 7:11974. doi: 10.1038/ncomms11974

94. Husmann D, Gozani O. Histone lysine methyltransferases in biology and disease. *Nat Struct Mol Biol* (2019) 26:880–9. doi: 10.1038/s41594-019-0298-7

95. Black JC, Van Rechem C, Whetstine JR. Histone lysine methylation dynamics: Establishment, regulation, and biological impact. *Mol Cell* (2012) 48:491–507. doi: 10.1016/j.molcel.2012.11.006

96. Taverna SD, Li H, Ruthenburg AJ, Allis CD, Patel DJ. How chromatin-binding modules interpret histone modifications: lessons from professional pocket pickers. *Nat Struct Mol Biol* (2007) 14:1025–40. doi: 10.1038/nsmb1338

97. Heintzman ND, Stuart RK, Hon G, Fu Y, Ching CW, Hawkins RD, et al. Distinct and predictive chromatin signatures of transcriptional promoters and enhancers in the human genome. *Nat Genet* (2007) 39:311–8. doi: 10.1038/ng1966

98. Greer EL, Shi Y. Histone methylation: a dynamic mark in health, disease and inheritance. *Nat Rev Genet* (2012) 13:343–57. doi: 10.1038/nrg3173

99. Migliori V, Müller J, Phalke S, Low D, Bezzi M, Mok WC, et al. Symmetric dimethylation of H3R2 is a newly identified histone mark that supports euchromatin maintenance. *Nat Struct Mol Biol* (2012) 19:136–44. doi: 10.1038/nsmb.2209

100. Shilatifard A. The COMPASS family of histone H3K4 methylases: Mechanisms of regulation in development and disease pathogenesis. *Annu Rev Biochem* (2012) 81:65–95. doi: 10.1146/annurev-biochem-051710-134100

101. Yuan C-C, Matthews AGW, Jin Y, Chen CF, Chapman BA, Ohsumi TK, et al. Histone H3R2 symmetric dimethylation and histone H3K4 trimethylation are tightly correlated in eukaryotic genomes. *Cell Rep* (2012) 1:83–90. doi: 10.1016/j.celrep.2011.12.008

102. Zhao Q, Rank G, Tan YT, Li H, Moritz RL, Simpson RJ, et al. PRMT5-mediated methylation of histone H4R3 recruits DNMT3A, coupling histone and DNA methylation in gene silencing. *Nat Struct Mol Biol* (2009) 16:304–11. doi: 10.1038/nsmb.1568

103. Bedford MT, Clarke SG. Protein arginine methylation in mammals: Who, what, and why. *Mol Cell* (2009) 33:1–13. doi: 10.1016/j.molcel.2008.12.013

104. Bernstein BE, Mikkelsen TS, Xie X, Kamal M, Huebert DJ, Cuff J, et al. A bivalent chromatin structure marks key developmental genes in embryonic stem cells. *Cell* (2006) 125:315–26. doi: 10.1016/j.cell.2006.02.041

105. Sareddy GR, Viswanadhapalli S, Surapaneni P, Suzuki T, Brenner A, Vadlamudi RK, et al. Novel KDM1A inhibitors induce differentiation and apoptosis of glioma stem cells *via* unfolded protein response pathway. *Oncogene* (2017) 36:2423–34. doi: 10.1038/onc.2016.395

106. Singh MM, Manton CA, Bhat KP, Tsai W-W, Aldape K, Barton MC, et al. Inhibition of LSD1 sensitizes glioblastoma cells to histone deacetylase inhibitors. *Neuro-Oncol* (2011) 13:894–903. doi: 10.1093/neuonc/nor049

107. Sareddy GR, Nair BC, Krishnan SK, Gonugunta VK, Zhang Q, Miyata N, et al. KDM1 is a novel therapeutic target for the treatment of gliomas. *Oncotarget* (2012) 4:18–28. doi: 10.18632/oncotarget.725

108. Kozono D, Li J, Nitta M, Sampetrean O, Gonda D, Kushwaha DS, et al. Dynamic epigenetic regulation of glioblastoma tumorigenicity through LSD1 modulation of MYC expression. *Proc Natl Acad Sci U. S. A.* (2015) 112:E4055–4064. doi: 10.1073/pnas.1501967112

109. Zhou A, Lin K, Zhang S, Chen Y, Zhang N, Xue J, et al. Nuclear GSK3β promotes tumorigenesis by phosphorylating KDM1A and inducing its deubiquitylation by USP22. *Nat Cell Biol* (2016) 18:954–66. doi: 10.1038/ncb3396

110. Shou T, Yang H, Lv J, Liu D, Sun X. MicroRNA−3666 suppresses the growth and migration of glioblastoma cells by targeting KDM2A. *Mol Med Rep* (2019) 19:1049–55. doi: 10.3892/mmr.2018.9698

111. Staberg M, Rasmussen RD, Michaelsen SR, Pedersen H, Jensen KE, Villingshøj M, et al. Targeting glioma stem-like cell survival and chemoresistance through inhibition of lysine-specific histone demethylase KDM2B. *Mol Oncol* (2018) 12:406–20. doi: 10.1002/1878-0261.12174

112. Kurt IC, Sur I, Kaya E, Cingoz A, Kazancioglu S, Kahya Z, et al. KDM2B, an H3K36-specific demethylase, regulates apoptotic response of GBM cells to TRAIL. *Cell death dis* (2017) 8:e2897. doi: 10.1038/cddis.2017.288

113. Banelli B, Carra E, Barbieri F, Würth R, Parodi F, Pattarozzi A, et al. The histone demethylase KDM5A is a key factor for the resistance to temozolomide in glioblastoma. *Cell Cycle Georget. Tex* (2015) 14:3418–29. doi: 10.1080/15384101.2015.1090063

114. Wang B, Fan X, Ma C, Lei H, Long Q, Chai Y, et al. Downregulation of KDM4A suppresses the survival of glioma cells by promoting autophagy. *J Mol Neurosci MN* (2016) 60:137–44. doi: 10.1007/s12031-016-0796-6

115. Li M, Cheng J, Ma Y, Guo H, Shu H, Huang H, et al. The histone demethylase JMJD2A promotes glioma cell growth *via* targeting akt-mTOR signaling. *Cancer Cell Int* (2020) 20:101. doi: 10.1186/s12935-020-01177-z

116. Mallm J-P, et al. Glioblastoma initiating cells are sensitive to histone demethylase inhibition due to epigenetic deregulation. *Int J Cancer* (2020) 146:1281–92. doi: 10.1002/ijc.32649

117. Lee DH, Kim GW, Yoo J, Lee SW, Jeon YH, Kim SY, et al. Histone demethylase KDM4C controls tumorigenesis of glioblastoma by epigenetically regulating p53 and c-myc. *Cell Death Dis* (2021) 12:89. doi: 10.1038/s41419-020-03380-2

118. Banelli B, Daga A, Forlani A, Allemanni G, Marubbi D, Pistillo MP, et al. Small molecules targeting histone demethylase genes (KDMs) inhibit growth of temozolomide-resistant glioblastoma cells. *Oncotarget* (2017) 8:34896–910. doi: 10.18632/oncotarget.16820

119. Dai B, Hu Z, Huang H, Zhu G, Xiao Z, Wan W, et al. Overexpressed KDM5B is associated with the progression of glioma and promotes glioma cell growth *via* downregulating p21. *Biochem Biophys Res Commun* (2014) 454:221–7. doi: 10.1016/j.bbrc.2014.10.078

120. Romani M, Daga A, Forlani A, Pistillo MP, Banelli B. Targeting of histone demethylases KDM5A and KDM6B inhibits the proliferation of temozolomide-resistant glioblastoma cells. *Cancers* (2019) 11:E878. doi: 10.3390/cancers11060878

121. Sherry-Lynes MM, Sengupta S, Kulkarni S, Cochran BH. Regulation of the JMJD3 (KDM6B) histone demethylase in glioblastoma stem cells by STAT3. *PloS One* (2017) 12:e0174775. doi: 10.1371/journal.pone.0174775

122. Hayami S, Kelly JD, Cho H-S, Yoshimatsu M, Unoki M, Tsunoda T, et al. Overexpression of LSD1 contributes to human carcinogenesis through chromatin regulation in various cancers. *Int J Cancer* (2011) 128:574–86. doi: 10.1002/ijc.25349

123. Sharma SV, Lee DY, Li B, Quinlan MP, Takahashi F, Maheswaran S, et al. A chromatin-mediated reversible drug-tolerant state in cancer cell subpopulations. *Cell* (2010) 141:69–80. doi: 10.1016/j.cell.2010.02.027

124. Margueron R, Justin N, Ohno K, Sharpe ML, Son J, Drury WJ III, et al. Role of the polycomb protein EED in the propagation of repressive histone marks. *Nature* (2009) 461:762–7. doi: 10.1038/nature08398

125. Nolz JC, Gomez TS, Billadeau DD. The Ezh2 methyltransferase complex: actin up in the cytosol. *Trends Cell Biol* (2005) 15:514–7. doi: 10.1016/j.tcb.2005.08.003

126. Ezponda T, Licht JD. Molecular pathways: deregulation of histone h3 lysine 27 methylation in cancer-different paths, same destination. *Clin Cancer Res Off J Am Assoc Cancer Res* (2014) 20:5001–8. doi: 10.1158/1078-0432.CCR-13-2499

127. Ott M, Litzenburger UM, Sahm F, Rauschenbach KJ, Tudoran R, Hartmann C, et al. Promotion of glioblastoma cell motility by enhancer of zeste homolog 2 (EZH2) is mediated by AXL receptor kinase. *PloS One* (2012) 7:e47663. doi: 10.1371/journal.pone.0047663

128. Pang B, Zheng X-R, Tian J-X, Gao T-H, Gu G-Y, Zhang R, et al. EZH2 promotes metabolic reprogramming in glioblastomas through epigenetic repression of EAF2-HIF1α signaling. *Oncotarget* (2016) 7:45134–43. doi: 10.18632/oncotarget.9761

129. Chen H, Hou G, Yang J, Chen W, Guo L, Mao Q, et al. SOX9-activated PXN-AS1 promotes the tumorigenesis of glioblastoma by EZH2-mediated methylation of DKK1. *J Cell Mol Med* (2020) 24:6070–82. doi: 10.1111/jcmm.15189

130. Chen X, Hao A, Li X, Du Z, Li H, Wang H, et al. Melatonin inhibits tumorigenicity of glioblastoma stem-like cells *via* the AKT–EZH2–STAT3 signaling axis. *J Pineal Res* (2016) 61:208–17. doi: 10.1111/jpi.12341

131. Natsume A, Ito M, Katsushima K, Ohka F, Hatanaka A, Shinjo K, et al. Chromatin regulator PRC2 is a key regulator of epigenetic plasticity in glioblastoma. *Cancer Res* (2013) 73:4559–70. doi: 10.1158/0008-5472.CAN-13-0109

132. Ning X, Shi Z, Liu X, Zhang A, Han L, Jiang K, et al. DNMT1 and EZH2 mediated methylation silences the microRNA-200b/a/429 gene and promotes tumor progression. *Cancer Lett* (2015) 359:198–205. doi: 10.1016/j.canlet.2015.01.005

133. Cheng T, Xu Y. Effects of enhancer of zeste homolog 2 (EZH2) expression on brain glioma cell proliferation and tumorigenesis. *Med Sci Monit* (2018) 24:7249–55. doi: 10.12659/MSM.909814

134. Lee J, Son MJ, Woolard K, Donin NM, Li A, Cheng CH, et al. Epigenetic-mediated dysfunction of the bone morphogenetic protein pathway inhibits differentiation of glioblastoma-initiating cells. *Cancer Cell* (2008) 13:69–80. doi: 10.1016/j.ccr.2007.12.005

135. Ohka F, Shinjo K, Deguchi S, Matsui Y, Okuno Y, Katsushima K, et al. Pathogenic epigenetic consequences of genetic alterations in IDH-Wild-Type diffuse astrocytic gliomas. *Cancer Res* (2019) 79:4814–27. doi: 10.1158/0008-5472.CAN-19-1272

136. Mortimer T, Wainwright EN, Patel H, Siow BM, Jaunmuktane Z, Brandner S, et al. Redistribution of EZH2 promotes malignant phenotypes by rewiring developmental programmes. *EMBO Rep* (2019) 20:e48155. doi: 10.15252/embr.201948155

137. Zhang W, Lv S, Liu J, Zang Z, Yin J, An N, et al. PCI-24781 down-regulates EZH2 expression and then promotes glioma apoptosis by suppressing the PIK3K/Akt/mTOR pathway. *Genet Mol Biol* (2014) 37:716–24. doi: 10.1590/S1415-47572014005000011

138. Fan T-Y, Wang H, Xiang P, Liu Y-W, Li H-Z, Lei B-X, et al. Inhibition of EZH2 reverses chemotherapeutic drug TMZ chemosensitivity in glioblastoma. *Int J Clin Exp Pathol* (2014) 7:6662–70.

139. Stazi G, Taglieri L, Nicolai A, Romanelli A, Fioravanti R, Morrone S, et al. Dissecting the role of novel EZH2 inhibitors in primary glioblastoma cell cultures: effects on proliferation, epithelial-mesenchymal transition, migration, and on the pro-inflammatory phenotype. *Clin Epigenet* (2019) 11:173. doi: 10.1186/s13148-019-0763-5

140. Ahmad F, Patrick S, Sheikh T, Sharma V, Pathak P, Malgulwar PB, et al. Telomerase reverse transcriptase (TERT) - enhancer of zeste homolog 2 (EZH2) network regulates lipid metabolism and DNA damage responses in glioblastoma. *J Neurochem* (2017) 143:671–83. doi: 10.1111/jnc.14152

141. de Vries NA, Hulsman D, Akhtar W, de Jong J, Miles DC, Blom M, et al. Prolonged Ezh2 depletion in glioblastoma causes a robust switch in cell fate resulting in tumor progression. *Cell Rep* (2015) 10:383–97. doi: 10.1016/j.celrep.2014.12.028

142. Shivram H, Le SV, Iyer VR. PRC2 activates interferon-stimulated genes indirectly by repressing miRNAs in glioblastoma. *PloS One* (2019) 14:e0222435. doi: 10.1371/journal.pone.0222435

143. Zhong J, Yang X, Chen J, He K, Gao X, Wu X, et al. Circular EZH2-encoded EZH2-92aa mediates immune evasion in glioblastoma *via* inhibition of surface NKG2D ligands. *Nat Commun* (2022) 13:4795. doi: 10.1038/s41467-022-32311-2

144. Chen Q, Cai J, Wang Q, Wang Y, Liu M, Yang J, et al. Long noncoding RNA NEAT1, regulated by the EGFR pathway, contributes to glioblastoma progression through the WNT/β-catenin pathway by scaffolding EZH2. *Clin Cancer Res Off J Am Assoc Cancer Res* (2018) 24:684–95. doi: 10.1158/1078-0432.CCR-17-0605

145. Ma J, Benitez JA, Li J, Miki S, Ponte de Albuquerque C, Galatro T, et al. Inhibition of nuclear PTEN tyrosine phosphorylation enhances glioma radiation sensitivity through attenuated DNA repair. *Cancer Cell* (2019) 35:504–518.e7. doi: 10.1016/j.ccell.2019.01.020

146. Venneti S, Thompson CB. Metabolic modulation of epigenetics in gliomas. *Brain Pathol Zurich Switz.* (2013) 23:217–21. doi: 10.1111/bpa.12022

147. Shankar SR, Bahirvani AG, Rao VK, Bharathy N, Ow JR, Taneja R, et al. G9a, a multipotent regulator of gene expression. *Epigenetics* (2013) 8:16–22. doi: 10.4161/epi.23331

148. Tao H, Li H, Su Y, Feng D, Wang X, Zhang C, et al. Histone methyltransferase G9a and H3K9 dimethylation inhibit the self-renewal of glioma cancer stem cells. *Mol Cell Biochem* (2014) 394:23–30. doi: 10.1007/s11010-014-2077-4

149. Bao L, Chen Y, Lai H-T, Wu S-Y, Wang JE, Hatanpaa KJ, et al. Methylation of hypoxia-inducible factor (HIF)-1α by G9a/GLP inhibits HIF-1 transcriptional activity and cell migration. *Nucleic Acids Res* (2018) 46:6576–91. doi: 10.1093/nar/gky449

150. Ke XX, Zhang R, Zhong X, Zhang L, Cui H. Deficiency of G9a inhibits cell proliferation and activates autophagy *via* transcriptionally regulating c-myc expression in glioblastoma. *Front Cell Dev Biol* (2020) 8:593964. doi: 10.3389/fcell.2020.593964

151. Ciechomska IA, Przanowski P, Jackl J, Wojtas B, Kaminska B. BIX01294, an inhibitor of histone methyltransferase, induces autophagy-dependent differentiation of glioma stem-like cells. *Sci Rep* (2016) 6:38723. doi: 10.1038/srep38723

152. Ghildiyal R, Sen E. Concerted action of histone methyltransferases G9a and PRMT-1 regulates PGC-1α-RIG-I axis in IFNγ treated glioma cells. *Cytokine* (2017) 89:185–93. doi: 10.1016/j.cyto.2015.12.008

153. Melcher M, Schmid M, Aagaard L, Selenko P, Laible G, Jenuwein T. Structure-function analysis of SUV39H1 reveals a dominant role in heterochromatin organization, chromosome segregation, and mitotic progression. *Mol Cell Biol* (2000) 20:3728–41. doi: 10.1093/emboj/18.7.1923

154. Schultz DC, Ayyanathan K, Negorev D, Maul GG, Rauscher FJ. SETDB1: a novel KAP-1-associated histone H3, lysine 9-specific methyltransferase that contributes to HP1-mediated silencing of euchromatic genes by KRAB zinc-finger proteins. *Genes Dev* (2002) 16:919–32. doi: 10.1101/gad.973302

155. Spyropoulou A, Gargalionis A, Dalagiorgou G, Adamopoulos C, Papavassiliou KA, Lea RW, et al. Role of histone lysine methyltransferases SUV39H1 and SETDB1 in gliomagenesis: Modulation of cell proliferation, migration, and colony formation. *NeuroMolecular Med* (2014) 16:70–82. doi: 10.1007/s12017-013-8254-x

156. Sepsa A, Levidou G, Gargalionis A, Adamopoulos C, Spyropoulou A, Dalagiorgou G, et al. Emerging role of linker histone variant H1x as a biomarker with prognostic value in astrocytic gliomas. a multivariate analysis including trimethylation of H3K9 and H4K20. *PloS One* (2015) 10:e0115101. doi: 10.1371/journal.pone.0115101

157. Rahman Z, Mohd. R, Devabattula G, Mohd. A. & Godugu, C. Targeting H3K9 methyltransferase G9a and its related molecule GLP as a potential therapeutic strategy for cancer. *J Biochem Mol Toxicol* (2021) 35:e22674. doi: 10.1002/jbt.22674

158. Wysocka J, Allis CD, Coonrod S. Histone arginine methylation and its dynamic regulation. *Front Biosci.-Landmark* (2006) 11:344–55. doi: 10.2741/1802

159. Tarighat SS, Santhanam R, Frankhouser D, Radomska HS, Lai H, Anghelina M, et al. The dual epigenetic role of PRMT5 in acute myeloid leukemia: gene activation and repression *via* histone arginine methylation. *Leukemia* (2016) 30:789–99. doi: 10.1038/leu.2015.308

160. Tamiya H, Kim H, Klymenko O, Kim H, Feng Y, Zhang T, et al. SHARPIN-mediated regulation of protein arginine methyltransferase 5 controls melanoma growth. *J Clin Invest.* (2018) 128:517–30. doi: 10.1172/JCI95410

161. Han X, Li R, Zhang W, Yang X, Wheeler CG, Friedman GK, et al. Expression of PRMT5 correlates with malignant grade in gliomas and plays a pivotal role in tumor growth *in vitro*. *J Neurooncol.* (2014) 118:61–72. doi: 10.1007/s11060-014-1419-0

162. Huang T, Yang Y, Song X, Wan X, Wu B, Sastry N, et al. PRMT6 methylation of RCC1 regulates mitosis, tumorigenicity, and radiation response of glioblastoma stem cells. *Mol Cell* (2021) 81:1276–1291.e9. doi: 10.1016/j.molcel.2021.01.015

163. Liao Y, Luo Z, Lin Y, Chen H, Chen T, Xu L, et al. PRMT3 drives glioblastoma progression by enhancing HIF1A and glycolytic metabolism. *Cell Death Dis* (2022) 13:1–14. doi: 10.1038/s41419-022-05389-1

164. Banasavadi-Siddegowda YK, Russell L, Frair E, Karkhanis VA, Relation T, Yoo JY, et al. PRMT5–PTEN molecular pathway regulates senescence and self-renewal of primary glioblastoma neurosphere cells. *Oncogene* (2017) 36:263–74. doi: 10.1038/onc.2016.199

165. Banasavadi-Siddegowda YK, Welker AM, An M, Yang X, Zhou W, Shi G, et al. PRMT5 as a druggable target for glioblastoma therapy. *Neuro-Oncol* (2018) 20:753–63. doi: 10.1093/neuonc/nox206

166. Holmes B, Benavides-Serrato A, Saunders JT, Landon KA, Schreck AJ, Nishimura RN, et al. The protein arginine methyltransferase PRMT5 confers therapeutic resistance to mTOR inhibition in glioblastoma. *J Neurooncol.* (2019) 145:11–22. doi: 10.1007/s11060-019-03274-0

167. Sachamitr P, Ho JC, Ciamponi FE, Ba-Alawi W, Coutinho FJ, Guilhamon P, et al. PRMT5 inhibition disrupts splicing and stemness in glioblastoma. *Nat Commun* (2021) 12:979. doi: 10.1038/s41467-021-21204-5

168. Heddleston JM, Wu Q, Rivera M, Minhas S, Lathia JD, Sloan AE, et al. Hypoxia-induced mixed-lineage leukemia 1 regulates glioma stem cell tumorigenic potential. *Cell Death Differ* (2012) 19:428–39. doi: 10.1038/cdd.2011.109

169. Gallo M, Coutinho FJ, Vanner RJ, Gayden T, Mack SC, Murison A, et al. MLL5 orchestrates a cancer self-renewal state by repressing the histone variant H3.3 and globally reorganizing chromatin. *Cancer Cell* (2015) 28:715–29. doi: 10.1016/j.ccell.2015.10.005

170. Dixit D, Prager BC, Gimple RC, Miller TE, Wu Q, Yomtoubian S, et al. Glioblastoma stem cells reprogram chromatin *in vivo* to generate selective therapeutic dependencies on DPY30 and phosphodiesterases. *Sci Transl Med 14 eabf3917* (2022) 14:eabf3917. doi: 10.1126/scitranslmed.abf3917

171. Liu H, Sun Y, Zhang Q, Jin W, Gordon RE, Zhang Y, et al. Pro-inflammatory and proliferative microglia drive progression of glioblastoma. *Cell Rep* (2021) 36:109718. doi: 10.1016/j.celrep.2021.109718

172. Fan X, Sun S, Yang H, Ma H, Zhao C, Niu W, et al. SETD2 palmitoylation mediated by ZDHHC16 in epidermal growth factor receptor-mutated glioblastoma promotes ionizing radiation-induced DNA damage. *Int J Radiat. Oncol* (2022) 113:648–60. doi: 10.1016/j.ijrobp.2022.02.018

173. Rhodes CT, Sandstrom RS, Huang S-WA, Wang Y, Schotta G, Berger MS, et al. Cross-species analyses unravel the complexity of H3K27me3 and H4K20me3 in the context of neural stem progenitor cells. *Neuroepigenetics* (2016) 6:10–25. doi: 10.1016/j.nepig.2016.04.001

174. Bottino C, Peserico A, Simone C, Caretti G. SMYD3: An oncogenic driver targeting epigenetic regulation and signaling pathways. *Cancers* (2020) 12:142. doi: 10.1038/nrc3929

175. Rao RC, Dou Y. Hijacked in cancer: the KMT2 (MLL) family of methyltransferases. *Nat Rev Cancer* (2015) 15:334–46. doi: 10.1523/JNEUROSCI.0968-09.2009

176. Abdouh M, Facchino S, Chatoo W, Balasingam V, Ferreira J, Bernier G. BMI1 sustains human glioblastoma multiforme stem cell renewal. *J Neurosci* (2009) 29:8884–96. doi: 10.1523/JNEUROSCI.0968-09.2009

177. Sun J, Zheng G, Gu Z, Guo Z. MiR-137 inhibits proliferation and angiogenesis of human glioblastoma cells by targeting EZH2. *J Neurooncol.* (2015) 122:481–9. doi: 10.1007/s11060-015-1753-x

178. Sharma V, Malgulwar PB, Purkait S, Patil V, Pathak P, Agrawal R, et al. Genome-wide ChIP-seq analysis of EZH2-mediated H3K27me3 target gene profile highlights differences between low- and high-grade astrocytic tumors. *Carcinogenesis* (2017) 38:152–61. doi: 10.1093/carcin/bgw126

179. Grinshtein N, Rioseco CC, Marcellus R, Uehling D, Aman A, Lun X, et al. Small molecule epigenetic screen identifies novel EZH2 and HDAC inhibitors that target glioblastoma brain tumor-initiating cells. *Oncotarget* (2016) 7:59360–76. doi: 10.18632/oncotarget.10661

180. Purkait S, Sharma V, Kumar A, Pathak P, Mallick S, Jha P, et al. Expression of DNA methyltransferases 1 and 3B correlates with EZH2 and this 3-marker epigenetic signature predicts outcome in glioblastomas. *Exp Mol Pathol* (2016) 100:312–20. doi: 10.1016/j.yexmp.2016.02.002

181. Jin X, Kim LJY, Wu Q, Wallace LC, Prager BC, Sanvoranart T, et al. Targeting glioma stem cells through combined BMI1 and EZH2 inhibition. *Nat Med* (2017) 23:1352–61. doi: 10.1038/nm.4415

182. Zhang L, Liu Y, Wang M, Wu Z, Li N, Zhang J, et al. EZH2-, CHD4-, and IDH-linked epigenetic perturbation and its association with survival in glioma patients. *J Mol Cell Biol* (2017) 9:477–88. doi: 10.1093/jmcb/mjx056

183. Luo W, Li X, Song Z, Zhu X, Zhao S. Long non-coding RNA AGAP2-AS1 exerts oncogenic properties in glioblastoma by epigenetically silencing TFPI2 through EZH2 and LSD1. *Aging* (2019) 11:3811–23. doi: 10.18632/aging.102018

184. Li Y, Ren Y, Wang Y, Tan Y, Wang Q, Cai J, et al. A compound AC1Q3QWB selectively disrupts HOTAIR-mediated recruitment of PRC2 and enhances cancer therapy of DZNep. *Theranostics* (2019) 9:4608–23. doi: 10.7150/thno.35188

185. Yang R, Wang M, Zhang G, Bao Y, Wu Y, Li X, et al. E2F7–EZH2 axis regulates PTEN/AKT/mTOR signalling and glioblastoma progression. *Br J Cancer* (2020) 123:1445–55. doi: 10.1038/s41416-020-01032-y

186. Chen Y, Hou S, Jiang R, Sun J, Cheng C, Qian Z, et al. EZH2 is a potential prognostic predictor of glioma. *J Cell Mol Med* (2021) 25:925–36. doi: 10.1111/jcmm.16149

187. Guo A-S, Huang Y-Q, Ma X-D, Lin R-S. Mechanism of G9a inhibitor BIX–01294 acting on U251 glioma cells. *Mol Med Rep* (2016) 14:4613–21. doi: 10.3892/mmr.2016.5815

188. Dai B, Wan W, Zhang P, Zhang Y, Pan C, Meng G, et al. SET and MYND domain-containing protein 3 is overexpressed in human glioma and contributes to tumorigenicity. *Oncol Rep* (2015) 34:2722–30. doi: 10.3892/or.2015.4239

189. Miller TE, Liau BB, Wallace LC, Morton AR, Xie Q, Dixit D, et al. Transcription elongation factors represent *in vivo* cancer dependencies in glioblastoma. *Nature* (2017) 547:355–9. doi: 10.1038/nature23000

190. Alexanian AR, Huang Y-W. Specific combinations of the chromatin-modifying enzyme modulators significantly attenuate glioblastoma cell proliferation and viability while exerting minimal effect on normal adult stem cells growth. *Tumour Biol J Int Soc Oncodevelopmental Biol Med* (2015) 36:9067–72. doi: 10.1007/s13277-015-3654-1

191. Lee J-Y, Lee S-H, Heo S-H, Kim K-S, Kim C, Kim D-K, et al. Novel function of lysine methyltransferase G9a in the regulation of Sox2 protein stability. *PloS One* (2015) 10:e0141118. doi: 10.1371/journal.pone.0141118

192. Zhang Y, Máté G, Müller P, Hillebrandt S, Krufczik M, Bach M, et al. Radiation induced chromatin conformation changes analysed by fluorescent localization microscopy, statistical physics, and graph theory. *PloS One* (2015) 10:e0128555. doi: 10.1371/journal.pone.0128555

193. Rheinbay E, Suvà ML, Gillespie SM, Wakimoto H, Patel AP, Shahid M, et al. An aberrant transcription factor network essential for wnt signaling and stem cell maintenance in glioblastoma. *Cell Rep* (2013) 3:1567–79. doi: 10.1016/j.celrep.2013.04.021

194. Park NI, Guilhamon P, Desai K, McAdam RF, Langille E, O'Connor M, et al. ASCL1 reorganizes chromatin to direct neuronal fate and suppress tumorigenicity of glioblastoma stem cells. *Cell Stem Cell* (2017) 21:209–224.e7. doi: 10.1016/j.stem.2017.06.004

195. Vue TY, Kollipara RK, Borromeo MD, Smith T, Mashimo T, Burns DK, et al. ASCL1 regulates neurodevelopmental transcription factors and cell cycle genes in brain tumors of glioma mouse models. *Glia* (2020) 68:2613–30. doi: 10.1002/glia.23873

196. Lin B, Lee H, Yoon J-G, Madan A, Wayner E, Tonning S, et al. Global analysis of H3K4me3 and H3K27me3 profiles in glioblastoma stem cells and identification of SLC17A7 as a bivalent tumor suppressor gene. *Oncotarget* (2015) 6:5369–81. doi: 10.18632/oncotarget.3030

197. Hall AW, Battenhouse AM, Shivram H, Morris AR, Cowperthwaite MC, Shpak M, et al. Bivalent chromatin domains in glioblastoma reveal a subtype-specific signature of glioma stem cells. *Cancer Res* (2018) 78:2463–74. doi: 10.1158/0008-5472.CAN-17-1724

198. Yoo S, Bieda MC. Differences among brain tumor stem cell types and fetal neural stem cells in focal regions of histone modifications and DNA methylation, broad regions of modifications, and bivalent promoters. *BMC Genomics* (2014) 15:724. doi: 10.1186/1471-2164-15-724

199. Zhou D, Alver BM, Li S, Hlady RA, Thompson JJ, Schroeder MA, et al. Distinctive epigenomes characterize glioma stem cells and their response to differentiation cues. *Genome Biol* (2018) 19:43. doi: 10.1186/s13059-018-1420-6

200. Bogeas A, Morvan-Dubois G, El-Habr EA, Lejeune F-X, Defrance M, Narayanan A, et al. Changes in chromatin state reveal ARNT2 at a node of a tumorigenic transcription factor signature driving glioblastoma cell aggressiveness. *Acta Neuropathol. (Berl.)* (2018) 135:267–83. doi: 10.1007/s00401-017-1783-x

201. Xu L, Chen Y, Huang Y, Sandanaraj E, Yu JS, Lin RY-T, et al. Topography of transcriptionally active chromatin in glioblastoma. *Sci Adv* (2021) 7:eabd4676. doi: 10.1126/sciadv.abd4676

202. Stępniak K, Machnicka MA, Mieczkowski J, Macioszek A, Wojtaś B, Gielniewski B, et al. Mapping chromatin accessibility and active regulatory elements reveals pathological mechanisms in human gliomas. *Nat Commun* (2021) 12:3621. doi: 10.1038/s41467-021-23922-2

203. Shiozawa Y, Havens AM, Jung Y, Ziegler AM, Pedersen EA, Wang J, et al. Annexin II/Annexin II receptor axis regulates adhesion, migration, homing, and growth of prostate cancer. *J Cell Biochem* (2008) 105:370–80. doi: 10.1002/jcb.21835

204. Chaligne R, Gaiti F, Silverbush D, Schiffman JS, Weisman HR, Kluegel L, et al. Epigenetic encoding, heritability and plasticity of glioma transcriptional cell states. *Nat Genet* (2021) 53:1469–79. doi: 10.1038/s41588-021-00927-7

205. Lee J, Kotliarova S, Kotliarov Y, Li A, Su Q, Donin NM, et al. Tumor stem cells derived from glioblastomas cultured in bFGF and EGF more closely mirror the phenotype and genotype of primary tumors than do serum-cultured cell lines. *Cancer Cell* (2006) 9:391–403. doi: 10.1016/j.ccr.2006.03.030

206. Allen M, Bjerke M, Edlund H, Nelander S, Westermark B. Origin of the U87MG glioma cell line: Good news and bad news. *Sci Transl Med* (2016) 8:354re3.

207. Linkous A, Balamatsias D, Snuderl M, Edwards L, Miyaguchi K, Milner T, et al. Modeling patient-derived glioblastoma with cerebral organoids. *Cell Rep* (2019) 26:3203–3211.e5. doi: 10.1016/j.celrep.2019.02.063

208. Koga T, Chaim IA, Benitez JA, Markmiller S, Parisian AD, Hevner RF, et al. Longitudinal assessment of tumor development using cancer avatars derived from genetically engineered pluripotent stem cells. *Nat Commun* (2020) 11:550. doi: 10.1038/s41467-020-14312-1

209. Sullivan JK, Fahey PP, Agho KE, Hurley SP, Feng Z, Day RO, et al. Valproic acid as a radio-sensitizer in glioma: A systematic review and meta-analysis. *Neuro-Oncol. Pract* (2023) 10:13–23. doi: 10.1093/nop/npac078

210. Brighi C, Salimova E, de Veer M, Puttick S, Egan G. Translation of focused ultrasound for blood-brain barrier opening in glioma. *J Controlled Release* (2022) 345:443–63. doi: 10.1016/j.jconrel.2022.03.035

211. Salehi A, Paturu MR, Patel B, Cain MD, Mahlokozera T, Yang AB, et al. Therapeutic enhancement of blood–brain and blood–tumor barriers permeability by laser interstitial thermal therapy. *Neuro-Oncol. Adv* (2020) 2:1–12. doi: 10.1093/noajnl/vdaa071

212. Szatmári T, Lumniczky K, Désaknai S, Trajcevski S, Hídvégi EJ, Hamada H, et al. Detailed characterization of the mouse glioma 261 tumor model for experimental glioblastoma therapy. *Cancer Sci* (2006) 97:546–53. doi: 10.1111/j.1349-7006.2006.00208.x

213. Genoud V, Marinari E, Nikolaev SI, Castle JC, Bukur V, Dietrich P-Y, et al. Responsiveness to anti-PD-1 and anti-CTLA-4 immune checkpoint blockade in SB28 and GL261 mouse glioma models. *OncoImmunology* (2018) 7:e1501137. doi: 10.1080/2162402X.2018.1501137

214. Franson A, McClellan BL, Varela ML, Comba A, Syed MF, Banerjee K, et al. Development of immunotherapy for high-grade gliomas: Overcoming the immunosuppressive tumor microenvironment. *Front Med* (2022) 9. doi: 10.3389/fmed.2022.966458

215. Faisal SM, Comba A, Varela ML, Argento AE, Brumley E, Abel C, et al. The complex interactions between the cellular and non-cellular components of the brain tumor microenvironmental landscape and their therapeutic implications. *Front Oncol* (2022) 12. doi: 10.3389/fonc.2022.1005069

216. Gangoso E, Southgate B, Bradley L, Rus S, Galvez-Cancino F, McGivern N, et al. Glioblastomas acquire myeloid-affiliated transcriptional programs *via* epigenetic immunoediting to elicit immune evasion. *Cell* (2021) 184:2454–2470.e26. doi: 10.1016/j.cell.2021.03.023

217. Kroesen M, Gielen PR, Brok IC, Armandari I, Hoogerbrugge PM, Adema GJ, et al. HDAC inhibitors and immunotherapy; a double edged sword? *Oncotarget* (2014) 5:6558–72. doi: 10.18632/oncotarget.2289

218. Bode KA, Schroder K, Hume DA, Ravasi T, Heeg K, Sweet MJ, et al. Histone deacetylase inhibitors decrease toll-like receptor-mediated activation of proinflammatory gene expression by impairing transcription factor recruitment. *Immunology* (2007) 122:596–606. doi: 10.1111/j.1365-2567.2007.02678.x

219. Deng S, Hu Q, Zhang H, Yang F, Peng C, Huang C, et al. HDAC3 inhibition upregulates PD-L1 expression in b-cell lymphomas and augments the efficacy of anti–PD-L1 therapy. *Mol Cancer Ther* (2019) 18:900–8. doi: 10.1158/1535-7163.MCT-18-1068

220. Bridle BW, Chen L, Lemay CG, Diallo J-S, Pol J, Nguyen A, et al. HDAC inhibition suppresses primary immune responses, enhances secondary immune responses, and abrogates autoimmunity during tumor immunotherapy. *Mol Ther* (2013) 21:887–94. doi: 10.1038/mt.2012.265

221. Tiper IV, Webb TJ. Histone deacetylase inhibitors enhance CD1d-dependent NKT cell responses to lymphoma. *Cancer Immunol Immunother.* (2016) 65:1411–21. doi: 10.1007/s00262-016-1900-z

Frontiers in Oncology

Advances knowledge of carcinogenesis and tumor progression for better treatment and management

The third most-cited oncology journal, which highlights research in carcinogenesis and tumor progression, bridging the gap between basic research and applications to imrpove diagnosis, therapeutics and management strategies.

Discover the latest Research Topics

See more →

Frontiers

Avenue du Tribunal-Fédéral 34
1005 Lausanne, Switzerland
frontiersin.org

Contact us

+41 (0)21 510 17 00
frontiersin.org/about/contact